HYDRODYNAMIC PERFORMANCE OF AN ARTIFICIAL AORTIC VALVE IMPLANT

by

MOHAMMAD AMINZADEH

B.A.Sc., University of Windsor,
Windsor, Ontario, 1969

A THESIS SUBMITTED IN PARTIAL FULFILMENT OF
THE REQUIREMENT FOR THE DEGREE OF
DOCTOR OF PHILOSOPHY

in the Department
of
Mechanical Engineering

We accept this thesis as conforming to the
required standard

THE UNIVERSITY OF BRITISH COLUMBIA

January, 1975

In presenting this thesis in partial fulfillment of the requirements for an advanced degree at the University of British Columbia, I agree that the Library shall make it freely available for reference and study. I further agree that permission for extensive copying of this thesis for scholarly purposes may be granted by the Head of my Department or by his representatives. It is understood that publication, in part or in whole, or the copying of this thesis for financial gain shall not be allowed without my written permission.

MOHAMMAD AMINZADEH

Department of Mechanical Engineering

The University of British Columbia,
Vancouver V6T 1W5, Canada

Date March 6, 1975

ABSTRACT

The project aims at studying fluid dynamics of a prosthetic aortic heart valve through an organized experimental programme with a view to obtain better appreciation of factors affecting its performance and eventual failure. The problem is approached in stages representing an increasing order of difficulties in terms of experimental set-up and interpretation of data.

Design, construction and calibration of the glycerol tunnel, which formed the fundamental test facility for the project, are described briefly in the beginning followed by an introduction to the test models and monitoring instrumentation. A simple theory for wedge shaped hot film anemometer is developed and velocity profiles with and without models in the test section presented.

Essentially the test programme consists of three stages:

(i) a single sphere by itself during stationary and oscillating conditions, R_n = 74 - 5838;

(ii) a stationary spherical poppet occupying different positions in the cage representing quasi-steady opening and closing of the valve, R_n = 220 - 1200;

(iii) poppet pulsating according to the recorded displacement-time history when implanted in a patient, R_n = 290 - 650.

A careful choice of reference pressure and velocity results in presentation of data in a manner that would permit reproduction and comparison of results by investigators using different test facilities.

The static pressure distribution data and resulting information on the average base pressure, separating shear layers, its movement, etc. are obtained for closed and open bypass conditions of the tunnel, the latter representative of regurgitation.

An extensive flow visualization programme using the dye injection procedure in conjunction with still and high speed movie photography complemented the experimental data. It resulted in better appreciation of the physical character of the flow.

Studies with a single sphere vividly showed the progress of formation, elongation and instability of the vortex ring with the Reynolds number. Of particular interest was the distinct rise in the minimum and base pressures in the Reynolds number range of 240 - 475, which was found to be associated with the onset of instability of the vortex ring leading to its periodic shedding. In general, the Reynolds number effects were confined to the region near and downstream of the minimum pressure point. The experimental results clearly suggested inherent limitations in the analytical procedures for predicting pressure distribution as proposed by several investigators. On the other

hand, the pressure integrated drag results compared favourably with the directly measured drag data reported in the literature thus substantiating the reliability of the pressure measurements.

Coming to the pulsating sphere, effects of the oscillation frequency, Reynolds number and sphere position are investigated during both forward and reverse strokes of a cycle. Influence of the Beta number is confined to the local changes in the character of the base pressure plots without substantially affecting their average magnitudes. A decrease in y_s leads to increase in the minimum and average wake pressures together with a forward movement of the separation point during the forward stroke. The general character of the pressure profiles remains the same during the reverse stroke, however, the magnitudes involved are markedly different.

Next, the thesis discusses a more realistic situation, from the configuration consideration, of a stationary poppet occupying different positions in the cage. The Reynolds number influence, which is more significant for $y_b < 0.2$, is essentially reflected in the increase of the wake pressure. A significant rise in the negative pressure coefficient at $y_b \leq 0.1$ would suggest large shearing stresses leading to possible deformation and destruction of the red blood cells. The presence of distributed vorticity and the associated centrifugal field in the wake

are suspected to be the fundamental factors promoting dissociation of the blood into its constituents and finally their deposition on the body of the valve.

Finally, the case of poppet oscillating inside the valve is considered which shows the effect of valve opening on C_p to be far greater than that observed during the stationary case. The high negative pressure, at the pulsation frequency, in the wake region and the associated large periodic shear stresses are likely to cause not only coagulation of the cells leading to clotting but may be responsible for rupturing of the suture lines in the implanted prosthetic valve, as often encountered in practice.

TABLE OF CONTENTS

Chapter Page

Chapter | Page

LIST OF TABLES

LIST OF FIGURES

Figure Page

Figure Page

Figure Page

Figure | Page

LIST OF APPENDIX FIGURES

ACKNOWLEDGEMENT

I would like to take this opportunity to express my gratitude and sincere thanks to Professor V.J. Modi for the enthusiastic guidance given throughout the research program and helpful suggestions during the preparation of the thesis. His help and encouragement have been invaluable.

The cheerful assistance of the technical staff is gratefully acknowledged. Their skillful assistance greatly accelerated the research program.

Mention should be made of the occasional discussions with Dr. C.E. Rotem, Cardiologist at the Shaughnessy Hospital, Vancouver, British Columbia.

The investigation was supported by the Medical Research Council of Canada, Grant No. MA-2637 and the National Research Council of Canada, Grants No. A-2181 and A-2772.

Finally, special appreciation is extended to my wife, Shaheen, for her encouragement and for her patience and understanding during difficult times.

LIST OF SYMBOLS

a	overheat ratio, $(R_0-R_c)/R_c$
b	hot film width
B_n	Beta number, $R_n^{1/2}S_n^{1/2} = D(f/\nu)^{1/2}$
c	speed of sound in air at the reference temperature
C	specific heat
C_d	sectional pressure drag coefficient based on sphere diameter (D), $F/(\frac{1}{2}\rho U^2)$ (diameteral cross-sectional area)
C_n	percentage concentration of glycerol-water solution by weight
C_p	static pressure coefficient, $(P_\theta-P_{60°})/(P_0-P_{60°})$
$\hat{C}_p$	static pressure coefficient as suggested by Grove et al.[124], $(P_\theta-P_r)/(\frac{1}{2}\rho U_r^2)$
C_{p_b}	base pressure coefficient, average static pressure coefficient over the portion of the body extending into the wake ($\theta \simeq 120°-180°$)
d	orifice diameter
d_s	diameter of the stem supporting the sphere
D	ball diameter
E_t	ejection time
f	pulsation frequency, cpm
F	sectional pressure drag
g	gravitational acceleration
g_b	ball acceleration

G_r	Grashof number, $[g\beta b^3(T_w-T_f)\cos\delta]/\nu^2$
h	head across the pump
K_f, K_g	thermal conductivity of the test fluid and glass support, respectively
ℓ	hot film length
L	axial distance in a tube viscometer
M	torque
M_n	Mach number, U/c
N_p	Prandtl number, $C\rho/K_f$
N_u	Nusselt number, $qb/K_f(T_w-T_f)$
P	static pressure
P_θ	static pressure on the surface of the sphere at an angle of θ from the front stagnation point
P_0	static pressure on the surface of the sphere at the front stagnation point
$P_{60°}$	static pressure on the surface of the sphere at $\theta = 60°$
P_r	reference static pressure as suggested by Grove et al.[124]
q	heat flux per unit area
Q	total heat flux
$\dot{Q}$	volume flow rate
r	radius of the rotating cylinder in a viscometer
r_1, r_2	radius of the inner and outer cylinder, respectively

R	electrical resistance
R_c, R_0	cold and operating resistance of the hot film probe, respectively
R_n	Reynolds number, UD/ν
$\hat{R}_n$	Reynolds number based on U_r as suggested by Grove et al.[124], $U_r D/\nu$
s	stroke length
S_n	Strouhal number, fD/U
t	time
t_0, t_c, t_{sc}, t_{s0}	opening time, closing time, closing duration and opening duration of an artificial aortic valve, respectively
T	temperature
T_f, T_m	bulk and mean temperature of the fluid
T_w	wall temperature
U	average velocity in the test section based on a flow rate as given by the orifice meter
U_0	poppet velocity during the reverse stroke (opening of the valve)
U_b	ball velocity during its pulsatile motion
U_c	poppet velocity during the forward stroke (closing of the valve)
U_r	reference velocity, taken as the centerline velocity
U_z	local velocity as measured by a hot film probe

V	D.C. voltage output of a constant temperature anemometer
X	piston displacement of an air cylinder
y_b	dimensionless valve opening, $\bar{y}_b/s$
$\bar{y}_b$	valve opening
y_p	probe's distance from the tunnel inlet
y_s	dimensionless sphere displacement
$\bar{y}_s$	sphere displacement
Y	horizontal coordinate parallel to the tunnel axis with origin at the tunnel entrance, positive in the direction of the flow
Z	vertical coordinate with origin at the bottom of the test section
α	angle between the cone and the plate in a cone-plate viscometer
β	coefficient of thermal expansion
γ	shear rate
γ_ω	shear rate at the wall
δ	wedge angle of the hot film probe
θ	angular location of a pressure tap with reference to the front stagnation point
θ_s	angular location of the separating shear layer with respect to the rear stagnation point
λ	coefficient of thermal resistivity of the hot film probe

μ	dynamic viscosity
μ_c	Casson viscosity[152]
ν	kinematic viscosity, μ/ρ
ρ	density
σ	yield stress of blood
τ	shear stress
τ_w	shear stress at the wall
ϕ	differential pressure across the orifice plate
χ	downstream coordinate along the probe face
ω	angular velocity of a rotational viscometer

GLOSSARY

Aortic incompetence, insufficiency	Diseases of the aortic cusps and ring causing the reverse flow of blood into the left ventricle during diastole due to incomplete closure of the aortic valve
Aortic leakage	Seepage of blood from aorta to the left ventricular chamber during diastole because of improper closure of the prosthetic aortic valve
Aortic valve	A valve (composed of three cusps of equal size attached symmetrically around the circumference) between left ventricle and aorta
Arteries	Vessels carrying blood from the left or the right ventricles to the tissues
Blood	A suspension of red cells (erythrocytes), white cells (leucocytes) and the platelets (thrombocytes) in the fluid plasma, the average

	number of each per mm^3 of blood being about 5×10^6, 10^4, and 3×10^5, respectively
Capillaries	The finest blood vessels, normally about 5-6 μm. in diameter, and about 0.5 mm. long in the systemic circulation
Cardiac Index	The cardiac output as determined by the product of the heart rate and stroke volume, L^3T^{-1}
Cavitation	The formation of cavities filled with vapour or gas within a moving liquid due to local pressure being reduced to below the vapour pressure for the liquid
Clotting	Occurrence of certain irreversible chemical and mechanical reactions leading to coagulation of blood
Diastole	The normal rhythmical dialation of the heart during which the chambers are filling with blood (the resting phase of the cardiac cycle)

Ejection Time	Duration of the ejection phase which lasts about 0.25 sec.; approximately two thirds of the ventricular stroke volume is pumped into the great vessels during the first half of this period
Electrocardiogram	A record of the electrical activity of the heart, normally obtained with electrodes on skin
Haematocrit	The relative volume of the cell in blood, normally about 45%
Heart	The mammalian heart consists of four chambers, right and left atria, right and left ventricles. The atria are thin walled chambers into which blood flows at low pressure from the veins. Between atria and ventricles are the tricuspid (right) and mitral (left) valves. Blood at high pressure leaves the ventricles by the pulmonary artery (right) and aorta (left); there are valves at the origin of each of these. The

	blood supply to the heart itself comes from the coronary arteries which spring from the aorta at its origin. Normally both atria beat together a short time before the synchronous beat of the ventricles
Hemolysis	The breaking down of the red blood cells with liberation of hemoglobin
In Vitro	Within an artificial environment, as a test tube
In Vivo	Within a living organism
Lesion	An injury or other change in an organ or tissue of the body tending to result in impairment or loss of function
Ligature	A thread or wire used to tie up a blood vessel
Low Output Syndrome	Heart condition, with features of simultaneous failure of ventricles, resulting in a low cardiac output

Mean Systolic Ejection Rate	The amount of blood ejected per second per square meter of body surface area
Morbid Complications	Impending failure caused by diseased condition
Regurgitation	A backward flow of blood due to imperfect closure of a heart valve
Scar	A mark left on the skin or other tissue after a wound
Stenosis	A narrowing of a blood vessel or of a valve
Systole	The normal rhythmical contration of the heart during which the ventricles are ejecting the blood
Suture Ring	A ring used for sewing or joining together a severed vein
Thrombosis	Coagulation of the blood in the heart or a blood vessel forming a clot
Thromboembolism	The blocking of a blood vessel by an embalus (blood clot) that has

	broken away from a thrombus at its site of formation
Thrombus	Fibrinous clot attached at the site of thrombosis

This thesis is dedicated to the memory of the late Professor Zeëv Rotem .

1. INTRODUCTION

1.1 Preliminary Remarks

The topic of the present thesis is the investigation of the performance of artificial aortic valve implants. A few historical remarks about the origin of these artificial non-organic devices would be in order here.

Between 1944 and 1952 the first extensive experimental studies concerning permanent replacement of diseased natural valves were undertaken[1-3]. The repair of damaged valves in situ had, of course, been carried out for many years, but in some cases the complete valve replacement seemed the only way to restore proper function.

The first clinical correction of aortic insufficiency was performed in 1952, employing a ball type valve prosthesis[4]. The plastic valve, evolved following the success of the permanent intubation of the aorta, is essentially a modification of the tube. Primarily it consists of an inlet, a chamber containing a ball, and an outlet. The entire valve, made of polyethylene, is molded into a single piece to provide extremely smooth and seamless inner surface. The hollow ball with no outside seam is normally made of methyl methacrylate with the specific gravity slightly less than one. At each end of the valve, there is a groove on the outer surface to hold the aorta by means of a fixation ring

of solid semiflexible nylon. The outside surface of the fixation ring is grooved so as to maintain in position the heavy braided silk ligature. The arrangement is schematically shown in Figure 1-1a(i).

It was well recognized at that time that complete control of aortic leakage was not possible because of technical difficulties involved in reaching the aortic root, but this introduced a new concept of surgical treatment of a lesion for which previously complete correction had been impossible. The successful demonstration that such a prosthesis could function satisfactorily for prolonged periods of time stimulated other efforts to develop prostheses which could be placed in the normal valvular position and be useful in correction of both aortic stenosis and insufficiency[5-7]. These efforts took three major directions:

(i) The development of trileaflet flexible valves or individual Teflon cusp which tend to approach quite closely the natural valve configuration[8,9]. Among these prostheses individual cusps, designed by Bahnson, were first applied clinically in 1959[8].

(ii) A modification of the ball valve for the use as an aortic or mitral valve. One of these prostheses in current use is the Starr-Edwards ball valve[10]. It consists of a silicone rubber ball

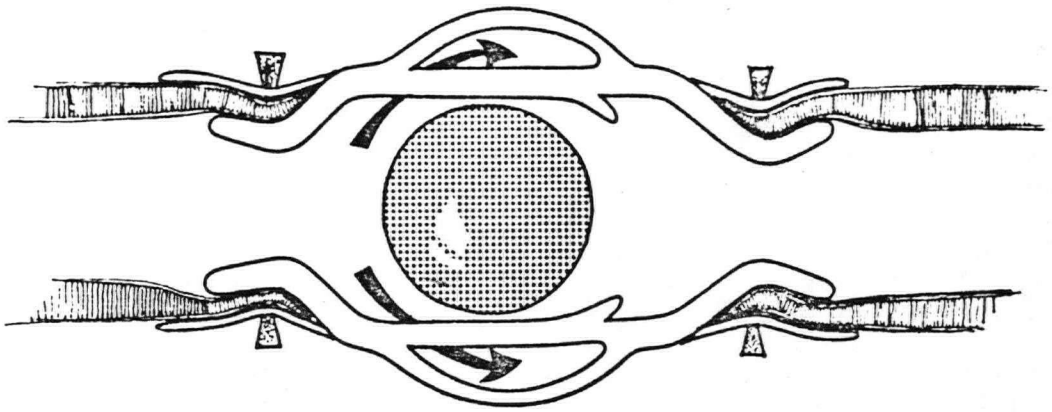

(i)

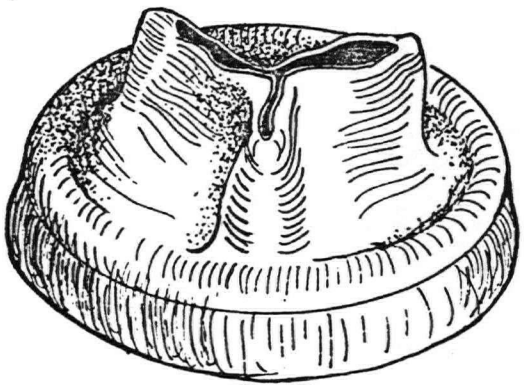

(ii)

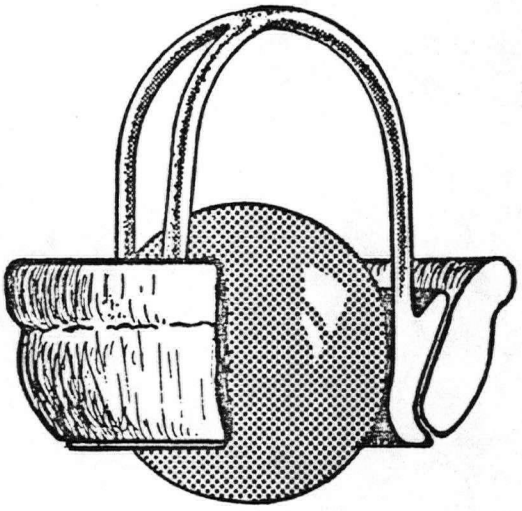

(iii)

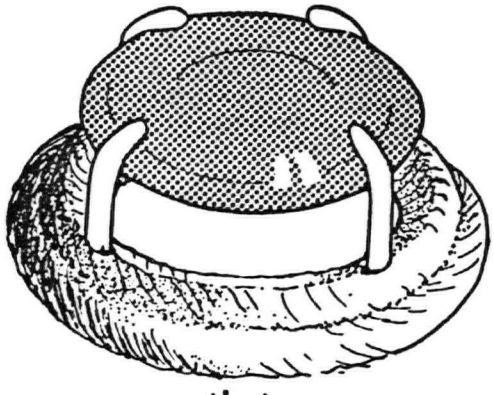

(iv)

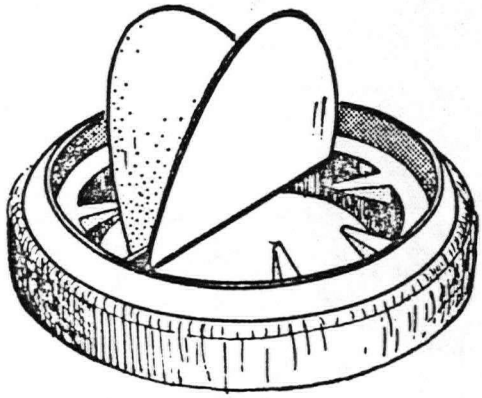

(v)

Figure 1-1 Several models of prosthetic aortic heart valves (a) earlier models: (i) Hufengal ball valve; (ii) Bahnson trileaflet valve; (iii) Starr and Edwards ball valve; (iv) disc valve; (v) Hufengal butterfly hinged leaflet valve

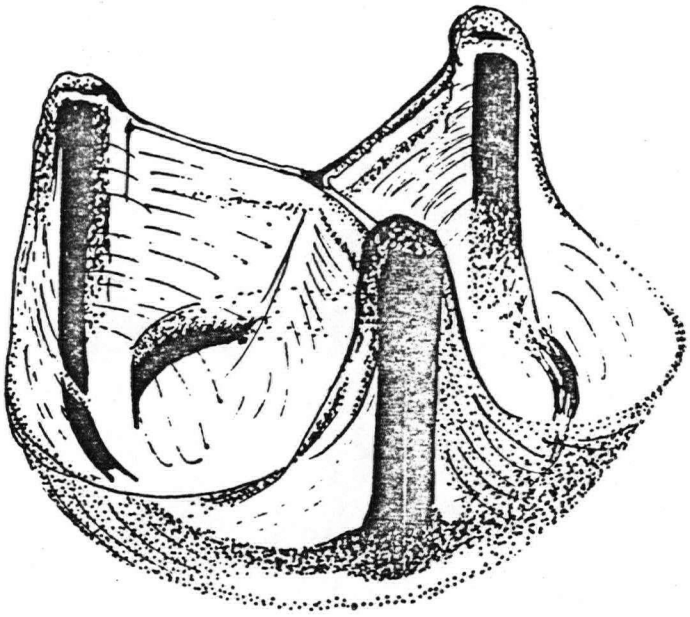

(i)

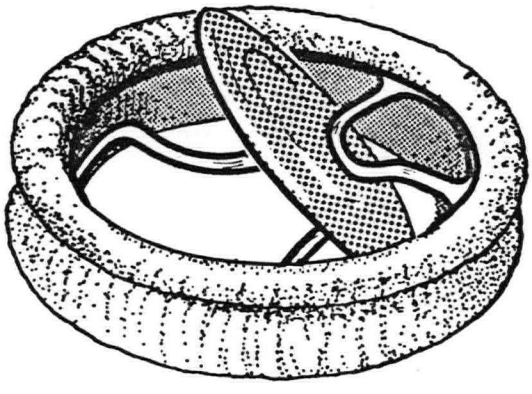

(ii)

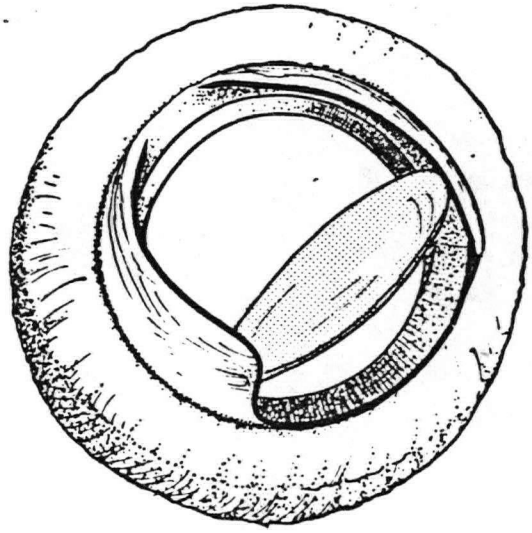

(iii)

Figure 1-1 Several models of prosthetic aortic heart valves (b) some of the newer designs: (i) silastic trileaflet aortic valve; (ii) tilting disc valve; (iii) pivoting disc valve

enclosed in a highly polished cage of Stellite 21. A bloodtight seal is produced by a circular seat at the bottom of the cage. Fixation in clinical implantation is afforded by a tightly knitted short Teflon cloth sleeve which projects upward from the prosthesis.

(iii) The use of hinged disc or other free moving valvular mechanisms[11-13]. The important features of these valves are the low profile housing, a relatively large orifice, and modest stress on sutureline.

Some of these configurations are also sketched in Figure 1-1(a).

Many alternative valve configurations have been devised since the introduction of the ball valve prosthesis. Among the newer designs are silastic trileaflet aortic valve[9], tilting disc valve[12], and pivoting disc valve[14] (Figure 1-1b).

In spite of great achievements with prosthetic heart valves there has been continued interest in improving its performance. The leaflet valve models used frequently in the past are now known to develop, almost invariably, stenosis or incompetence after prolonged use due to scarring with retraction of the surrounding aorta or, on the other hand, incompetence due to fatigue fracture[15-17]. Björk

and associates have also concluded that significant thickening and decreased mobility of the Bahnson Cusps can result from fibrin ingrowth into the Teflon fabric. Recent clinical reports on the performance of the disc valves reveal that none of these valves is free from the complications of thromboembolism, structural failure, infection, and blood destruction[18-22]. On the other hand, the ball valve designs have shown excellent durability and relative freedom from clotting difficulties. But they have been found, quite often in postoperative studies, to produce residual stenosis, varying from mild to severe[23-25].

Requirements of acceptable designs for an artificial replacement would be:

(i) compatibility of material with body fluids;
(ii) negligible tendency to cause either thrombus growth or adjacent tissue damage;
(iii) good hydrodynamic performance and mechanical efficiency maintained over the lifetime of the valve;
(iv) long fatigue life;
(v) ease of installation; and ideally
(vi) low cost.

Obviously, not all of these requirements can be met, hence a compromise is inevitable so as to arrive at an optimum configuration under imposed constraints. One of the designs evolved in this manner is represented by the ball valve.

So far none of the existing ball valves has been entirely successful in operation from all aspects enumerated above, due to, among others, certain inadequacies with respect to the hemodynamic performance (partial stenosis and/or incompetence as mentioned earlier), the morbid complications such as thromboembolism[26-32], left ventricular outflow obstruction when used in mitral position, and "low output syndrome" caused by obstruction to free outflow in patients with wide aortic annulus and narrow ascending aorta[33,34].

Successful operation of artificial heart valves in general and ball type valves in particular depend upon reliable in vitro and in vivo evaluation. Considering that moving parts are characteristic of practically all designs, the demand on prosthetic materials used are considerable. Therefore it is imperative to simulate the operating condition of prosthetic valves in order to establish whether a particular combination of design, fabric, and implantation is adequate, and compatible with requirements.

In testing prosthetic valves, in vitro studies should logically precede in vivo testing. The disadvantage of choosing the reverse sequence is underlined by reflecting upon the very large number of design parameters which have to be evaluated: available prosthetic materials; the variety of mechanical valve designs; various methods of fabrication and installation. The number of parameters

is such that the evaluation of each one of them by in vivo testing is impossible, more particularly so as not all of these are independent of one another. Lastly, even if in vivo studies were carried out using theoretically satisfactory valves, with the heart rate of common laboratory animals similar to that of the human rate, the time for complete evaluation would be excessively long. This would mean that only a day-by-day comparison of the valve and its components could be made. In other words, it would take five year tests after implantation to satisfy oneself that a particular valve would be satisfactory in humans over the same period.

Two main objects should be achieved in preliminary testing. The first concerns the mechanical strength of the valve and therefore its ability to withstand for many years unsteady pressures similar to those that it would experience in the human body. The second problem is to determine whether the flow characteristics of the prosthetic valve are suitable for clinical use. Many pulse duplicator and fatigue machines have been designed mainly to answer the first question; however, little attention has been paid to the latter aspect[35-38].

Experience with prosthetic heart valves has shown that a basic knowledge of pulsatile flow through the valve is necessary if both clotting and hemolysis are to be eliminated. Theoretical approaches to this problem are

limited because of the complex geometries and the time dependent character of the non-Newtonian fluid involved[39]. Current studies of idealized laminar and turbulent flows in elastic tubes are not directly applicable to flow in aortic and mitral valvular areas[40,41]. Consequently, one is forced to resort to experimental techniques for better appreciation of flow characteristics associated with artificial heart valves. Because of difficulties of duplicating the pulsatile pressure and flow conditions present in the heart, quasi-steady tests have been used quite frequently[42-45].

The first successful attempts at visual observation of heart valve movements were those by Smith[46] and Kantrowitz[47] and their associates, but it was McMillan[48,49] who developed post mortem cinematography as a practical technique for studying valve action. Leyse[50], Meisnere[51] and others have investigated the flow pattern associated with heart valves using two dimensional models in birefringent solution of bentonite clay in aqueous-glycerol. Davila[52,53] employed the bentonite clay visualization technique to observe turbulence generated by artificial heart valves, and to evaluate its role in the production of thrombosis. Dye injection[54,55] as well as suspension of aluminum particles in conjunction with slit illumination[56-59] have also been attempted to this end. Surprisingly Davey et al.[56] found no stagnant regions for any

position of the ball and absence of separation (with associated turbulence downstream) for fully open position of the valve.

An alternate approach to the problem and probably a more realistic one, would be to explore hydrodynamic character of prosthetic devices using pulse simulators. The object here is to reproduce pulsatile character of the flow in the aortic region using a positive displacement pump[35], a cam drive mechanism[36], a rotary valve[37], and a reciprocating piston pump between constant head tanks[55], etc. Unfortunately, most of the earlier studies using this procedure are confined only to the pressure measurement across the valve for different flow rates and/or different orifice designs[59,60]. Smeloff and associates[57] compared the flow characteristics for five different prostheses (Roe molded leaflet valve, Gott leaflet valve, Kay-Suzuki discoid valve, Starr-Edwards ball valve, and Smeloff-Cutter ball valve) and concluded the Smeloff-Cutter ball valve to have several favorable features which are helpful in reducing the incidence of thromboembolism. On the other hand, using the results of their investigation with six valves (Gott leaflet, Teardrop discoid, Pin teardrop, Starr-Edwards, Trileaflet, Heavy Teflon, and Hammersmith) Kelvin et al.[61] found (based on orifice size, time of actuation and regurgitation) Starr-Edwards ball valve and Gott hinged leaflet valve to be most suitable for the aortic and mitral position, respectively.

Kaster et al.[62,63] conducted comparative tests on eleven prostheses (Meniscus disc, Smeloff-Cutter ball #2,3, 4,5, Starr-Edwards ball, pivoting disc, Kay-Shiley disc #4,5, Toroidal disc, Gott-Dagget leaflet). Their findings indicate that the ball, pivoting disc, and butterfly leaflet valves generally show good flow volumes with minimal pressure gradients. They also observed that the leaflet valve requires less mechanical energy for activation than the disc or ball valve and allows minimal retrogation of flow during diastole. Finally, it was concluded that the Smeloff-Cutter full flow orifice ball valves have good flow characteristics together with a modest pressure gradient. Wieting and his associates[59] investigated flow characteristics of five different aortic valves (Starr-Edwards 12A, Kay-Shiley disc #5, Benson Roe flexible cusp 27 mm, Gott hinged leaflet 29 mm, and Barnard Poppet LICT A06). All of them were found to have similar aortic, left ventricular, and mean left arterial pressure contours, but none could match that of the human aortic valve. Furthermore, it was observed that the flexible cusp, hinged leaflet and caged disc valves have less regurgitation compared to the ball valve. This, to some extent, contradicts the conclusion of Kelvin et al.[61] mentioned earlier. Several important parameters of the prosthetic valve characteristics such as mean diastolic pressure, incompetence, mechanical movements, and flow disturbances were studied by Wright[64]. He found:

(i) many of the prostheses to produce mild to moderate stenosis;

(ii) only valves with large orifice diameter (22 mm or larger) to be free of significant stenosis;

(iii) disc valves to produce a steep velocity profile near the wall of the ventricle;

(iv) the Starr-Edwards 6120/3M to cause more high frequency turbulence than the other valves.

Vigger[65] has emphasized the importance of pressure drop and associated work load on the heart in any prosthetic valve design. Based on the measured pressure drop, an empirical hydraulic efficiency parameter is suggested to assess effectiveness of an artificial device in relation to that of the natural valve. It is concluded that, despite the wear and variance that has occurred with a relatively few prosthesis ball occluders, the ball valve concept is sound, should be studied further and improved.

Any systematic approach to the problem should include investigation of the behavior of the spherical poppet moving through a fluid. It is only through studies of such a fundamental configuration that one can hope to gain better understanding of rather complex fluid mechanics associated with the prosthetic heart valve.

1.2 A Brief Review of the Relevant Literature on the Flow Past a Sphere

Interest in the behavior of a sphere moving through a fluid goes back many years with the first recorded measurements related to sphere drag attributed to Sir Isaac Newton. Following this and prior to 1930, numerous measurements on the drag of sphere falling through various fluids were made, and a body of information was generated for $10^{-1}<R_n<10^6$. However, these data, which usually show a significant degree of scatter,[66-68 et al.] and hence are approximated by a single line called the "standard" drag curve[69], represent only a rough estimate of the drag coefficient. Ever since, theoretical and practical interest in the subject has resulted in a large volume of literature, and the contributions up to 1960 have been sited by Torobin and Gauvin in their admirable and comprehensive review of the field[70].

In 1963, Heinrich et al.[71] carried out sphere drag measurements in a wind tunnel for $2 \times 10^3 < R_n < 2 \times 10^4$ and $0.078 < M_n < 0.39$. Their data, however, are significantly higher than the standard values. The discrepancy was attributed to the free stream turbulence. Sivier[72] has measured the drag of magnetically supported spheres in a wind tunnel with a free stream turbulence intensity up to 8%. His results are also considerably higher than the standard drag values. Zarin[73] refined the magnetic balance system used by Sivier[72] and varied the free stream turbulent

intensity level. Even at the turbulence level less than 1%, he found, for $R_n > 10^3$, drag to be markedly greater than the standard values. However, for $R_n < 10^3$, the results were in good agreement with the standard values. From this study, Zarin concluded that, in the higher Reynolds number range ($R_n > 10^3$), a small degree of free stream turbulence results in increased drag values.

Ross and Willmarth[74] conducted drag measurements for sphere moving rectilinearly through the glycerine-water mixture for $5 < R_n < 10^5$. Their results agree fairly well with the standard data for $R_n < 2 \times 10^3$ but are somewhat greater for the Reynolds number exceeding this value. The study revealed that the drag on a sphere is not significantly affected by the vortex shedding (5% variation). It was also shown that drag on a sphere accelerated from rest to a constant velocity exceeds the steady state drag by as much as 30% at high R_n, until the final quasi-steady state wake configuration becomes established. Furthermore, they concluded that the 'potential flow apparent mass' concept is valid for the first diameter of motion of a sphere undergoing constant acceleration such that $R_n \simeq 30{,}000$ when sphere has moved one diameter; beyond this point, the drag is reasonably well approximated by the steady state drag corresponding to the instantaneous sphere velocity. Baily and Hiatt[75] carried out sphere drag measurements in a ballistic range for $0.1 < M_n < 6.0$ and $20 < R_n < 10^5$ for

$T_w/T_\infty = 1$ (T_w = temperature at the wall). There is a reasonable agreement between their low speed data and the classical standard drag curve. Based on their own results and other published data they were able to predict the effect of wall temperature on C_d when $T_w/T_\infty \neq 1.0$.

Experimental investigation involving flow visualization and photographing of the wake behind a sphere in the low Reynolds number range of $5 < R_n \simeq 300$ was carried out by Taneda[76] using a water tank. The results showed that the critical R_n at which the permanent "vortex-ring" begins to form in the rear of a sphere is about 24, size of the ring is nearly proportional to the logarithm of the R_n, and the wake behind the ring begins to oscillate for $R_n \simeq 130$. Magarvey and Bishop[77] studied the transition ranges for three dimensional wakes produced by the motion of a drop of an immiscible liquid in the Reynolds number range $0 < R_n < 2500$. They distinguished the observed wakes as steady or periodic with several subclassifications in each of the categories, and concluded (as can be anticipated) that the wake pattern depends entirely on the Reynolds number regardless of the liquid-liquid system employed. Furthermore, it was observed that the general values of the transition Reynolds numbers cannot be obtained as they depend on the drop deformation. However, for all the cases considered the transition in the wake patterns were limited to Reynolds number spread of less than 20. A qualitative interpretation of heat and

mass transfer mechanisms in the wake region of a sphere in low speed flow (R_n < 410) is presented by Lee and Barrow[78] who employ measurements of the velocity field in the wake through flow visualization by dye injection. The observed flow patterns generally confirmed Taneda's results. An important characteristic of the near-wake is the reversed flow, at the velocity much smaller than the free stream velocity, along the axis of the sphere towards the rear stagnation point. The wake transition and Strouhal number for the incompressible wake of various bodies was studied by Goldburg and Florsheim[79]. Based on the experimental results, it was suggested that the transition could be approximately correlated for a range of spheres and cones by a Reynolds number based on the total wake momentum thickness. Furthermore, it was found that for regular vortex shedding the data for spheres and cones could be correlated with Rayleigh-Strouhal formula based on the same criterion.

Measurements of vortex shedding frequency, wake dimensions and static pressure in the wake for a sphere have been reported by Calvert[80]. Based on these data, the Strouhal number has a value of 0.188, with a scatter of ± 0.0008 for $2 \times 10^4 < R_n < 6 \times 10^4$. The results showed the base pressure coefficient to be substantially dependent on R_n with the variation of -0.270 to -0.356 over $R_n = 1.5 \times 10^4 - 6 \times 10^4$. The effect of a trip wire was to shift the origin of the wake, leaving the scale unchanged. Eddy

shedding from a sphere in turbulent free streams was investigated by Mujumdar and Douglas[81]. Test data showed that for 0.5% turbulence and for $5.6 \times 10^3 < R_n < 11.6 \times 10^3$ the Strouhal number for sphere is 0.20, a value typical of circular cylinders in cross-flow in the same Reynolds number range. It was also suggested that in a turbulent flow there is no regular, well defined eddy-shedding.

Theoretical investigation of even a steady viscous incompressible flow past a sphere is very complex. It was first considered by Stokes (1851)[82], and has been discussed by many authors since then. A large portion of these studies have been concerned with the solutions for vanishingly small R_n.

Stokes solved the problem by neglecting the inertia of the fluid. Later, Whitehead[83] tried to improve upon this solution by introducing higher approximations to the flow when the Reynolds number is not negligible. But as is now well known, his solution is not valid in problems of uniform streaming[84]. Oseen[85] solved Whitehead's paradox by assuming that the sphere caused a small perturbation in the uniform parallel flow and neglected second order perturbation velocities, thus taking the inertia terms into account to a limited extent. Oseen's solution for linearized equation has been improved by Goldstein[86], Tomotika et al.[87], and Pearcey et al.[88] However, as can be anticipated, linearization renders these analysis inadequate for $R_n > 2$.

Of considerable interest are two independent solutions: one by Kawaguti[89] who satisfied an integrated form of the Navier-Stokes equation for first and second-order terms when expanded by Legendre Polynomials and the other by Proudman and Pearson[84] who linearized the Navier-Stokes equation by two approximations, one valid at a distance from the sphere, and the other valid near the surface of the sphere. Kawaguti[90] has also developed an alternative procedure to solve the Navier-Stokes equation using the finite difference method. Unfortunately, the technique, valid for flow around spheres up to $R_n = 20$, proves to be extremely laborious. Fox et al.[91,92] and Allen et al.[93] have partially alleviated this difficulty by transferring the technique into the relaxation procedures. On the other hand, Jenson[94] applied the relaxation method directly to the governing equations for vorticity and stream function in modified spherical coordinates to obtain solutions for flow around spheres at $R_n = 5, 10, 20, 40$. Hamielec et al.[95-97] have also used a similar method, but with finer grid size to obtain numerical solutions of the Navier-Stokes equations for slow viscous flow around spheres. Fourier expansions for the flow variables were used to solve the problem over a wide range of the Reynolds number by Dennis and Walker[98]. Rimon and Cheng[99] derived steady state solutions for $1 < R_n < 1000$ by impulsively starting a sphere from rest with uniform velocity and used a time

dependent integration to carry the solution to the steady state. More recently, Dennis and Walker[100] have presented a series truncation method, first proposed by Van Dyke[101], employing a family of Legendre functions to solve the Navier-Stokes equations for flow around spheres in the Reynolds number range of 1-40.

1.3 Purpose and Scope of the Investigation

The development of artificial heart valves depends upon reliable knowledge of the hemodynamic performance and physiology of the human cardiovascular system, in addition to a fair understanding of the associated fluid mechanics. It is evident from the literature survey that in spite of extensive tests (in vitro as well as in vivo) of the aortic ball valves, critical information bearing on valve performance is quite unavailable. Pressure distribution on the surface of the ball, exact location of separation points, regions of stagnant flow, and the intensity of turbulence generated by the ball: all these have not received proper attention. The present thesis aims at taking a modest step in exploring some of these fundamental parameters.

In the beginning, design, construction and calibration of a glycerol tunnel is presented. This is followed by a brief description of the pump drive system, hot film

anemometry, pressure transducing set-up, aortic heart valve model, and pulsating drive mechanism.

Next, the test procedures adopted in measuring:

(i) velocity profiles in the test length of the tunnel;

(ii) mean pressure distribution on stationary spheres and oscillating poppet;

(iii) mean pressure on a stationary and oscillating spherical poppet located inside the valve

are described in some detail, results presented and discussed. Related information from literature is also included where appropriate for comparison and to help establish trends. The results are given for both the cases — valve bypass closed as well as open — the latter condition representative of regurgitation.

Finally, an extensive programme of flow visualization using dye injection technique in conjunction with still and 16 mm movie photography is introduced. The objective is to obtain qualitative visual substantiation of the conclusions based on measured parameters.

Figure 1-2 schematically summarizes the proposed plan of study.

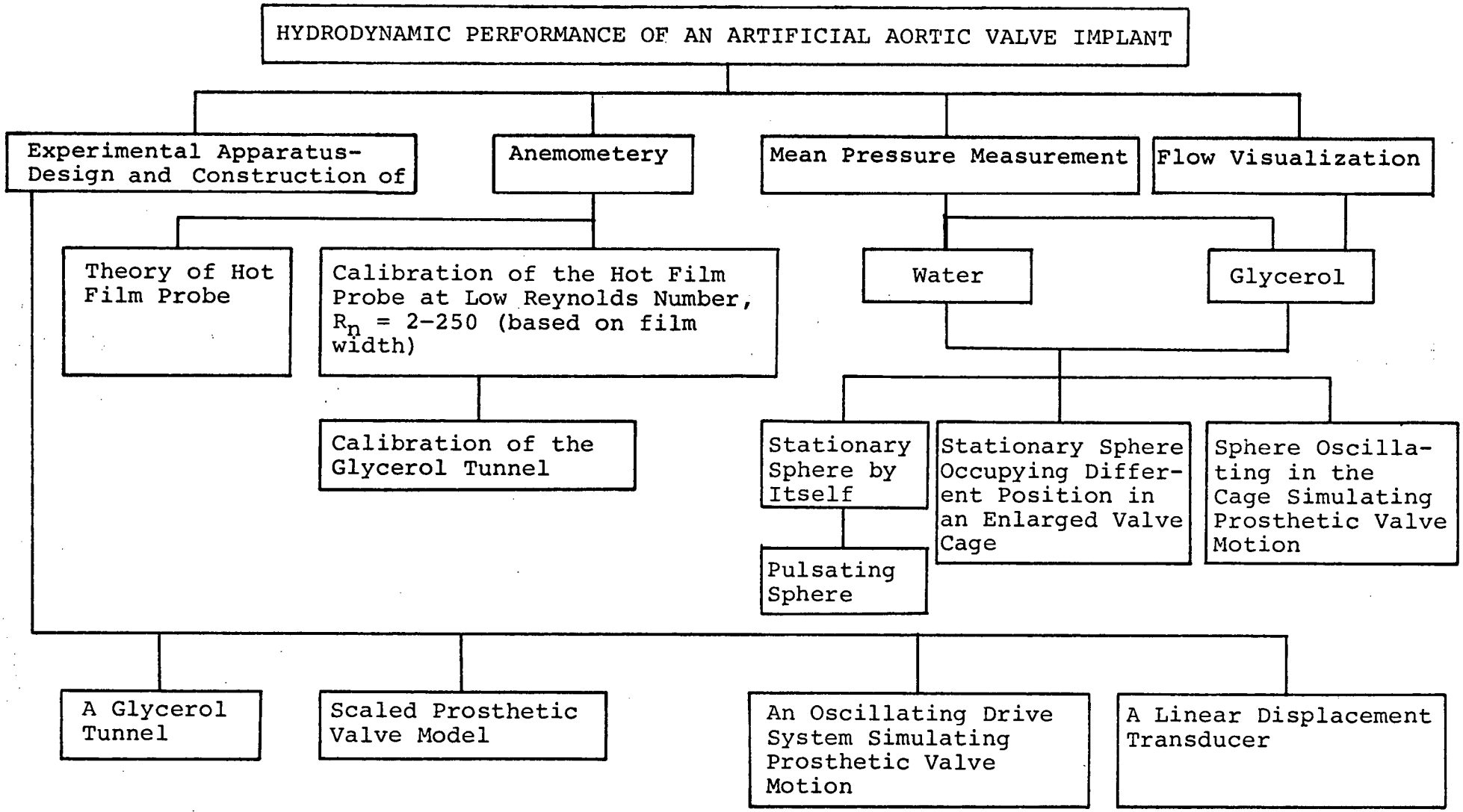

Figure 1-2 A schematic diagram of the plan of study

2. EXPERIMENTAL APPARATUS AND CALIBRATION

This chapter attempts to introduce the test facility used in the experimental program. Some of the instrumentation constitutes the standard equipment in any well equipped fluid mechanics laboratory and hence needs no elaboration. On the other hand, design and constructional details involved in the development of specific equipments are often numerous and hence, though important and relevant, cannot be covered in their entirety. One is therefore, forced to confine attention to more salient features. Undoubtedly, the most demanding equipment in terms of time and effort was the glycerol tunnel, which is described first. This is followed by brief descriptions of hot film anemometry, model design, pulsating mechanism, pressure and displacement transducer, etc. Wherever appropriate, calibration procedures are explained and corresponding charts included.

2.1 Glycerol Tunnel

The fundamental facility for the test program is the glycerol tunnel designed and fabricated entirely in the department. The main criterion governing the design was the Reynolds number, which for the anticipated model size,

was around 400-3000 based on the spherical poppet diameter and average flow velocity. The choice of concentration of the working fluid provided a degree of flexibility, but only to a certain extent as governed by the characteristics of the power unit. The tunnel is shown schematically in Figure 2-1.

Primarily it consists of three subassemblies: the test section; the fluid return system; and the power unit consisting of a pump and a drive motor.

The test section is built of four plexiglas walls 8 ft. long, 0.750 in. thick and wide enough to produce an inside cross-section of 8 x 8 in. The long length was purposely chosen to ensure sufficient room for the installation of flow distributing and straightening devices, and to leave a relatively large region for model positioning. A vent, 4 in. in diameter and one foot high, located on the downstream end of the "box" (5 in. from the outlet end) provided for fluid expansion as well as an escape route for the air bubbles. It also serves as an effective check against the overpressurization of the test section, particularly, near the model location, irrespective of the pump's operating condition. There are three accesses to the inside of the section, through each end and via a porthole at the top of the "box". The porthole, 5 in. in diameter, is judiciously, located 33 in. from the entrance to admit an arm to reach, position and adjust models. During operation

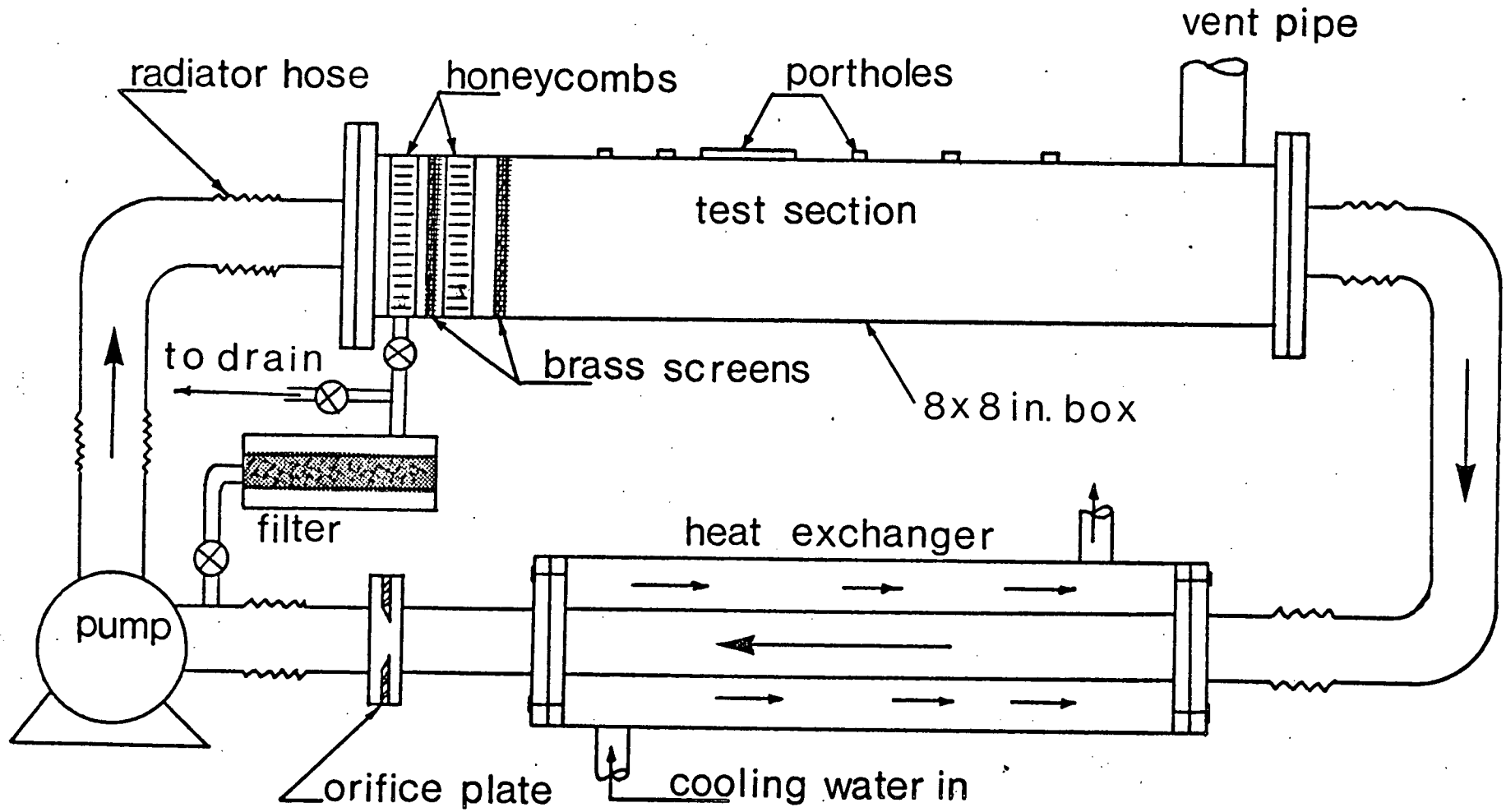

Figure 2-1 A schematic diagram of the glycerol tunnel

the porthole is sealed watertight employing an "O"-ring. In addition, several smaller portholes which could take 5/8 in. N-C plugs were drilled and tapped on the top of the plastic "box". These openings were used to mount models, take out pressure conducting lines and to support a hot film probe in the test section. When not in use they were sealed off employing the plugs with "O"-rings. Two glass plates, 25 x 5 1/2 x 1/2 in., recess-mounted in the sides of the test section provided optically flat, homogeneous and thermally stable walls for inspection and photography. A drain positioned at the bottom of the "box" facilitated complete draining and flush cleaning of the tunnel.

Of critical importance, from velocity profile consideration, was the transition of the flow from the pump outlet (3 in. diameter) to the 8 x 8 in. "box". The jet like flow has to be diffused and spread evenly across the test cross-section. To achieve this the following arrangements were used:

(i) deflection annular vanes were positioned in the incoming stream to force some of the fluid away from the center of the stream;

(ii) several sections of honeycombs followed the annular vanes to straighten the flow through turbulent exchange and laminar damping;

(iii) brass screens of different pore size with or without fiberglass wool in between.

In view of the available information on velocity distribution at the entrance of the aortic passage[102], it was desirable to obtain uniform velocity profile in the test section. A preliminary calculation of the boundary layer growth on a flat plate indicated adequate region of uniform flow one foot downstream of the honeycomb. Later on, experimental measurements confirmed this observation. An incidental advantage of the test in a uniform flow is, of course, the ease of comparison of data obtained in different tunnels.

Aluminum honeycombs used originally were susceptible to pitting due to electrogalvanic action and fungus growth on its surface. A coating of epoxy resin decelerated the process but failed to solve the problem permanently. Finally plastic honeycomb sections, 6 in. thick, were employed with success. Ethylene Diamine Tetraacetate (EDTA) in small quantity (1:120) helped suppress biological growth.

Located between the end of the plexiglas "box" and the power drive system is the return section essentially comprising of heat exchanger, Poly Vinyl Chloride (PVC) pipes and elbows with connecting flanges and radiator hose. A copper pipe, 10 ft. x 3 in., in conjunction with 8 ft. x 6 in. PVC plastic sewer pipe formed an annular single pass heat exchanger. With the coolant supplied by a water main it was possible to maintain temperature of the working fluid within ±.0.2°C. PVC elbows and sections of the radiator hose provided relatively easy, anti-corrosion and vibration free connections between the test section and heat exchanger.

The power unit consists of a centrifugal pump (Auora type GAPB, 200 gal/min, 25 ft. head, 1750 rpm) driven by a three horsepower variable speed D.C. motor. The pump impeller and housing are of cast brass to guard against possible corrosion. The motor is energized by a three phase grid, the voltage being adjusted through an autotransformer (Variac model 4T11) and rectified by selenium diodes. No further smoothing of the D.C. output was required.

To minimize fluctuation in pump performance, it was desirable to operate on the stable (descending) leg of its characteristics. Unfortunately, performance charts as supplied by the manufacturer are only for water. Hence, test results with oil of different viscosity as obtained by Abdurashitov et al.[103] were used to estimate pump behaviour in glycerol. Later on, when the system was operational, it was possible to evaluate the pump performance with the specific concentration of glycerol used to obtain the desired Reynolds number. This plot is shown in Figure 2-2. It is of interest to recognize that the pump performance remains virtually unaffected by an increase in viscosity as high as 7-10 times that of water. This confirms the test data presented by Abdurashitov et al.[103] as well as the American Hydraulic Institute[104].

To promote damping and isolation of vibrations generated by the pump motor assembly, a concrete foundation of 6 x 2 x 1 ft. was used with the unit mounted on a steel

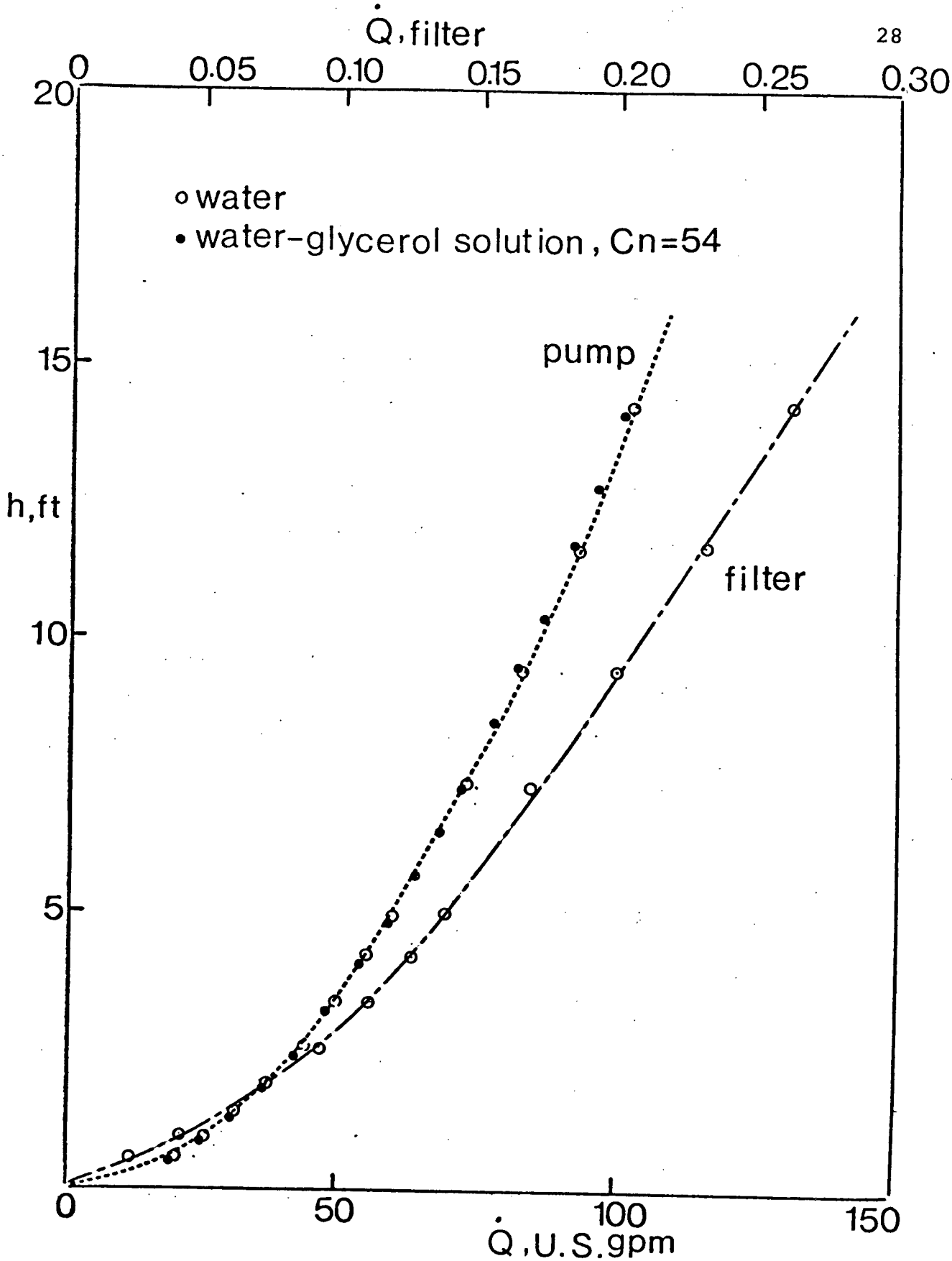

Figure 2-2 Pump characteristic curves for water and glycerol-water solution

channel base and shafts aligned within ±0.002 in. A flexible coupling with a damping insert was used to connect the drive shafts. Radiator hose were used to attach the pump inlet and outlet to the tunnel.

Flow rate in the tunnel was monitored using a sharp edge orifice plate mounted two feet upstream of the pump inlet. The plate location was selected so as to make its reading relatively independent of upstream and downstream disturbances in the form of elbows, change in section at the pump inlet, pump suction, etc. Before final assembly, the orifice plate and associated plumbing were calibrated, under simulated test conditions, by pumping water from a large sump into a weighing tank. For various flow rates, adjusted by means of a gate valve, time taken to collect 1000 lb. of water was recorded along with pressure difference across the orifice plate. For each setting of the valve sufficient time was allowed for the flow to reach the steady state condition In all, ten valve settings were used to give the flow rate variation from 2.5-15.0 cm/sec. For a given setting the procedure was repeated three times and their arithmetic mean was used to obtain the final calibration chart (Figure 2-3).

It was important to minimize dirt contamination of fluid. This was achieved by incorporating a filter (10 μ) in a bypass circuit across the pump. The system filters the entire volume at least once in twenty four hours of operation (Figure 2-2). A photograph of the glycerol tunnel is shown in Figure 2-4.

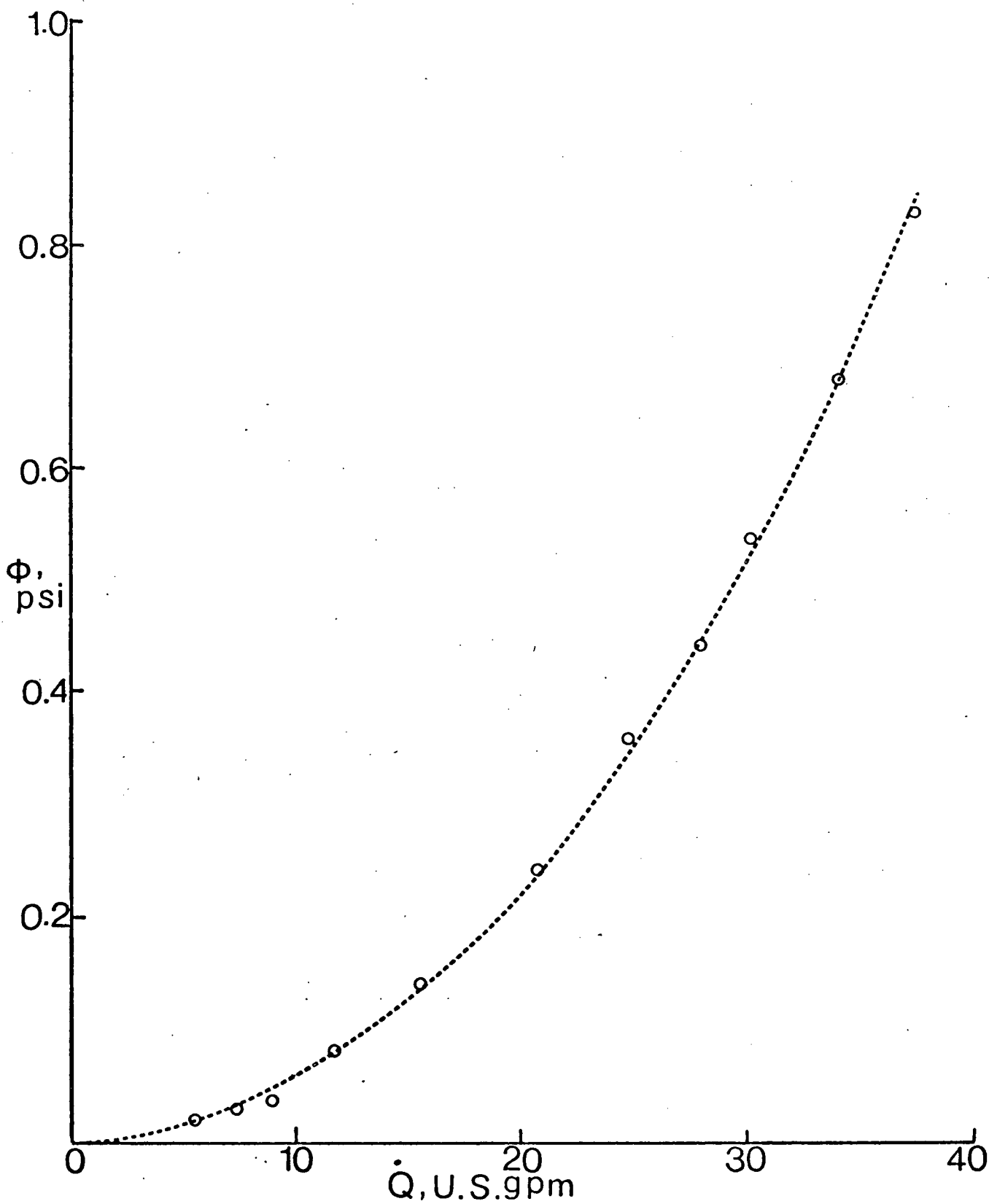

Figure 2-3 The orifice calibration plot

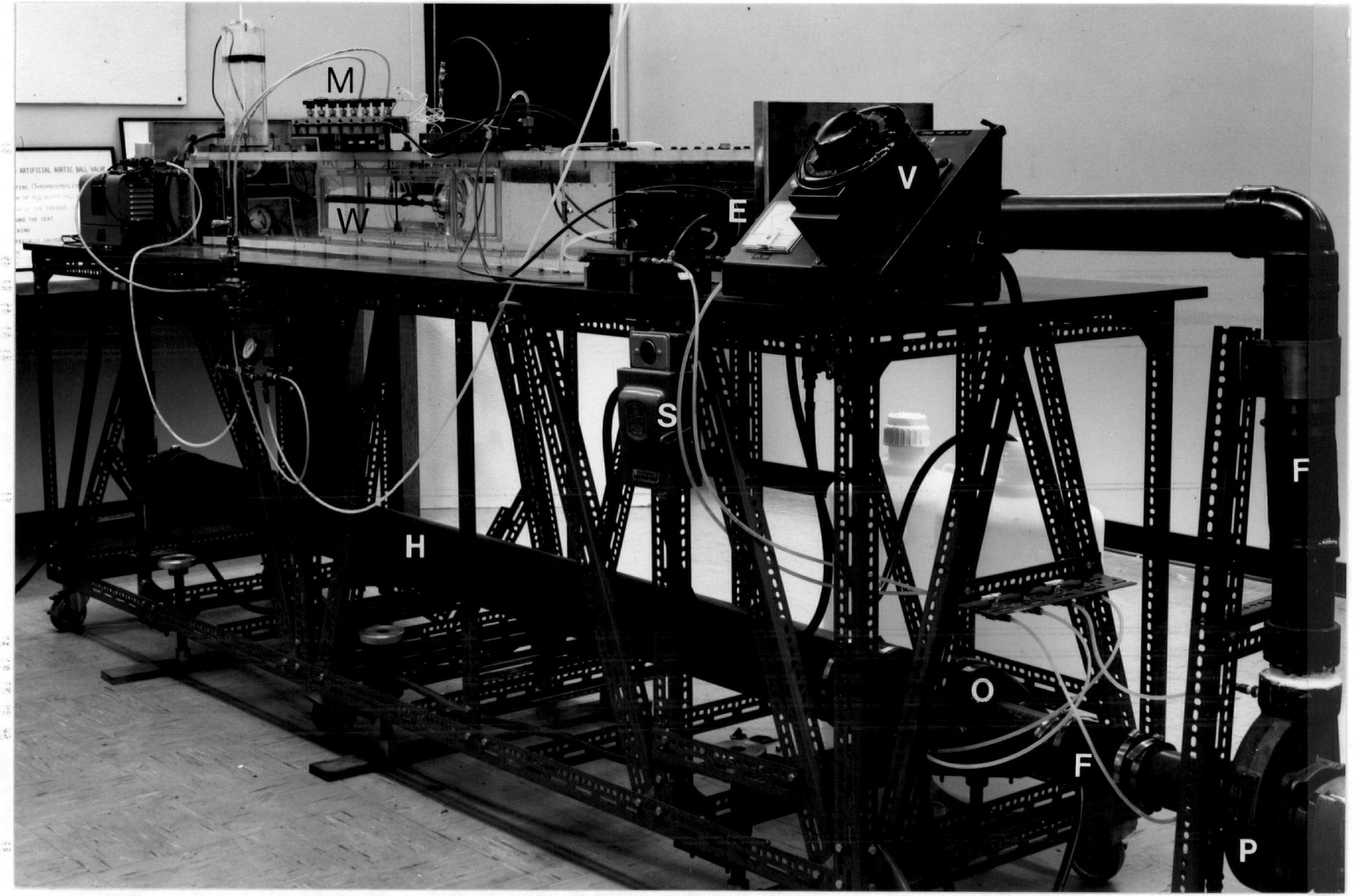

Figure 2-4 A photograph of the glycerol tunnel: E, honeycombs; F, flexible couplings; H, heat exchanger; M, manifold; O, orifice plate; P, pump; S, power switch; V, variac; W, plate-glass window

2.2 Hot Film Anemometry

The next logical step would be to calibrate the glycerol tunnel. In the Reynolds number range of interest this presents several problems and hence requires careful evaluation of the available procedures.

During the course of the experimental work it was required to measure flow velocities of the order 2.5-15 cm/sec. with a fair degree of accuracy, in order to achieve dynamic similarity between the model and the prototype (Appendix I). Measurement of fluid velocities at low values of Reynolds number (R_n) has long been known to be exceptionally difficult. Boundary layer theory is available for sufficiently large R_n; the dynamic head may then be measured, e.g. with a Pitot tube, and as the pressure of the "outer" essentially inviscid flow is impressed upon the boundary (i.e., the outer envelope of the Pitot tube) it can be converted directly to a reading of velocity. Hot film probes in conjunction with the theory of laminar flow forced convection[105] can also yield predictable characteristics (Appendix II). Should R_n be very low (up to 1.5), Stokes' calculation for drag on a spherical body with Oseen's (subsequently Proudman and Pearson's[84]) improvement will enable the interpretation of a pressure read by an impact tube. The results depend, however, on probe shape, and pressures tend to be so low as to be virtually unrecordable. In principle, a theory for hot film probes may also be obtained for this range (e.g. Reference 106 for a spherical surface) but free convective heat transfer from the probe

renders the analytical result of no value[107]. In the range of R_n = 2-150 there is at present no theory available which will relate measured values of the total head, as of the convective heat dissipation, to flow velocities. It is therefore necessary to resort to careful selection and calibration of a probe which could perform successfully in this range.

Apart from laser-doppler anemometer, which was still in the stage of development when calibration of the tunnel was undertaken (1970), a hot film probe appeared to be the only instrument to meet the requirements of high resolution in time and space of flow velocities. Hence a quartz coated wedge shaped platinum film probe (DISA 55A83) was used in conjunction with standard constant temperature anemometric equipment (DISA model 55A01). Despite the existence of a comprehensive literature on measurement in gases, very few papers deal with the use of hot film anemometry for investigation of slow liquid flow. It is mainly because of several difficulties involved in adapting the anemometer to use in water or other liquids:

(i) Electrolysis is by far the worst source of trouble, causing corrosion of the probe, generation of gases and instability in the electronic control circuitry. This particular problem does not arise in non-conducting liquids, such as distilled water or kerosene.

Another way of avoiding serious corrosion could be the use of high frequency alternating current to heat the probe, and/or coating the probe to provide electrical insulation from the liquid.

(ii) Often the formation of bubbles on the sensor causes incorrect and unstable operation of the probe[108]. Bubble formation can be reduced by cleaning the probe in a solvent, e.g. methyl alcohol, with the anemometer in "stand-by" condition, and/or by adding some surface reactants to reduce fluid surface tension, thus preventing the formation of bubbles and their attachment to the sensor. In the case of water a "wetting agent" (Kodak Photo-Flo 200.) can be used.

(iii) Contamination of the probe by dust particles or other deposits reduces and modifies its sensitivity[109]. To eliminate dirt contamination the surface of the liquid should be shielded. Continuous filtration of a part of the circulating fluid should also help in minimizing the problem. Both these methods and frequent cleaning of the probe were found necessary in the present set of experiments.

For the reasons cited above each probe had to be calibrated independently before it was used. There are many ways to calibrate hot film probes[110,111]. The choice of method depends on the availability of a suitable standard of comparison, the ease of measurement, and the desired degree of accuracy. In most cases, the velocity measured by mechanical means at a specific point in the fluid field is compared with the electrical signal of the anemometer. The degree of accuracy then depends mainly on the accuracy with which the reference velocity is known. Two calibration procedures were used mainly to substantiate the methods adopted. In the first case,a probe was mounted on the tool holder of a lathe and towed at controlled speeds in a slotted flume, employing the feed mechanism. The multispeed gear box allows satisfactory determination of the tow velocities. The probe was immersed in the fluid to a depth of at least ten times its diameter. The arrangement worked satisfactorily up to a velocity of about 15.0 cm/sec. beyond which noise caused by spurious vibration substantially affected the signal. Furthermore, at higher velocities the towing time became so short, due to limited length of the flume (5 ft.),that the output signal from the probe could not reach the steady state condition. A photograph of the arrangement is given in Figure 2-5.

In the alternative arrangement the probe was held stationary in a rotating dish, 1 ft. diameter and 10 in. high,

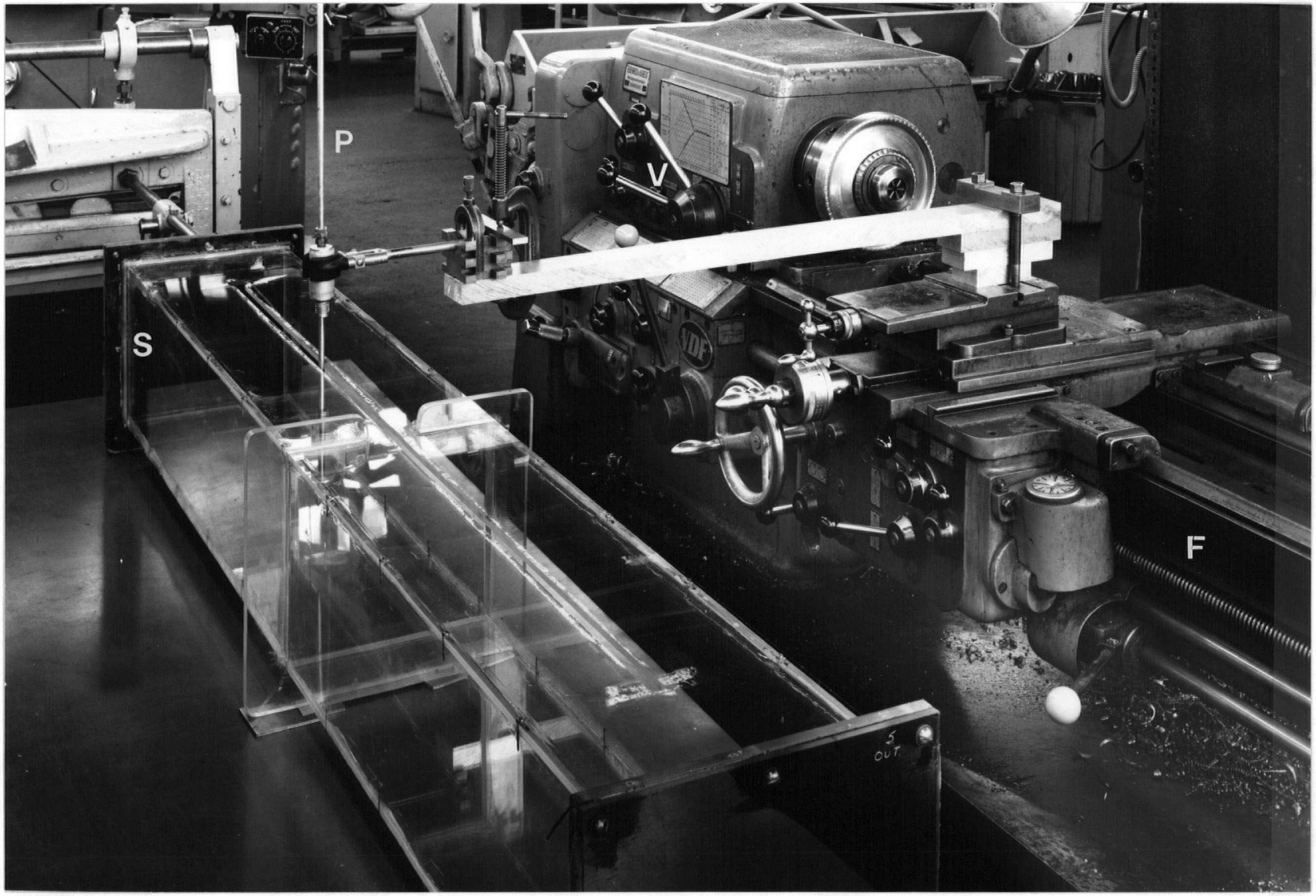

Figure 2-5 A photograph of the probe towing mechanism and associated flume: F, feed worm; P, probe; S, flume; V, speed control gear box

mounted horizontally on a turntable with infinitely variable speed drive (Figure 2-6). This arrangement was found satisfactory over the velocity range of interest. Sufficient time had to be allowed for a quasi steady state of motion to be set-up[112]. The motion obtained was very closely solid body rotation when the probe was not too far from the cylindrical or bottom walls of the dish. The circular dish had to be sufficiently large to allow for the dissipation of vorticity generated by the probe between successive passes; obviously the time constant of this effect is of the order ν/r^2 [113] (r = distance from the probe to the axis of rotation). Absolute cleanliness was found to be essential in these tests. The complete rig was kept in a glass enclosure which greatly reduced the frequency of probe cleaning required.

In general, if properly designed, either of the procedures can be expected to yield reliable results. This was indeed the case with the calibration plots obtained, which correspond precisely. However, the second arrangement, because of its rather limited volume, was anticipated to be more susceptible to temperature variations, and at high speeds to mechanical vibrations. Hence the first procedure was used when a recalibration was desired.

Calibration tests were carried out in tap water, distilled water and water-glycerol solutions of several concentrations (Figure 2-7). As anticipated, the experimental points clustered around a straight line down to quite low

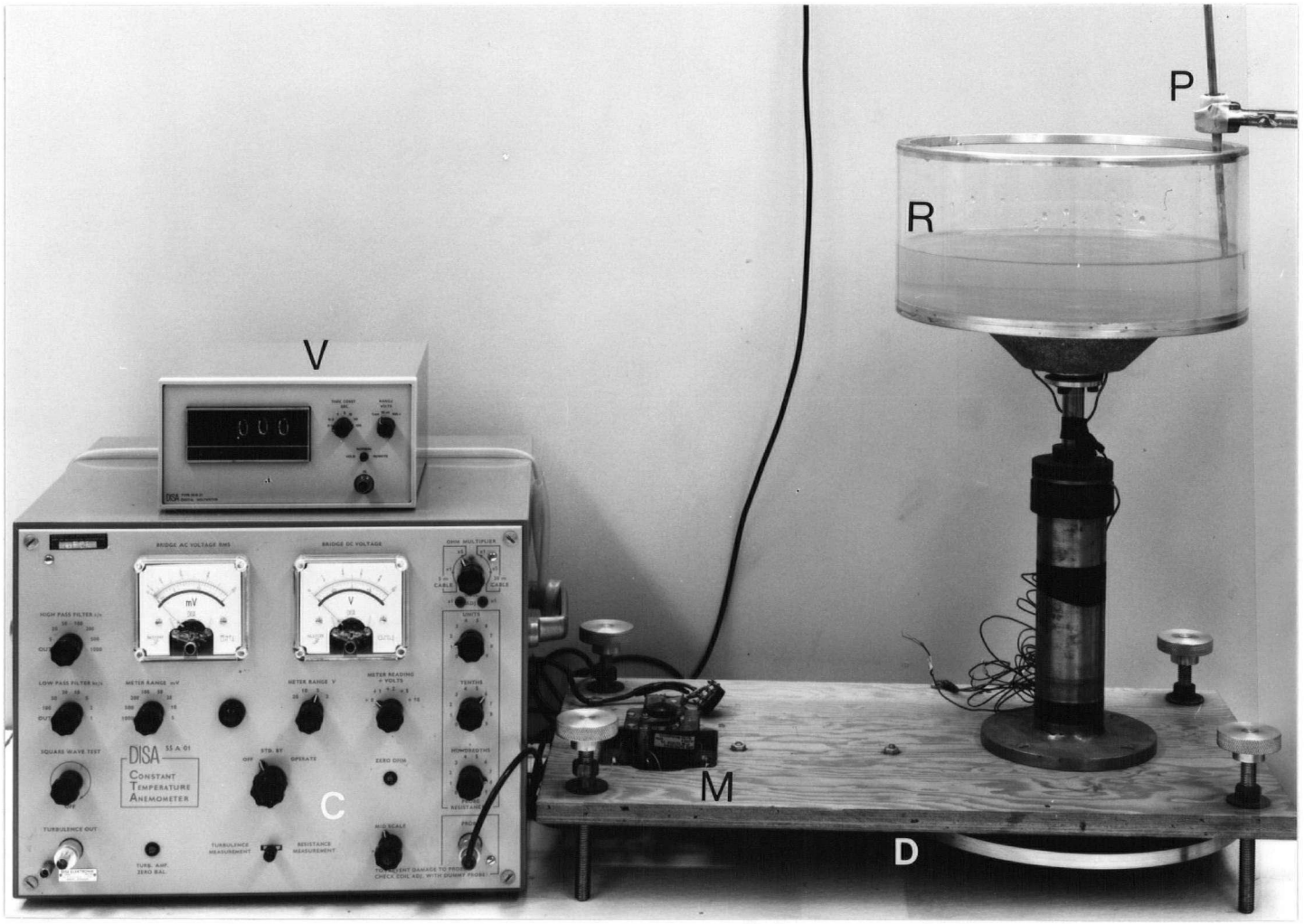

Figure 2-6 A photograph showing the rotating dish arrangement for calibration of hot-film probe: C, constant temperature anemometer; D, drive wheel; M, drive motor; P, probe; R, rotating dish; V, D.C. digital voltmeter

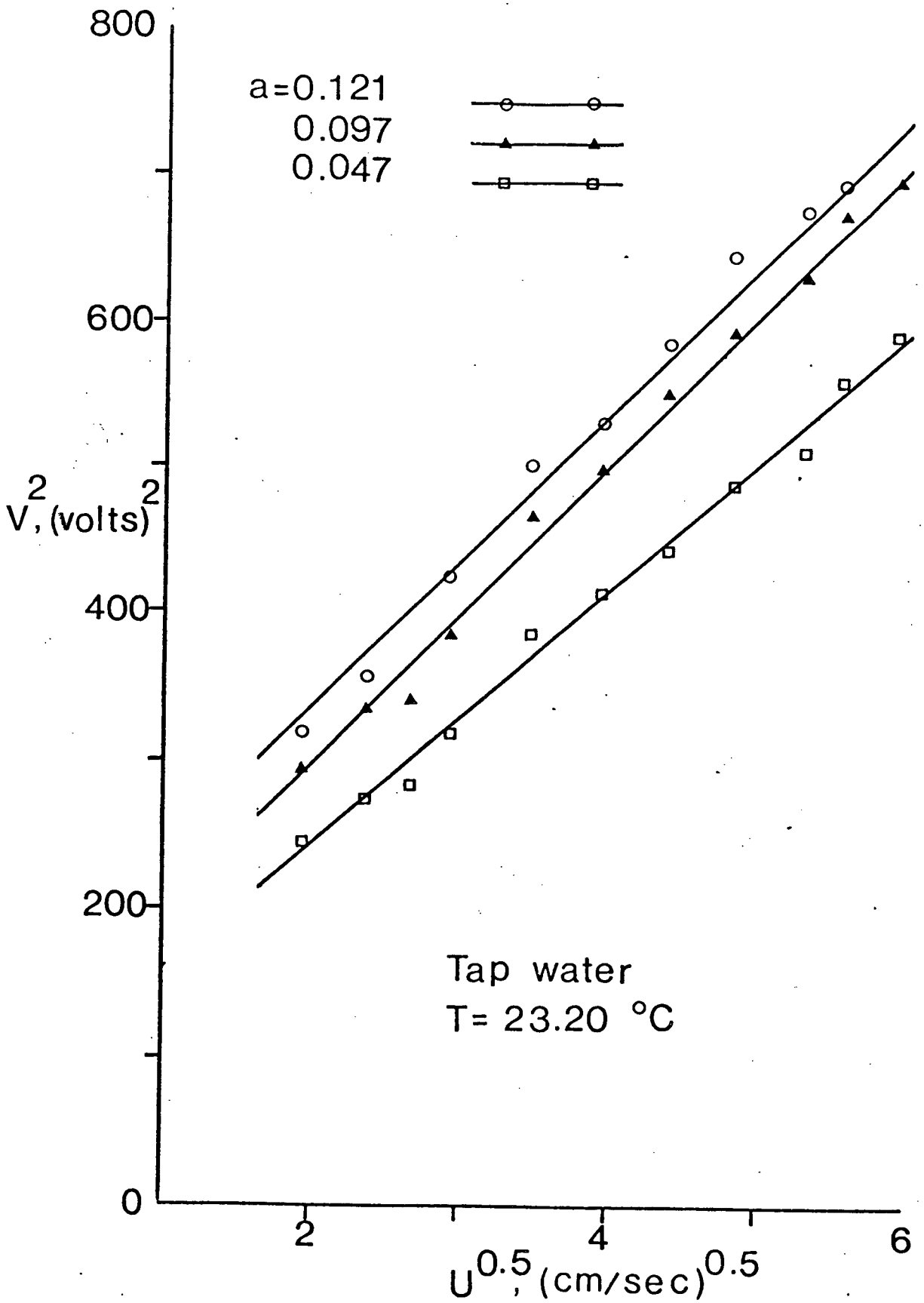

Figure 2-7 Calibration data for the hot film probe in: (a) tap water

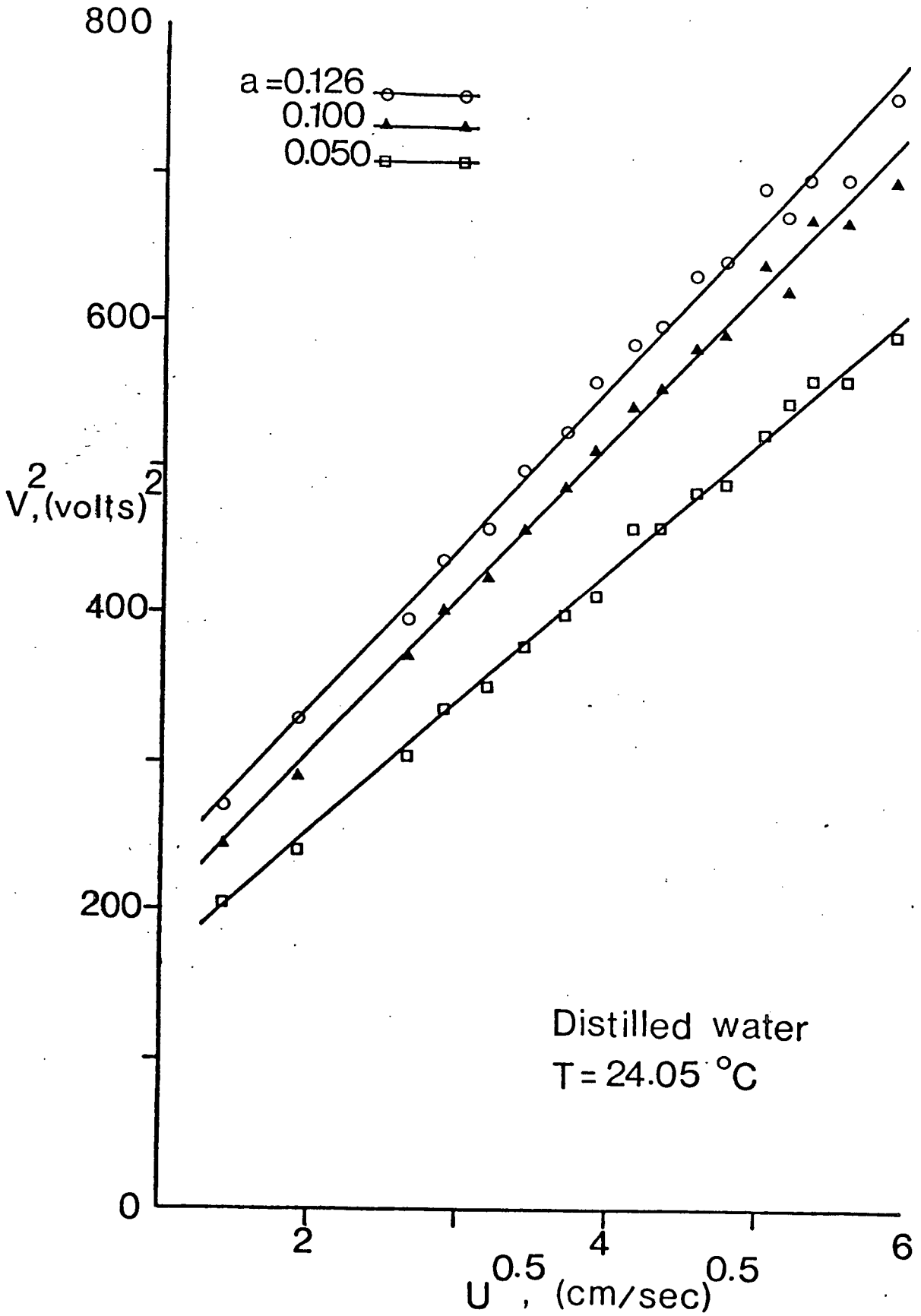

Figure 2-7 Calibration data for the hot film probe in: (b) distilled water

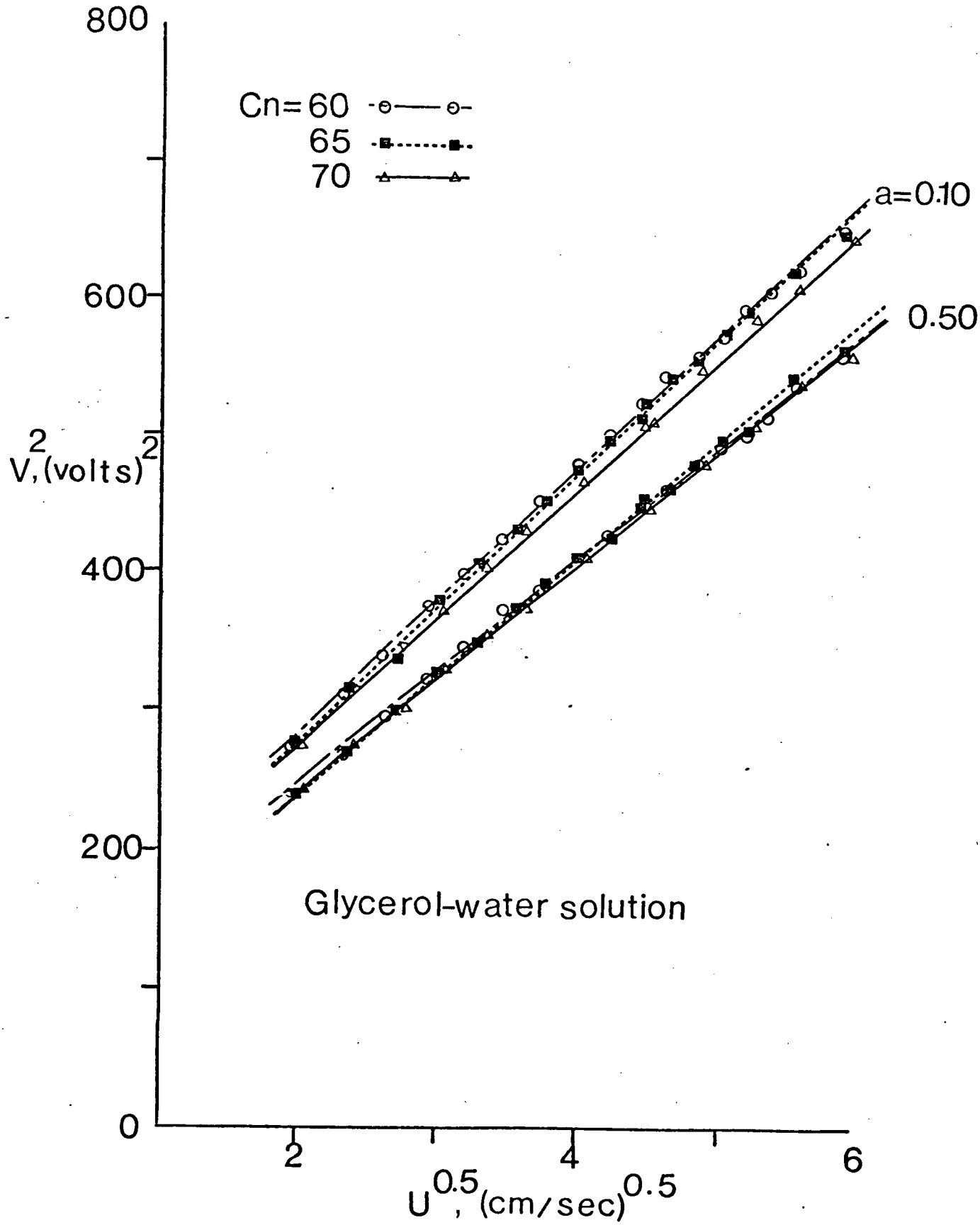

Figure 2-7 Calibration data for the hot film probe in: (c) water-glycerol solutions of various concentrations

values of the true velocity. The indicated straight line is a least mean square fit through the measured data. The maximum percentage deviation from the fit is 8.8% for tap water and the minimum is 0.40% for water-glycerol solution of 60% concentration. The scatter of experimental results is of the order of that which is expected from the ancillary equipment alone. Though the viscosity of glycerol is rather sensitive to changes in temperature, the effect of rates of heating in standard film equipment appears low enough to be negligible.

Since the hot film temperature T_m is kept constant by virtue of the overheat ratio, a change of R_c (probe's cold resistance) during the measurements would imply a change of T_m. It is, therefore, useful to investigate drift in the overheat ratio induced by variations in R_c. This would give some appreciation as to the changes in the ambient temperature that can be tolerated during a given test.

To this end, dependence of probe cold resistance on fluid temperature was measured using a constant temperature bath. Figure 2-8 shows these results for various concentrations of glycerol solution. All the curves have almost the same slope suggesting the constant coefficient of resistivity. In the worst case, the maximum deviation was observed to be about 1.2%. The arrangement was also used to locate the intersection of the velocity calibration curves with axis $V = 0$.

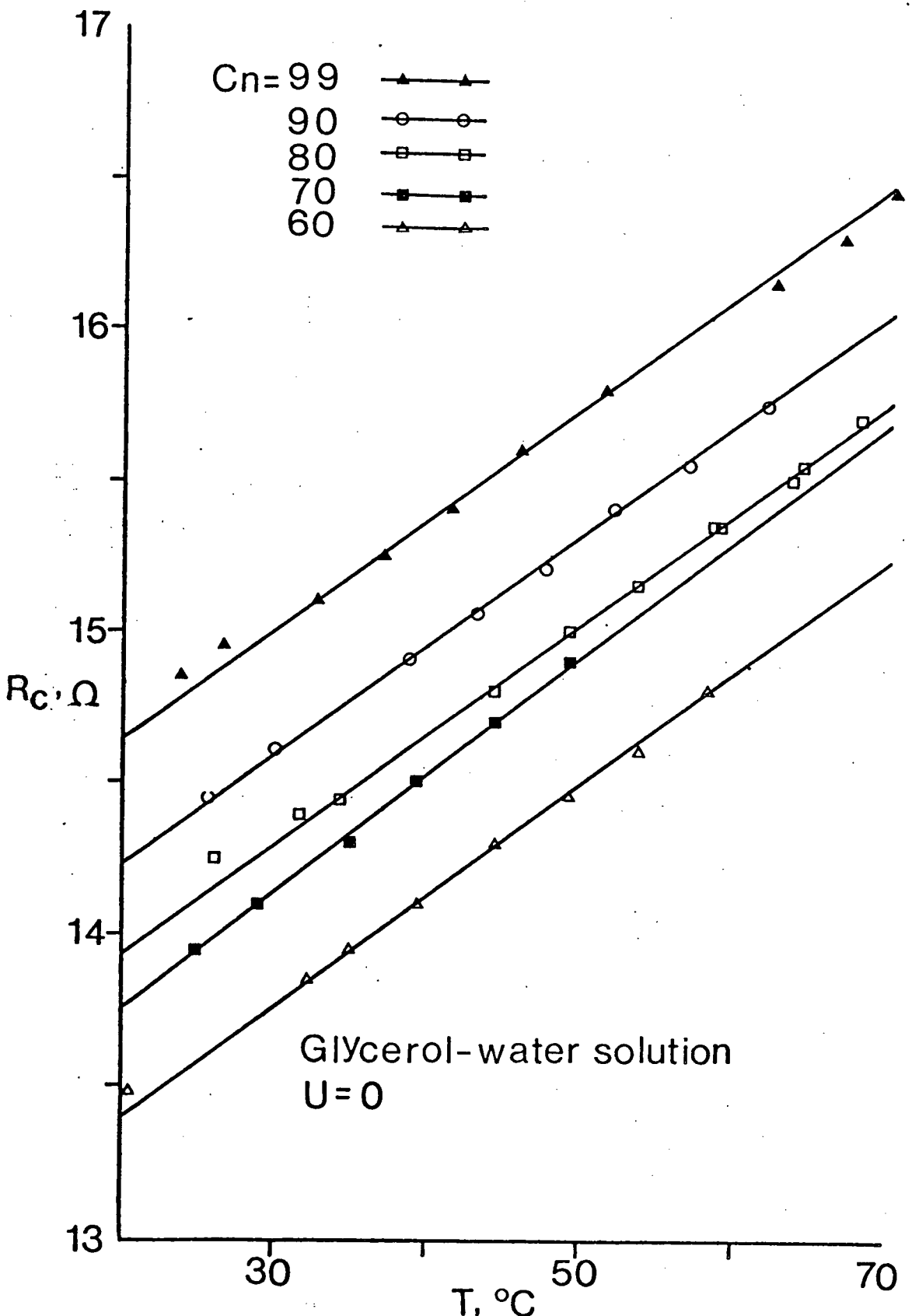

Figure 2-8 Calibration plots showing the effect of temperature on probe's cold resistance when immersed in glycerol-water solution of different concentrations

2.3 Pressure Transducer

The mean pressure component, being extremely small (of the order of 10^{-4}psi), demanded a highly sensitive instrumentation for its measurement. This was accomplished using a "Barocel Modular Pressure Transducing System" developed by Datametric Inc. of Waltham, Massachusetts. The type 550-5 Barocel sensor is designed to operate with fluids over the pressure range of 0-10 psia. The unit is a high precision, stable capacitive voltage divider, the variable element of which is a thin prestressed steel diaphragm positioned between fixed capacitor plates. The diaphragm deflects proportionally to the magnitude of the applied pressure. To isolate the external pressure medium from the sensor diaphragm-capacitance system, the unit uses highly sensitive metallic bellows. The volume between the bellows, isolator and sensor diaphragm is filled with degassed silicone oil which serves both as pressure transmitting fluid and as a dielectric. The pressure signal from the external liquid medium is transmitted by the bellows to the silicone oil which in turn deflects the diaphragm to produce the required change in capacitance. An A.C. carrier voltage at 10 Kc/sec. is applied to the stationary capacitor plates, and a bridge circuit determines an output voltage dependent on the ratio of the capacitance of the diaphragm to each of the stationary plates. The carrier voltage is therefore modulated according to the input pressure. The unit sensitivity is 10^{-5} psi provided the pressure sensor

is fully isolated from external sources of vibration and noise. It was imperative to ensure removal of all traces of air pockets from the pressure ducting for satisfactory operation. Barocel is accurately calibrated for steady pressures. Figure 2-9 presents a schematic diagram of the pressure transducer.

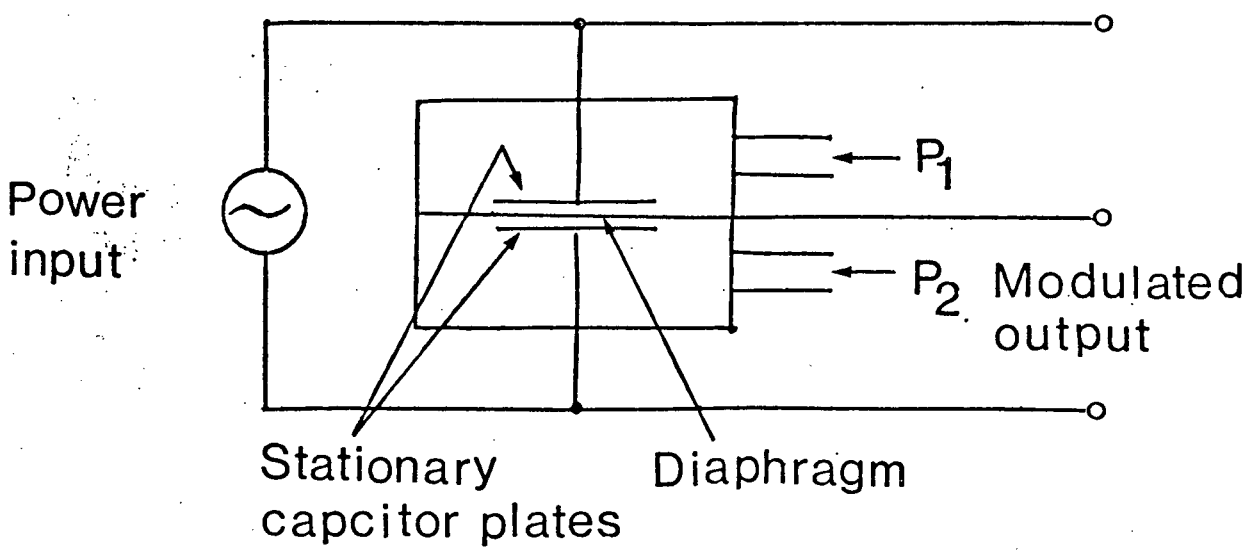

Figure 2-9 Schematic diagram of a Barocel pressure transducer

It was important to minimize the effect of ambient temperature excursions on the Barocel's performance. This was achieved by mounting the transducer on a heat sink, a large aluminum block with working fluid circulating inside. The arrangement virtually eliminated the influence of temperature transients.

2.4 Aortic Heart Valve Model

Aortic replacement ball values presently in use consist of the following parts (Figure 2-10):

(i) a metal cage of a highly polished uncoated casting of Stellite 21, a cobalt alloy noted for high strength and excellent corrosion resistance;

(ii) a spherical ball of silicone rubber with diameter ranging from 0.482 - 0.868 in.;

(iii) a metal seat, normally called orifice, carrying a sewing margin of knitted Teflon cloth.

Unfortunately, the actual aortic valve is far too small for the purpose of pressure measurement on the ball surface and its wake. Furthermore, velocity data upstream and downstream of the ball would be affected because of the flow disturbances produced by the presence of the hot film probe and its stem. Hence it was decided to use an enlarged

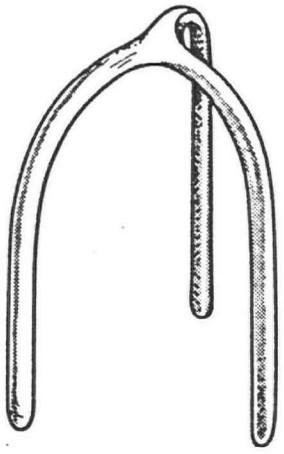

(i) cage

(ii) ball

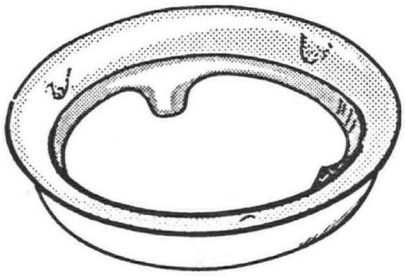

(iii) seat

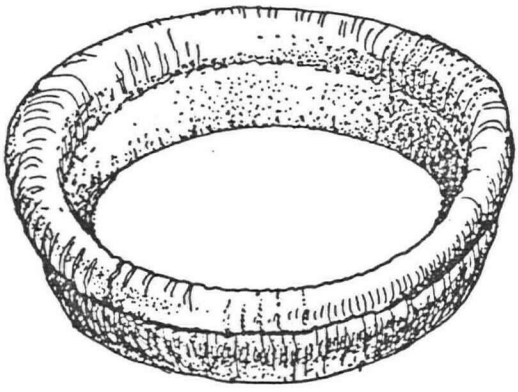

(iv) suture ring

Figure 2-10 Exploded view of the Starr and Edwards aortic ball valve prosthesis: (i) case; (ii) ball; (iii) orifice ring; (iv) suture ring

model of the aortic ball valve for test evaluation. The enlargement ratio was governed by the following factors:

(i) attainability of the dynamic similarity;

(ii) size of the tunnel test section;

(iii) sufficiently large sphere to provide adequate number of pressure ports and room for pressure conducting tubings;

(iv) practical difficulties involved in pulsating the ball.

Above considerations in conjunction with a few compromises led to a 5:1 enlargement of an actual prosthetic valve for experimental investigation. It consists of:

(i) A plexiglas spherical ball of 2.5 in. diameter with fourteen pressure taps drilled radially to accommodate "Intramedic" polyethylene tubing of 0.038 in. O.D., 0.023 in. I.D. and 3 ft. in length. The exact location of the pressure ports are indicated in Figure 2-11.

(ii) A stainless steel tube of 0.375 O.D., 0.325 I.D., and 6 in. long is inserted into the ball, in the plane of pressure taps, by means of a plexiglas plug with 0.750 N.C. threads. The tube acts both as a stem to position the ball centrally with respect to the seat as well as a conduit

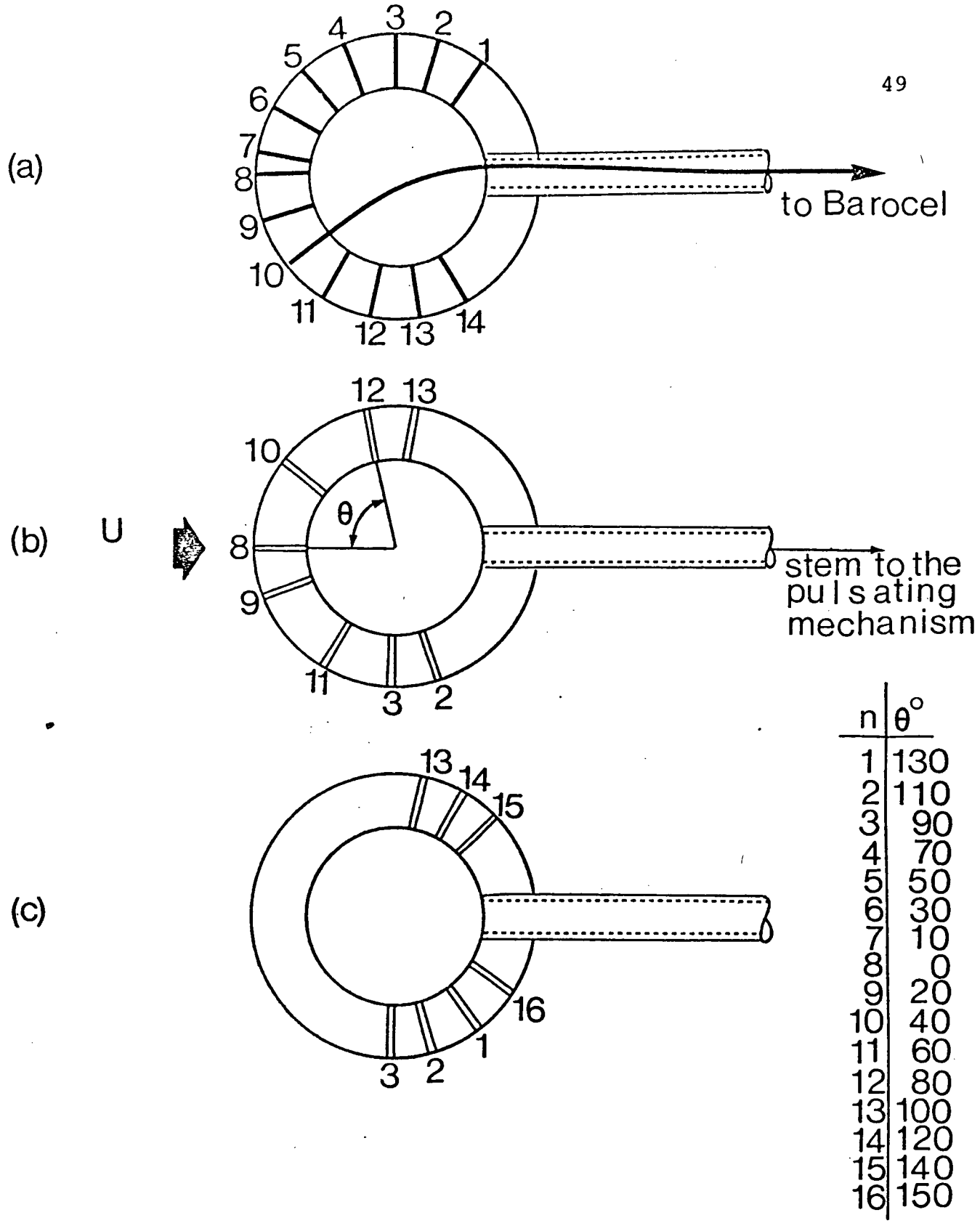

n	θ°
1	130
2	110
3	90
4	70
5	50
6	30
7	10
8	0
9	20
10	40
11	60
12	80
13	100
14	120
15	140
16	150

Figure 2-11 A schematic diagram showing the location of pressure ports on the surface of the poppet:
(a) used in water, θ = 0 - 130°
(b) employed in glycerol-water solution, θ = 0 - 110°
(c) used in glycerol-water solution, θ = 90 - 150°

accommodating polyethylene tubings conveying pressure signals to the externally located transducer.

(iii) A three prong cage, made of 0.184 in. O.D., 0.125 in. I.D. brass tubing, encloses the ball and restricts its movement. A port, 0.061 in. diameter, is drilled in each of the prongs to help estimate pressure variations in the wake of the ball. The cage is fixed to the base ring, acting as a seat, by a bayonet fixture arrangement. The junction of the prongs forming the downstream end of the cage carries a brass bushing which acts as an external support for the stem. The bushing is lined with a Teflon cylinder to reduce friction wear.

(iv) A plexiglas seat, 6 in. O.D., 2.250 in. I.D., 1 in. thick, consisting of three lips spaced circumferentially at 120°, is so machined as to produce watertight fit through matching curvatures when the ball is pressed against it. The arrangement is essential in actual valves to reduce contact stresses through increased impact area;

(v) Two concentric plexiglas cylinders, held in position by means of four rectangular plexiglas ribs, result in an annular space to serve as a

bypass when the valve is shut. This is essential to prevent possible water hammer damage to the tunnel. Connected at the outlet end is a brass fixture which supports a double acting air cylinder, an integral part of the pulsating mechanism described later. Two plexiglas plates, attached to the top and bottom of the outer cylinder by means of two rectangular plexiglas ribs, help mount the model inside the tunnel.

Figure 2-12(a) shows an exploded view of the model with a photograph of the components presented in Figure 2-12(b). The assembled model was slid into position through the outlet end of the test section and was locked in place by a stainless steel pin extending about 0.500 in. in the rib. A porthole (0.500 in. diameter), drilled through the tunnel wall and concentric cylinders facilitated velocity measurements in the wake of the poppet.

2.5 Pulsating Mechanism

Poppet of the prosthetic valve exhibits a rather complex time-displacement history. However, for dynamic similarity between the prototype and the model, it is essential to simulate important characteristics of this motion. The time history used in the program was based on a frame

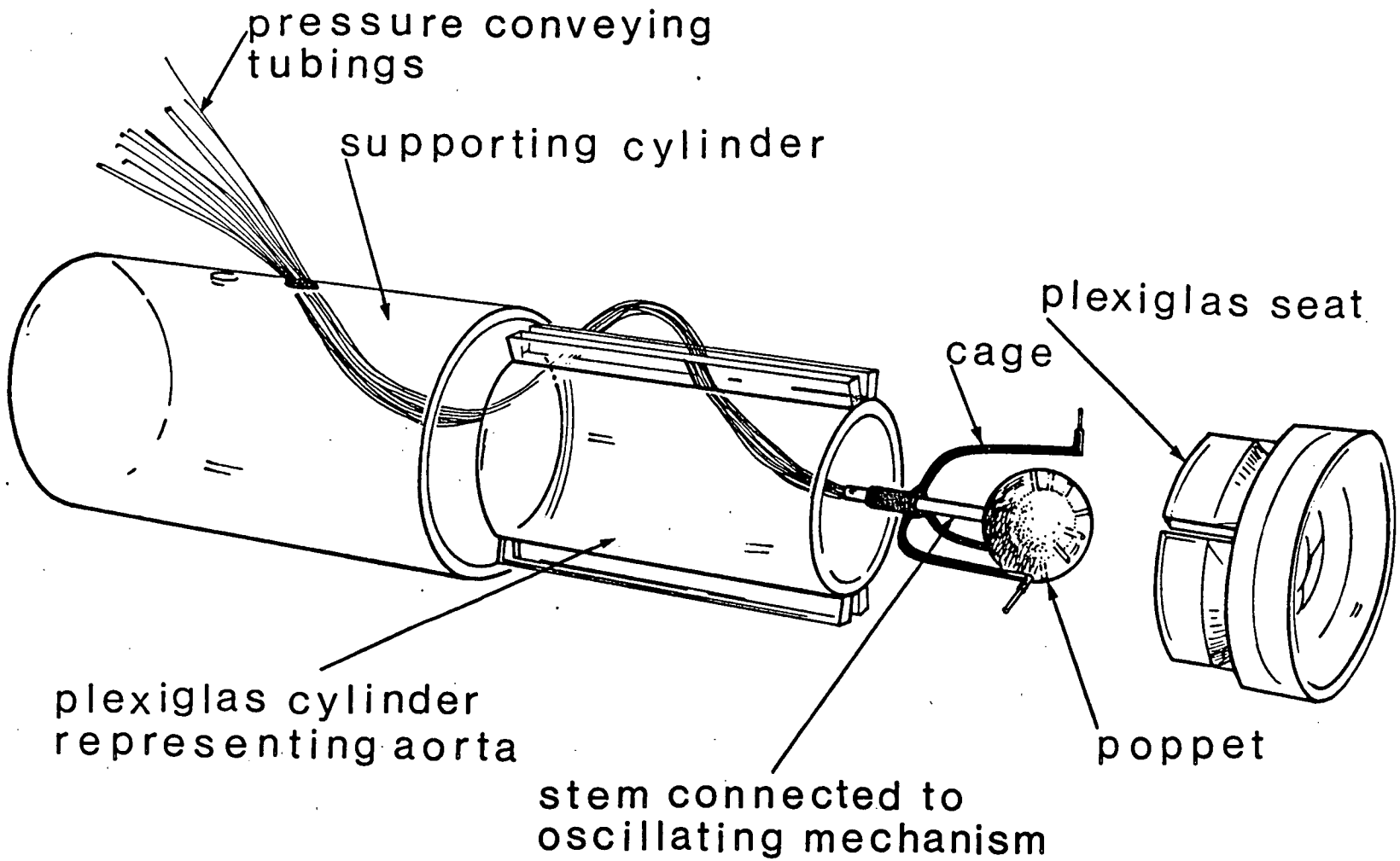

Figure 2-12 An exploded view of the heart valve model: (a) schematic drawing

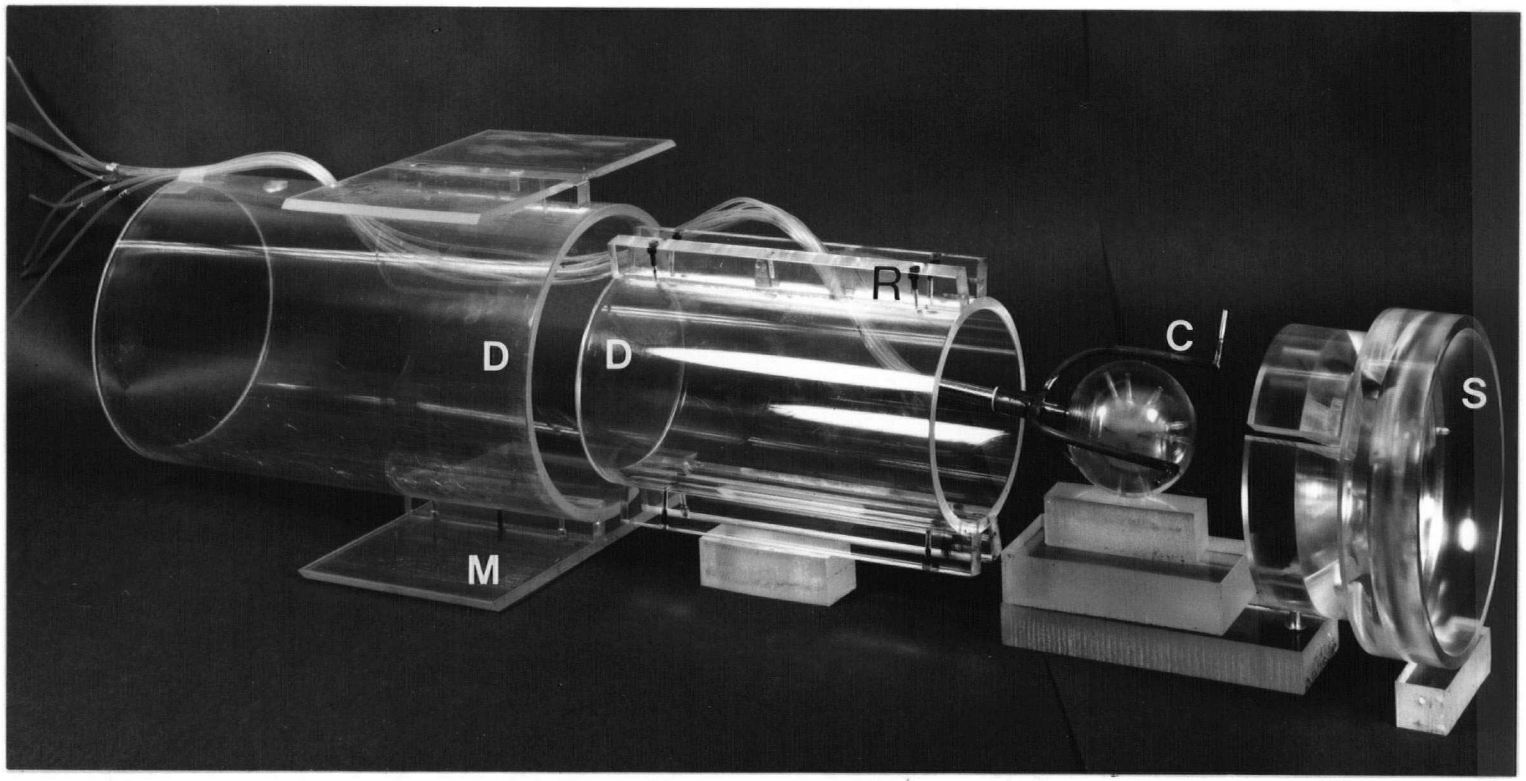

Figure 2-12 An exploded view of the heart valve model: (b) photograph of the components: C, cage; D, concentric circular cylinder; M, mounting plate; R, support ribs; S, orifice seat

by frame analysis of the x-ray movies (taken at Shaughnessy hospital) of patients with prosthetic valve employing special radio opaque poppet. Furthermore, there has been some information on this aspect recorded in literature. As can be expected, the displacement function varied from patient to patient. A typical plot is presented in Figure 2-13. In the test described in details later, a representative plot was selected for simulation.

The desired oscillating motion of the ball is produced by means of a double acting air cylinder (A) in conjunction with an electronic pulse duplicator and a specially designed pneumatic circuit (Figure 2-14). The supply of compressed air, held constant at 80 psig through a needle valve (N), is fed into two pressure regulating valves (R_1,R_2) adjusted to produce outlet pressures of 40 and 5 psig, respectively. The 40 psig air supply, controlled by a solenoid valve (s), is used to drive the pilot of a four way air valve (p). On the other side, the air supply at 5 psig is connected to the intake of the four way valve with its outlets connected to the air cylinder. As the solenoid opens the port, the pilot air activates the four way valve, which in turn causes the ball to move upstream until it rests against the orifice seat. When the solenoid shuts the valve, the ball returns to its original position under the reversed piston actuation. The speed of this fore and aft motion of the ball can be controlled by means of two needle valves (v) placed in line

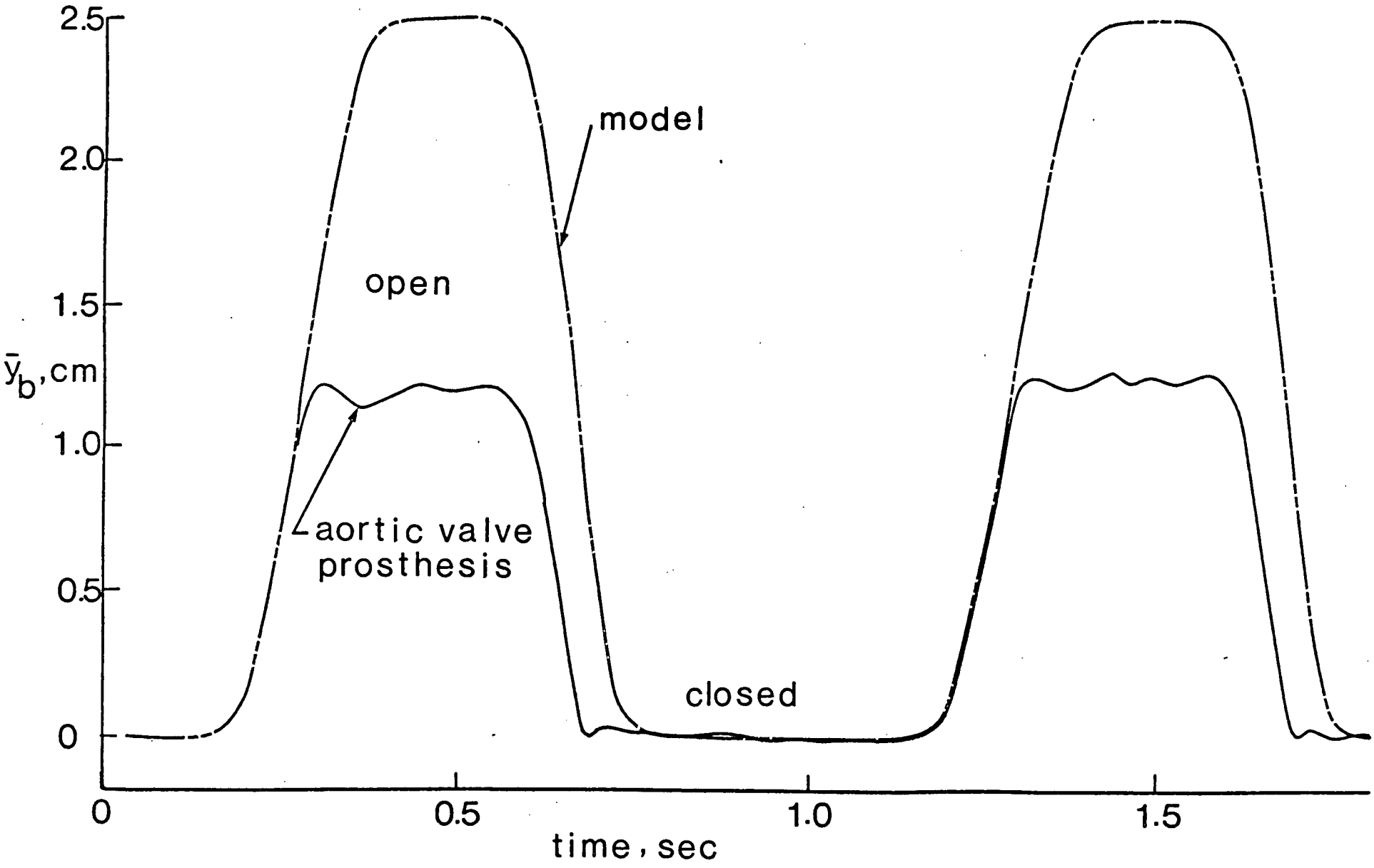

Figure 2-13 A comparison of the typical displacement-time histories for an aortic ball valve implant and the model

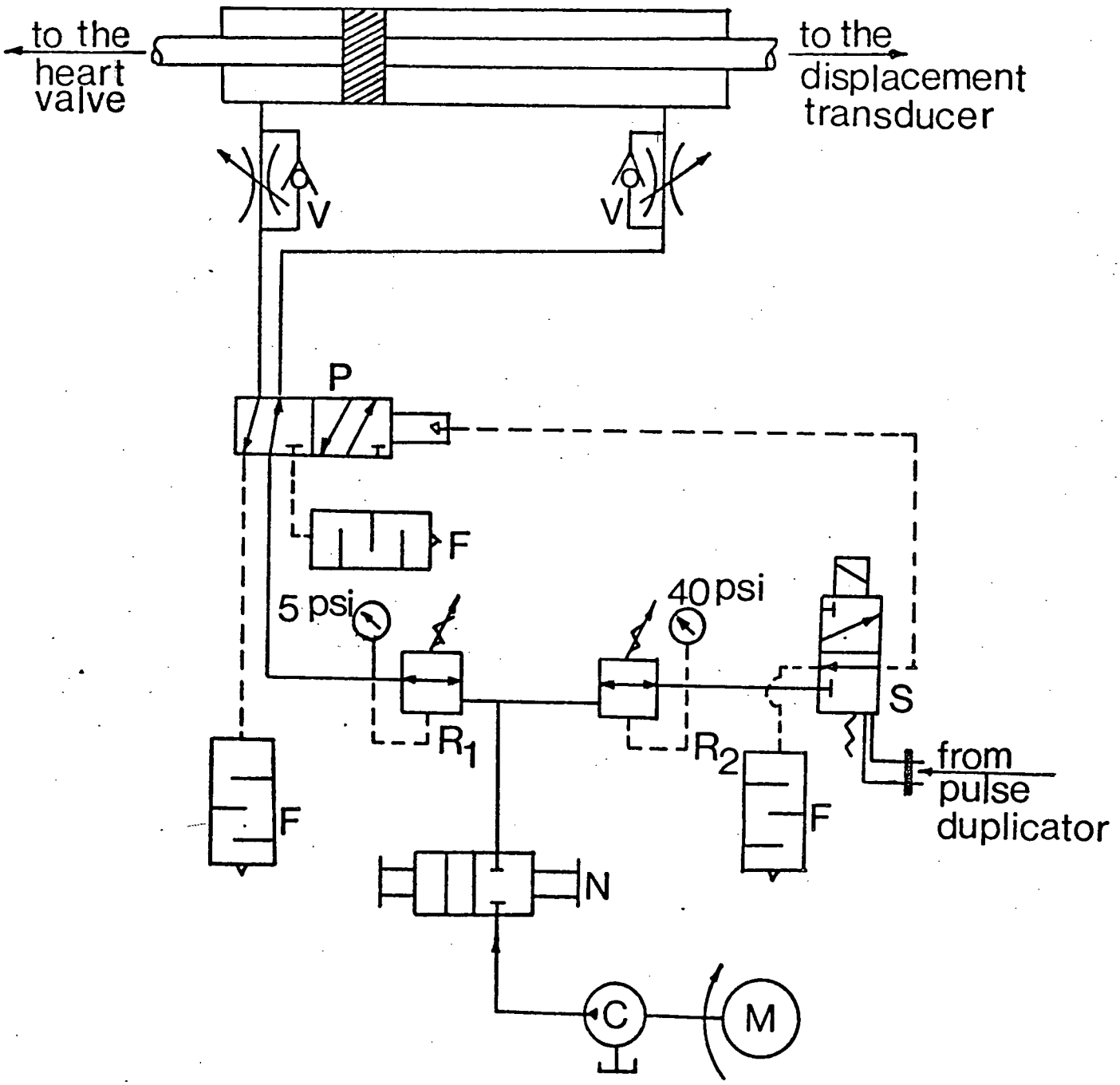

Figure 2-14 Details of the circuit used in pulsating the poppet of the heart valve model: C, compressor; F, adjustable muffler; M, motor; N, needle valve; P, four way air valve; R_1, fine control pressure regulating valve; R_2, pressure regulating valve with coarse setting; S, three way solenoid valve; V, one way fine control needle valve

at the intake of the air cylinder. Duration of each cycle and the travel time are adjusted through a pulse duplicator which controls the solenoid (Figure 2-15).

2.6 Linear Displacement Transducer

The time history of the pulsating poppet was monitored by a linear displacement transducer specifically designed for underwater application (Figure 2-16). The transducer employs the principle of differential transformer and consists of three main components:

(i) a soft iron core;

(ii) a non-conducting spool upon which the primary and secondary windings are wound;

(iii) a brass tubular casing.

A 10 Kc/sec., 10 volts rms signal from a function generator (Interstate Electronic Corporation) supplied to the primary is modulated by the core oscillation. This modulated signal from the secondary is rectified to 2.4 - 4.4 volts D.C. in linear proportion to the core displacements.

The transducer is calibrated to the accuracy of ±.001 in. employing a mechanical dial gauge in conjunction with a traversing mechanism. The transducer's body was held in a vise with the actuating rod connected to the

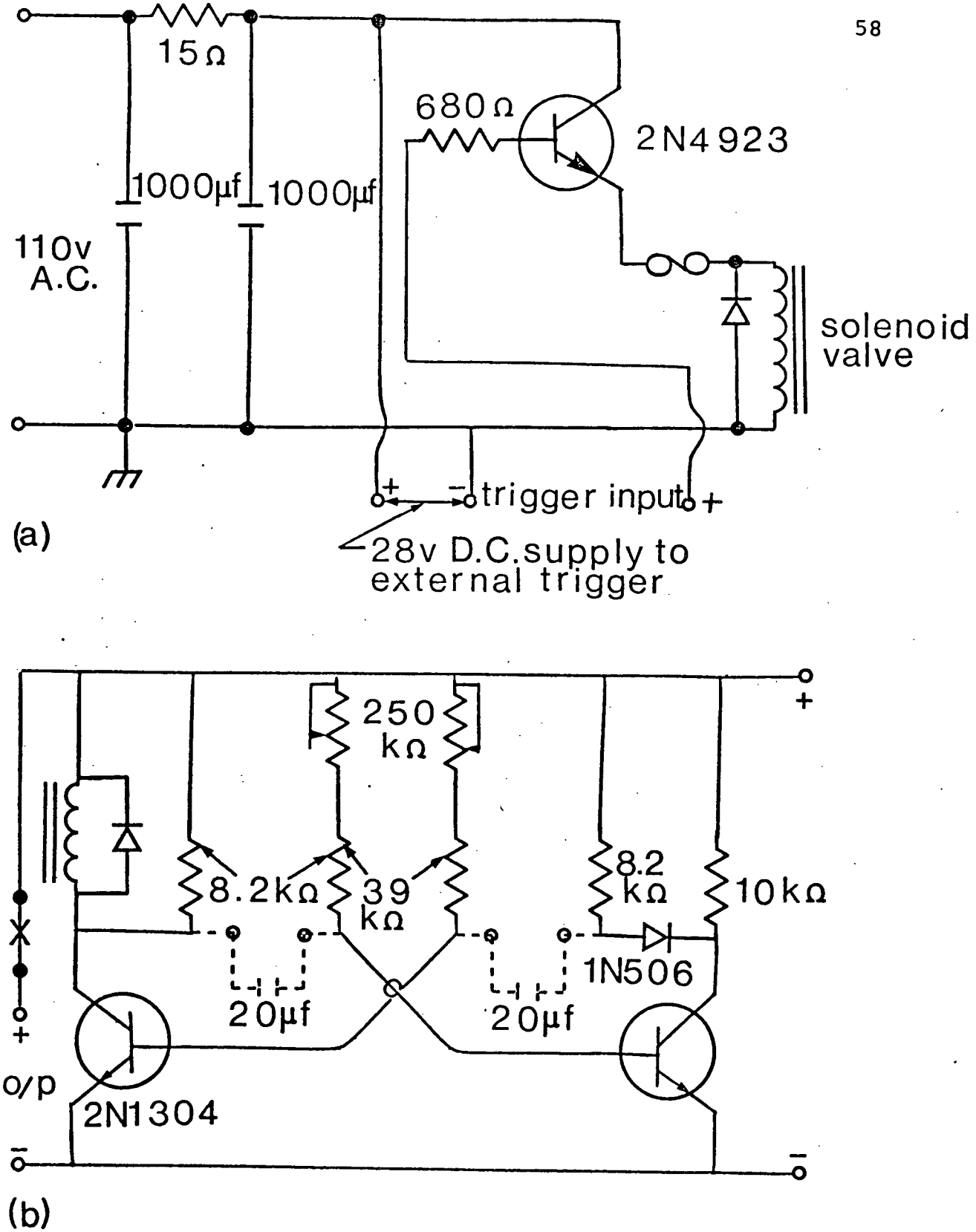

Figure 2-15 Circuit diagram for the pulse duplicator: (a) D.C. power supply for the solenoid valve and the (b) triggering mechanism

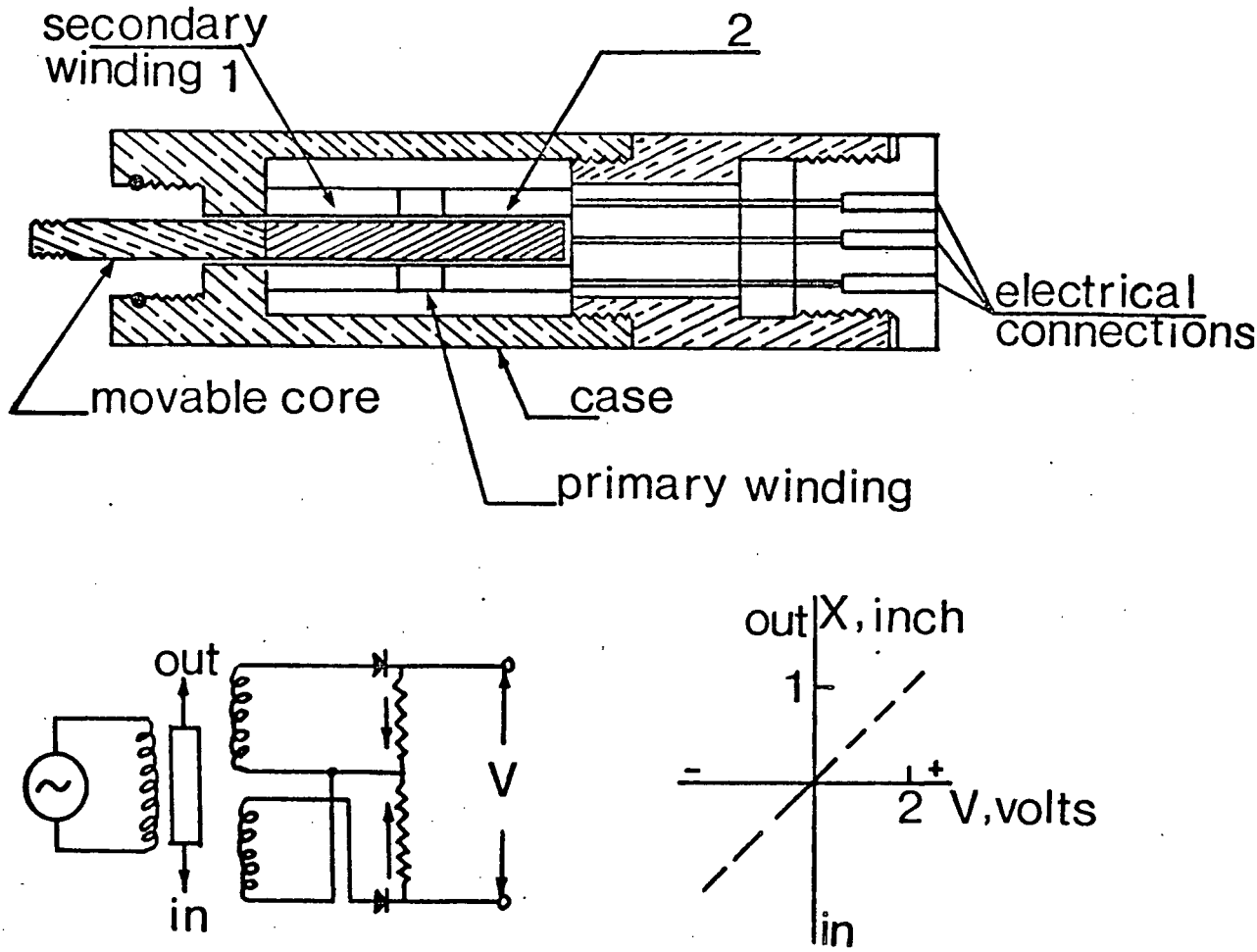

Figure 2-16 A schematic diagram of the displacement transducer and associated electronic circuitry

traversing gear. For each position of the rod, set by the traversing device and indicated by the dial gauge, the output voltage from the rectifier was recorded. The calibration plot thus obtained is shown in Figure 2-17. The straight line represents the least square fit to the test data.

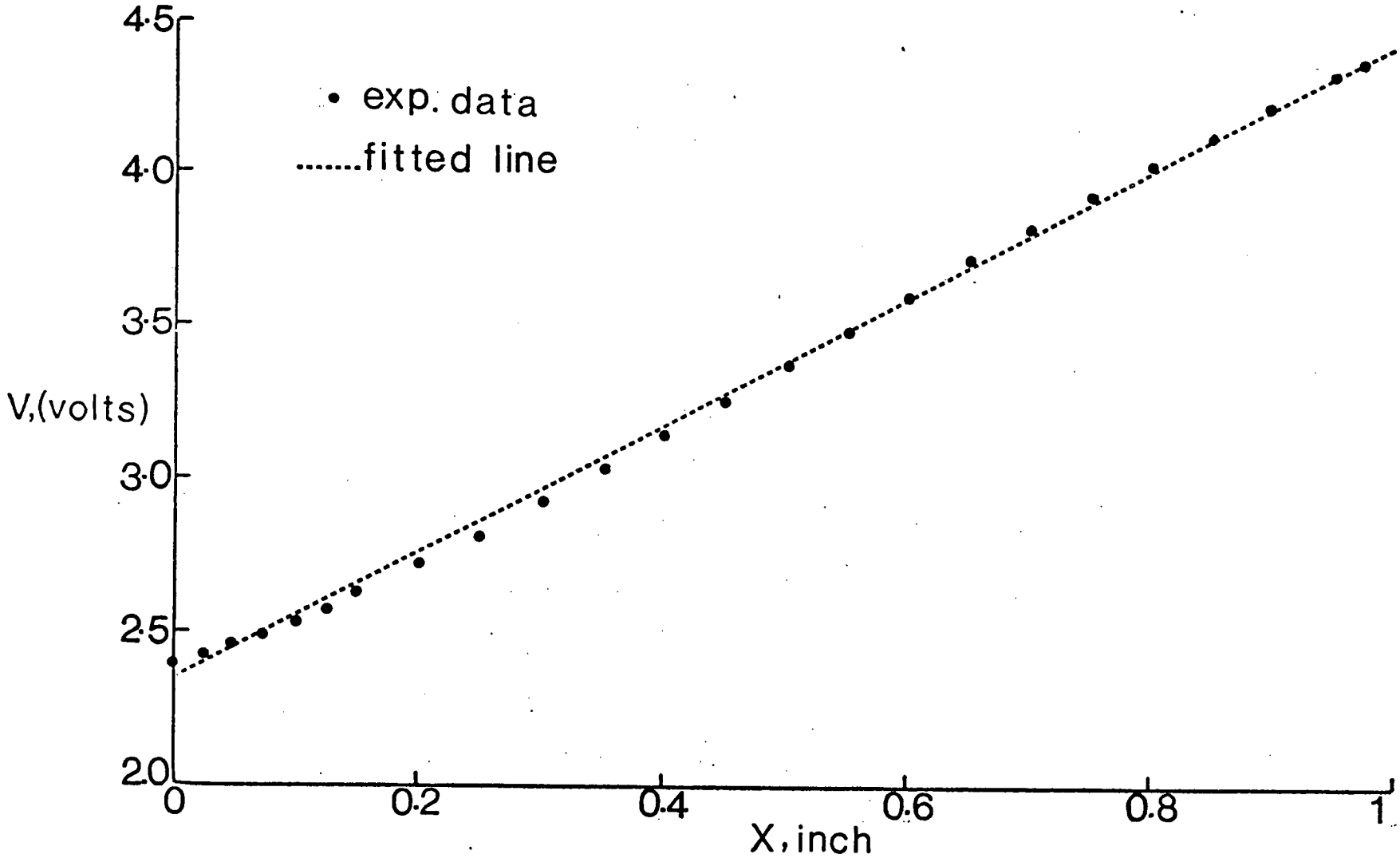

Figure 2-17 Calibration plot for the displacement transducer

3. TEST PROCEDURES

Before proceeding to present the test results and their discussion in detail, it would be appropriate to briefly describe some of the important test procedures. Mostly, the techniques employed are conceptually well known but their implementation attain complexity of a higher order, mainly because of the character of the working fluid (water or glycerol). Often peculiarities of specific experiments make certain measurements quite difficult. Throughout, the emphasis is on practical considerations involved in executing the experimental programme. At times the factors involved are, seemingly, so trivial that one would seldom give them a second look. However, a common experience of most experimenters is that resolution of apparently simple problems occasionally takes days, if not weeks or months. This chapter aims at touching upon such relevant points encountered during the present test programme.

3.1 Velocity Profiles Along the Test Section of the Tunnel

The first step in the test programme was to calibrate the tunnel, i.e., to obtain information about the boundary layer growth as reflected in the velocity profiles

along the test section. To this end, the tunnel (without the test model) was filled with the working liquid of a fixed concentration. All air pockets and bubbles were removed from the tunnel by circulating the test fluid, with the wetting agent, for at least eight hours at around 30°C. Velocity profiles at several test sections were then obtained using the calibrated hot film probe in conjunction with a traversing gear, which can position the probe with an accuracy of around ± 0.01 in. It should be pointed out that the probe movement is confined to the vertical direction in the central plane of the tunnel. Step size for the probe movement was regulated according to the velocity gradient so as to provide an accurate profile near the wall.

Initial tests revealed the regions where the velocity distribution deviated from the desired uniform value. Logical application of the available information[114-120] together with considerable amount of experimentation led to a suitable combination of honeycombs, brass screens and fiberglas wool, which produced a fairly uniform flow over the central portion of the test section in the desired range of the Reynolds number.

Deposition of dust particles and/or air bubbles on the probe, leading to a sudden change in the probe response, represented an occasional source of annoyance. Addition of the surface reactant and introduction of the filtering circuit reduced the problem but did not completely

eliminate it because of the gradual wear of the pump seal. To avoid dirt contamination the probe was washed in methyl alcohol after each run.

Figure 3-1 shows the instrumentation layout used during these measurements.

3.2 Static Pressure Distribution on Stationary and Oscillating Spheres

The main element of the valve being the spherical poppet, it seemed appropriate to conduct pressure measurements on an isolated sphere during both stationary and oscillating conditions. This would naturally serve as a useful reference in assessing effects of presence of the cage, seat and the surrounding cylinders approximately representing the aortic vein. Furthermore, an extensive review of the literature showed that most investigations on sphere are confined to the overall drag measurements. Detailed studies of the pressure distribution in the Reynolds number range of interest (100-5000) are rather scarce. Of course, with its symmetrical geometry together with the available information on the drag data, it is convenient to check the performance of the test set-up.

To cover a wide range of Reynolds number, seven different spheres (1/4, 3/8, 1/2, 1, 1 1/2, 2, 2 1/2 in. diameter) were employed as models with water

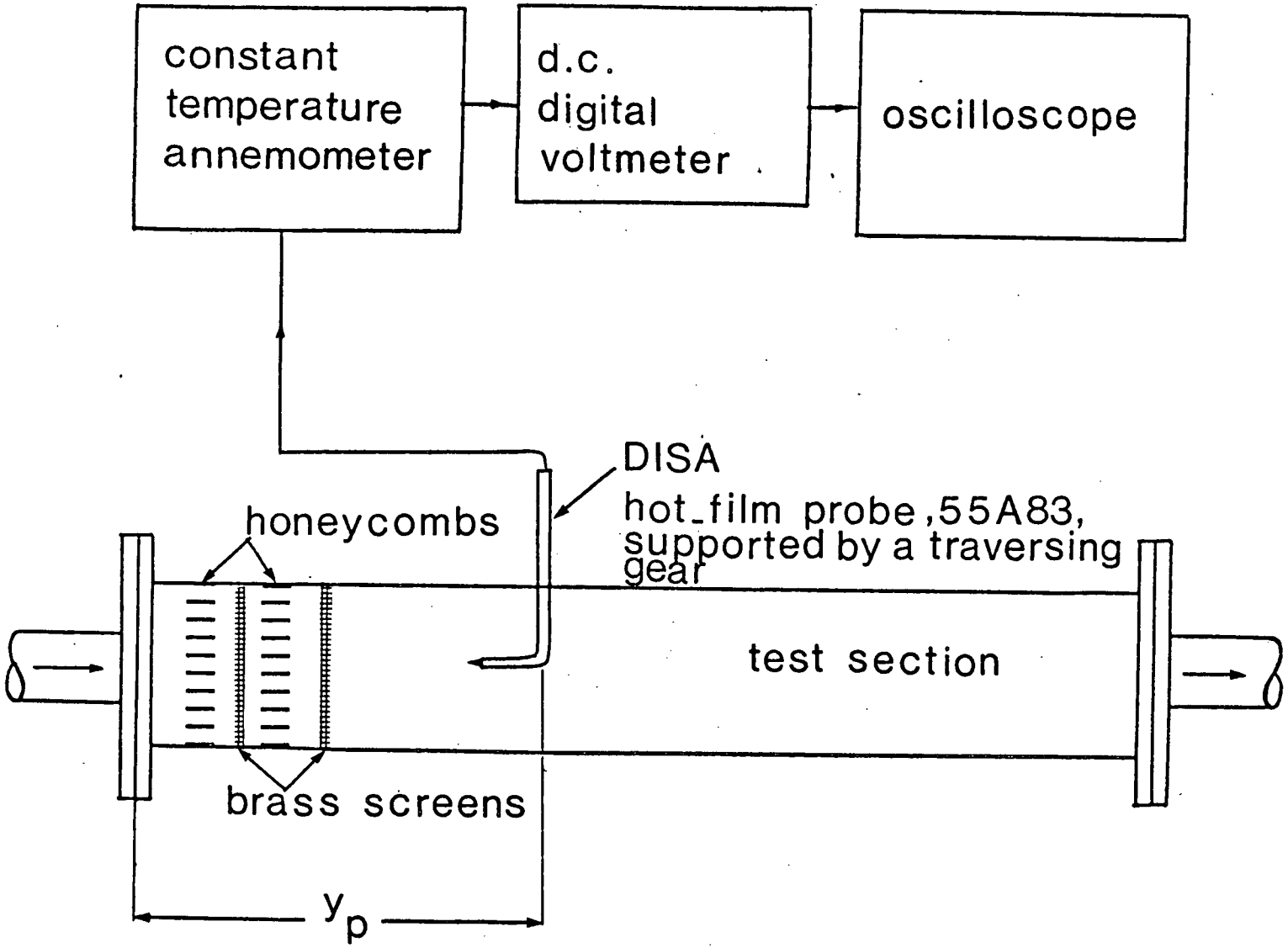

Figure 3-1 Instrumentation layout used during velocity profile measurement

($\nu = 1.05 \times 10^{-5}$ ft.^{2}/sec.) and glycerol-water solution (54% glycerin by weight, $\nu = 7 \times 10^{-5}$ ft.^{2}/sec.) as working fluids. After a complete removal of air bubbles from the fluid, a model was positioned in the test section with its center 18 in. downstream of the last screen. Next, the pressure ducting was filled with the test fluid and was connected to a Barocel pressure transducer via a manifold, which facilitated removal of the air pockets from the line and provided a central station for connection of the pressure tubings. The pressure sensing unit was balanced to read zero output in the no-flow condition. With the pump operating at a preselected speed to give a desired Reynolds number and the test fluid held at a constant temperature, the mean pressure distribution around the horizontal meridional cross-section was measured. For each run the velocity profile upstream of the sphere was also recorded. The hot film probe, mounted on a traversing gear, was positioned 10 in. upstream of the sphere. The procedure was repeated over a range of mean flow rates.

A point concerning an appropriate choice of the size of the pressure tubings must be emphasized here. A systematic study with tubes of different size and associated time to reach steady state pressure showed the tubes with internal diameter less than 0.062 in. to have an excessively large time constant (>20 min.) Of course, as suggested by several theoretical and experimental studies on the dynamic response of fluid lines[121-123], the time constant would depend on a

number of parameters including the diameter and length of the tubings, viscosity of the fluid, inline volume including the transducer's cavity, character of pressure signals, etc. For the mean pressure measurements under consideration, it was convenient to use fluid lines of 0.023 - 0.187 in. I.D., depending on the size of the sphere and the fluid, resulting in the time constant of around five minutes.

To insure accuracy as well as repeatability of the measured data, it was of utmost importance to minimize and compensate for any drift of the pressure transducer and associated electronic circuitry. Minute character of the pressure signals (10^{-4} psi) together with the relatively long time involved in reaching the steady state made this all the more necessary. Chart recordings of the drift over periods of 24-48 hours showed them to be quite significant, at times as large as 50% of the actual signal, but of no well defined pattern. The drift compensation procedure involved careful measurements of pressures at a reference step (say $\theta = 60°$) before and after a given test and attributing the difference to the drift. The procedure yielded data that can be reproduced within the accuracy of ±2.0%.

Furthermore, any fluctuation in the line voltage would be reflected on the pump speed and hence on the pressure signals from the model. The speed fluctuations were monitored through variations in the orifice meter data. The output voltage from the pressure transducer was damped

using a DISA type 550 digital D.C. voltmeter equipped with a R-C damping circuit to provide an adjustable time constant of up to 100 seconds. Schematic diagram of the instrumentation layout is shown in Figure 3-2.

The pressure measurements were also conducted during controlled oscillations of the spherical poppet of the aortic heart valve model. For this, the poppet was connected to the end of a double acting air cylinder and the displacement transducer to the other. The entire assembly was placed inside the test section and locked in position. The power cables for the transducer and pressure conducting intramedic tubings were brought outside the test section through the portholes on the top of the tunnel. Compressed air line was connected to the cylinder ports and the actuating mechanism checked for any misalignment before introducing the working fluid. After satisfactory operation of the pulsating system the tunnel was filled with the test fluid and air bubbles removed. Few trial runs were carried out to check the performance of the pressure measuring unit and the displacement transducer. Upon assurance of successful operation of all the instruments involved, tests were carried out for two conditions. In the first, the poppet was oscillated at various frequencies (6-80 cpm) with a constant mean flow rate through the tunnel. In the alternate case, the pulse rate was held constant but the mean flow rate was varied. As before, for both the cases, the mean pressure measurements

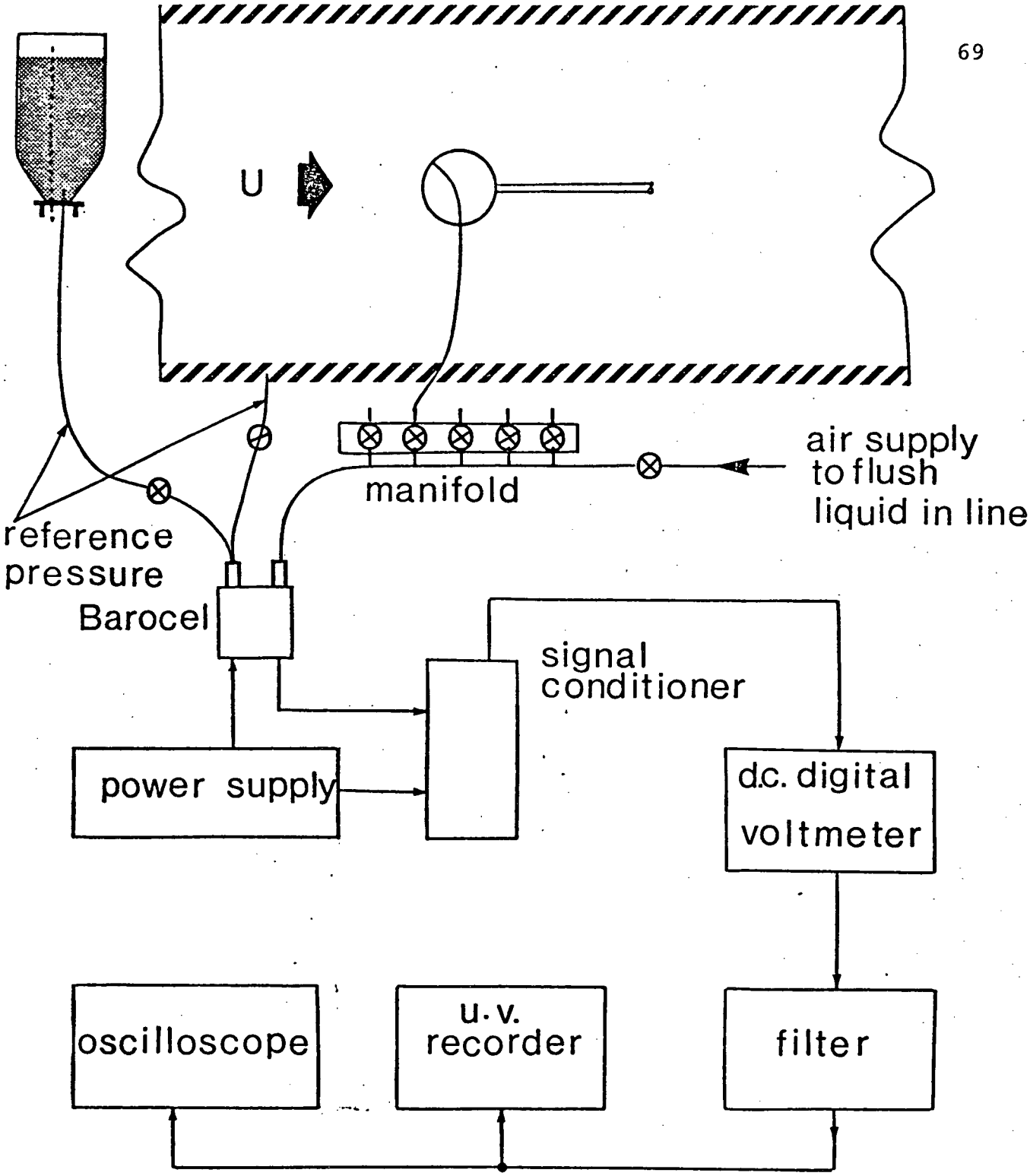

Figure 3-2 A line drawing of the instrumentation set-up used for pressure measurements

were confined to a meridional section of the poppet. Above tests were carried out with a constant amplitude of 1 in. in the range $300 < R_n < 1100$.

An aspect of considerable importance is the acceleration of the liquid body contained inside the pressure conveying lines leading to an additional signal. It was difficult to isolate entirely this inertia effect from the pressure signals due to the movement of the sphere and fluid surrounding it.

To overcome this problem several procedures were attempted, including:

(i) oscillation of a conveying line by itself and when connected to a pressure tap, the difference leading to the desired information;

(ii) differential pressure measurements with two lines connected to two different pressure taps, one of which used as a reference;

(iii) pulsating the poppet with no liquid inside the conveying tubes thus minimizing (though not eliminating) the latter's acceleration effect.

As the last method was found to be, relatively, more effective, it was decided to conduct pulsating sphere tests without any liquid (water or glycerol) inside the tubes. Accomplishment of this demanded a degree of ingenuity. With the sphere stationary and having established a desired flow

velocity, compressed air at 5 psig was pumped into a given tube to force the liquid column down to a minimum value (≈0.10 in.). The outlet end of the tube was now connected to a shut off valve leading to Barocel via a manifold. Inside of the tube at the entrance was coated with a low surface tension compound (shoe polish) to avoid breaking up of the liquid column resulting in trapped air and hence, erroneous signals. The poppet was now set into motion at a desired frequency and pressure measurements conducted, opening individual valves one at a time. The time history of the static pressure was logged continuously, after filtering the extraneous high frequency noise, using a U.V. recorder (S.E. Laboratories, Model 3006). The mean value of the signal was also obtained using a DISA TYPE 550 D.C. digital voltmeter employing a damping circuit with the maximum time constant of 100 sec. All pressure measurements were made with respect to a constant head provided by an external liquid column. To correlate pressure signals with the poppet travel during a cycle, the sphere displacement was also recorded on the same chart. Care was taken to flush pressure conveying lines before each set of tests.

Figure 3-3 shows the instrumentation set-up used during the measurements of the pulsating pressures.

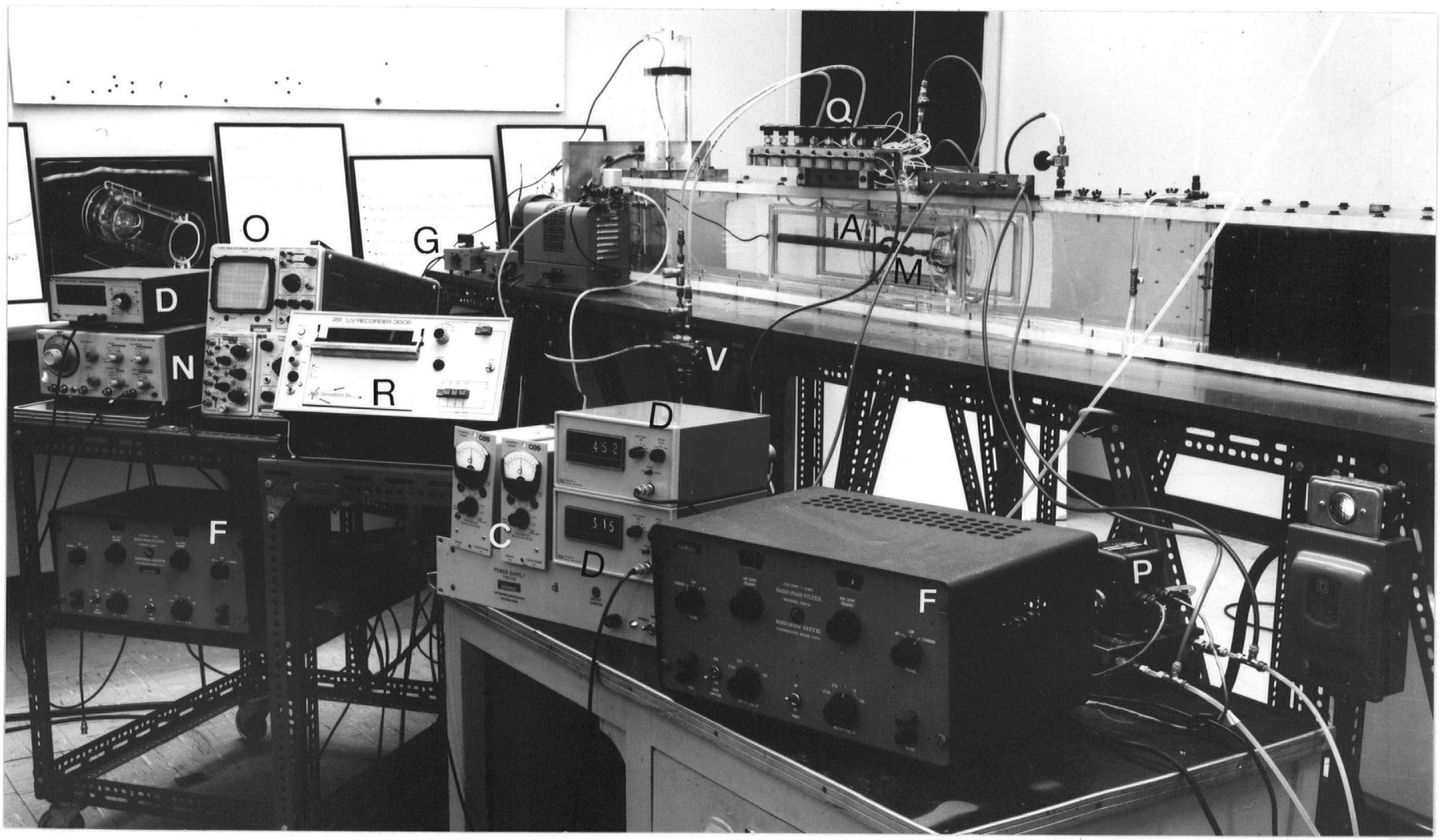

Figure 3-3 A photograph showing the instrumentation set-up used during measurements of the pulsating pressure: A, double acting air cylinder; C, signal conditioner; D, digital D.C. voltmeter; F, filter; G, electrical pulse duplicator; M, modelof the aortic heart valve; N, function generator; O, osciloscope; P, pressure transducer; Q, manifold; R, recorder

3.3 Pressure Distribution on the Stationary Poppet Representing Various Valve Openings

Here the complete heart valve model was placed inside the tunnel test section and locked in position. Employing a gear and rack system, the poppet was positioned so as to produce a preselected valve opening. The poppet position was indicated within ±0.001 in. using the linear displacement transducer. The test liquid was circulated until all air bubbles were removed (≃6 hrs.). For various openings of the valve and over a range of the Reynolds number, mean pressures around the meridional section of the poppet and three stations on the cage were measured. At the same time, velocity profiles at several stations upstream of the model were also recorded. The tests were conducted for both open and close bypass conditions. In the case of the open bypass, the valve opening ranged from 0-1 in., i.e. from fully closed to fully open positions of the valve, in the range $300 < R_n < 3100$. However, for the closed bypass, the minimum valve opening was restricted to 0.050 in. and the maximum Reynolds number to 1100 to avoid over stressing of the test section.

3.4 Mean Pressure Measurements on the Poppet while Oscillating Inside the Valve

For this study, it was necessary to oscillate the poppet in the manner so as to simulate actual motion of the

prosthetic valve in a patient. Thus the model arrangement in the tunnel remained essentially the same as before except for the pulsating mechanism and monitoring device. After mounting the double acting air cylinder and the displacement transducer, the entire assembly was slid into the test section and locked in position. Two sets of pressure conducting tubings were involved: one supplying the necessary compressed air for operation of the air cylinder and the other set of polyethylene tubes transmitting static pressures from the surface of the poppet to the externally located Barocel. These tubes were brought out of the test section through the downstream portholes at the top of the tunnel.

Now the tunnel was filled with the test liquid and air bubbles removed as before. With zero mean flow through the tunnel (i.e. no discharge from the pump), the poppet was forced to oscillate and its time displacement history was recorded using the displacement transducer (differential transformer) and a Honeywell Visicorder. After a few trial runs to check alignment of the air cylinder and proper functioning of the four way air valve, the pulse duplicator was set so as to simulate the actual motion of the prosthetic heart valve.

The tests were conducted for two sets of conditions. In the first, the frequency of oscillation was varied with no net flow through the tunnel. The second case involved a systematic variation of flow rate through the valve but

at a constant frequency. For both the cases, time history of pressures around the poppet and velocity profiles upstream of the valve were measured. As the pressure at the individual tap was recorded one at a time (only one unit of Barocel being available) it was quite important to maintain the precise character of the oscillating function. This was ascertained by a continuous recording of the poppet displacement and maintaining the constant actuating pressure. To reduce impact stresses resulting from the collision of the ball with the seat, air cushions were provided during the terminal portions of the forward and reverse strokes. The axial rotation of the poppet was prevented by a slotted sleeve, forced around its stem, and locked in position by a key on the air cylinder shaft. Care was taken to position the poppet so that the meridional section carrying the pressure taps was horizontal.

As before, the tests were carried out for both open and closed bypass conditions, and in the Reynolds number range of 300-1100. The pressure measuring technique was similar to the one described in Section 3.2.

3.5 Flow Visualization

To better appreciate the character of the flow through the aortic heart valve model and trends indicated by the pressure measurements, flow visualization was under-

taken. Among the several available techniques Schlieren, shadowgraph, and dye injection procedures were considered for their suitability. A preliminary study suggested that the Schlieren technique would present obvious problems of alignment and stability due to the flexible character of the wooden floor. Furthermore, there was also a possibility of excessive optical noise from the tunnel, liquid and model materials. The shadowgraph technique was discarded because of the limitations in marking the flow (heating or cooling the liquid upstream of the model). Here three different procedures were attempted:

(i) introduction of a heating element in the form of a tungsten wire (6 in. long) to mark the flow;

(ii) injection of hot or cold test fluid upstream of the model;

(iii) introduction of glycerol-water solution of higher density than the test fluid upstream of the model.

Unfortunately, none of the above attempts proved satisfactory in terms of high resolution flow patterns that can be photographed with clarity and interpreted. Consequently, dye injection method was used.

The dyed glycerol-water solution of the same concentration as that of the test fluid was injected 10 in.

upstream of the model. The dye employed was an imitation Cochineal food colour. Appropriate volumes of the dye and pure glycerin were mixed to produce a glycerol-water solution of the same density as that of the test fluid. At first the dyed solution was injected through a set of five syringe needles (#16) as shown in Figure 3-4(a). Although the arrangement worked fairly well, it was felt that the diameter of the injecting needles was a little too large (0.052 in.) and could be reduced. With this in mind, a new injecting probe consisting of seven #23 syringe needles (0.015 in.) placed 0.25-0.50 in. apart on a streamlined support, was constructed (Figure 3-4b). "Intramedic" tubings (0.023 in. I.D.) were used to connect the needles to a manifold. The rate of injection was controlled with brass needle valves. To ensure adequate flow through each needle, i.e. to provide sufficient head, the supply bottle was suspended from the ceiling 10 ft. above the injection level. A schematic diagram of the complete set-up is shown in Figure 3-5.

After ascertaining a successful operation of the entire assembly, flow patterns around the stationary and pulsating sphere, by itself and when located within the aortic heart valve model, were studied. The Reynolds number and oscillating frequency [Beta number = $(R_n S_n)^{1/2} = D(f/\nu)^{1/2}$] were varied systematically and flow patterns recorded.

It would be appropriate to point out here the type of lighting system used as it played a critical role in the

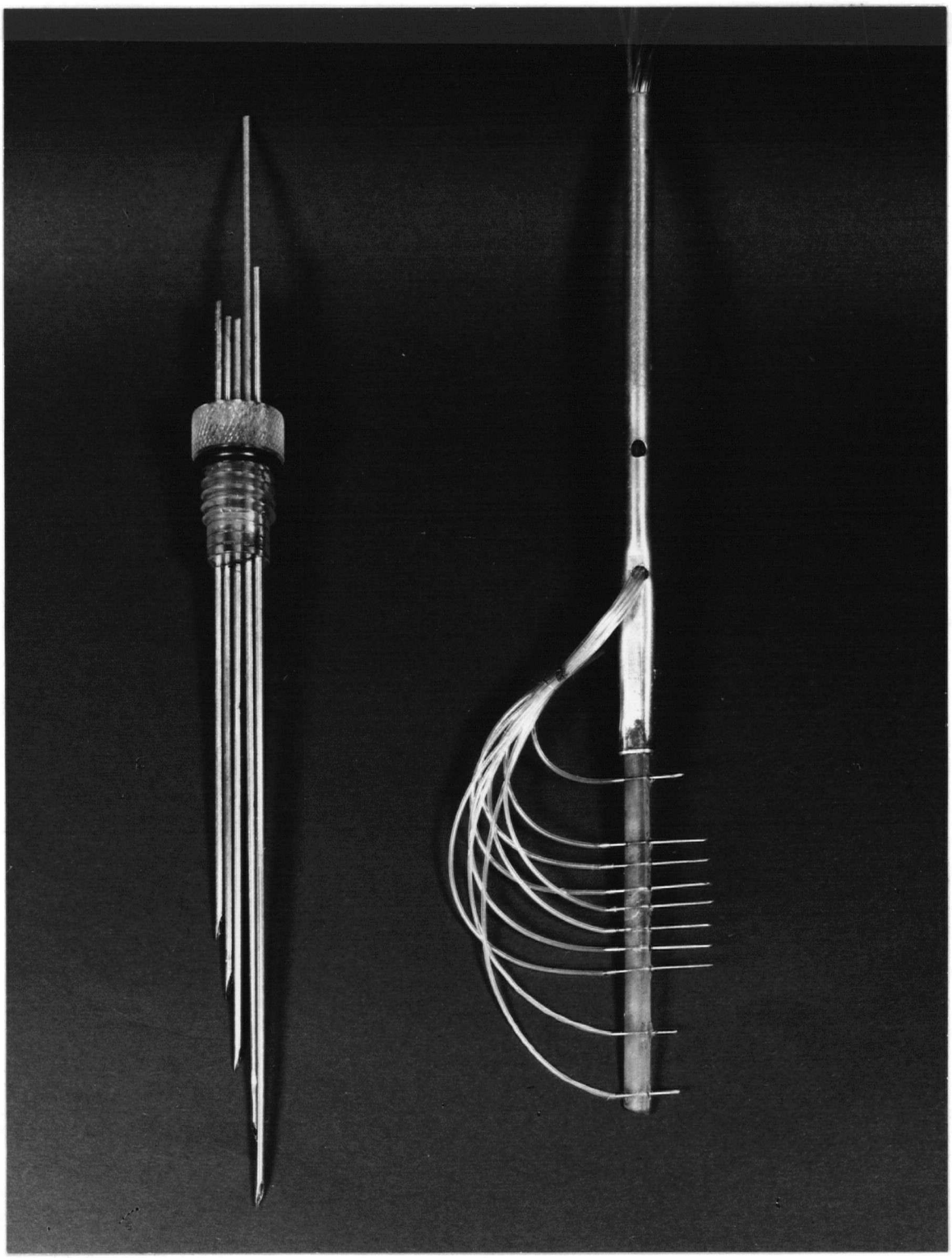

(a) (b)

Figure 3-4 A photograph of dye injecting probes:
(a) earlier model
(b) final streamlined probe

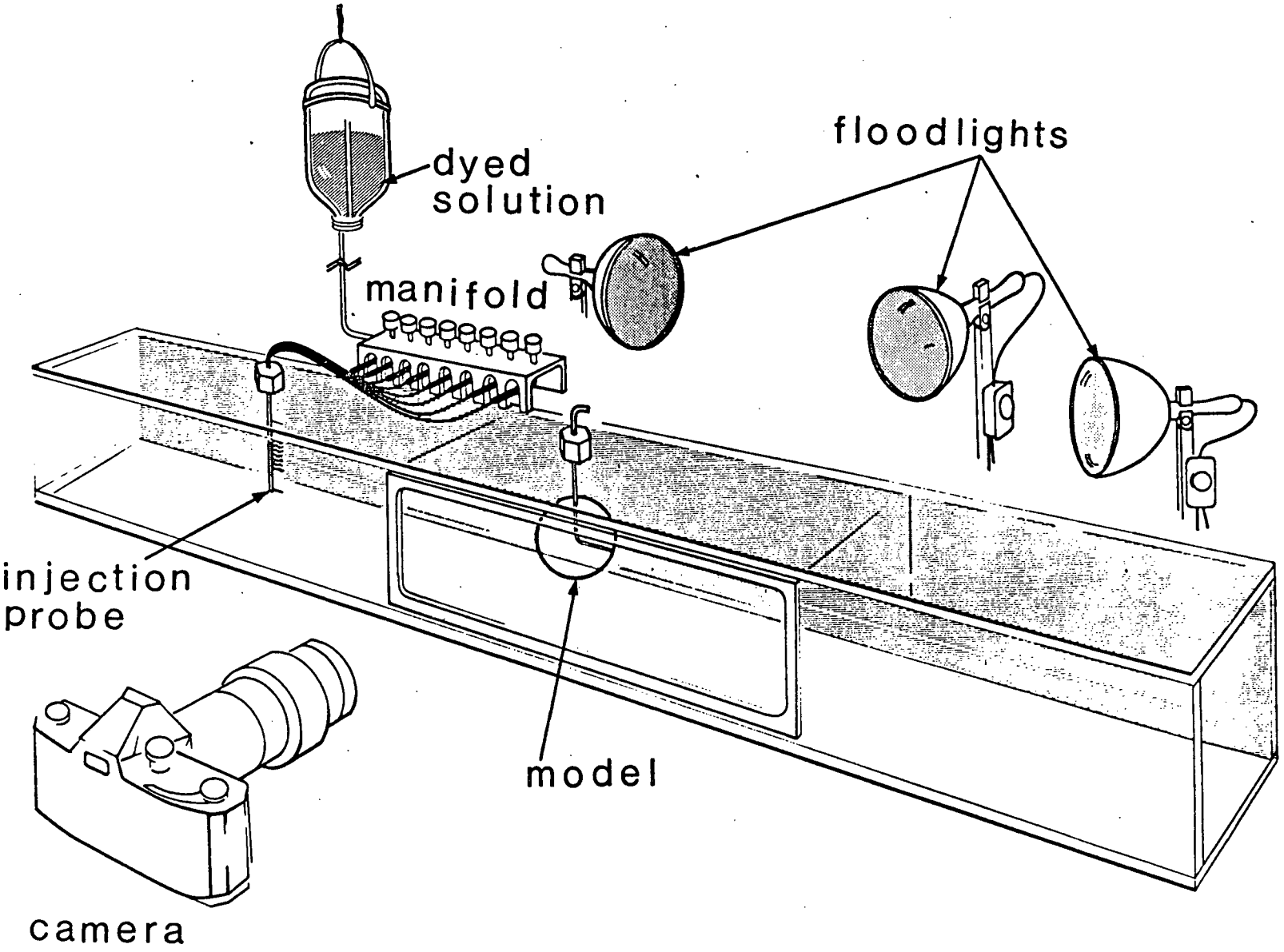

Figure 3-5 A sketch showing the equipment layout during flow visualization

photographing process. A combination of three variable intensity photo floods (maximum 500 watts, 3400°K) back-illuminated the subject through the tunnel glass window. To eliminate hot spots, the light beam was evenly diffused by masking the test section wall with a tracing paper. A set of trial runs helped arrive at the appropriate aperture setting and exposure time for the type of film used (still-Kodak high speed Ektachrome type EHB-135, tungsten, 3200°K, ASA 125, filter 81A; movie-Kodak Ektachrome EF7242, tungsten, 3200°K, ASA 125, filter 81A).

During the course of visualization study, it was discovered that in spite of the large volume of the test fluid (40 U.S. gallons), a relatively small amount of dye (8 fluid oz.) was sufficient to pollute the working fluid to the point that no clear photographs could be taken. This presented a rather serious problem in terms of time, effort and cost involved in replenishing the working fluid. Clearly, it was necessary to find an agent that would neutralize the dye without attacking the tunnel material or its circulating system and which does not alter the physical properties of the test fluid. Unfortunately, no such agent has been reported in the literature. A considerable amount of patient testing with numerous oxidizing agents led to sodium hypochlorite which has all the desirable attributes. Only 300 cc of the agent was sufficient to completely neutralize

the dye. To keep the concentration of the test fluid constant, sufficient amounts of glycerin were periodically added thus offsetting the diluting effect of the dye removing agent.

4. RESULTS AND DISCUSSION

With some appreciation of the background to the problem, instrumentation used and the experimental procedures adopted, we are ready to look into the test results and their interpretation. The amount of experimental data obtained is rather enormous, thus dictating a compromise between conciseness and comprehensibility. The guiding principle has been to include only those results which have immediate relevance to the study in hand, and help in establishing definite trends. In general, the sequence in which the results are presented also denote the chronological order of the tests. To begin with, velocity profiles along the test section are measured which give some indication as to the performance of the designed test facility. This is followed by the steady and instantaneous mean pressure on stationary and oscillating spheres, respectively. The study not only concerns one of the basic elements in the more complex configuration undertaken later, but also provides information of fundamental importance not recorded in literature. The next logical step was to study the hydrodynamics of the poppet in the simulated biological environment systematically — first with the spherical poppet occupying different positions in the valve followed by its oscillation in the precisely controlled fashion representing the time history of a

prosthetic valve in patient. The results of both the bypass open and closed situations are presented to have at least a qualitative appreciation of the influence of regurgitation and leaky valve. The flow visualization data are also included which generally substantiate the flow behavior predicted by pressure results. When available, published results from literature are included to aid comparison and help establish trends.

4.1 Tunnel Velocity Profiles

Velocity profiles were measured at several locations in the test section in the Reynolds number range 300-20,000 based on the hydraulic diameter of the test section and the average velocity as deduced from the flowmeter data. Both with water and glycerol as working fluids, a jet type of flow was observed over several localized regions typically illustrated by the plots in Figure 4-1. This suggested that the diffuser ring, honeycombs and screens introduced to uniformly distribute the flow were not completely effective. The undesirable behavior was substantially reduced (Figure 4-2) through the introduction of nylon wool in conjunction with existing straighteners in the entrance portion of the test section. Note that now the velocity profile is essentially flat at least over central 10 cm. of the tunnel

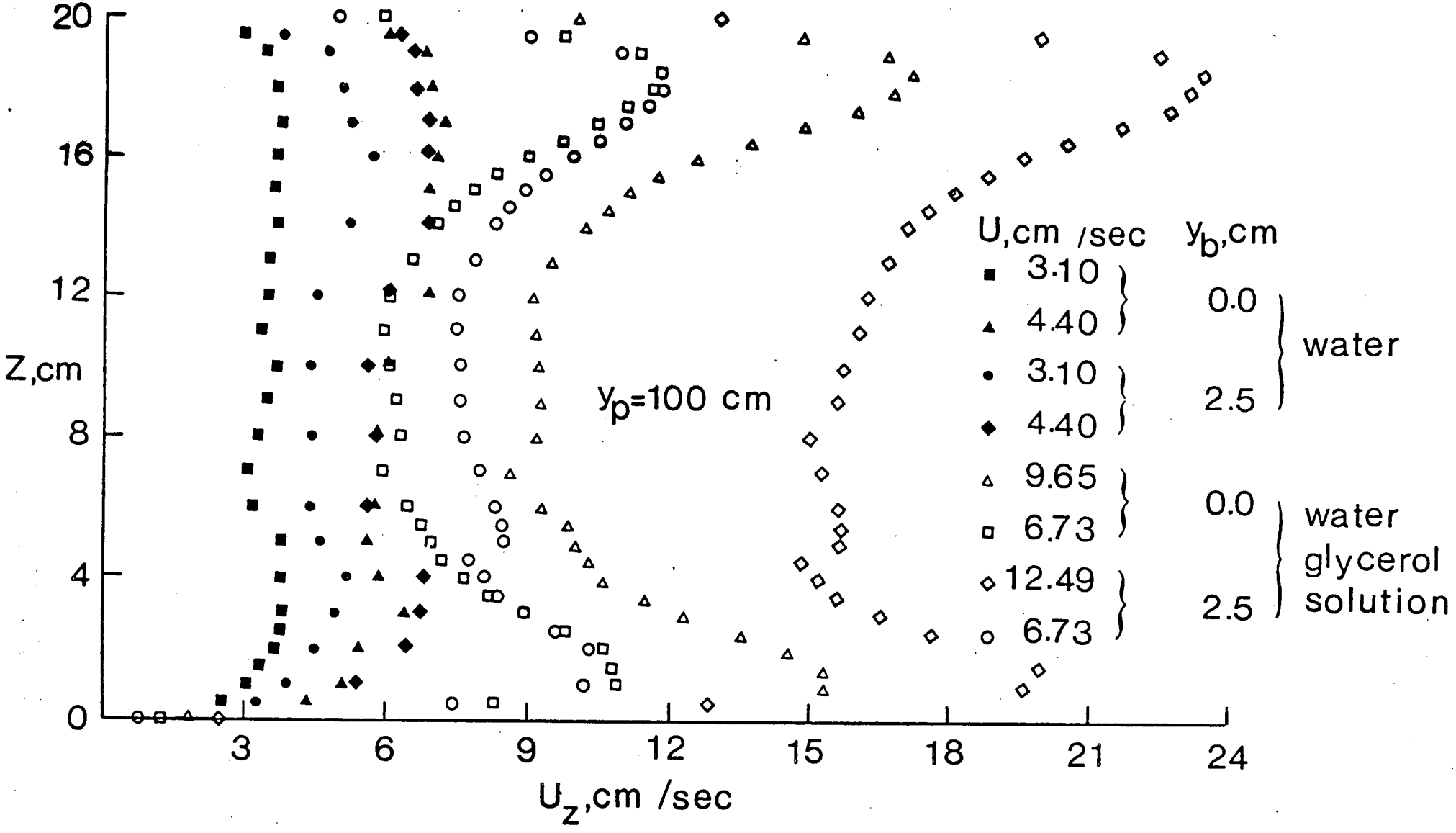

Figure 4-1 Typical tunnel velocity profiles indicating localized jet type flow

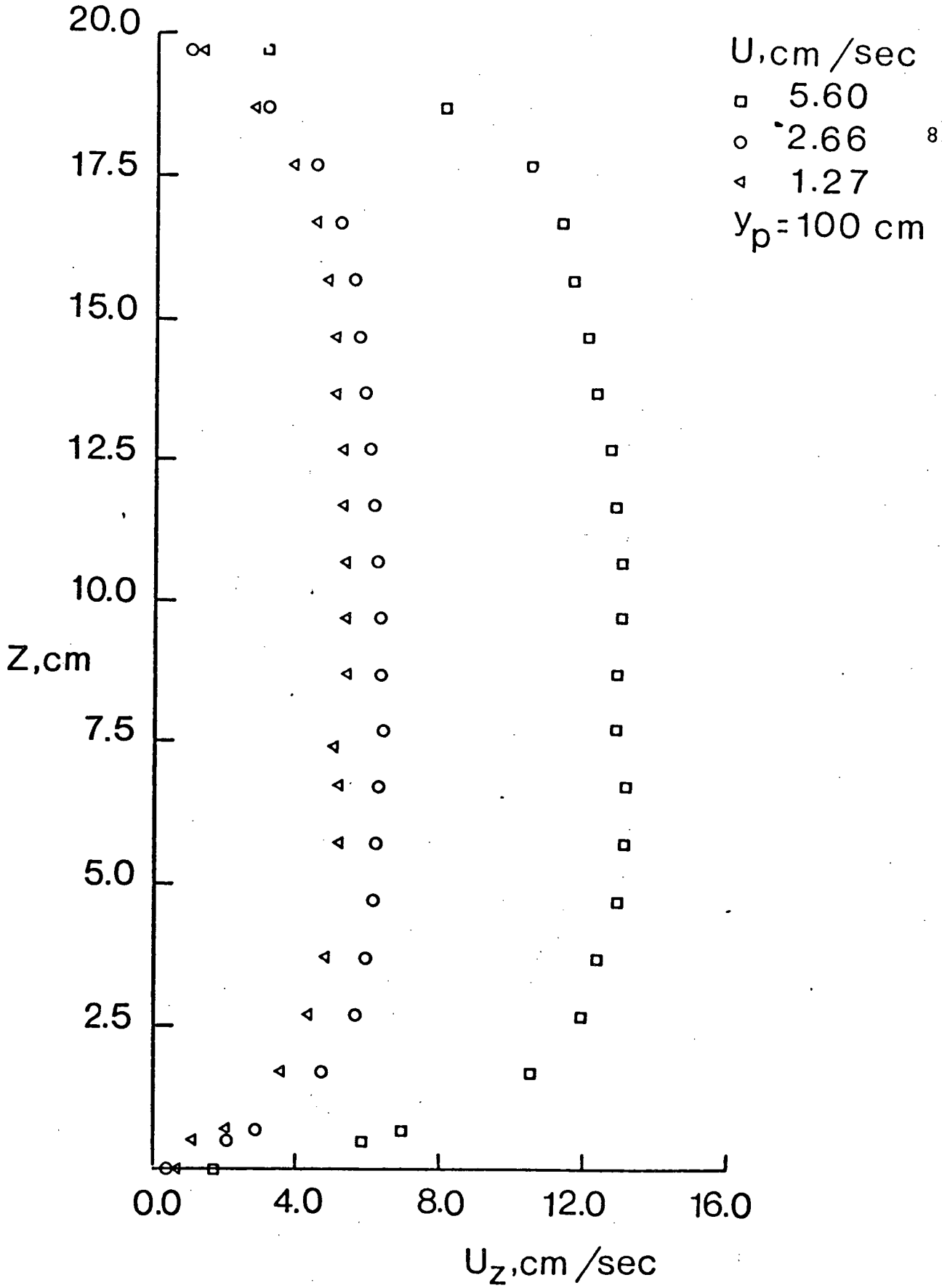

Figure 4-2 Representative velocity profiles showing effect of the introduction of nylon wool: (a) in water

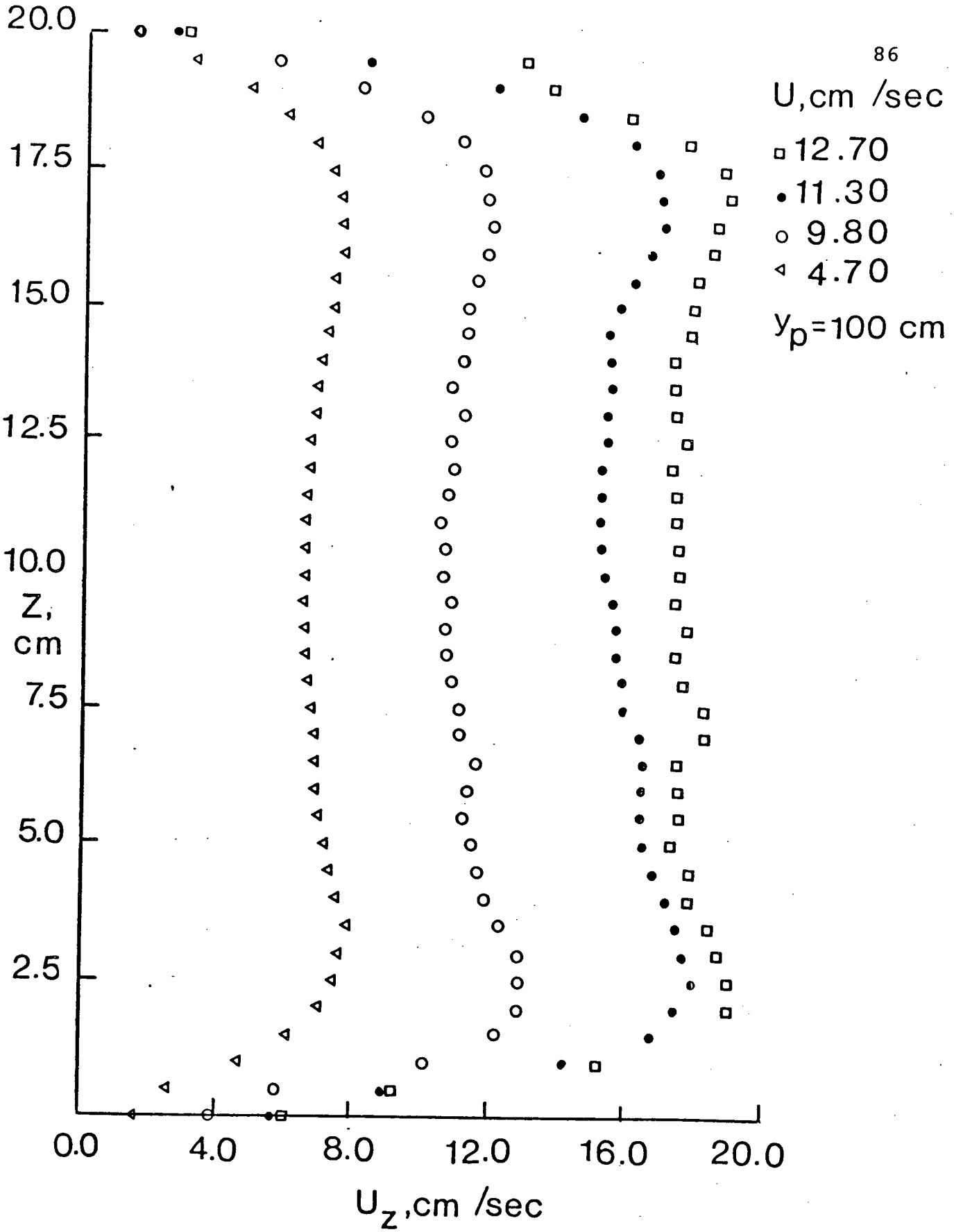

Figure 4-2 Representative velocity profiles showing effect of the introduction of nylon wool: (b) in glycerol-water solution, C_n = 54

height. Of course, this is desirable for reproduction and comparison of the test results. In general, the uniform portion of the profiles decreased with increase in distance from the tunnel inlet and velocity. This is to be expected in the light of the flow development downstream and strengthening of the jet effect with an increase in the flow rate.

Another point of interest was the character of the velocity profiles in presence of the models as shown in Figures 4-3, 4-4. In both the cases, the velocity results are for the plane 12.5 cm. ahead of the model (distance measured from the stem center line for the spherical model and from the orifice plane in the case of the valve model). Note that with the spherical model (Figure 4-3) the increase in resistance and irregularity of the profiles are relatively small compared to the valve model representing higher resistance (Figure 4-4). Apparently this is an outcome of rather complex interactions between interruption of the boundary layer growth, blockage, changed total circuit resistance and associated shift in the operating point of the pump.

Prosthetic valve openings also had a direct effect on velocity distributions. Smaller valve openings led to flatter profiles in water; however, no such discernable trend was observed in glycerol. The worst situation was represented by the valve model, fully open, in the glycerol

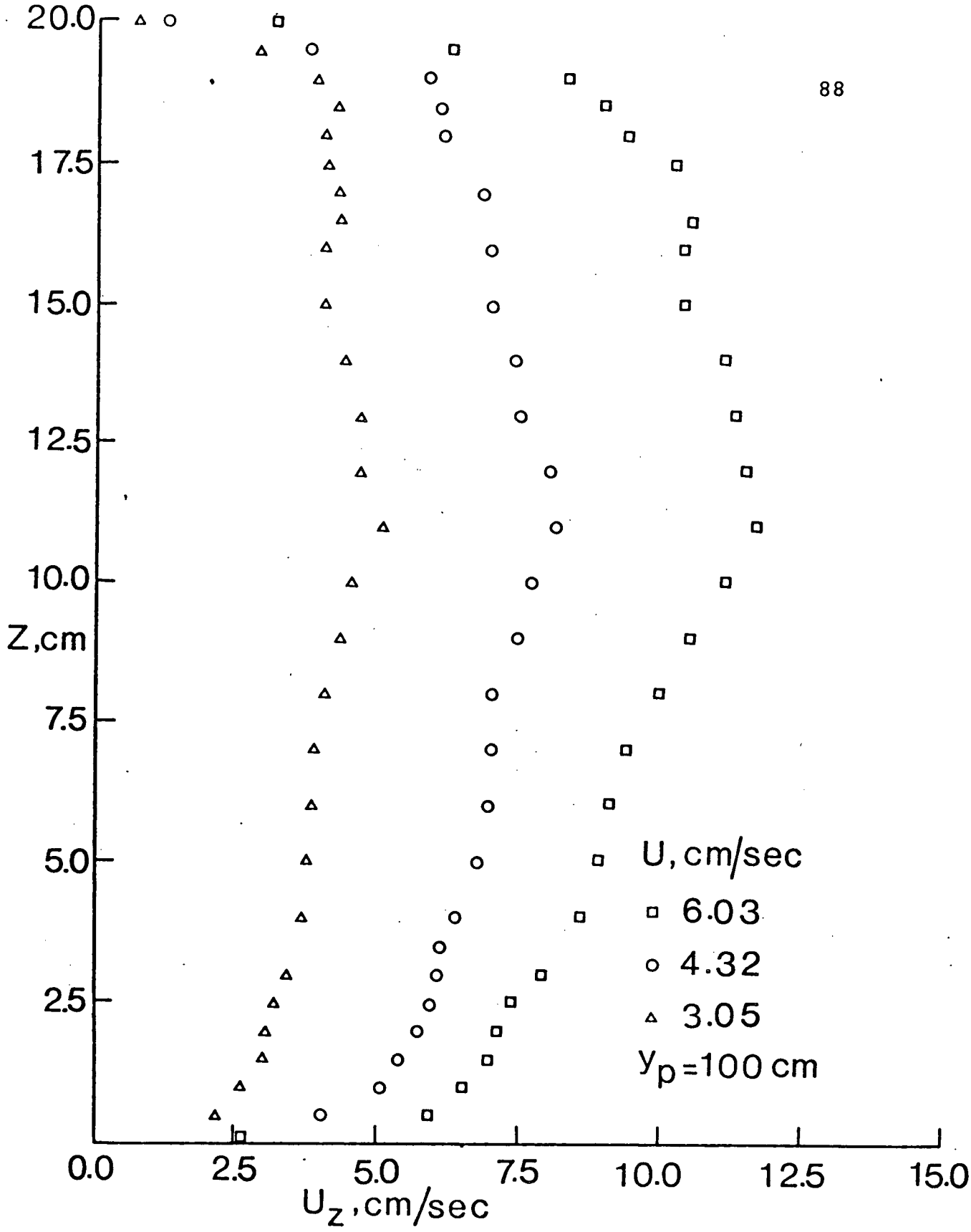

Figure 4-3 Effect of spherical model (d = 2.5 in.) on velocity profiles: (a) in water

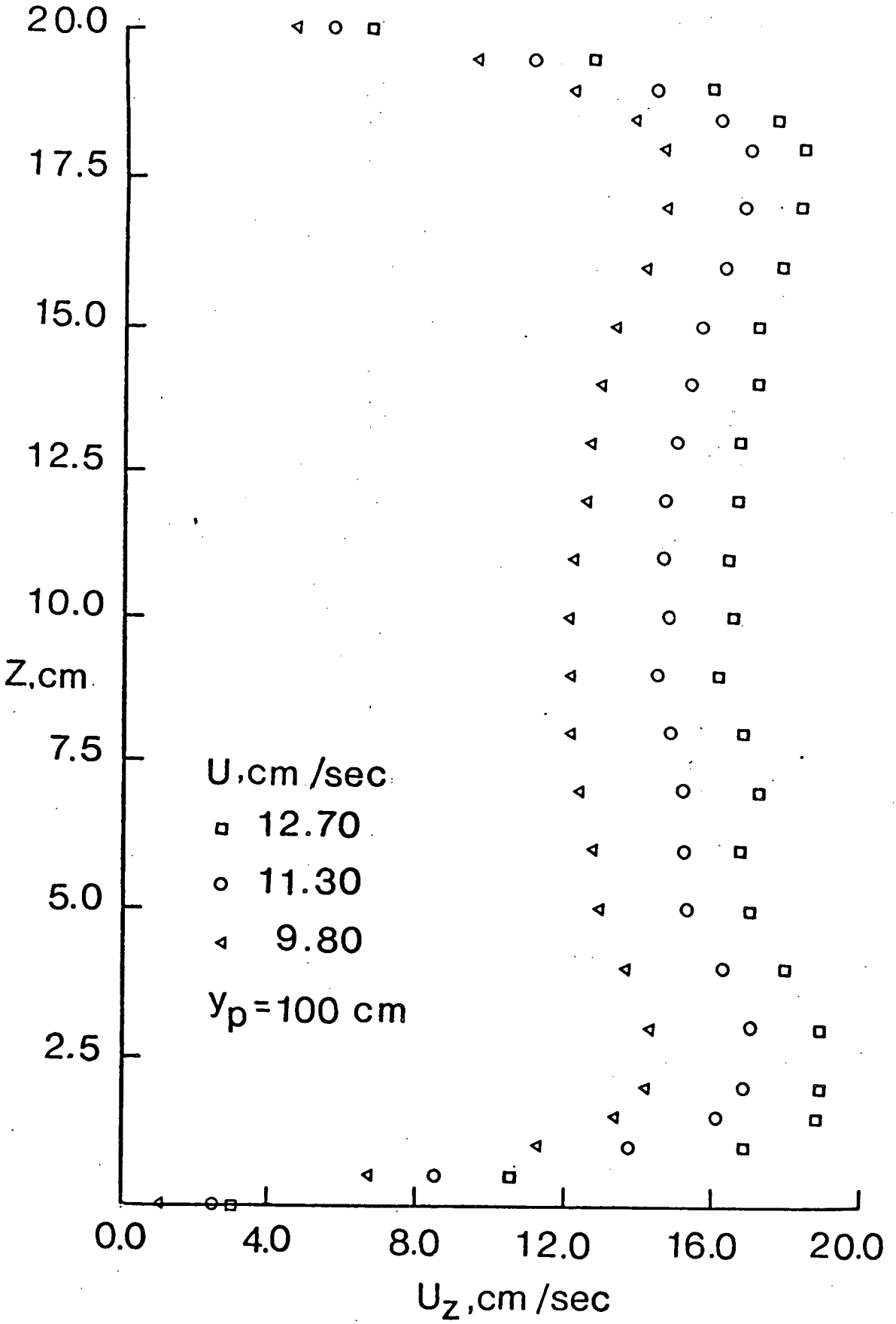

Figure 4-3 Effect of spherical model (d = 2.5 in.) on velocity profiles: (b) in glycerol-water solution, C_n = 54

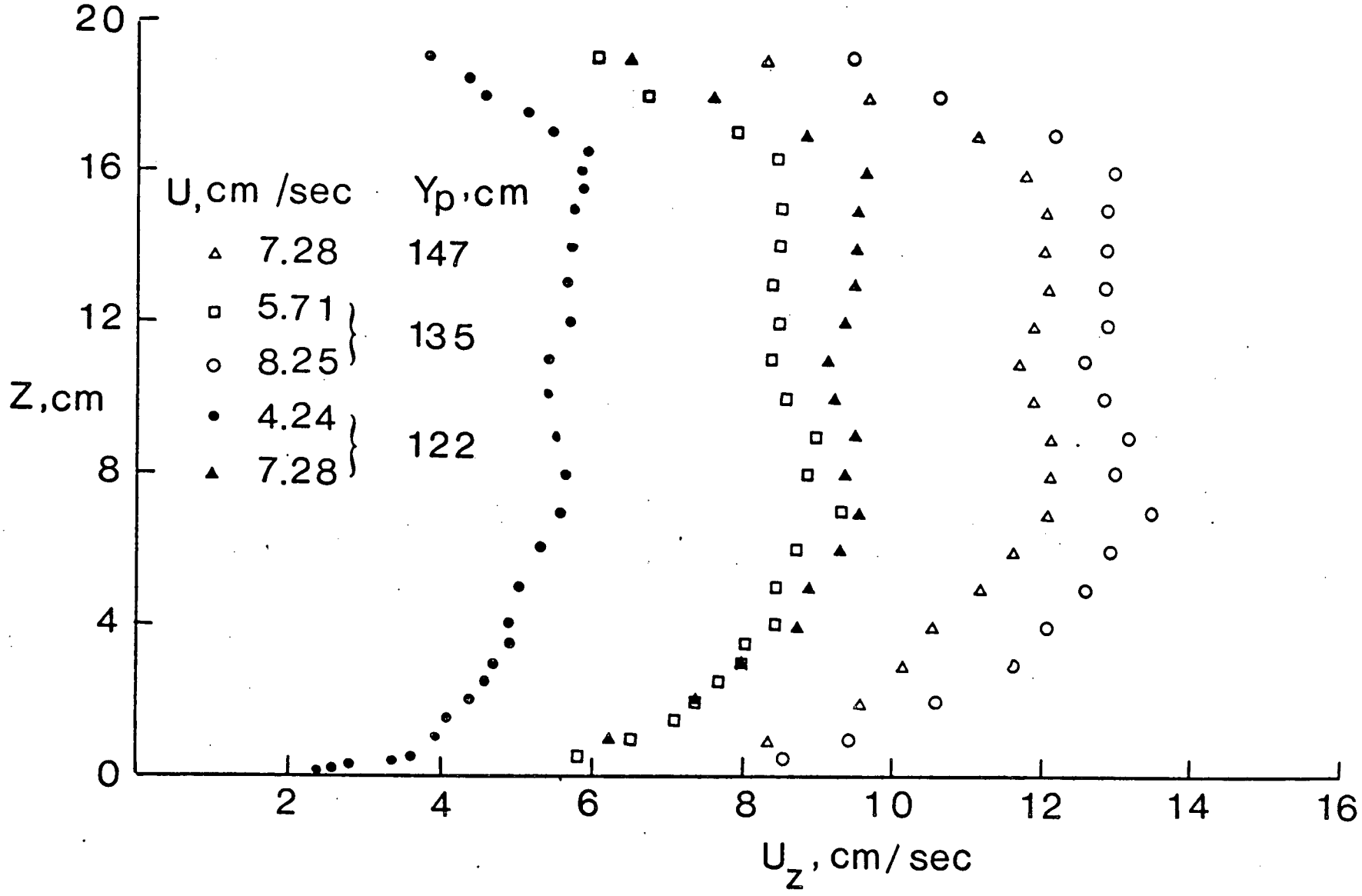

Figure 4-4 Velocity profiles as affected by the valve model

solution at the Reynolds number of 3000 (the highest for the glycerol solution in the test program). Even here, the maximum deviation from the mean over the valve entrance amounted to only 2.5%.

4.2 Choice of Reference Velocity and Pressure

The velocity profiles bring to light an important question of reference or characteristic velocity and pressure that can be used in presenting data. Clearly, with model immersed in an unbounded uniform stream there is no ambiguity in the definition of these parameters: it is the constant velocity and pressure of the stream far away from the model. For low Reynolds number flow in a tunnel, however, the fluid velocity and pressure vary significantly along the axis of the test section, even in the absence of the model due to the boundary layer growth along the walls. The presence of model and the associated wake would only accentuate this problem. Obviously some compromise is indicated in selection of these parameters.

Grove et al.[124,125] have suggested the use of the pressure directly below the centerline of their model as the reference static pressure and the centerline velocity, with the model absent but at the same setting of the pump, as the characteristic velocity. For models with small blockage

this choice of reference pressure may prove to be adequate but at a larger blockage, due to acceleration of the flow at the model location, the reference pressure is indeed affected and becomes a function of wall confinement (besides other parameters). To put it differently, the choice of reference pressure as suggested above has a degree of optimism implicit in it. It assumes that the effects of the upstream adverse pressure gradient created by the presence of the model exactly cancels the influence of the acceleration in the gaps at the model location thus giving the desired P_∞.

One possible improvement in the choice of P_∞ would be to take it as the pressure at the model location (but without the model) with operating condition of the tunnel kept the same as that used with the model in position. However, this still leaves us with the problem of selecting a suitable reference velocity.

Usefulness of the centerline velocity as a characteristic velocity also poses several questions. As indicated by Figures 4-1 to 4-4, the velocity profiles are substantially affected by location, boundary layer growth, screen's mesh size, blockage, pump speed and the total circuit resistance. Hence the U_∞ proposed by Grove et al. can hardly be considered a suitable reference.

Another possible compromise would be to take uniform portion of the velocity profile far upstream and use it as a characteristic velocity. However, the distance

involved to account for boundary layer effects would, in general, depend upon the tunnel used, model and its location.

A rather significant point to keep in mind in presenting data is to ensure its repeatability by other investigators, using different test facilities, to permit comparison. With this in mind and after careful consideration of the alternative methods discussed above in conjunction with the pressure and velocity data in hand, a compromise characteristic velocity, average velocity in the test section based on the mean flow rate, was adopted. This approach has several obvious advantages. It eliminates most of the problems mentioned above.

A series of tests conducted with and without models (but at the same pump setting as with the model) showed the reference velocity to vary by less than 8% (Figure 4-5). Thus, not only does it eliminate the question of model location, type of tunnel, flow straighteners used and size of the test section but also overcomes problems of pressure gradient and blockage. The choice would facilitate the duplication of R_n, reference velocity being more precisely defined. Furthermore, its measurement is quite simple and involves only conventional instrumentation. However, it must be emphasized that this does not correct for changes in velocity profile with distance and hence the location of the model.

We are still faced with that ellusive task of selecting P_∞. As discussed earlier, the P_∞ advocated by

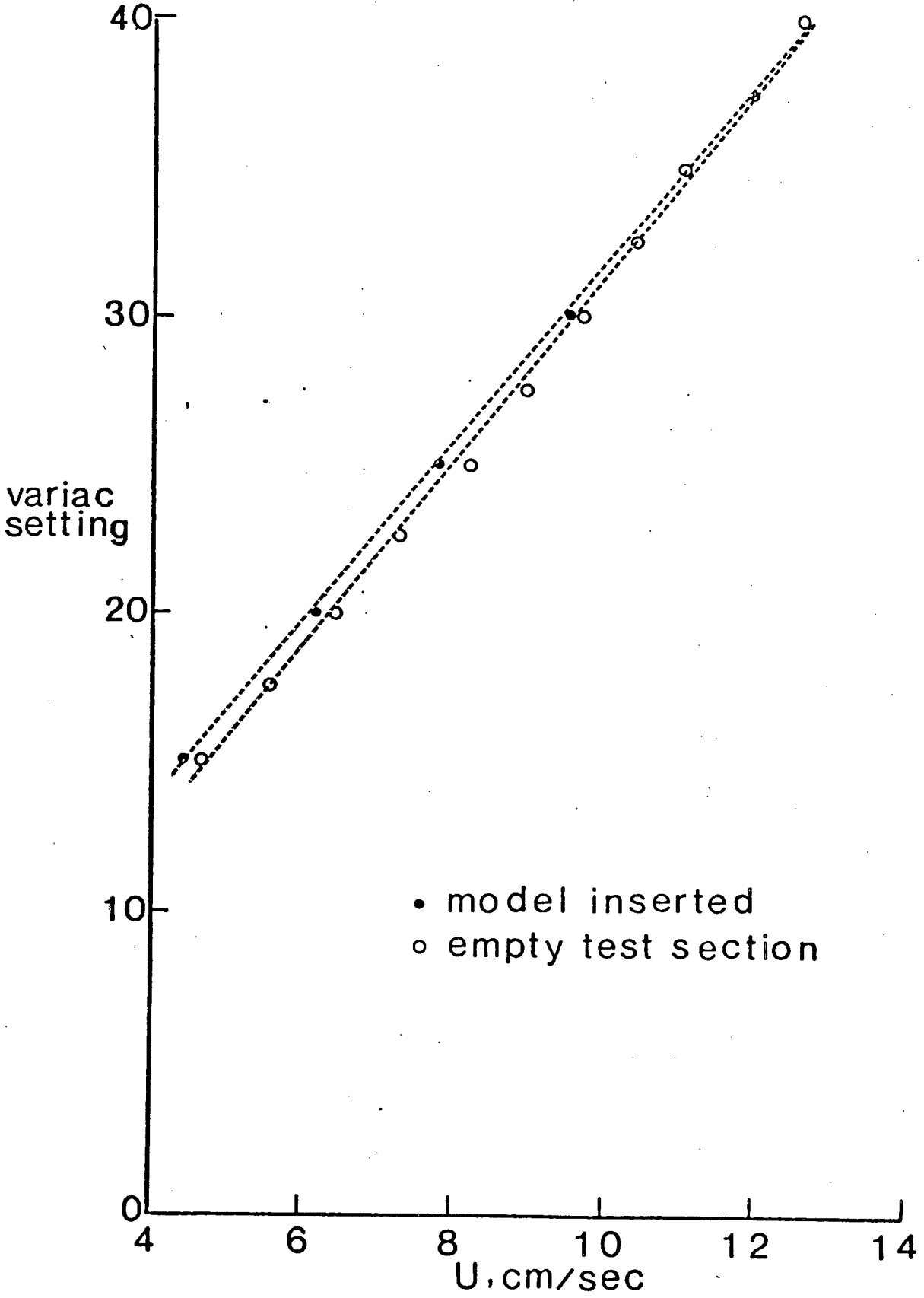

Figure 4-5 Blockage effect on the mean flow rate as indicated by the variac setting

Grove et al. has little meaning here in view of the large blockage presented by the model. From the point of view of repeatability and comparison of data, the use of pressure at a specified tap on the surface of the model as reference appears quite attractive. Although this cannot account for the local variation of blockage effects (from point to point at the surface of the model) it could compensate for it in an average fashion.

Thus one way to present pressure data in coefficient form would be as $\hat{C}_p = (P_\theta - P_r)/(\rho U_\infty^2/2)$ where P_r corresponds to the pressure at the specified tap on the surface of the poppet and U_∞ as calculated from the average flow rate (average flow rate/test-section area of 8 in. x 8 in.). However, this definition is still susceptible to errors introduced by non-uniformity of the velocity profile (at a pressure tap and the reference location). One way to virtually eliminate it is to express the pressure coefficient as explained below (Figure 4-6).

Let errors in pressure due to non-uniformity of the velocity profile be ε_0 at P_0, ε_θ at P_θ and ε_r at P_r. Expressing pressure coefficient as the ratio of the differential pressures, between that at a tap in question and the stagnation point with respect to the reference pressure, gives

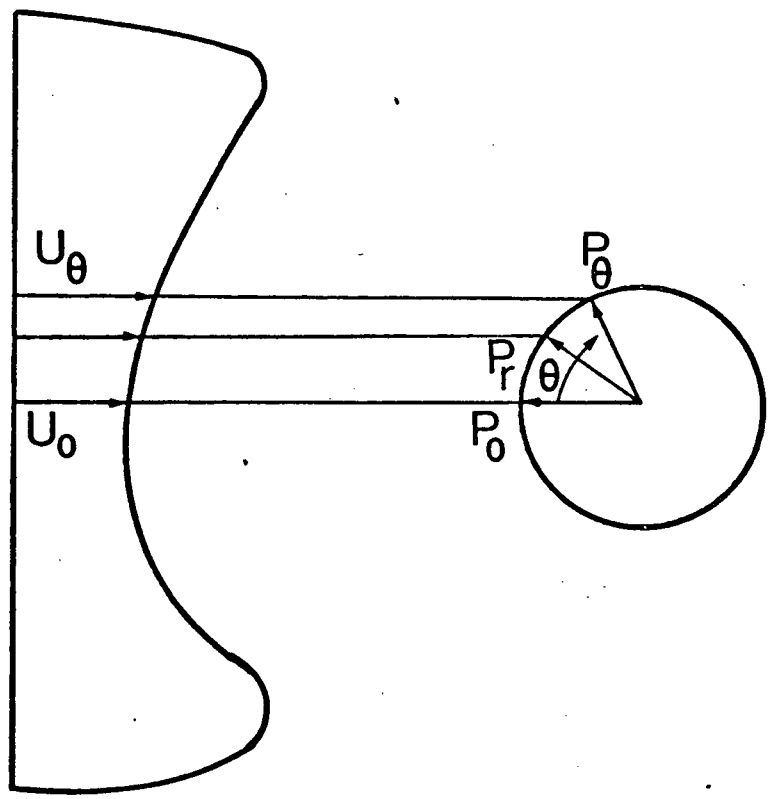

Figure 4-6 An illustration showing possible errors introduced by non-uniformity of the velocity profile

$$C_p = \frac{(P_\theta + \varepsilon_\theta) - (P_r + \varepsilon_r)}{(P_0 + \varepsilon_0) - (P_r + \varepsilon_r)}$$

where P_θ, P_r, P_0 correspond to pressures with uniform velocity profile. Thus

$$C_p = \left(\frac{P_\theta - P_r}{P_0 - P_r} \right) \left(\frac{1 + \dfrac{\varepsilon_\theta - \varepsilon_r}{P_\theta - P_r}}{1 + \dfrac{\varepsilon_0 - \varepsilon_r}{P_0 - P_r}} \right)$$

Note that $\varepsilon_\theta - \varepsilon_r$ and $\varepsilon_0 - \varepsilon_r$ are likely to be very small. On the other hand, $P_\theta - P_r$ and $P_0 - P_r$ represent relatively large quantities compared to the respective error differentials. Therefore, $\varepsilon_{\theta r} = \frac{\varepsilon_\theta - \varepsilon_r}{P_\theta - P_r}$ and $\varepsilon_{0r} = \frac{\varepsilon_0 - \varepsilon_r}{P_0 - P_r}$ are likely to be vanishingly small. Consequently, the term $\frac{1 + \varepsilon_{\theta r}}{1 + \varepsilon_{0r}} \simeq 1$ and $C_p \simeq \frac{P_\theta - P_r}{P_0 - P_r}$. This definition of the pressure coefficient promises to provide adequate compensation for errors introduced by non-uniformity of the velocity profile.

The reference location was taken to be at $\theta = 60°$. The choice was prompted by the test data which showed $\hat{C}_p$ to reach zero in the general vicinity of $\theta = 60°$, i.e. $P_{60} \simeq P_\infty$. Of course, in general, location of the reference pressure is entirely arbitrary. The pressure data presented in this chapter use the definition of pressure coefficient as

$$C_p = \frac{P_\theta - P_{60}}{P_0 - P_{60}}$$

It is easy to recognize the term $P_0 - P_{60}$ as an approximation of $0.50\ \rho U_\infty^2$. However, now we are likely to account for the errors introduced by non-uniformity of the velocity profile. Thus, in summary, this coefficient has several advantages: it tends to compensate for blockage effects, irregularity of the velocity profile and possible errors in pressure measurements caused by electrical drifts of the pressure measuring

system (the electrical drift was discussed in Chapter 3). Furthermore, in conjunction with the Reynolds number (based on average flow velocity and the poppet diameter), it promises to assist in duplication and comparison of similar data by other investigators using different test facilities.

4.3 Static Pressure Distribution

4.3.1 Stationary sphere

The tests were conducted on a set of spheres ranging in diameter from 0.5 - 2.5 in. in glycerol as well as water in the Reynolds number range of 74 - 5848. In all the cases, the model was supported by a vertical stem, a stainless steel tubing, which also served as a pressure conducting line. Its outside diameter was dictated by the relative size of the sphere and the stem influence on the pressure field. On the other hand, the inside diameter was governed by the time constant to reach the steady state pressure as discussed before. A series of tests conducted with 2.5 in. diameter sphere supported either by a vertical or horizontal stem showed that the sphere to stem diameter ratio must be least seven to make stem interference negligible (Figure 4-7). The pressure measurements were confined to the horizontal meridional section of the model. A 1/16 in. pressure tap

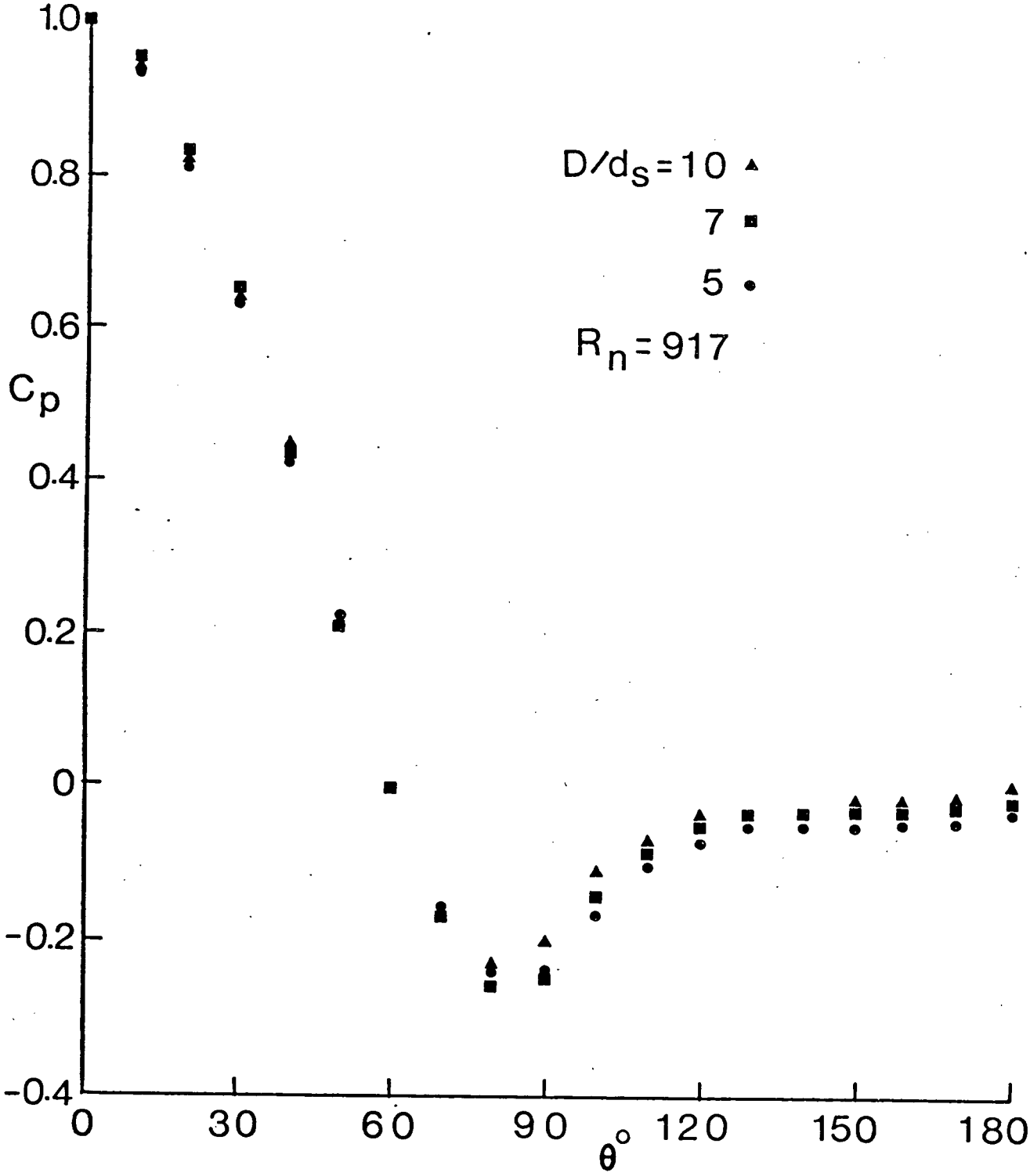

Figure 4-7 Effect of the supporting stem on the profiles for a 2.5 in. sphere

connected the stem through a groove (1/16 in. dia.) drilled in the body of the sphere (Figure 4-8). The entire horizontal plane was covered by a controlled rotation of the stem in a step size of 10°. Due to sectional symmetry, the measurements in general were confined to only one side of the sphere, except for occasional checks to confirm flow symmetry. The heat exchanger described earlier held temperature of the working fluid constant within 0.2°C during the test period.

Before proceeding to present and analyze the results in detail, it would be of interest to compare the data reduction procedure adopted here with that discussed by Grove et al. The comparison for a representative set of data is shown in Figure 4-9. Note the use of $\hat{R}_n$ in Figure 4-9(a) due to a different definition of the Reynolds number used by these authors. Several points of interest become apparent. Essentially linear drop from the front stagnation to zero pressure coefficients is exhibited by both the systems of data presentation. Note that $\hat{C}_p = 0$ at $\theta \simeq 50°$, thus our choice of P_r at $\theta_r = 60°$ is indeed going to be close to P_∞. However, the most important departure, and here the advantage of using C_p becomes evident, is in and around the separated region. The large spread in $\hat{C}_p$ data, which is due to the combined effects of the Reynolds number and blockage, is definitely reduced by the use of C_p as shown in Figure 4-9(b). This suggests at least partial compensation of the blockage effects as anticipated before in Section 4.2.

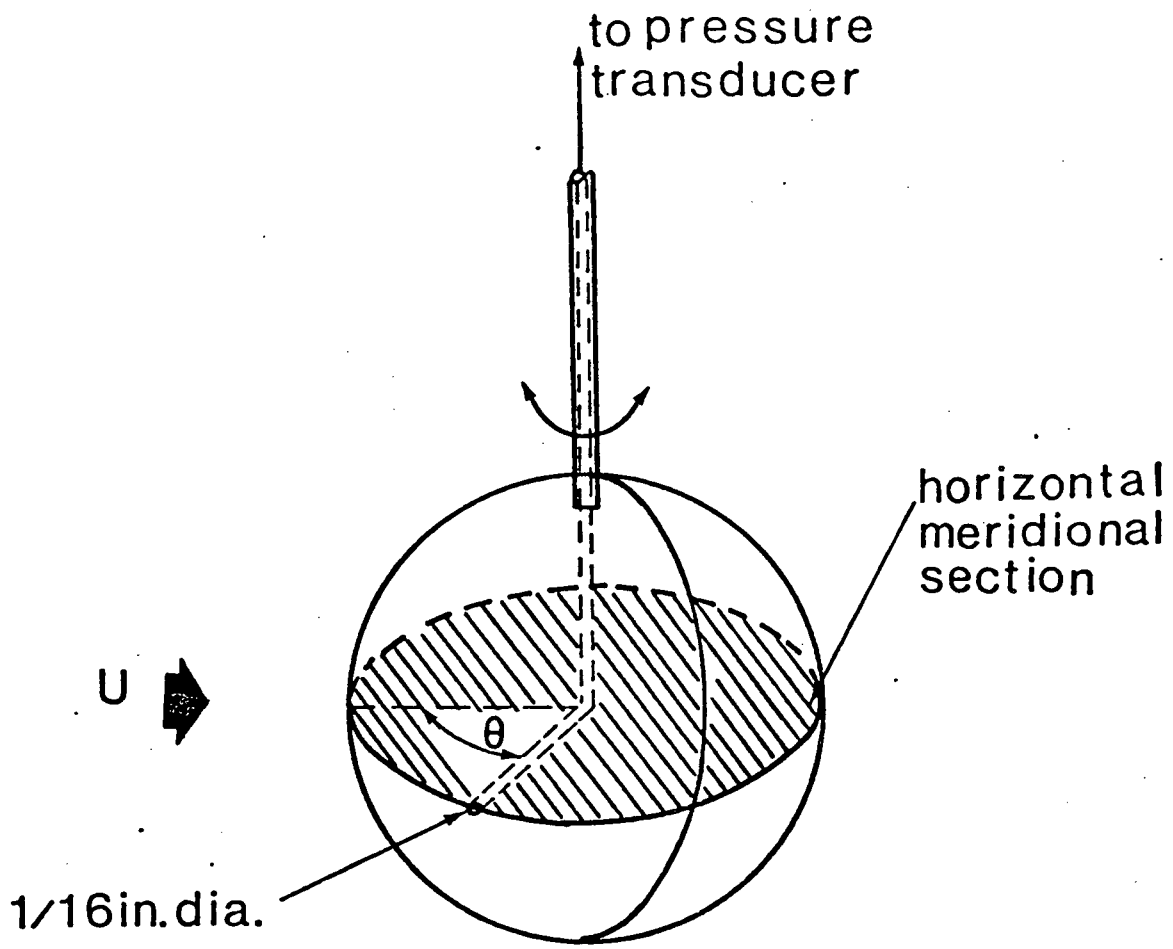

Figure 4-8 A schematic drawing showing the spherical model and its support during the pressure measurements

Reynolds number effects, over its discrete ranges, on the surface pressure distribution are presented in Figure 4-10. It is apparent that the region bounded by the front stagnation and zero pressure points is virtually independent of the Reynolds number (Figure 4-9 (b) also leads to the same conclusion). Note that location of the zero pressure point ($C_p = 0$) is fixed by the choice of the refer-

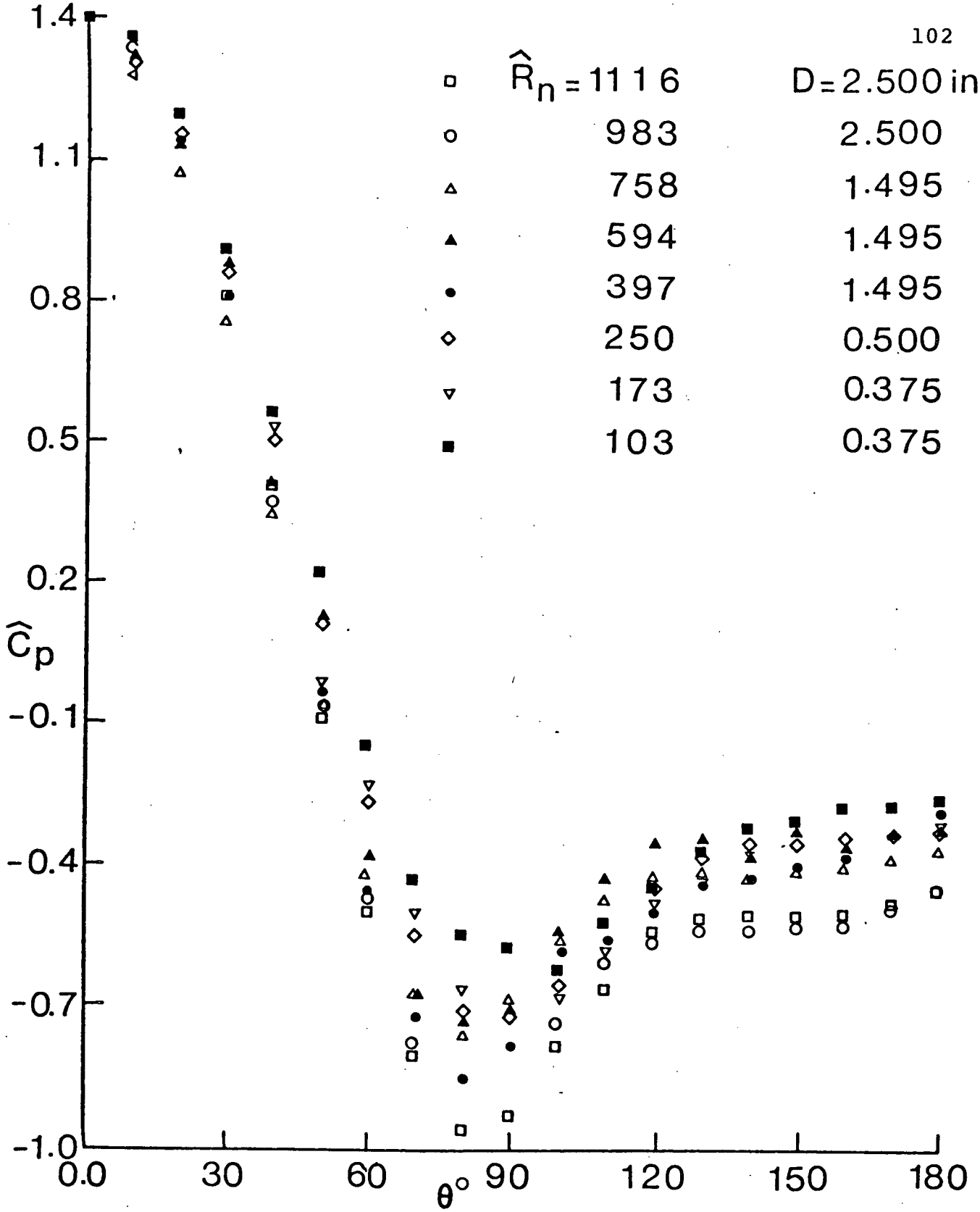

Figure 4-9 Typical C_p profiles around the meridional section of a sphere: (a) data reduced as suggested by Grove et al.[124]

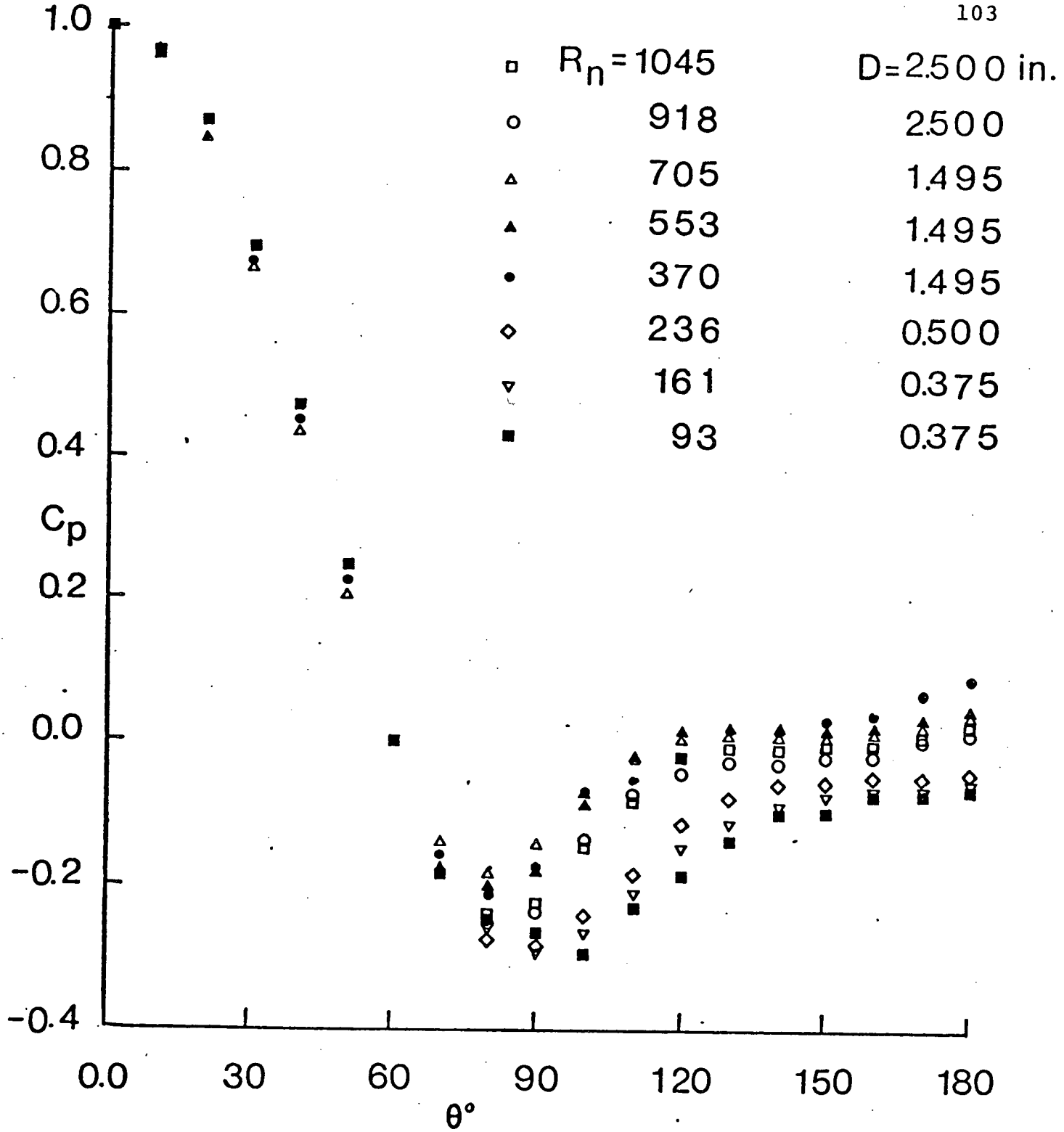

Figure 4-9 Typical C_p profiles around the meridional section of a sphere: (b) data reduced according to the proposed technique

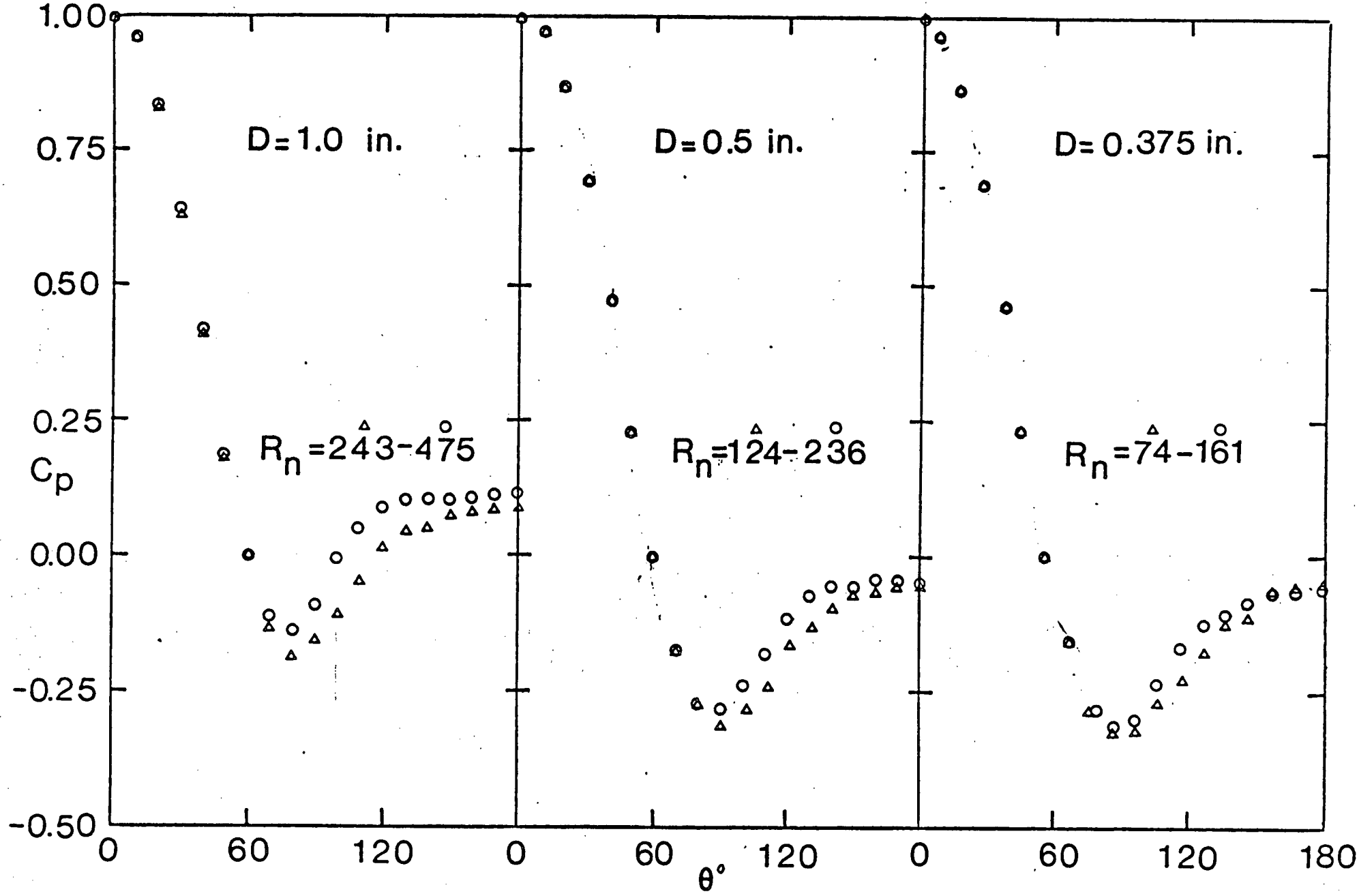

Figure 4-10 Reynolds number dependency of the pressure distribution around a sphere: (a) R_n = 74-475

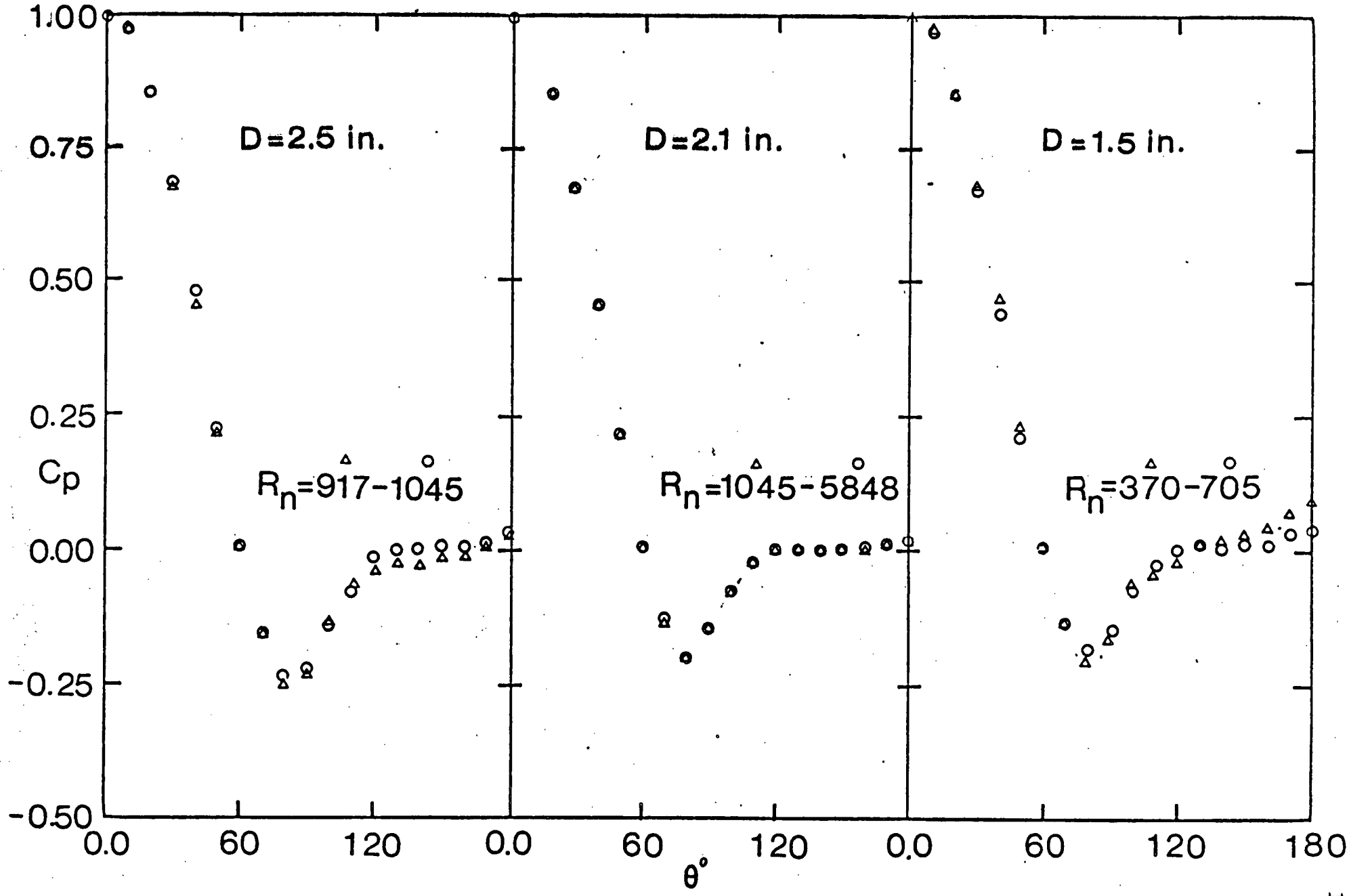

Figure 4-10 Reynolds number dependency of the pressure distribution around a sphere: (b) R_n = 370-1045

ence pressure. However, as indicated by Figure 4-9(a), even location of the zero pressure point $\hat{C}_p = 0$ remains essentially fixed in the Reynolds number range investigated. Thus influence of the Reynolds number is primarily confined to the region downstream of this location.

Figure 4-10 also shows an interesting trend of forward shift of both, location of the minimum pressure point and the separation point (approximately represented by the beginning of a flat profile in the wake) with increase in the Reynolds number. This can also be deduced from Figure 4-9(b). Magnitude of the minimum pressure remains essentially constant for $R_n < 240$ (Figure 4-10a). However, in the Reynolds number range of 240-475 it shows a sudden rise. Beyond this the minimum pressure again attains an almost constant value but at a slightly lower level (Figure 4-10b). In fact, this form of behavior is also exhibited by the pressure plots in separation and wake regions. To better visualize this sudden rise in pressure, both pressure at $\theta = 180°$ and average base pressure (average over the region $\theta = 120° - 180°$) are plotted in Figure 4-11. The rise in pressure is indeed quite spectacular. No definite explanation was readily available, however, it was suspected to be associated with a fundamental change in the character of the vortex ring and the wake downstream. In any case, it clearly suggested a need for flow visualization study to confirm this explanation.

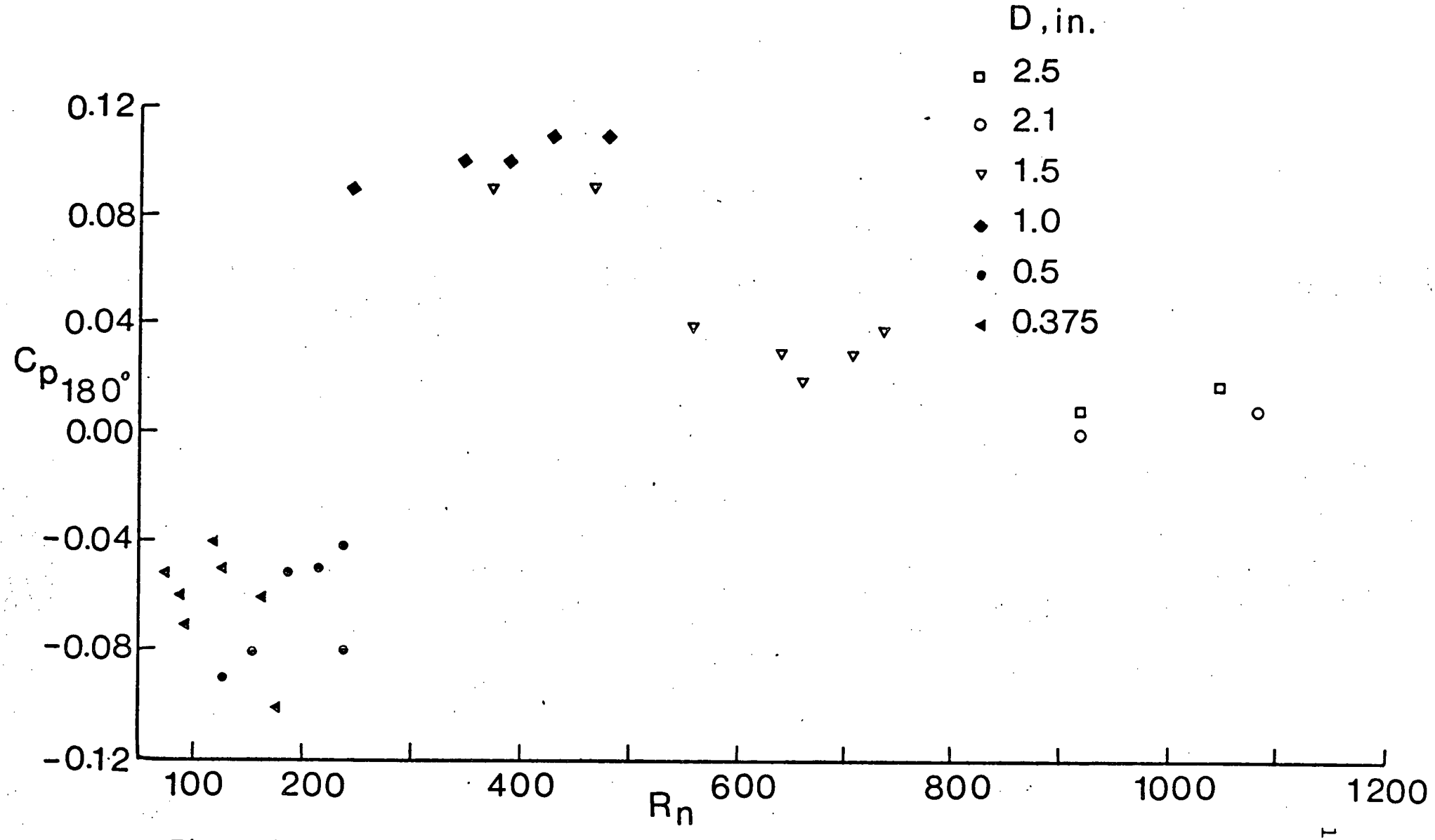

Figure 4-11 Effect of Reynolds number on base pressure coefficient: (a) pressure coefficient at $\theta = 180°$

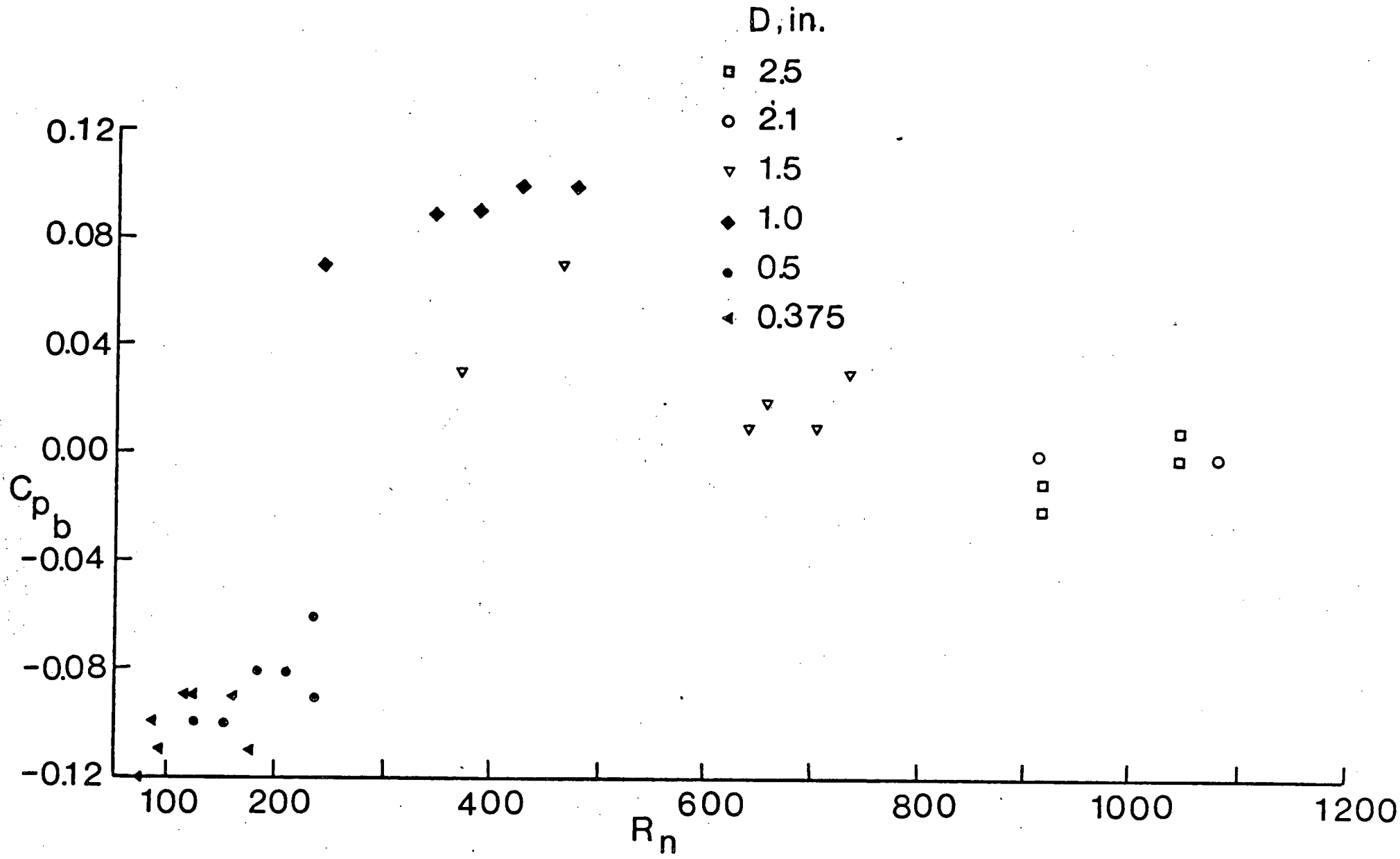

Figure 4-11 Effect of Reynolds number on base pressure coefficient: (b) average wake pressure

It must be emphasized here that such detailed measurements of pressure distribution on the surface of a sphere in the indicated low Reynolds number range (R_n = 90 - 5000) have not been recorded in literature. On the other hand, numerous analytical attempts do exist[82-101]. Probably the most relevant to the present range of Reynolds number is the numerical analysis by Rimon and Cheng[99] who solved the complete Navier-Stokes equations using a finite difference approximation to vorticity transport in conjunction with spherical polar grid system. Large velocity gradients encountered in the analysis raised some questions concerning the stability of the integration procedure. Rimon and Cheng's results (R_n = 1 - 1000) are compared with present experimental data in Figure 4-12. Discrepancies between the two sets of results in the vicinity of the separated region are rather striking and tend to increase with an increase in the Reynolds number. The numerical results consistently predict higher pressure in this region. The discrepancy may be attributed to the inherent limitations in the numerical procedure used and would lead to lower drag prediction. Furthermore, as pointed out by the authors themselves, their theoretical development is valid for axisymmetric flows. However, for $R_n \simeq 250 - 300$, the flow becomes asymmetric due to the onset of wake oscillation as explained in the following section. Thus validity of the theory beyond $R_n > 300$ is indeed questionable.

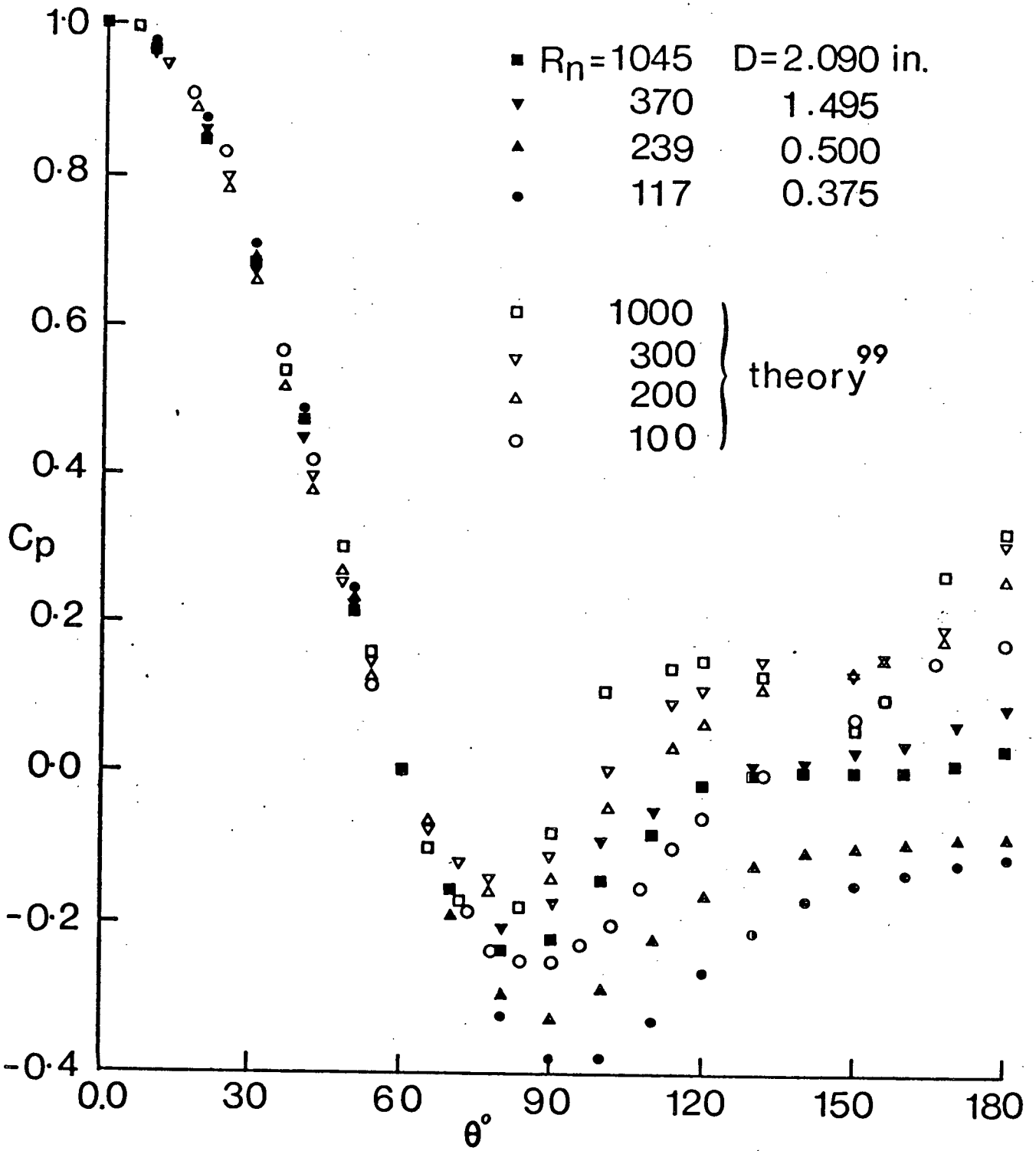

Figure 4-12 A comparison of the theoretical and experimental pressure distributions on the surface of a sphere

The pressure distribution data were integrated to obtain variation of C_d with the Reynolds number as shown in Figure 4-13. Important results of experiments and semi-empirical theory[126] as reported in the literature are also included for comparison. The classical drop in drag with the Reynolds number represents resultant influence of the minimum pressure, its location and the pressure distribution downstream of it. Considering the fact that the experimental data themselves show wide deviations[75] (often as much as 20%), the agreement may be considered rather good. This is indeed comforting and tends to substantiate reliability of the presented pressure data.

To provide better appreciation as well as substantiation of the certain behavior exhibited by the measured data, it was decided to undertake extensive flow visualization program. A set of spheres ranging in diameter from 0.5 - 2.0 in. were used in glycerol solution medium to provide lower end of the Reynolds number range of interest. The main objective was to observe the formation, development and instability of the vortex ring and the associated influence on the measured pressure data. It was also hoped that this would provide some indication concerning location of the separation point and its movement. The use of dye injection procedure, explained in detail earlier, proved to be quite effective in achieving these objectives. It showed the formation of vortex ring in a rather spectacular

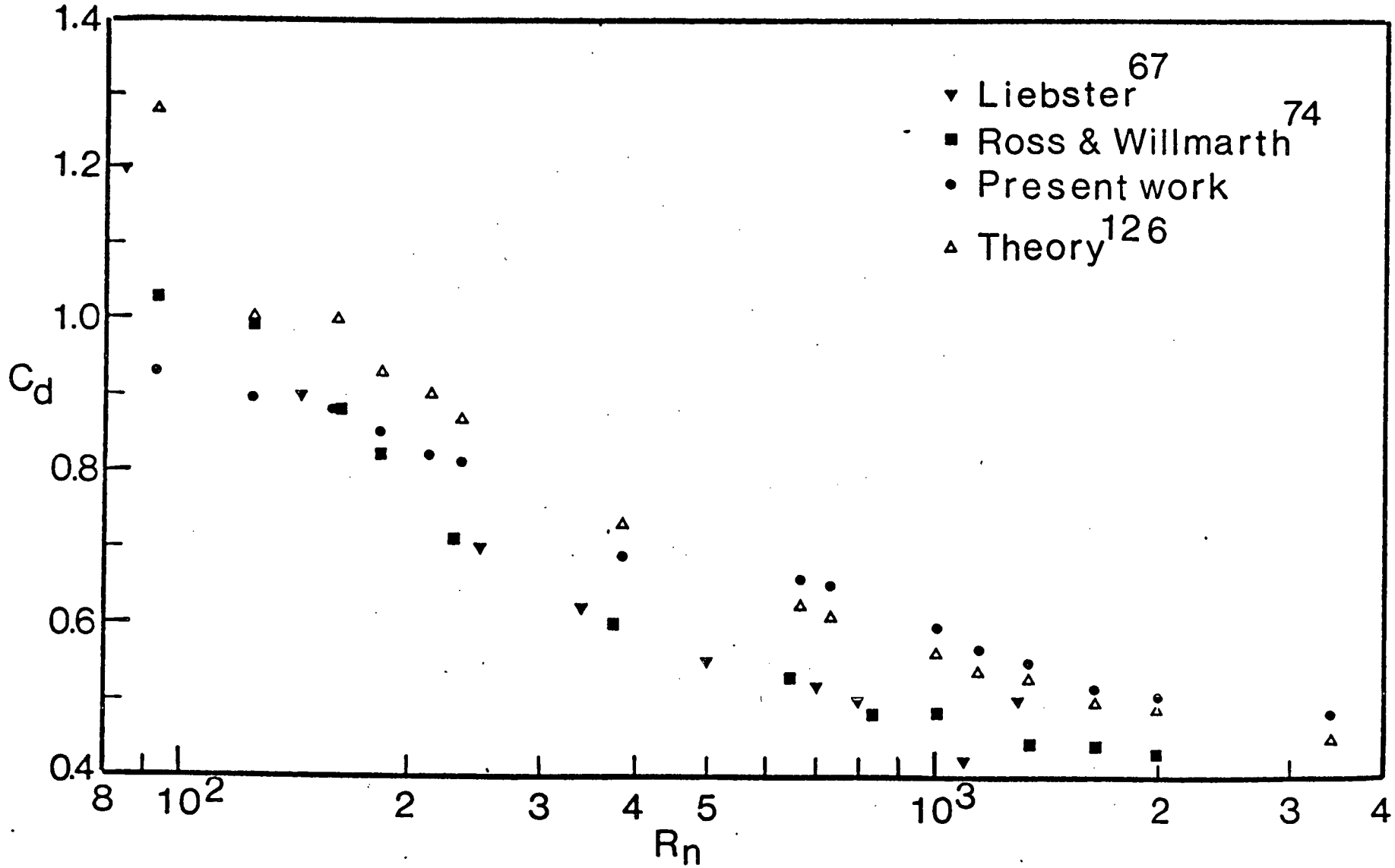

Figure 4-13 Variation of the sphere drag coefficient with Reynolds number

fashion as presented in Figure 4-14. Numerous photographs were taken at systematic increments of the Reynolds number. Only a few of the typical pictures illustrating formation, symmetric elongation, onset of asymmetry and instability followed by turbulent shedding are presented in Figure 4-15.

The existence of an axisymmetric, stable vortex ring for low Reynolds number in a stream, essentially free of macroscopic turbulence is shown in Figures 4-15(a) and (b). For the Reynolds number above a critical value (corresponding to the first formation of a stable ring, $10 < R_n < 25$), the streamlines separate from the surface and form a closed region immediately behind the sphere. A single stream emerges from the vortex of the closed region extending to a long distance behind the sphere. The size of the ring is such as to maintain an equilibrium between the rate at which vorticity is generated and dissipated into the main stream. As the Reynolds number is increased the vortex ring becomes elongated in the flow direction to maintain this equilibrium, and the separation points move upstream towards the front stagnation point (Figure 4-15a-d). This forward movement of the separation points was also suggested by the pressure plots presented earlier (Figure 4-9).

For Reynolds number between 170 - 230 an asymmetry in the circulatory motion within the vortex sheet produces a corresponding asymmetry in the circulatory motion in the sheet itself and a resultant shift from the center line.

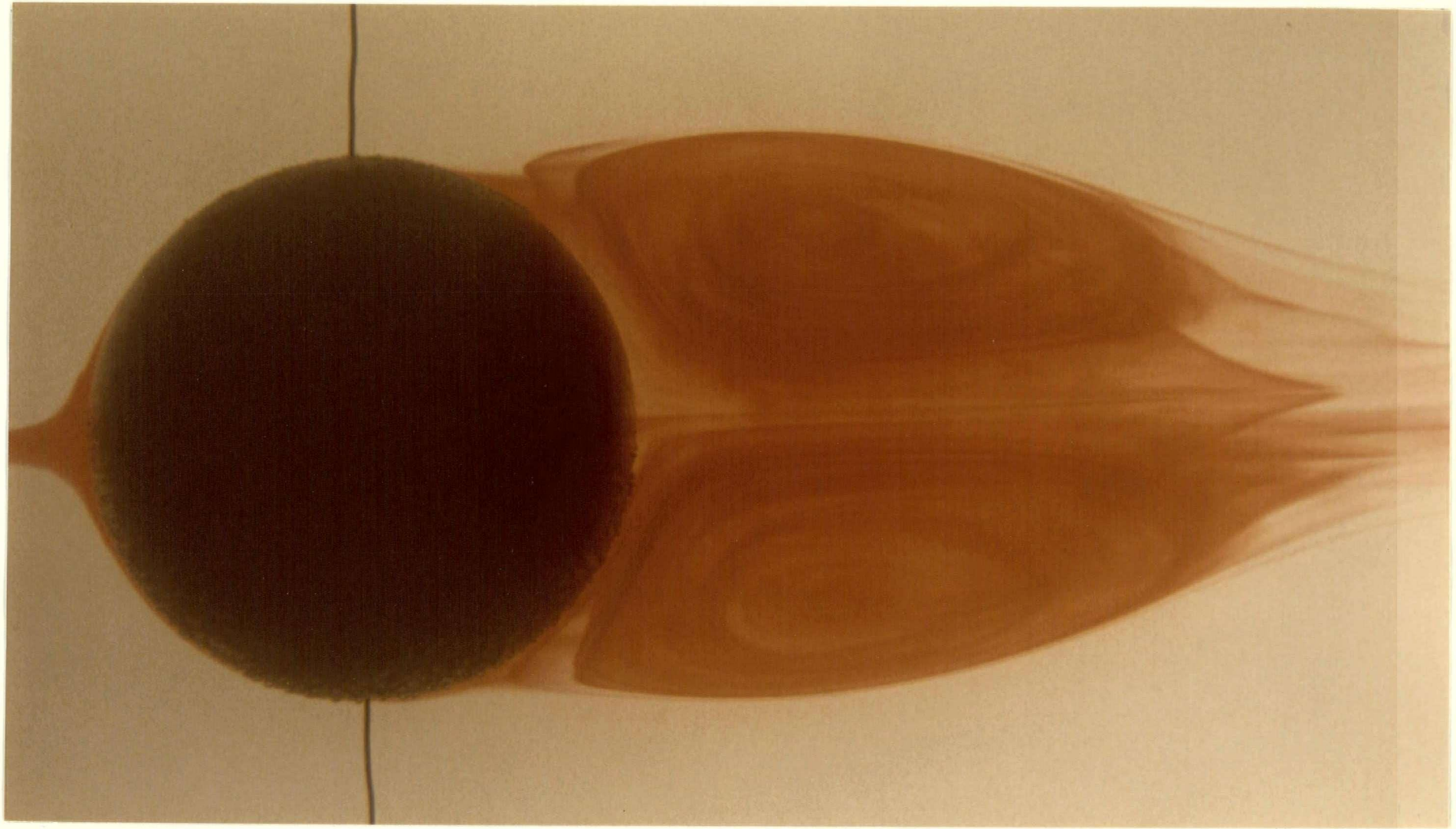

Figure 4-14 A typical photograph illustrating formation of a vortex ring behind sphere

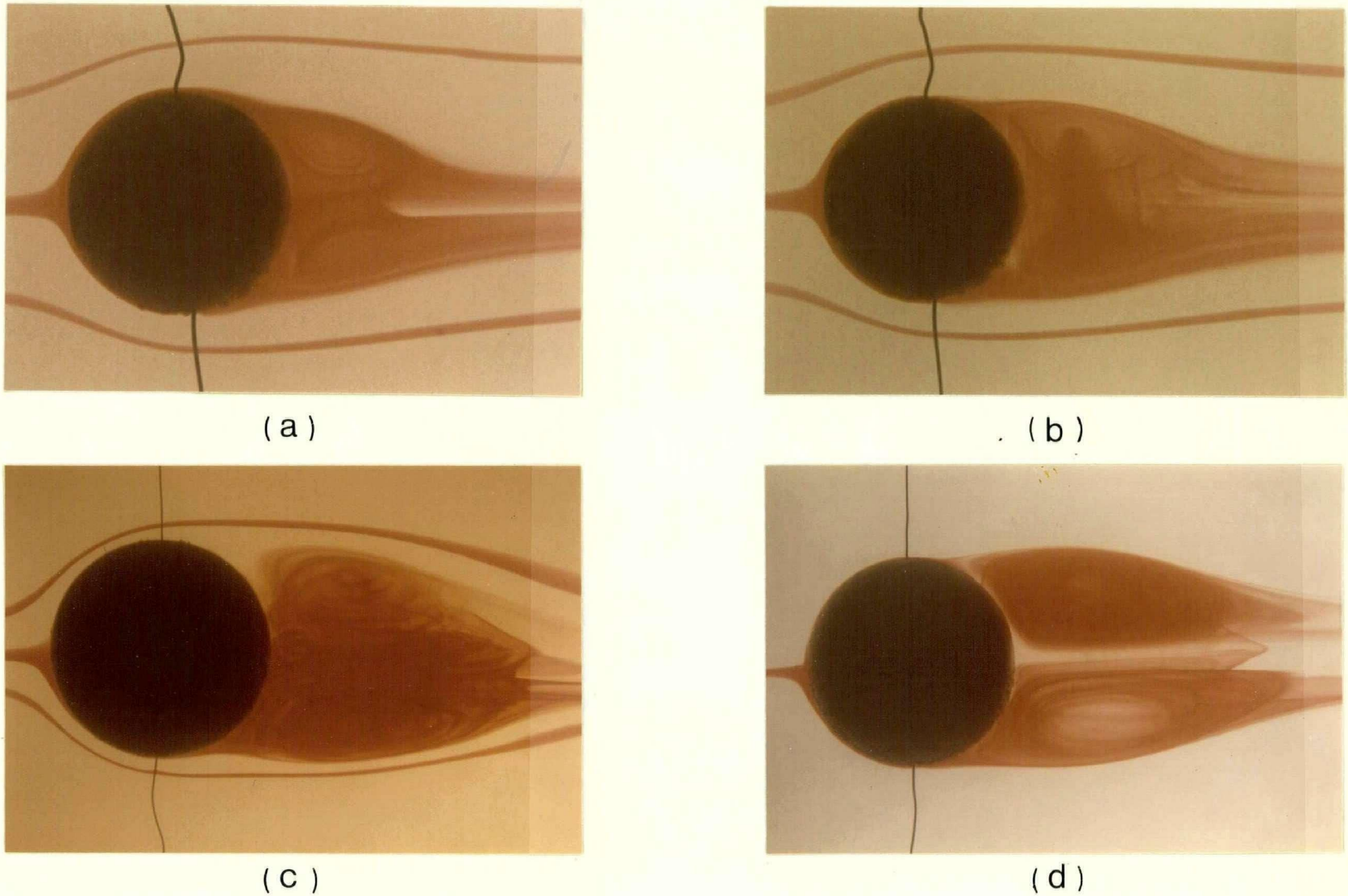

Figure 4-15 A flow visualization study showing development and instability of vortex ring with Reynolds number: (a) R_n=55; (b) R_n=92; (c) R_n=176; (d) R_n=221

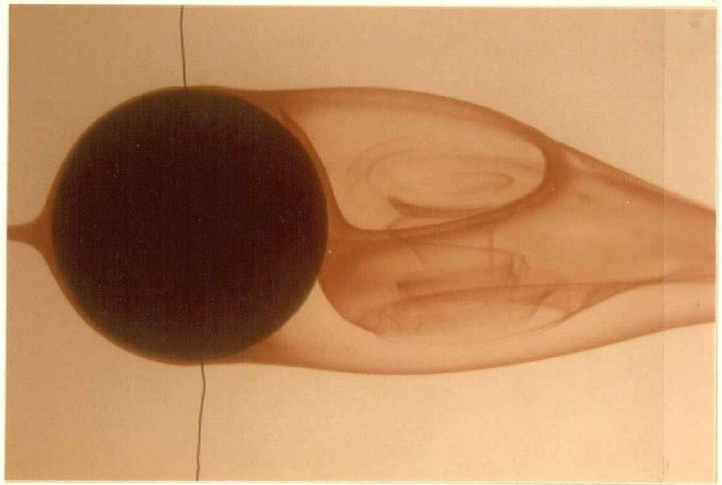

(e)

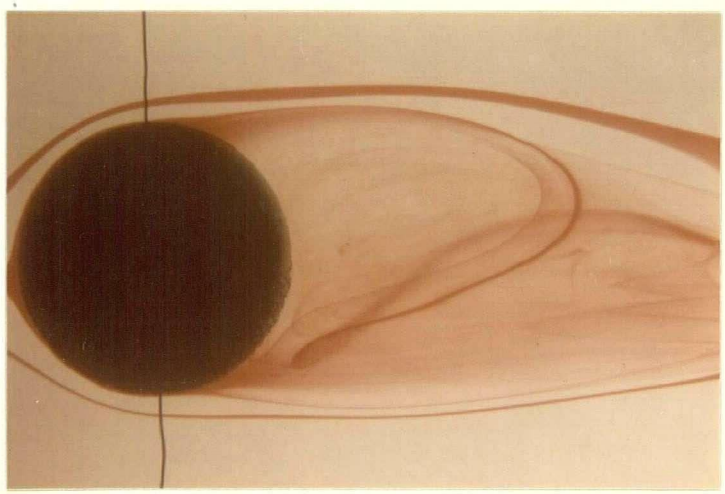

(f)

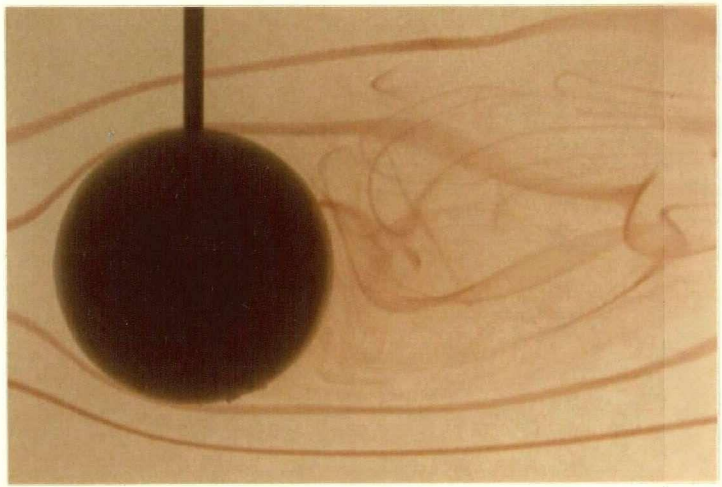

(g)

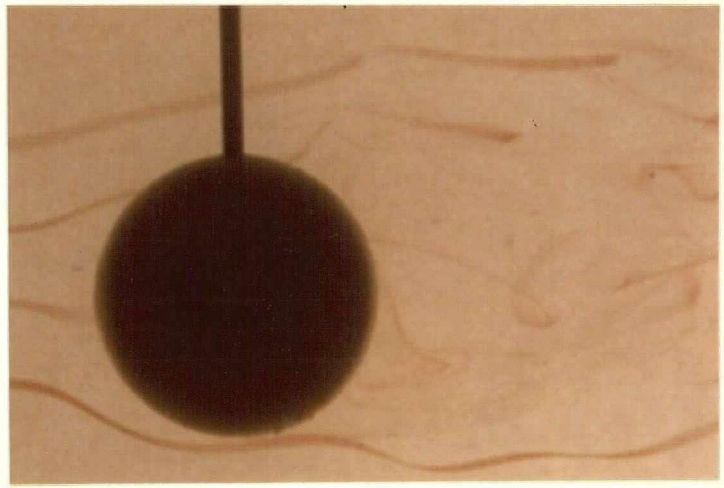

(h)

Figure 4-15 A flow visualization study showing development and instability of vortex ring with Reynolds number: (e) R_n=265; (f) R_n=289; (g) R_n=331; (h) R_n=395

This wake is followed by two distinctly inclined streamlines which maintain an equilibrium between rates of generation and diffusion of vorticity. As no rotation is observed, it is assumed that the lack of symmetry is responsible for the sidewise force component (Figure 4-15 e - f). Taneda[76] related the slight asymmetry of the vortex ring to the support effect. However, this could not be so as the asymmetry prevailed regardless of the support diameter d_s ($\frac{1}{150} < \frac{d_s}{D} < \frac{1}{16}$).

The state of unsymmetrical but steady wake is disturbed by further increase in the Reynolds number. The rate at which vorticity is diffused from the sheet into the main body of the fluid remains practically constant, but the increased rate at which it is transferred to the vortex ring creates unstable condition within the vortex sheet. Basically, the process is one of build-up and release, but no sizeable portion of the ring escapes through an opening in the end of the vortex sheet during the cycle. This in turn causes the oscillation of the asymmetrical wake about the axis of symmetry. When the vortex strength of the ring reaches a critical value, a sudden motion of the ring disturbs the sheet, which in turn is responsible for a release of vorticity and a consequent return of the ring to its original position and shape. This phenomenon appears to happen in the Reynolds number range of about 250 - 300 (Figures 4-15 e-f). Thus we have a clear explanation as to the sudden rise in wake pressure observed earlier (Figure

4-11b). It can now be attributed, with a measure of confidence, to the oscillating character of the asymmetrical ring and the attached filaments.

With further increase in the Reynolds number, the oscillatory motion of the vortex ring assumes higher frequency and the circulation within the sheet ceases to be symmetrical. In the cycle of build-up and release, the vorticity generated in the boundary layer becomes concentrated on diametrically opposite sides of the flow axis within the vortex sheet. The sections in which the vortex strength is greatest are alternately discharged into the main body of fluid. With each ejection a portion of the sheet is carried away. The vortex element discharged into the stream interacts with the disperse liquid to form a regular wake pattern. Figures 4-15 (g) and (h) represent the initiation and development of the unsteady wake which promotes regular vortex shedding.

The flow visualization results also provide useful substantiation as to the forward movement of the separation point as suggested by the pressure plots (Figure 4-9b). For this the photographs were analyzed systematically and the separation position plotted as a function of R_n as shown in Figure 4-16. Note that the separation point moves forward by as much as 17° over the R_n range of 55 - 315. For comparison, the analytical results of Rimon and Cheng[99] are also included. The results show increasing discrepancy at lower

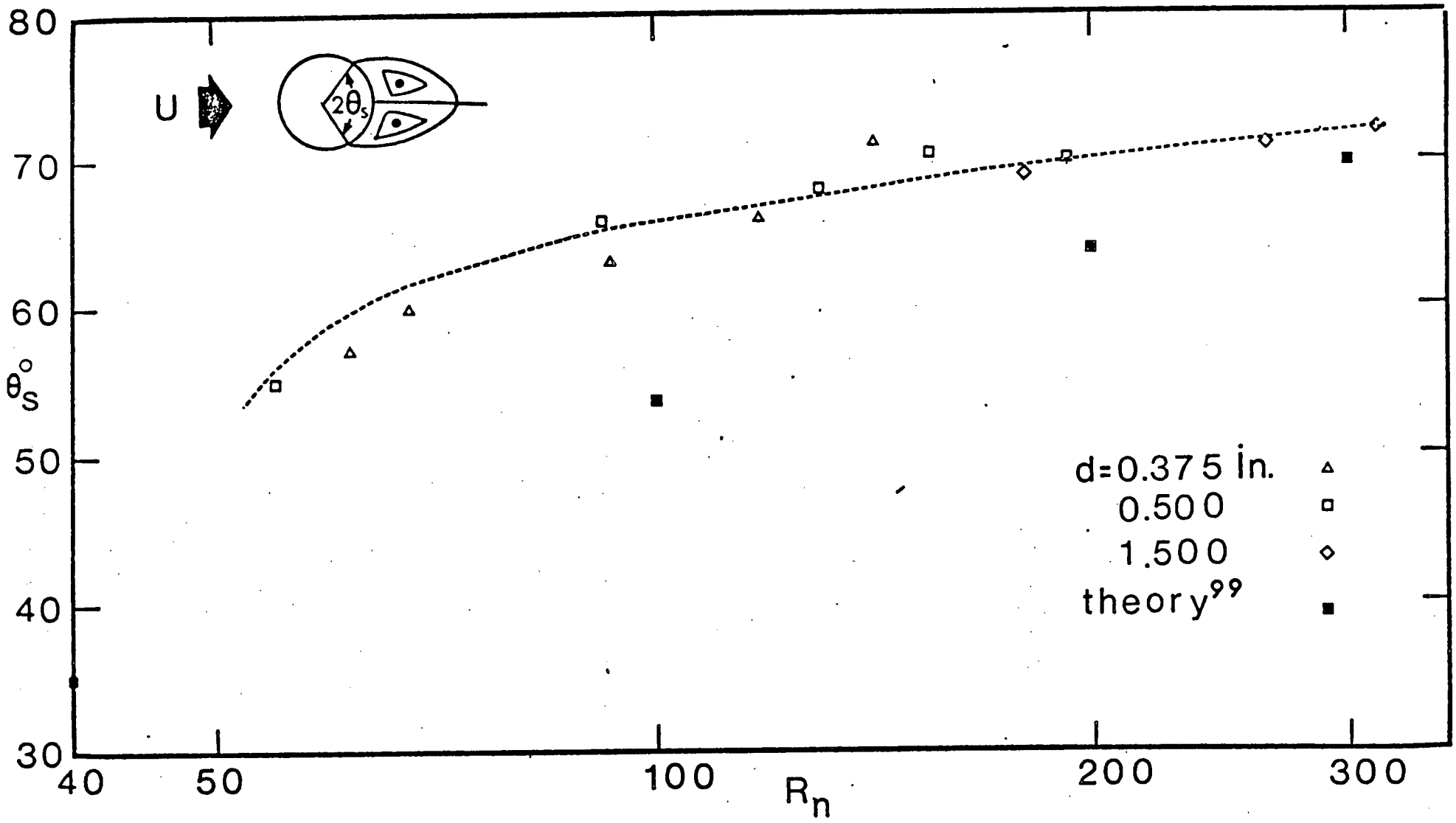

Figure 4-16 Effect of R_n on the separation angle θ_s

R_n suggesting inconsistency of some of the assumptions inherent in Rimon and Cheng's analysis. On the other hand, it must be emphasized that the visual determination of separation point is, at best, approximate. Considering this and the unstable character of the process, scatter in the experimental results is surprisingly small.

4.3.2 Pulsating sphere

The problem of dynamic forces exerted by real fluid on a submerged object when the relative velocities between the two change with time is classical and complex. As early as in 1851, Stokes[127] investigated simple harmonic and other rectilinear motions of several objects including spheres, but his approximate analysis neglected convective acceleration terms in the Navier-Stokes equations. Later Basset[128], Boussinesq[129], and Oseen[130] studied the same problem using essentially the same simplification concerning the convective terms, but with one useful conclusion. They observed that the force on the sphere depends not only on its instantaneous velocity and acceleration but also on an integral representing the effect of its entire history of acceleration. The force expression thus obtained is valid only for slowly moving but rapidly accelerating sphere.

A lull of nearly thirty years prevailed before any other important contribution in the field appeared.

Lin's[131] method for periodic external flows past a body of revolution relies on forming appropriate averages of the quantities under investigation and on a linearization of the equation describing oscillations of the laminar separation.

In the early sixties, Odar and Hamilton[132] undertook to eliminate the assumption of negligible convective acceleration terms and proposed a new force expression, which showed excellent agreement with their experimental data up to around the R_n of 60, for a sphere executing simple harmonic motion. The expression was also successful in predicting velocities of spheres during free fall in viscous fluid[133]. With appropriate modifications, Odar[134] was also able to use the expression for predicting forces on sphere accelerating along a circular trajectory.

As pointed out before, a numerical study of impulsively started sphere in the R_n range of 1 - 1000 was presented by Rimon and Cheng[99]. Using the "complete" Navier-Stokes equations in conjunction with time dependent stream function-vorticity formulation, the authors obtained pressure distribution and hence drag. Unfortunately, their steady state pressure data do not agree with the present experimental results (Figure 4-12) while their unsteady drag results showed considerable discrepancy with the experimental values of Ross and Willmarth[74].

Several items of interest become apparent at this stage:

(i) No attempt is recorded in literature to measure time history of the mean pressure on an oscillating sphere, even when the surrounding fluid is stationary (i.e. zero free stream velocity).

(ii) Any effort at theoretical and experimental correlation between the time dependent drag of oscillatory sphere is confined to the R_n of around 60.

(iii) Even here the comparison shows considerable discrepancy during the first 1.5 seconds[74].

This section studies time history of the mean pressure distributions in the R_n range of 600 - 1000, and complements the results with the flow visualization information to confirm several physical characteristics of the flow. It should be emphasized that here the time dependent displacement corresponds to a prosthetic valve in a patient (Figure 4-17). Furthermore, the free stream velocity is no longer zero as has been the case in the past.

Time history of the pressure at different surface taps on the poppet was obtained using a Barocel pressure transducer in conjunction with the U.V. recorder (Section 3.2). The displacement-time history of the poppet was recorded simultaneously along with the pressure signals. (Figure 4-17). With these in hand, C_p for a given θ can be calculated for any particular valve opening. Obviously,

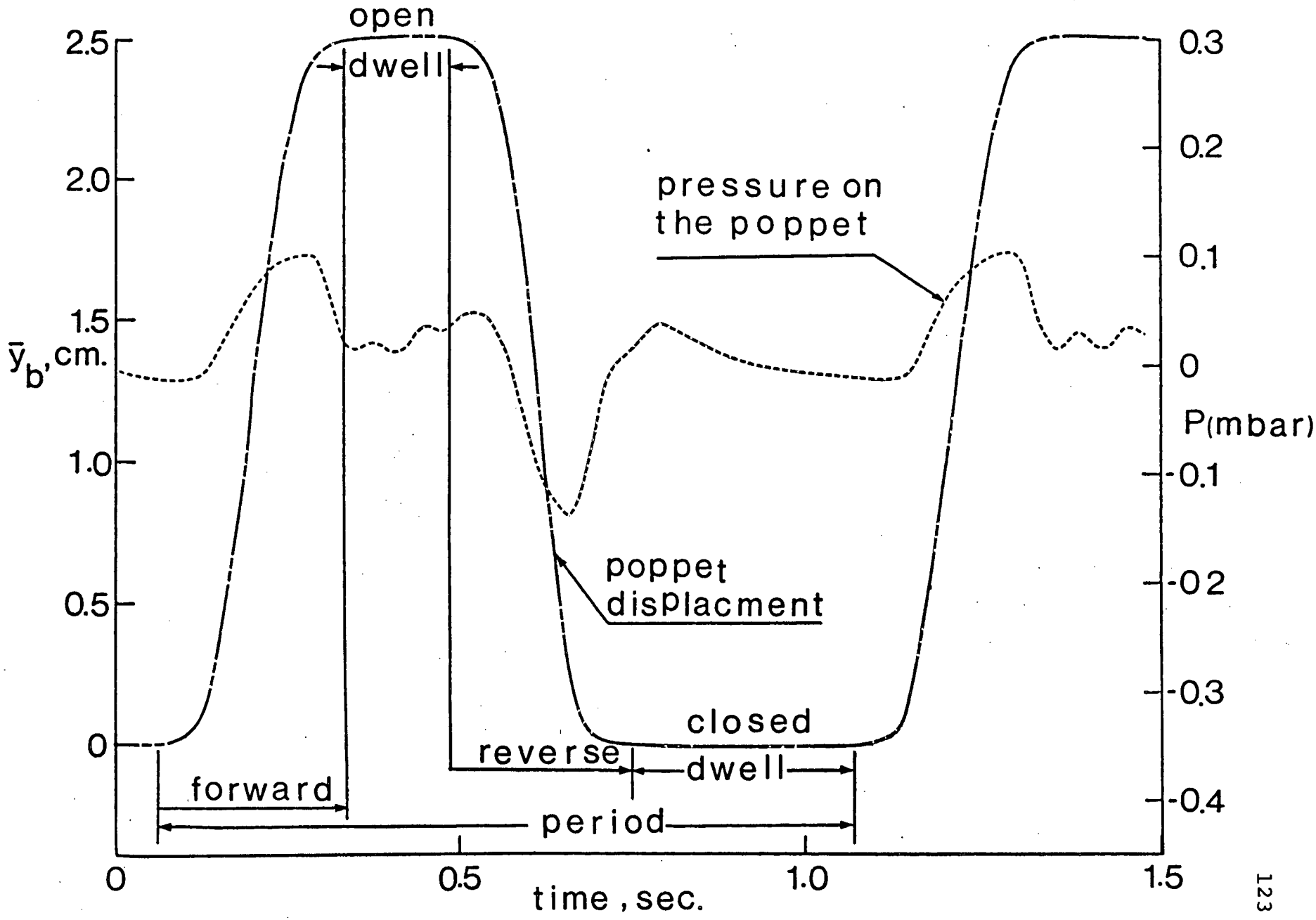

Figure 4-17 Displacement and pressure time histories for the pulsating sphere

depending on the number of values of y_b selected, many such C_p profiles can be constructed. However, for the sake of conciseness only a few of the representative profiles are given here.

Pressure distribution on the surface of an oscillating sphere placed in a uniform stream is shown in Figure 4-18. The plots correspond to four different instantaneous locations of the poppet corresponding to the valve being fully open, partially open and fully closed. Both forward and reverse portions of the cycle are considered together with two different values of the oscillation frequency. For comparison, the pressure distribution on a stationary sphere is also included.

(a) Forward stroke

During forward motion of the ball (i.e. moving upstream against the flow), it is apparent that the pressure distribution over the frontal region of the sphere ($\theta \simeq 0$-$60°$) is not significantly altered; however, beyond this the pressure data are markedly affected (Figure 4-18(i)). The mean pressure in the wake displayed a direct dependence upon the time history of the poppet position. Of particular interest is the increase in minimum and average wake pressures together with forward movement of the separation point with decreasing y_s. Although the movement of the separation point is not distinctly demonstrated by the C_p profiles

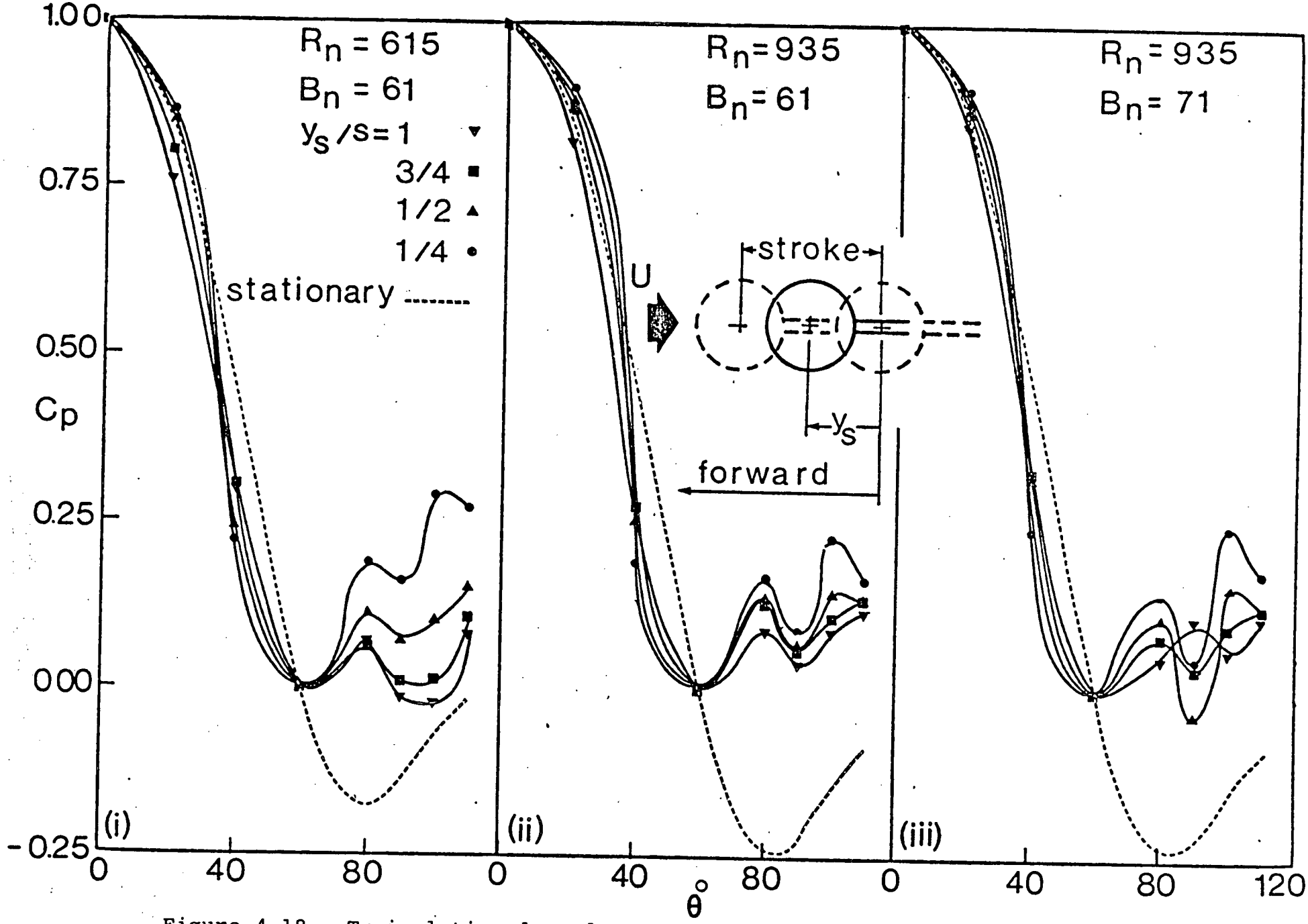

Figure 4-18 Typical time dependent pressure profiles for a sphere showing the effect of Reynolds number and pulsation frequency: (a) forward stroke

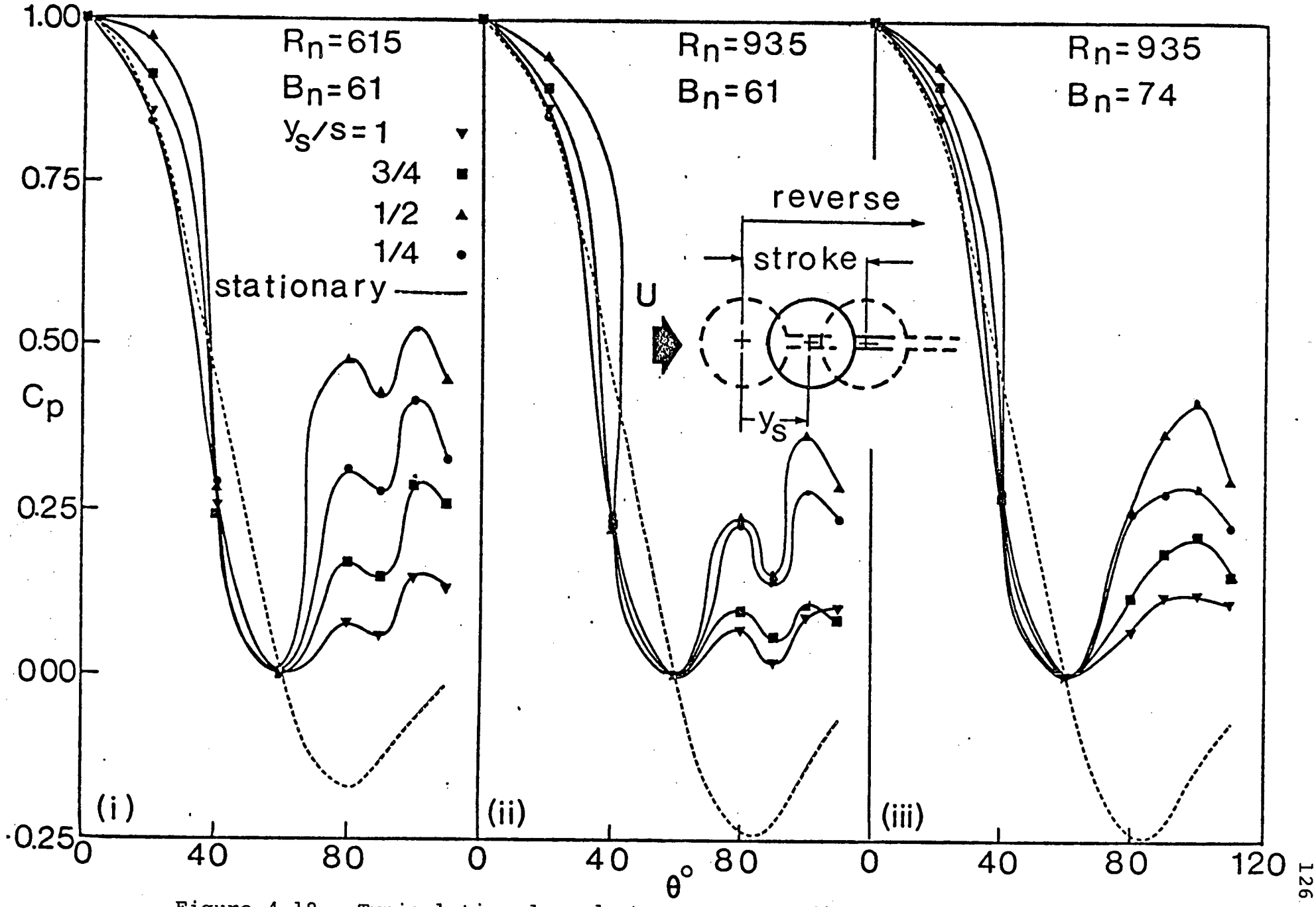

Figure 4-18 Typical time dependent pressure profiles for a sphere showing the effect of Reynolds number and pulsation frequency: (b) reverse stroke

(note that the available pressure distribution do not cover the entire wake region), it was substantiated by the flow visualization (Figure 4-19). The large changes in the wake pressure, in the beginning of the cycle, can be anticipated as here the ball undergoes a large acceleration before reaching a constant speed. Impact of the surrounding fluid, rushing in to fill the void created by the accelerating sphere, results in an increase in the wake pressure as indicated. With the attainment of a nearly uniform velocity, the rate of change of momentum in the wake is reduced leading to a relatively smaller pressure. Of course, a motion of the ball against the free stream direction leads to an increase in the effective R_n and an associated decrease in drag as depicted by the large positive pressure in the wake ($y_s = 1/4$). As the ball continues its forward movement at a constant velocity, the acceleration effect in the wake decays. Consequently, the drag increases compared to the previous case as indicated by smaller pressure in the wake region ($y_s = 3/4$). Further journey of the ball is at decelerating rates resulting in reduction of the ball velocity, i.e. lowering the effective R_n, leading to further reduction of the wake pressure. Thus recalling the effect of R_n upon C_p in the range of interest (Figure 4-10b), the observed time history of the pressure distribution is consistent with what one would expect. It is noteworthy that at the end of the stroke, $y_s = 1$, the pressure distribution is closest to the steady state condition.

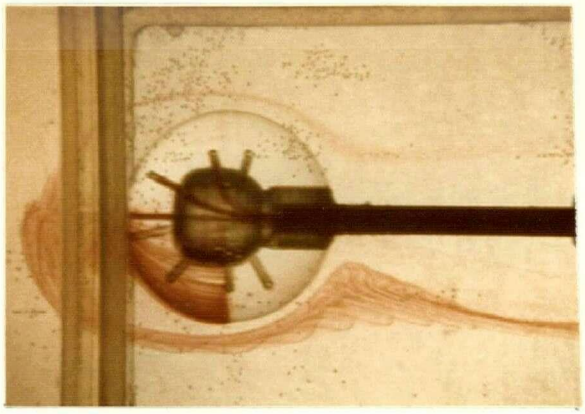

$y_s = 0.10$

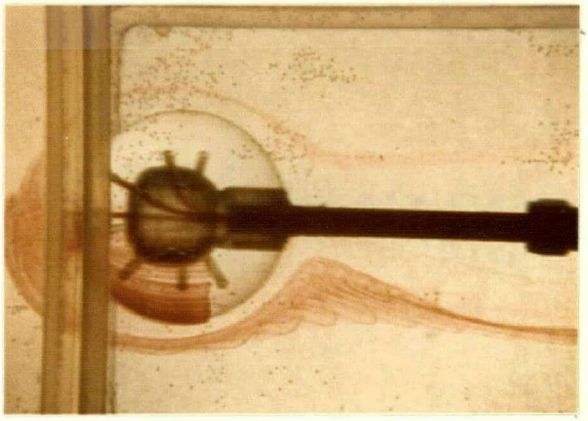

$y_s = 0.50$

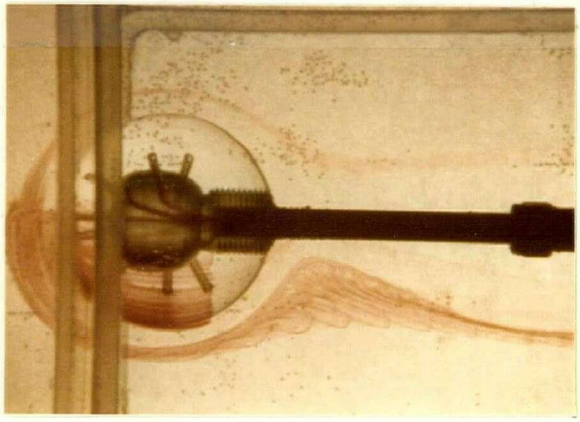

$y_s = 0.90$

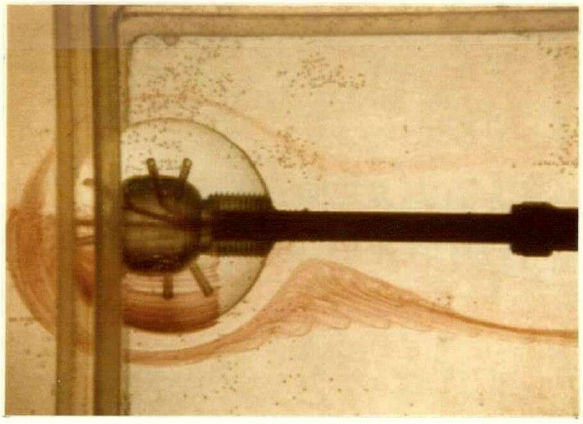

$y_s = 1.00$

Figure 4-19 A flow visualization study showing movement of separation point during pulsating motion of the sphere

Figure 4-18a(ii) shows the effect of increasing the free stream R_n on the time history of the pressure. The important aspect to notice is the clustering of pressure plots in the wake, suggesting their little dependence on the poppet position. Recognizing that the effective R_n variation for this case is in the range $935 \leq R_n \leq 3000$, where it has very little influence on C_p (Figure 4-9b), the behavior is in conformity with the expected trend.

Figure 4-18a(iii) shows the effect of Beta number [$B_n = D(\omega/\nu)^{0.5}$], which is a measure of the pulsation frequency, on C_p. In the R_n range considered and for the given variation in B_n, the pressure distribution plots are affected only by a small amount. In general, the effect of frequency is confined to local changes in the character of the base pressure plots without substantially affecting the average magnitude of the pressure. This behavior is better understood through recognition of the fact that an increase in B_n is accomplished by changing the dwell without affecting time history of the forward (and reverse) motion. At higher frequencies, obtained by further reduction of the dwell, the poppet would be essentially quasi-stationary suggesting the pressure plot to shift towards the stationary case.

(b) Reverse stroke

The time dependent pressure distribution on the surface of the poppet during the reverse stroke is shown in Figure 4-18(b). In general, the plots are similar to those

obtained for the forward stroke but with significant differences in detail. Although the pressure profiles are similar in shape, their magnitudes and dependence on the poppet position are markedly different. Note that for the values of R_n and oscillating frequency considered, the wake pressure peaks at around $y_s = 1/2$. The pressure in the wake is quite sensitive to the position parameter, certainly more than that observed during the forward stroke. These differences in pressure characteristics are understandable in light of the reduction in relative velocity and hence the effective R_n. Discontinuous reduction in the relatively small R_n range leads to distinct pressure profiles as observed earlier (Figure 4-9b). The minimum relative velocity occurs in the vicinity of the midstroke (Figure 4-17) causing the wake to attain its largest positive pressure. However, this region of near minimum velocity is rather short and the ball enters a period of high deceleration just before completing the cycle. This in turn shifts the corresponding C_p profiles towards the steady state condition.

Effect of R_n on C_p plots is quite similar to that observed during the case of the forward motion. Variation of C_p with B_n (Figure 4-18b(iii)) is also as expected: time constant of the pressure transducer being fixed, it eliminates local irregularities without substantially affecting the level of the base pressure. As before, the flow visualization study showed movement of the separation point and associated changes in the size of the wake.

During the past ten years, several investigators have conducted measurements of the fluctuating force on spheres[132,133]. However, there appears to be no published experimental or theoretical results on the pressure distribution in the R_n range of interest. The lack of information may be attributed to the intractable nature of the system, which is not amenable to known analytical procedures, and several challenging problems of instrumentation.

4.3.3 Poppet occupying different positions in the valve

Having obtained some appreciation as to the fluid dynamics of the poppet by itself, in a relatively unconfined condition, the next logical step would be to consider a more realistic situation of the ball operating in the cage. Two cases are of interest:

(i) Bypass open, i.e. when a part of the fluid flows through the valve while the remaining fluid is conveyed through the outside passages. Thus the arrangement provides for possible backflow (regurgitation) as encountered in a leaky valve. From the point of view of the tunnel's structural safety, this is a desirable condition.

(ii) Closed bypass condition corresponds to the normal operation of the heart valve but presents a danger of high pressure build up, particularly at a small opening of the valve, due to the increased resistance.

The test were conducted for both the cases over the desired range of R_n, however, for the latter case the highest R_n was purposely limited to 1200 from the consideration of the glycerol tunnel's structural integrity.

(a) Bypass open

Figure 4-20 gives a set of representative plots showing the Reynolds number effect on the pressure distributions at various valve openings. At the outset it is apparent that the Reynolds number effect is essentially confined to the negative pressure region. For relatively smaller valve openings, $0 < y_b < 0.2$, when this influence is more significant, the wake pressure increases with R_n (Figure 4-20a). This has a degree of similarity with the observed behavior of the single sphere in the range $90 < R_n < 300$ discussed earlier (Figure 4-10). Recognizing the fact that with a gradual closing of the valve more and more fluid is diverted into the bypass, the apparent discrepancy in R_n is readily explained. Thus although a free stream Reynolds number for smaller valve openings be the same, their effective values at the poppet will be vastly different due to the presence of the bypass.

Another factor of importance which promotes R_n dependency at smaller openings is related to the controlling effect produced by the poppet in the wake of the exit bell. As the poppet travels forward to reduce the outflow orifice

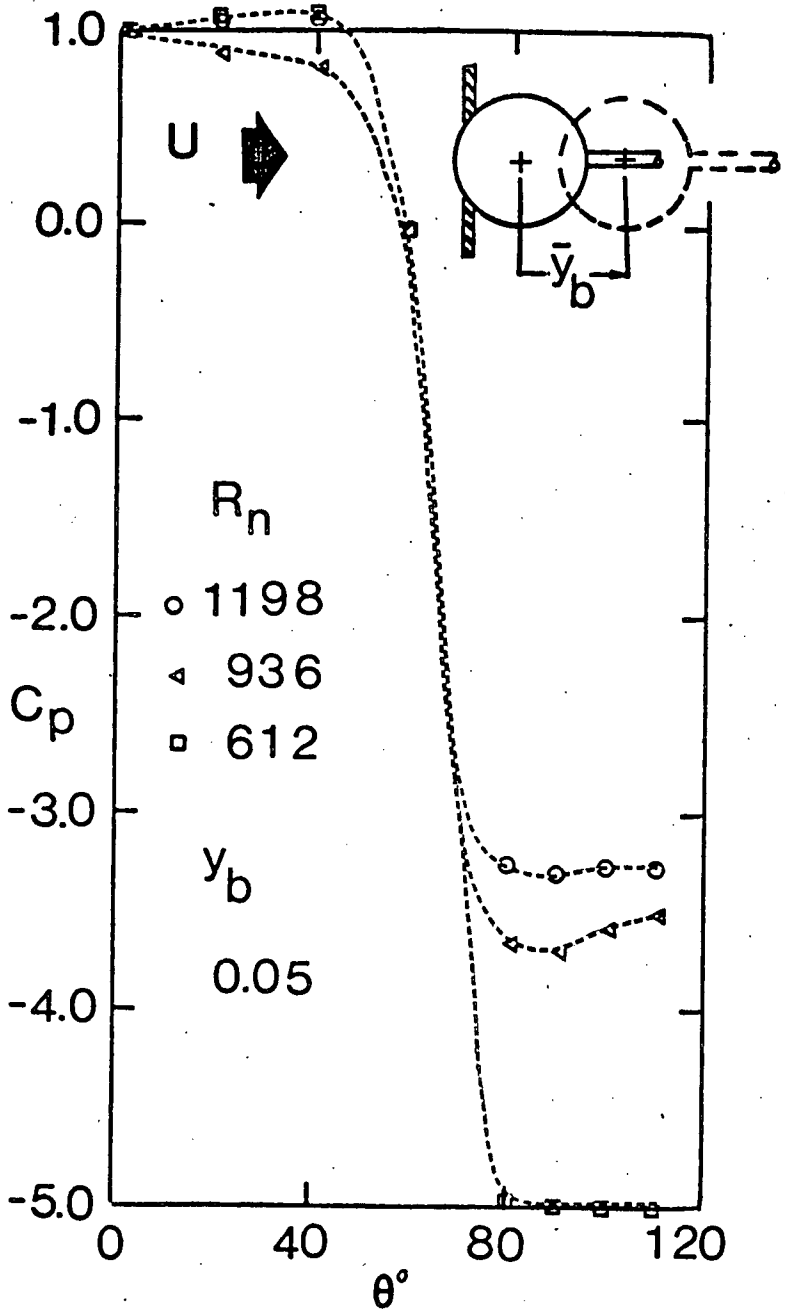

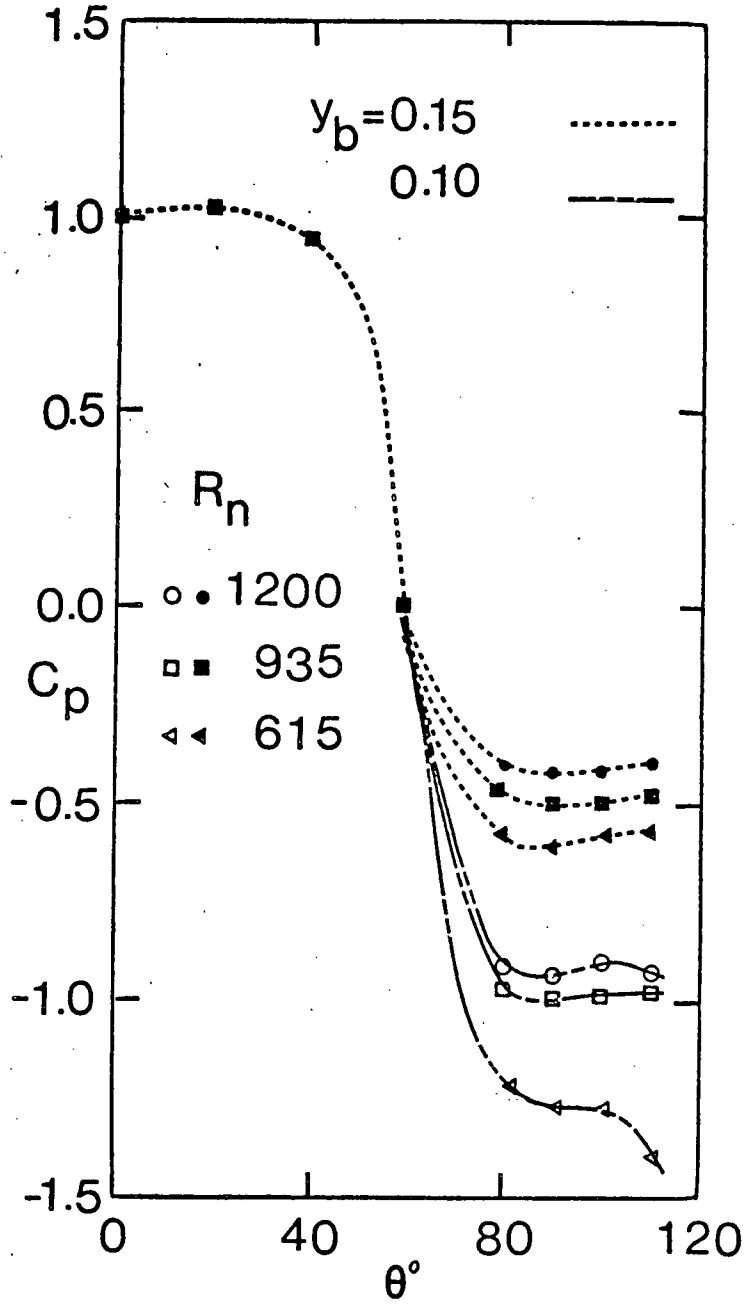

Figure 4-20 Pressure distribution on the poppet occupying different positions in the valve during the open bypass condition: (a) y_b = 0.05,0.10,0.15

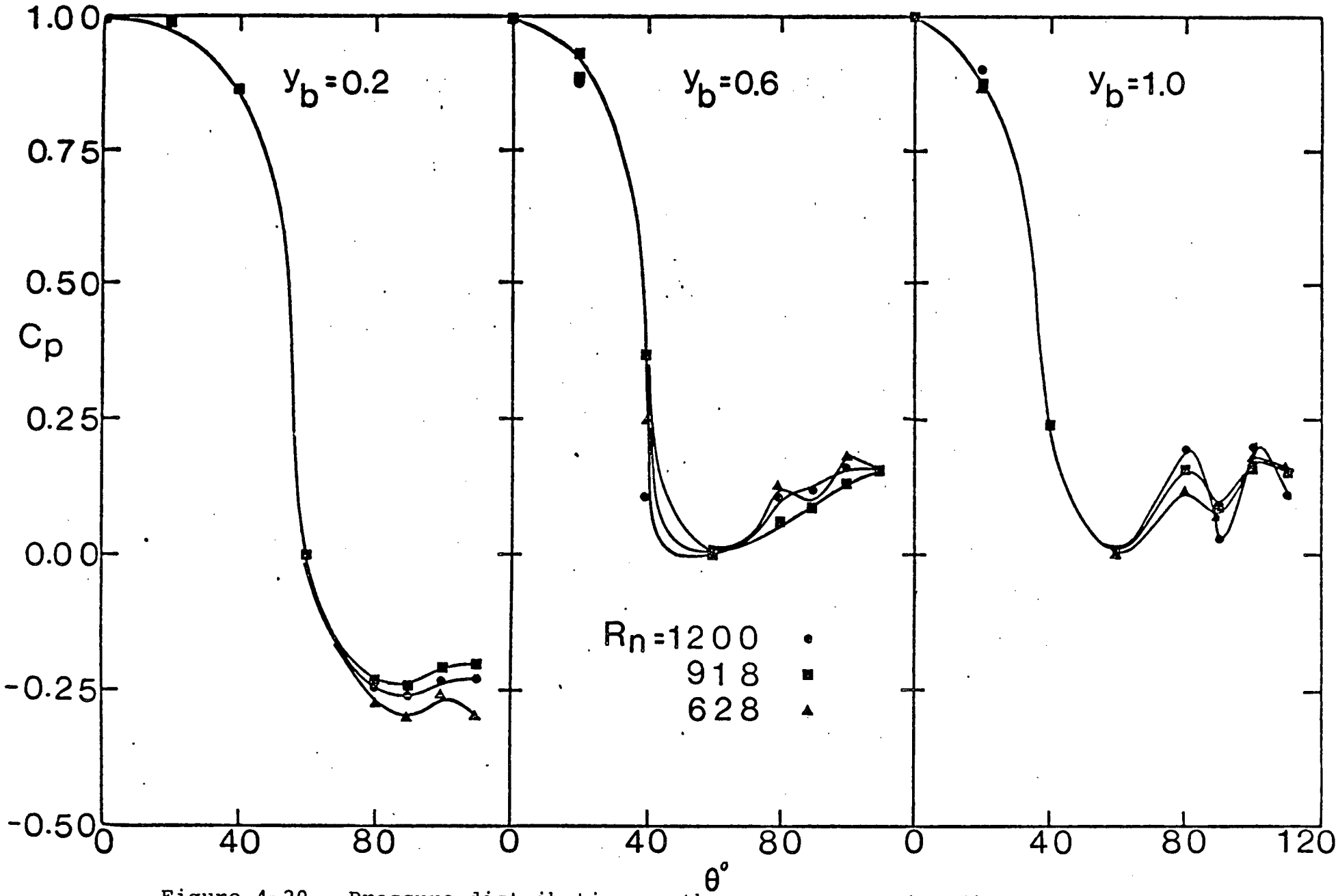

Figure 4-20 Pressure distribution on the poppet occupying different positions in the valve during the open bypass condition: (b) y_b = 0.2,0.6,1.0

(Figure 4-21), the separation from the exit bell is delayed or even suppressed. Consequently, the vorticity distribution immediately upstream of the poppet is controlled. This in turn produces a more uniform flow of low effective R_n which results in the delay of separation on the poppet.

On the other hand, for valve openings in the range $0.2 < y_b < 1.0$, the pressure distribution in the wake is virtually unaffected as shown in Figure 4-20(b). Recalling the results on the velocity profiles in the test section with the model present (Figure 4-4) and the relevant data for a single sphere in the corresponding range (Figure 4-9b) the above behavior appears consistent with what one would expect.

Figure 4-22 presents typical flow visualization photographs to illustrate distribution of flow past the poppet and through the bypass as affected by the valve opening. For an extremely small opening ($y_b \simeq 0.050$, Figure 4-22a) most fluid takes the bypass route. However, flow past the sphere gradually increases with opening ($y_b = 0.50$, Figure 4-22b) and with the valve fully open ($y_b = 1.00$, Figure 4-22c) considerable amounts of fluid flows through the inlet orifice. Variations in the effective R_n caused by the valve openings are thus apparent.

Dependence of the mean pressure distribution on the valve opening for a set of R_n is presented in Figure 4-23. In contrast to R_n, the valve opening substantially affects

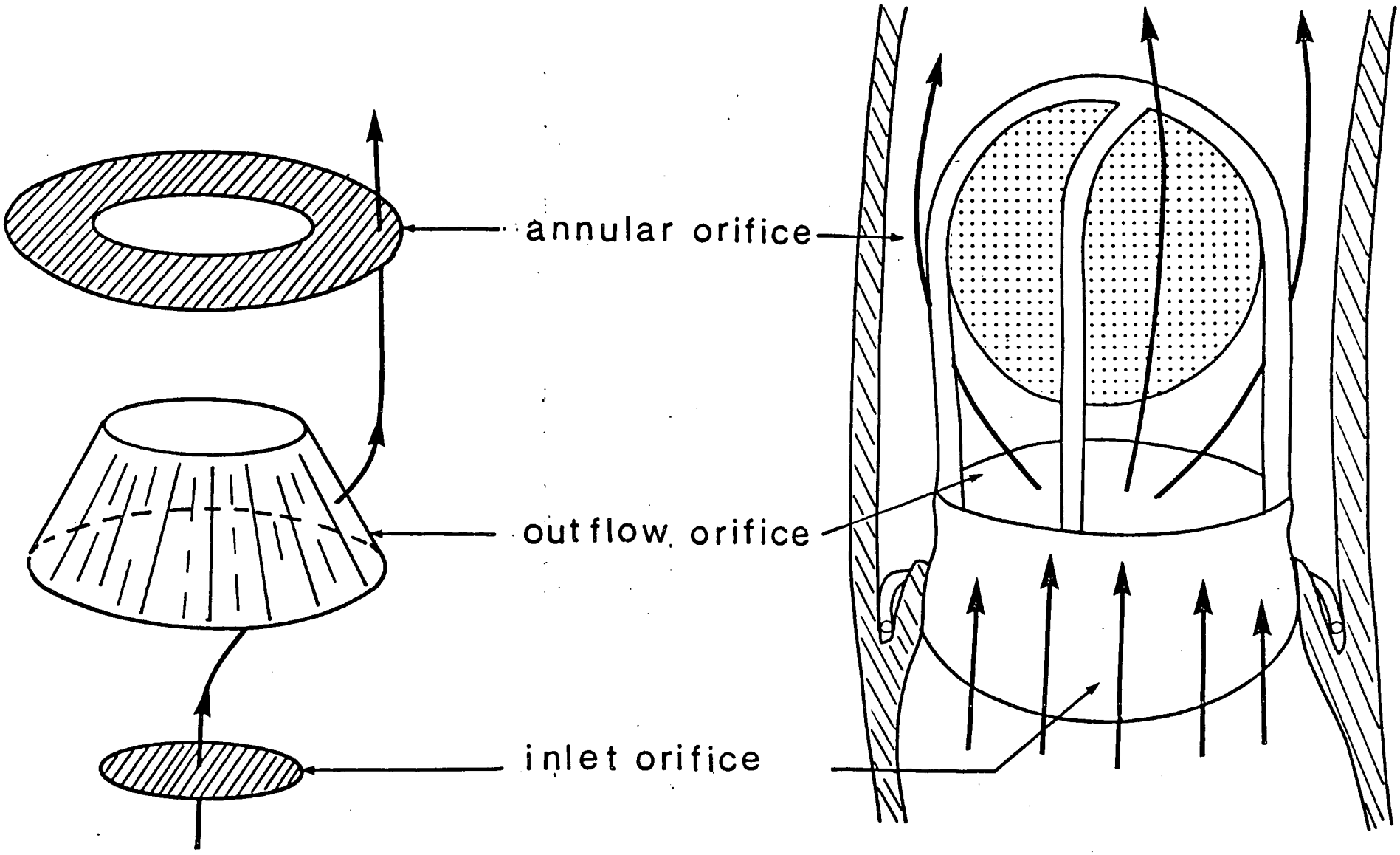

Figure 4-21 A schematic diagram showing passage of fluid in the immediate vicinity of the valve

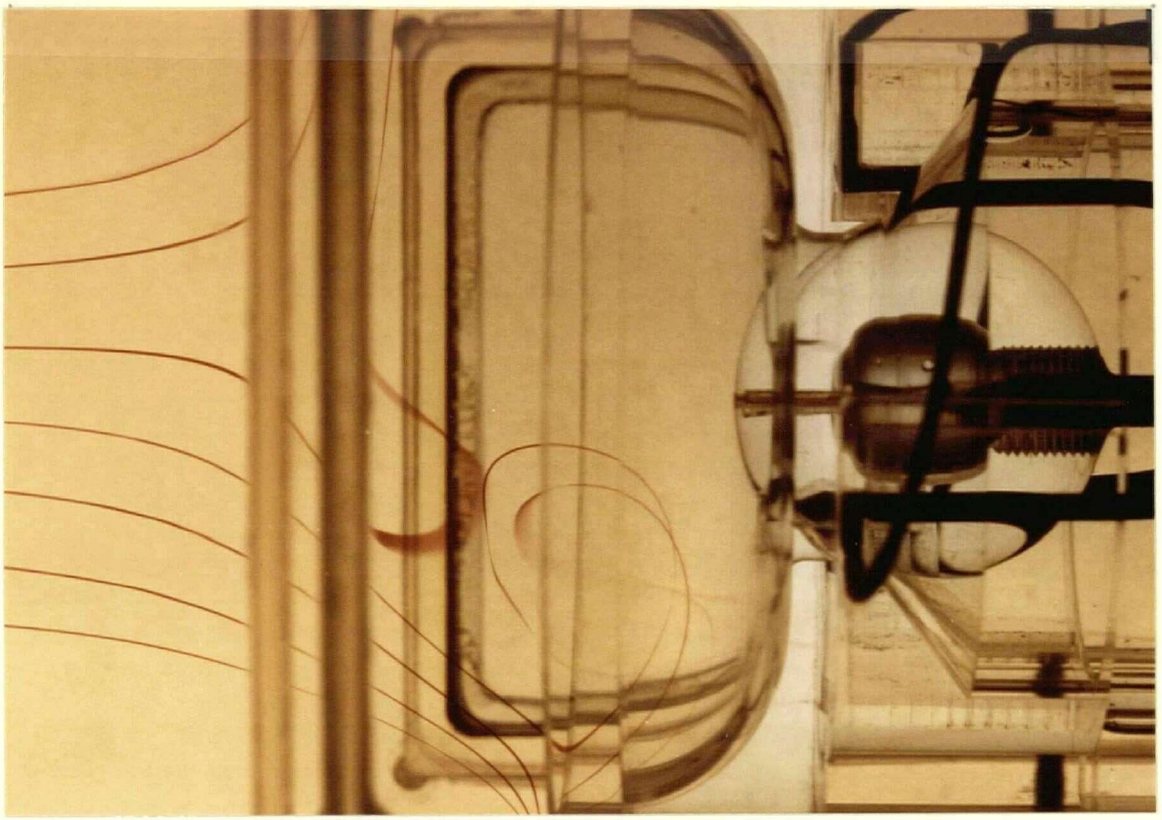

(a) $y_b = 0.05$

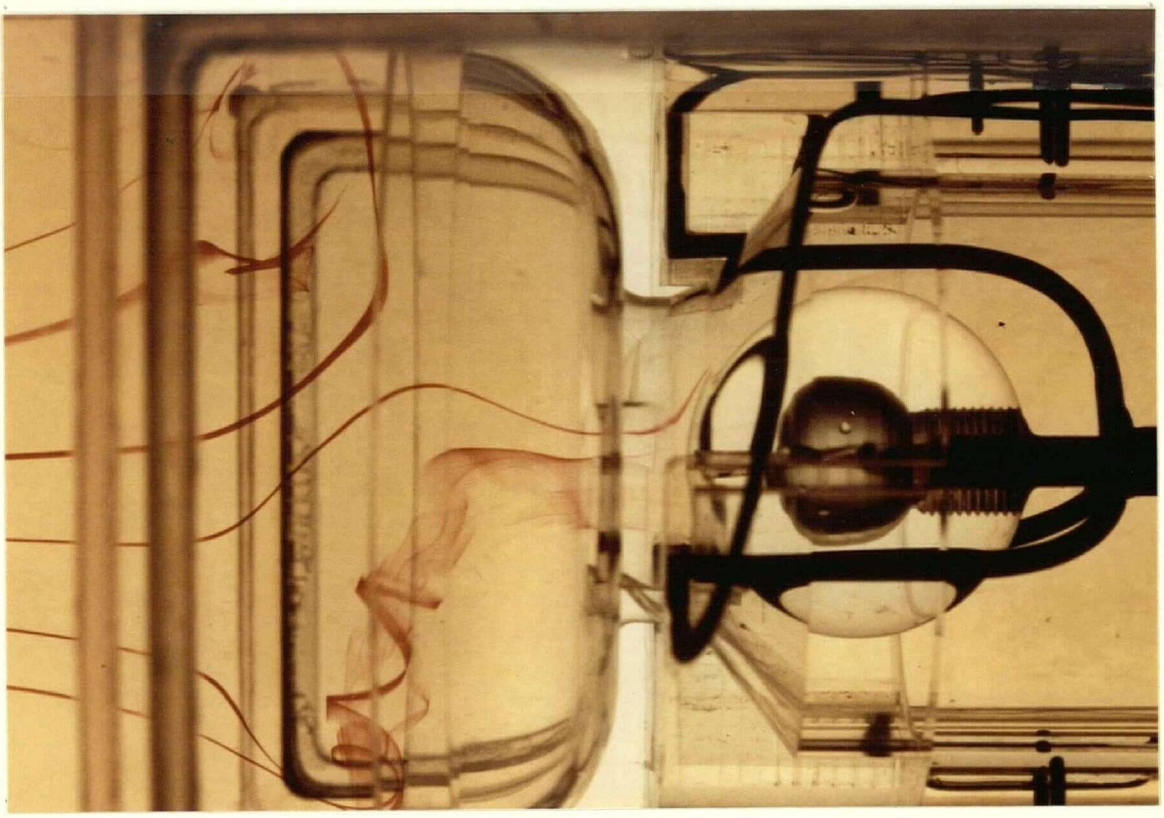

(b) $y_b = 0.50$

(continued)

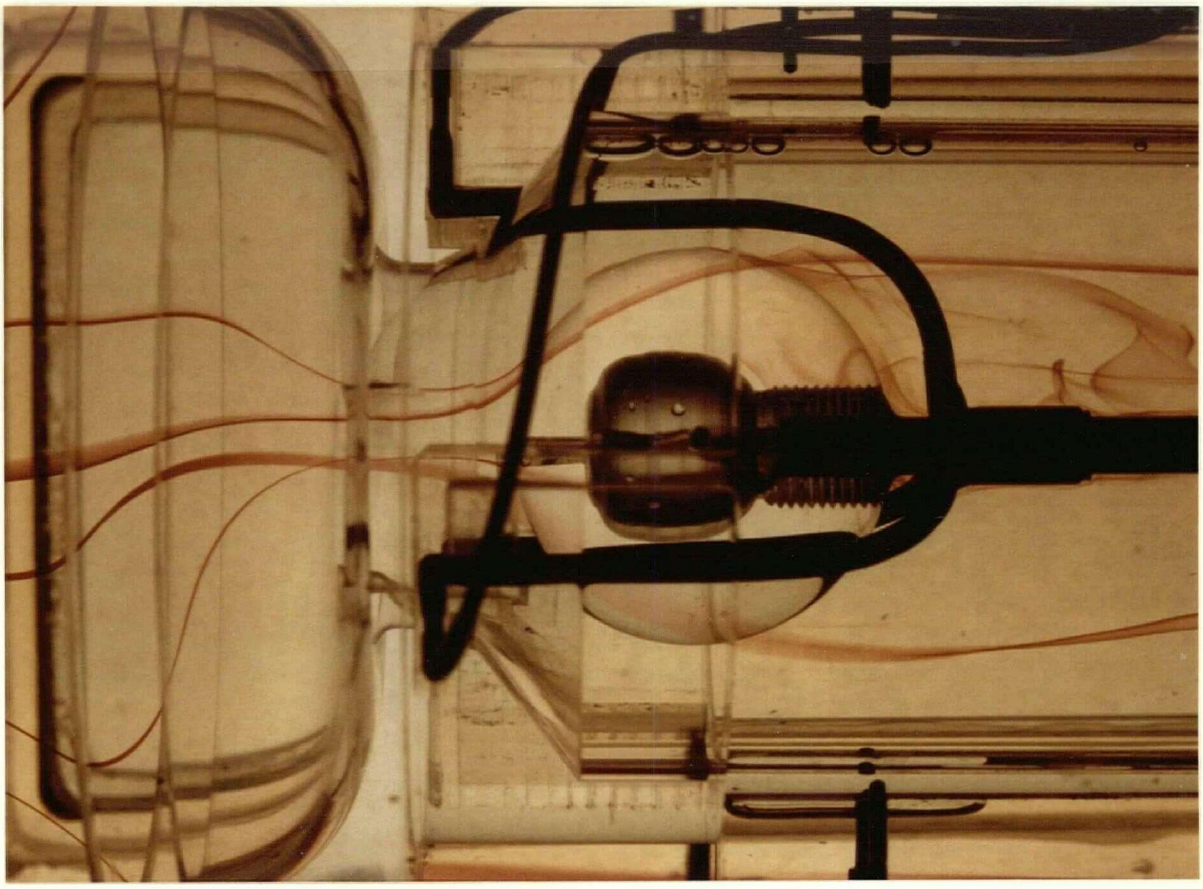

(c) $y_b = 1.0$

Figure 4-22 Visual study of flow patterns past the poppet and through the bypass as effected by the valve openings at $R_n = 290$

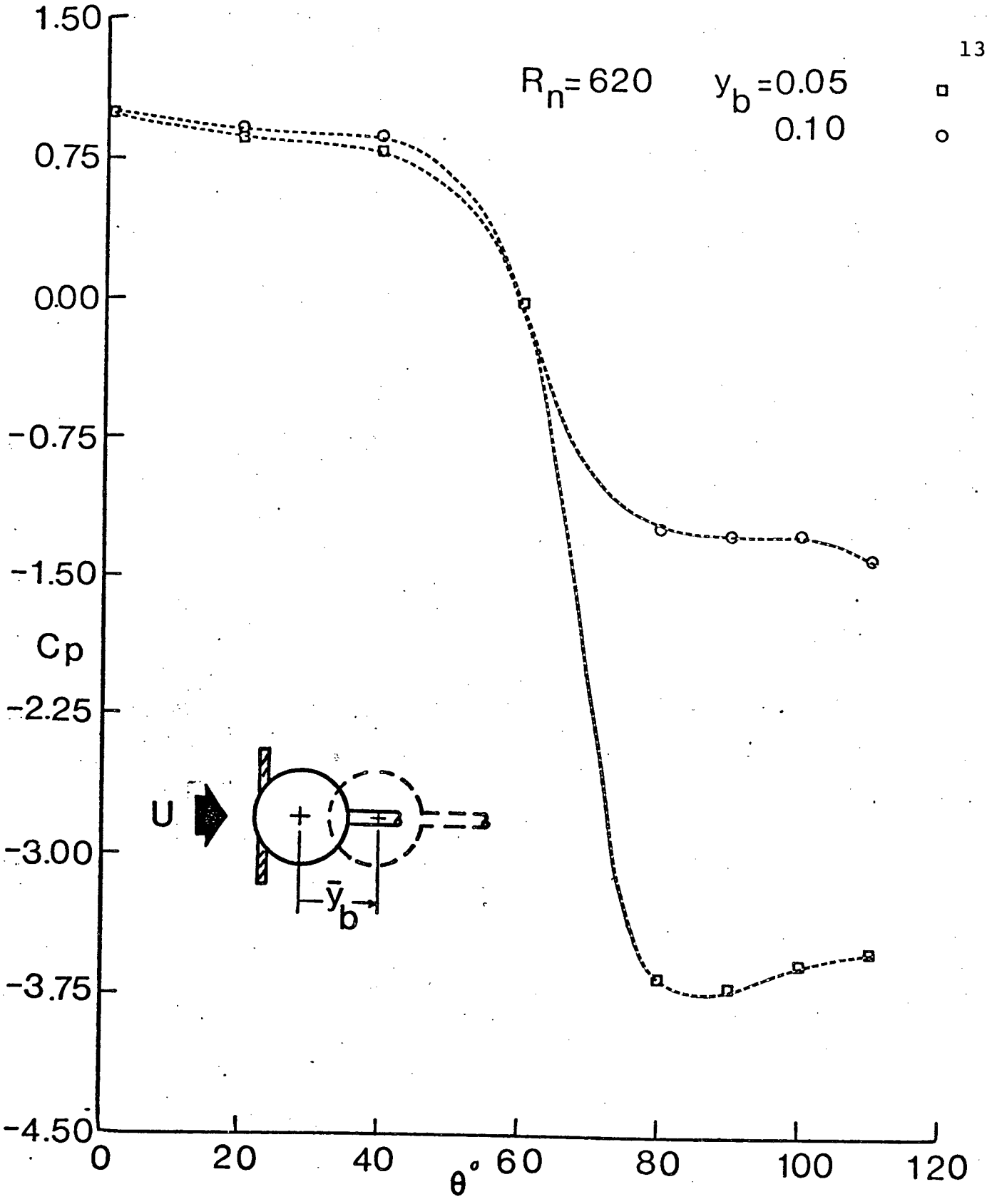

Figure 4-23 Variation of pressure distribution with the poppet position for the case of the open by-pass: (a1) very small openings, R_n = 620

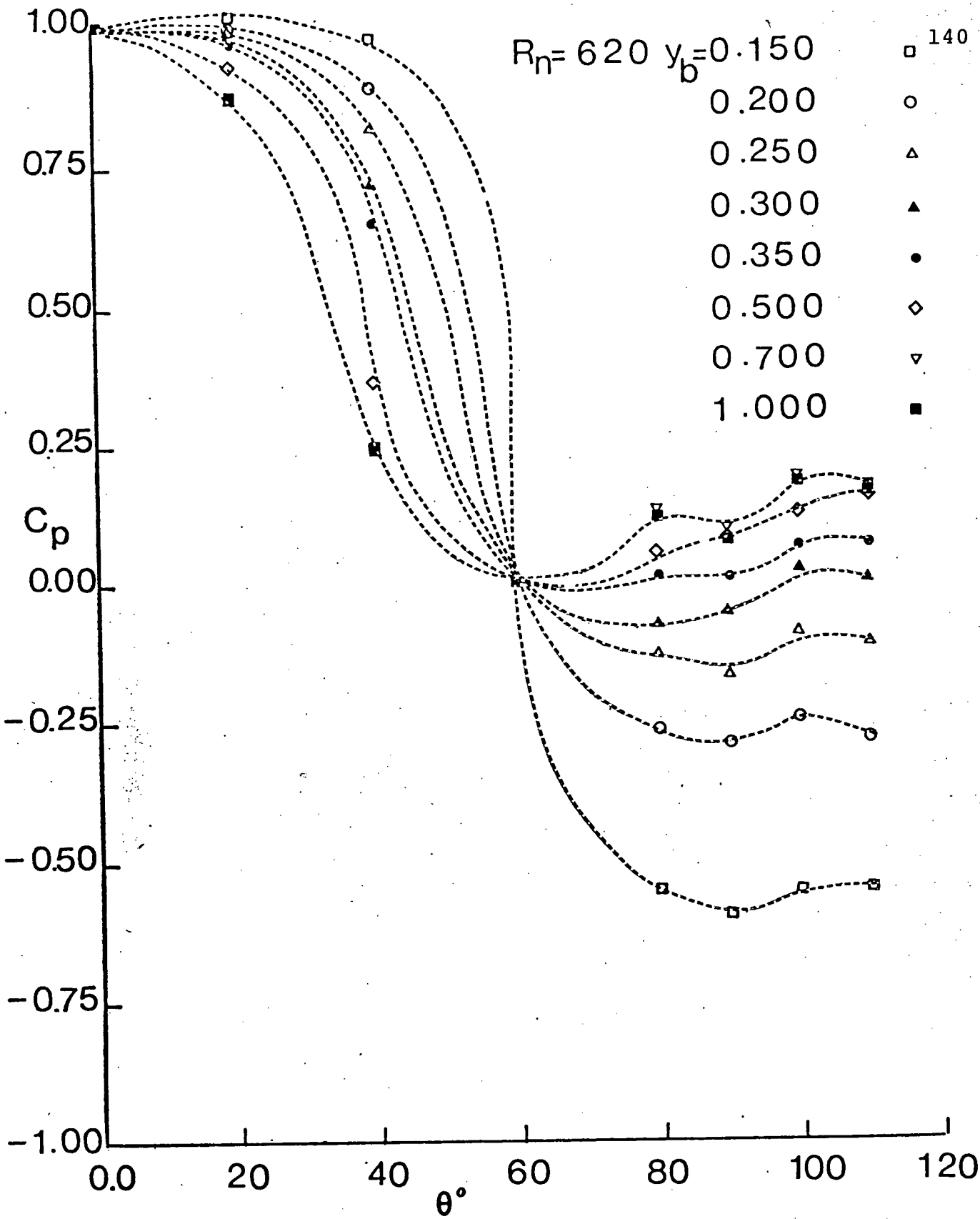

Figure 4-23 Variation of pressure distribution with the poppet position for the case of the open by-pass: (a2) intermediate and large openings, R_n = 620

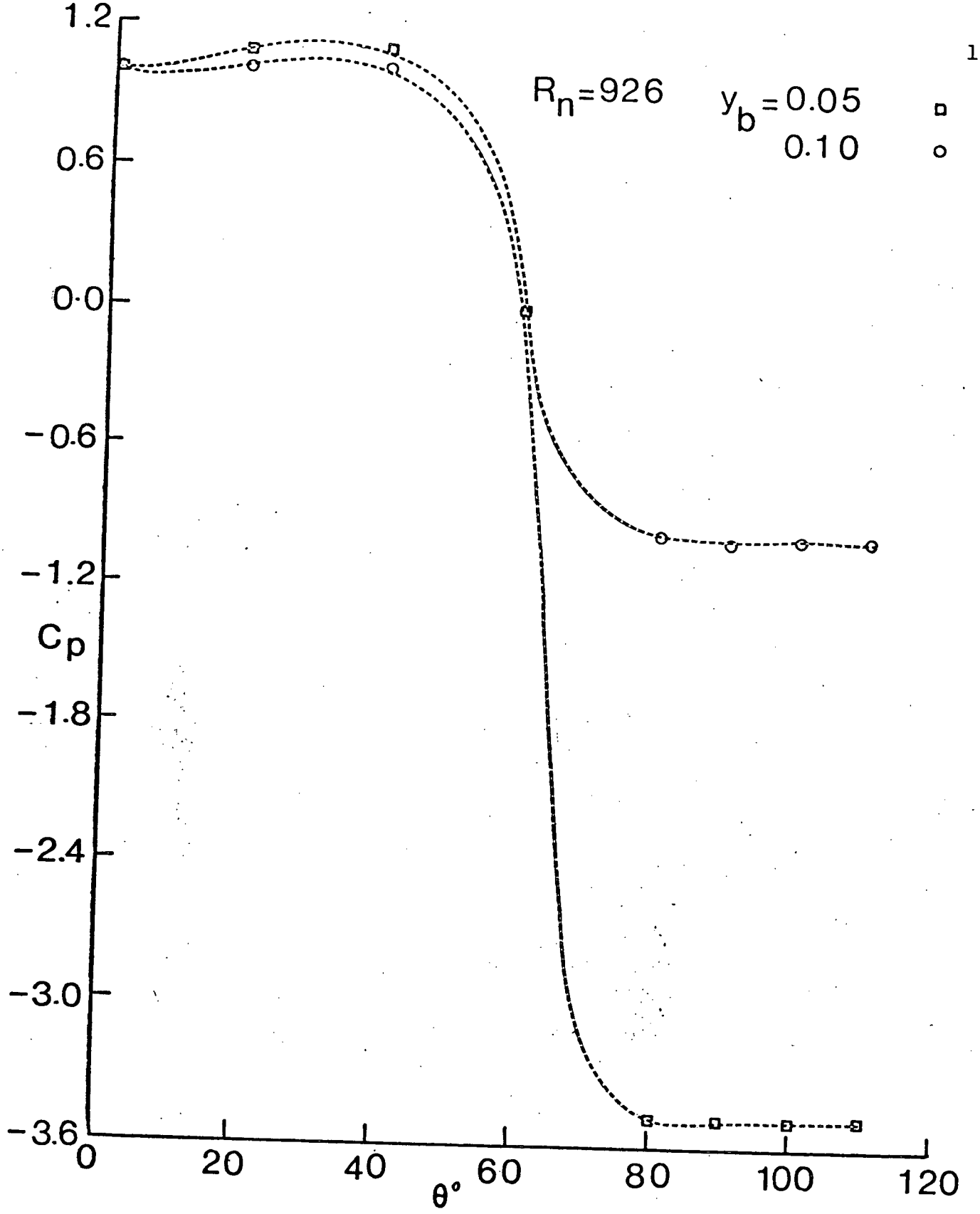

Figure 4-23 Variation of pressure distribution with the poppet position for the case of the open bypass: (b1) R_n = 926, y_b = 0.05, 0.10

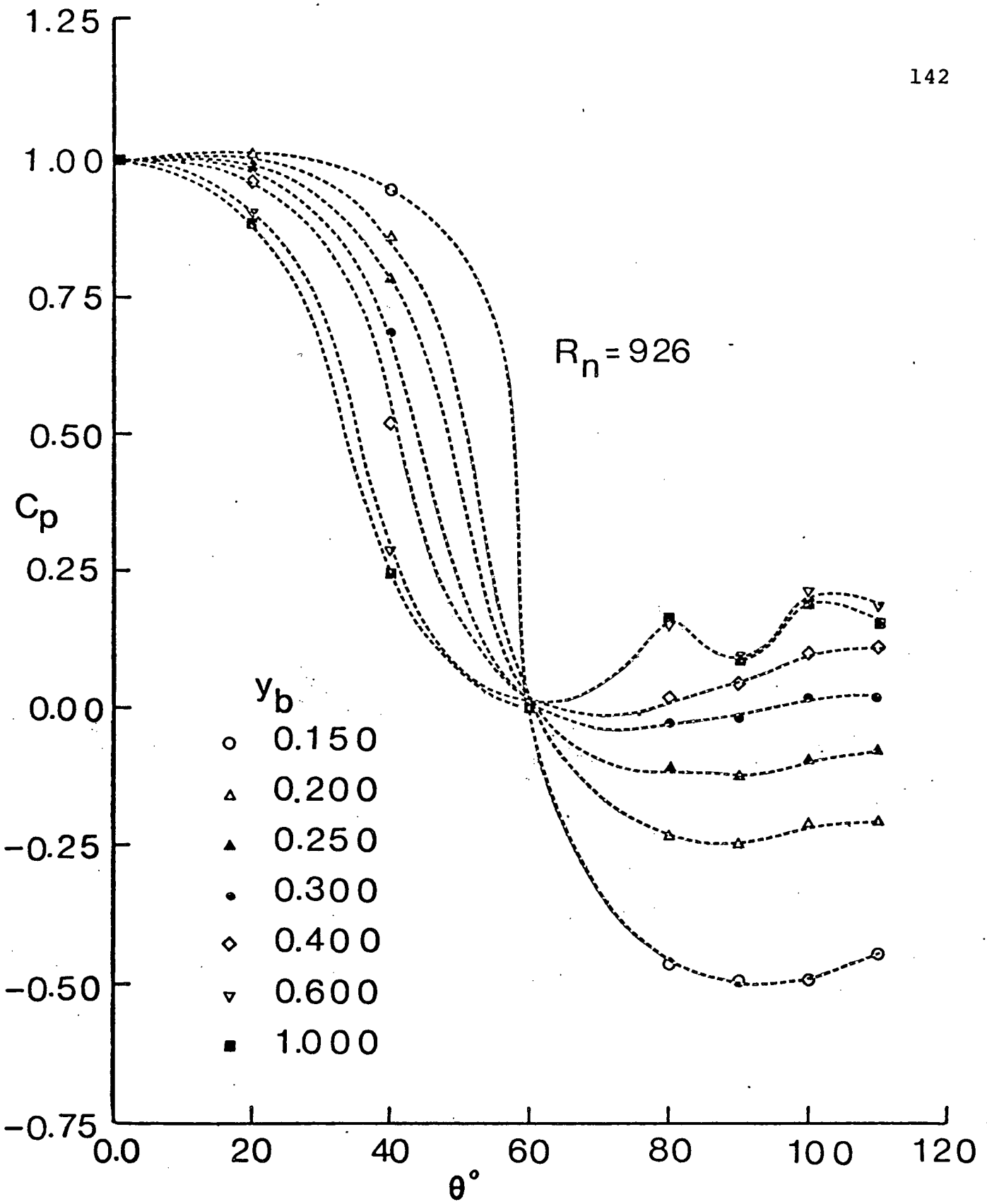

Figure 4-23 Variation of pressure distribution with the poppet position for the case of the open bypass: (b2) $R_n = 926, y_b = 0.15, 1.0$

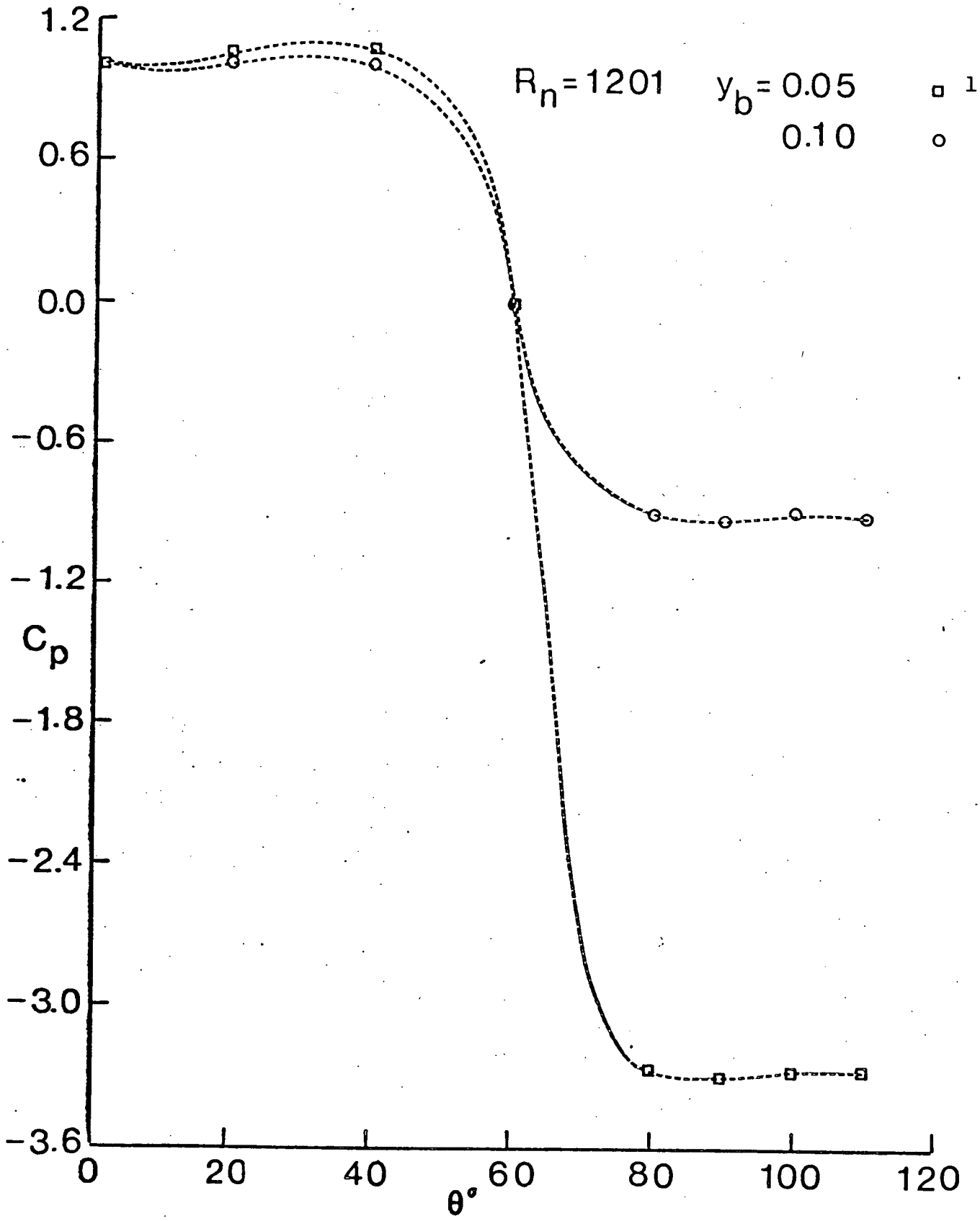

Figure 4-23 Variation of pressure distribution with the poppet position for the case of the open bypass: (c1) R_n = 1201, y_b = 0.05, 0.1

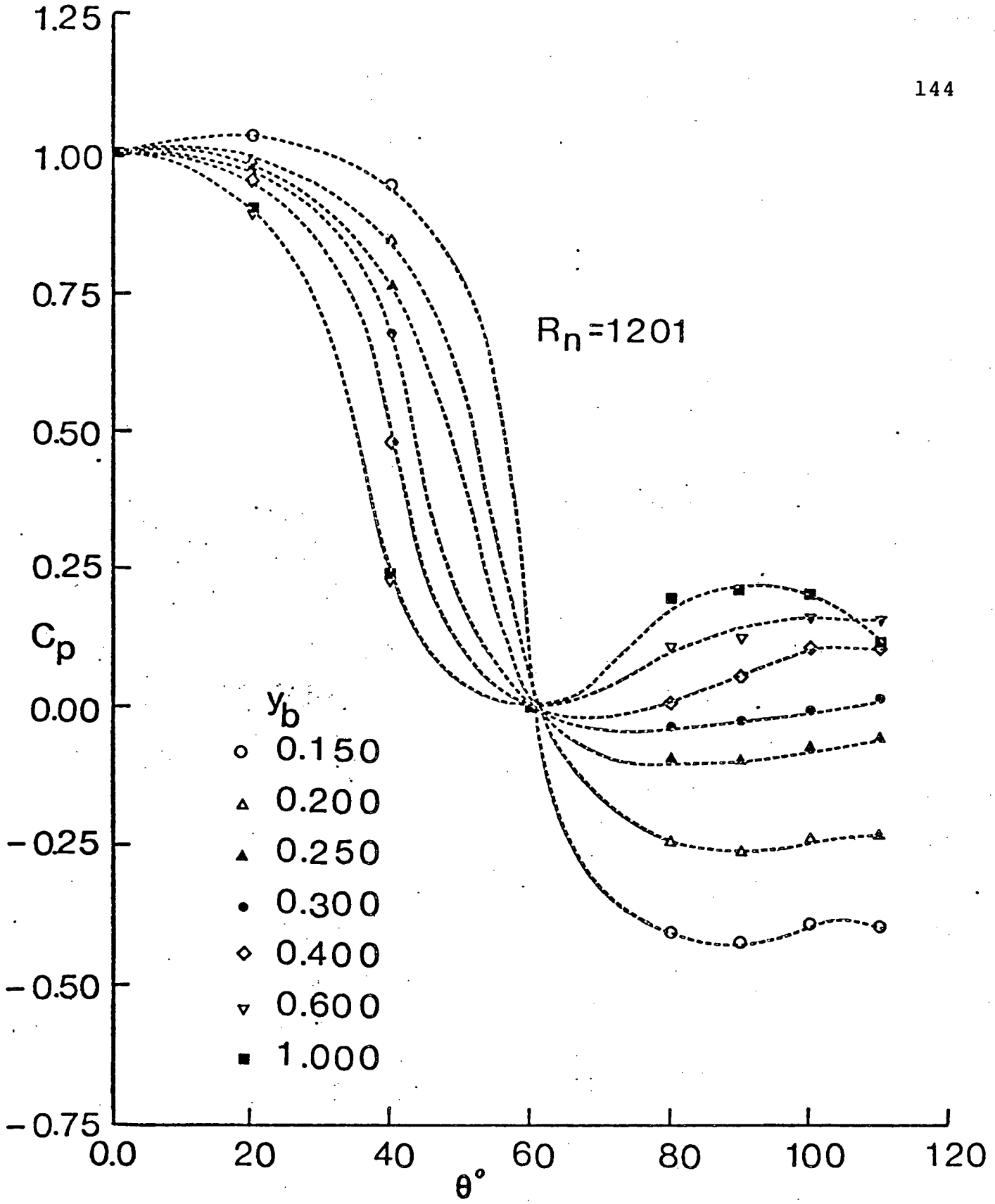

Figure 4-23 Variation of pressure distribution with the poppet position for the case of the open bypass: (c2) R_n = 1201, y_b = 0.15, 1.0

the pressure distribution over the entire surface of the poppet. In general, with progressive reduction in y_b (i.e. valve closing), the pressure on the frontal section of the sphere $\theta \simeq 0\text{-}60°$) increases while that on the downstream section ($\theta \simeq 60\text{-}180°$) diminishes. It is this increase in pressure on the frontal section that is responsible for the reversal of flow observed earlier (Figure 4-22a).

Of particular significance is the dramatic rise in the negative pressure coefficient at smaller openings ($y_b \leq 0.1$) in the near wake region. This would suggest large shearing stresses leading to possible deformations and destruction of the blood cells.[135] The presence of vorticity distribution characterizing the wake, generates a centrifugal field which may cause dissociation of the blood into its constituents and finally their deposition on the body of the valve.

(b) Closed bypass

As pointed out before, in this study the range of R_n (R_n = 221-900) and valve openings (y_b = 0.125-1.0) were carefully selected to obtain meaningful data without excessively stressing the test section. In general, the pressure results (Figure 4-24) exhibited the same trends as those observed during the open bypass case with one significant difference: closing of the bypass tends to increase the pressure on the downstream region of the poppet (i.e. $\theta > 60°$, Figure 4-25). This increase in pressure may be

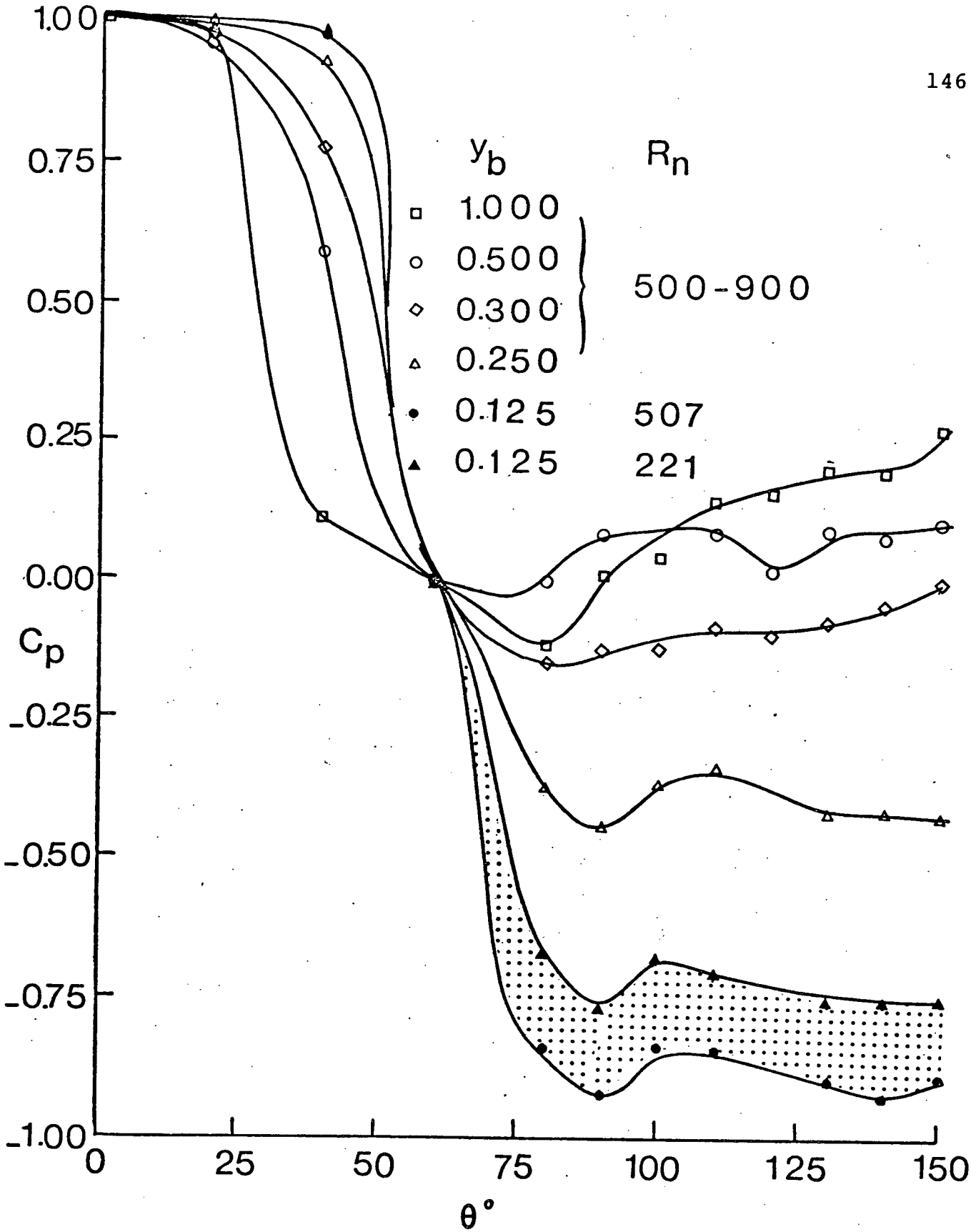

Figure 4-24 Pressure distribution on the poppet occupying different positions in the valve during the closed bypass condition

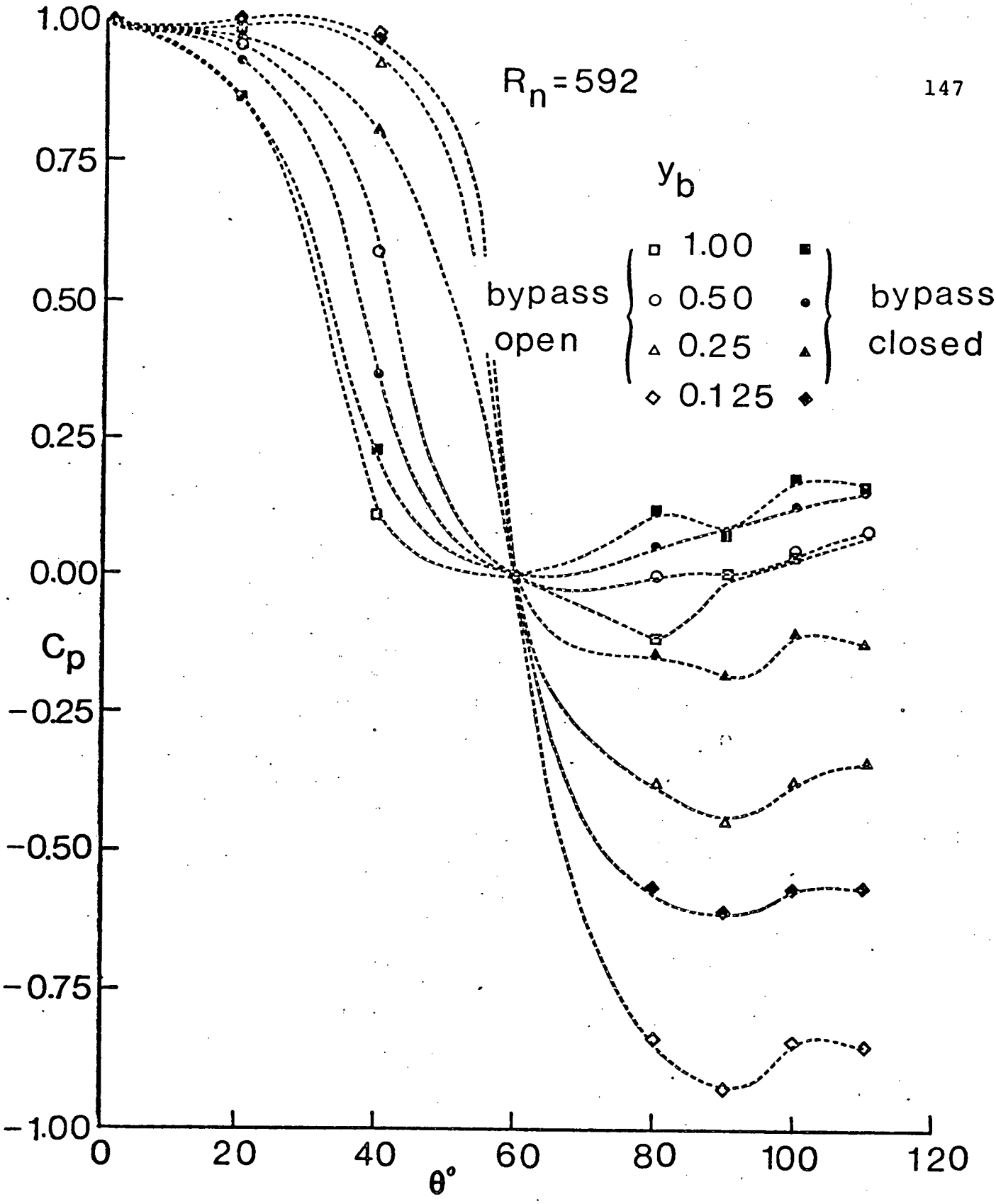

Figure 4-25 Comparison of pressure distributions on the poppet occupying various positions in the valve for the closed and open bypass conditions

attributed to a large difference in the local R_n for the two cases even when the free stream value is the same. With the bypass blocked the fluid must pass through the valve with the inlet much smaller than that of the test section. The jet-like flow issuing from the exit bell is accelerated past the poppet leading to a higher effective R_n. A preliminary calculation based on the area ratio showed the effective R_n to be several times the mean free stream value for the closed bypass case (3700-15300).

To ascertain the effect of such a dramatic increase in R_n a separate test program was undertaken using a set of spheres with glycerol as well as water as working fluids. The results are presented in Figure 4-26. Recognizing the fact that an increase in R_n in the range of interest leads to a corresponding increase in pressure on the downstream region of the sphere, the observed pressure distribution for the closed bypass case follows the logical trend.

As before, the flow visualization study proved to be quite effective in providing better appreciation of the phenomenon. Tests with dye injection were conducted at three Reynolds numbers: R_n = 450, 600, 900, and photographs of the flow pattern taken as shown in Figure 4-27. Several aspects of interest become apparent. Acceleration of the fluid through and downstream of the inlet orifice is vividly demonstrated by stretching of the dye filaments which become

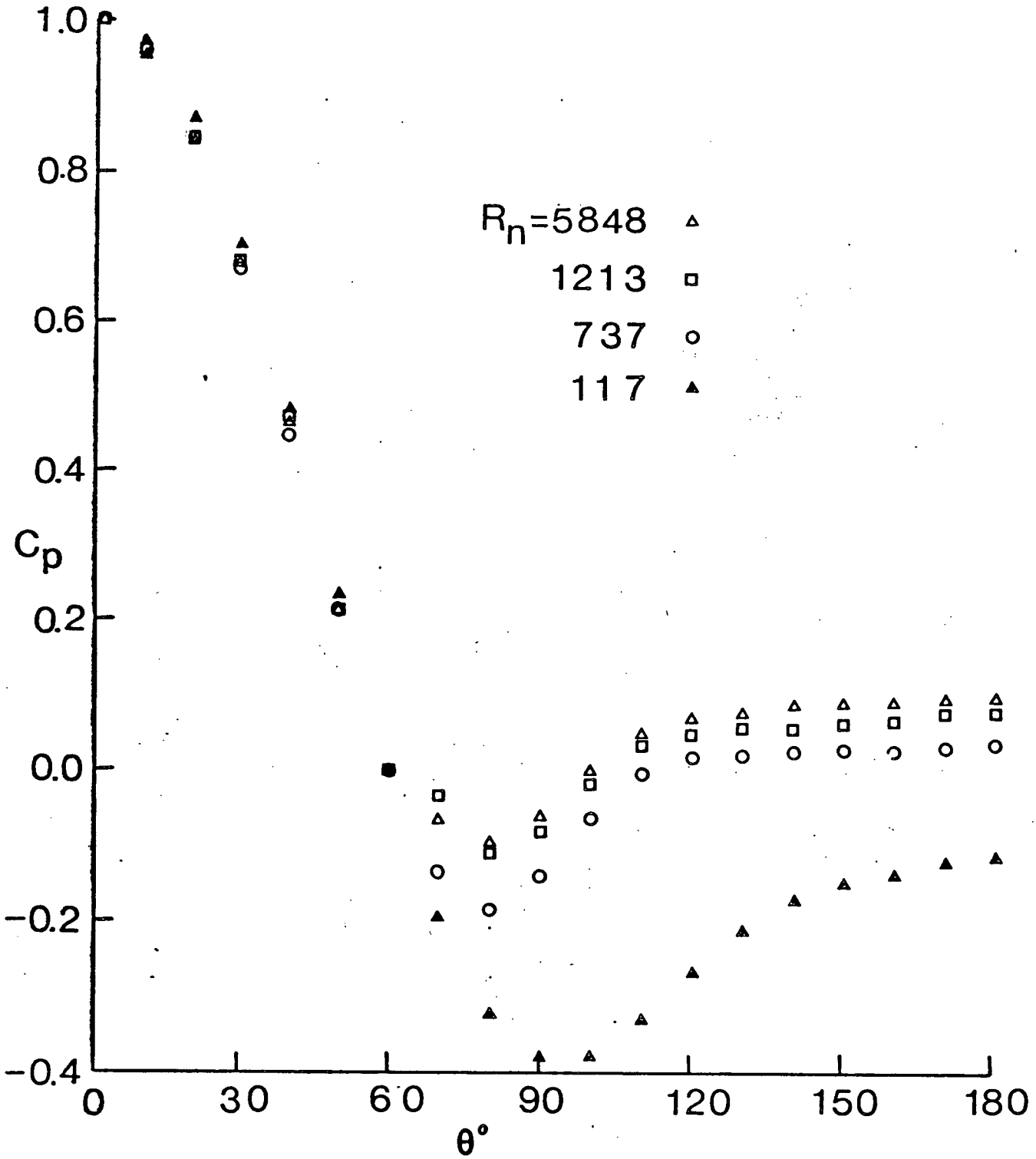

Figure 4-26 Reynolds number effect on C_p profiles for a sphere

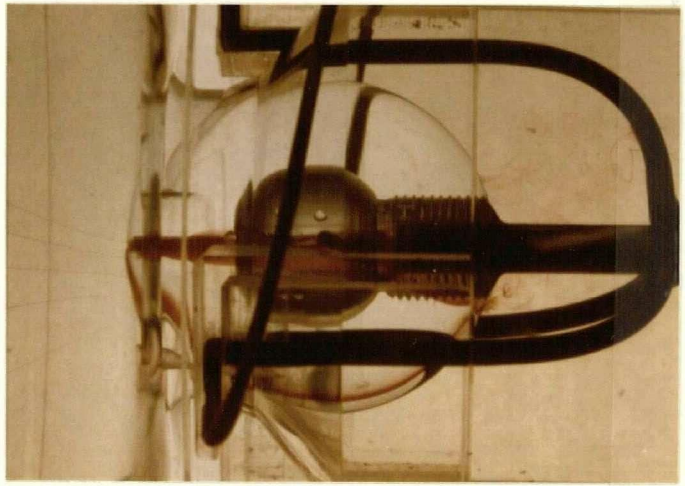

y_b=0.05

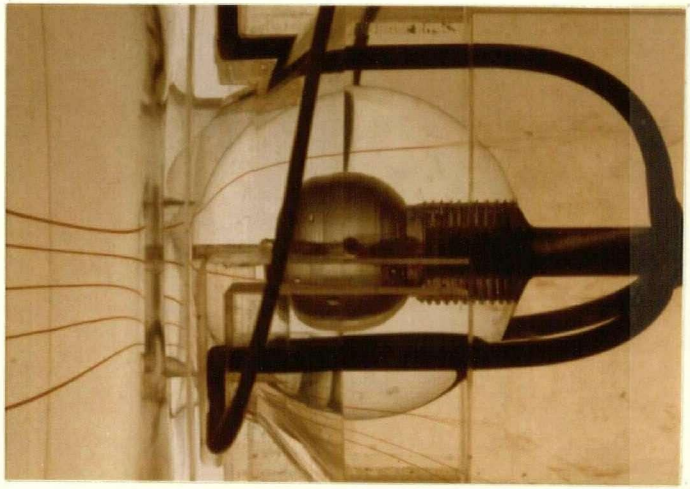

y_b=0.25

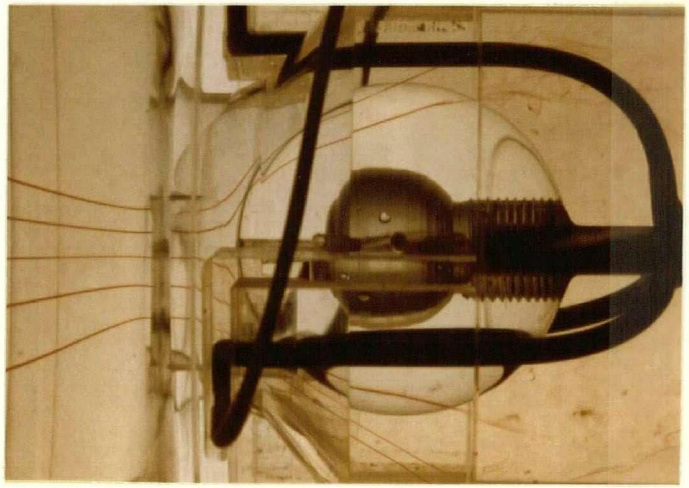

y_b=0.75

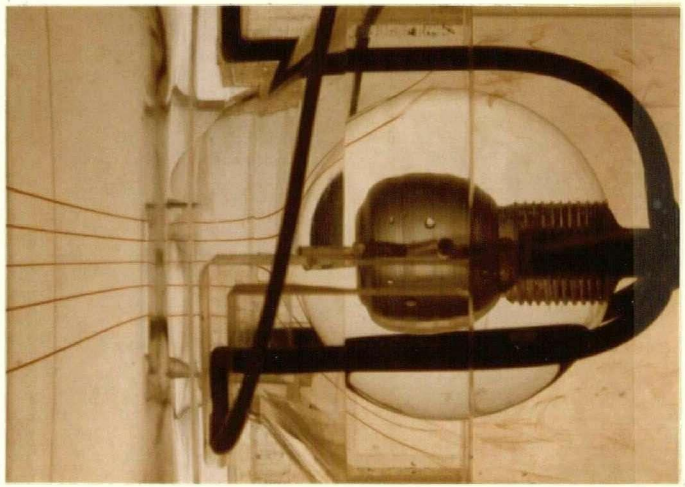

y_b=1.0

Figure 4-27 A flow visualization study showing the effect of valve openings on the flow past a spherical poppet during the closed bypass condition: (a) R_n = 450

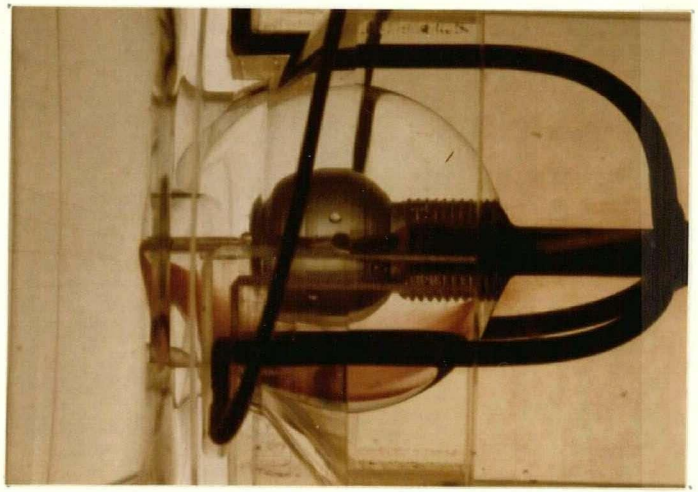

y_b=0.05

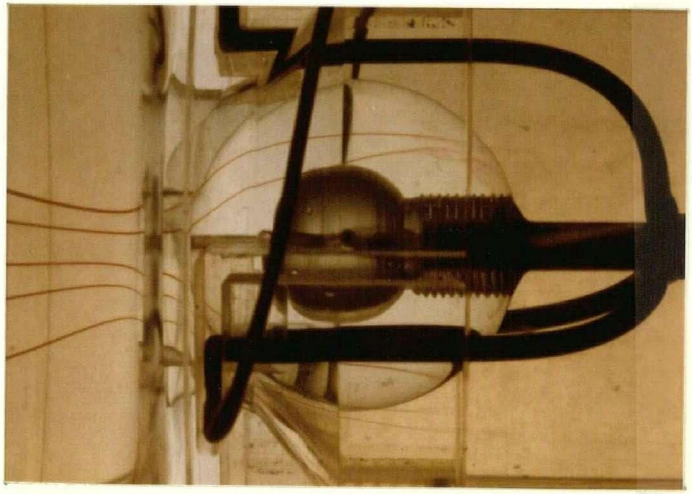

y_b=0.25

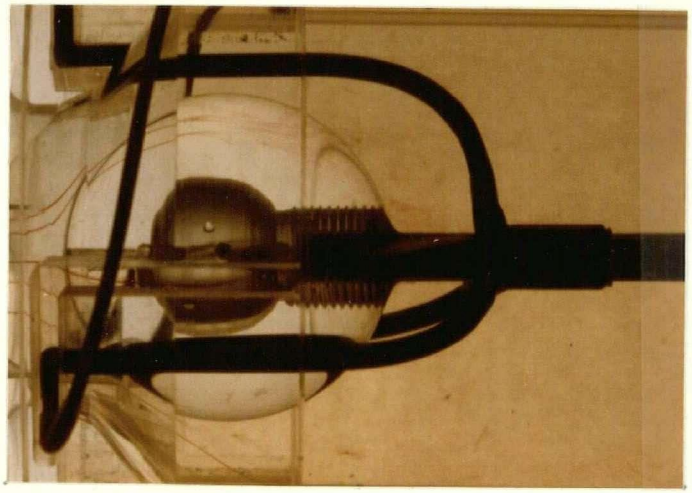

y_b=0.75

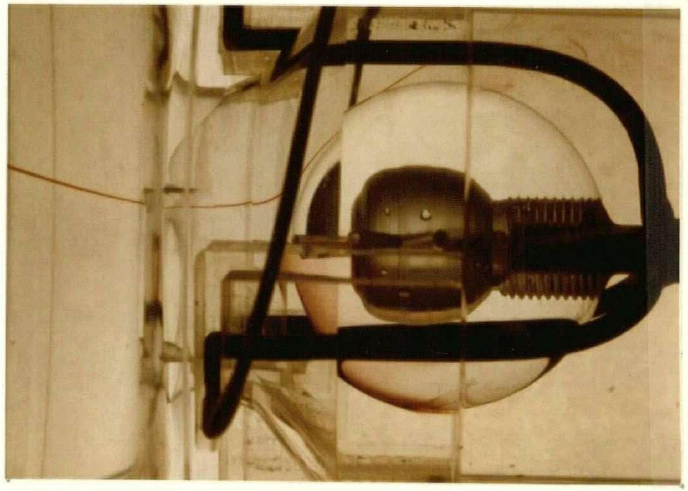

y_b=1.0

Figure 4-27 A flow visualization study showing the effect of valve openings on the flow past a spherical poppet during the closed bypass condition: (b) R_n = 600

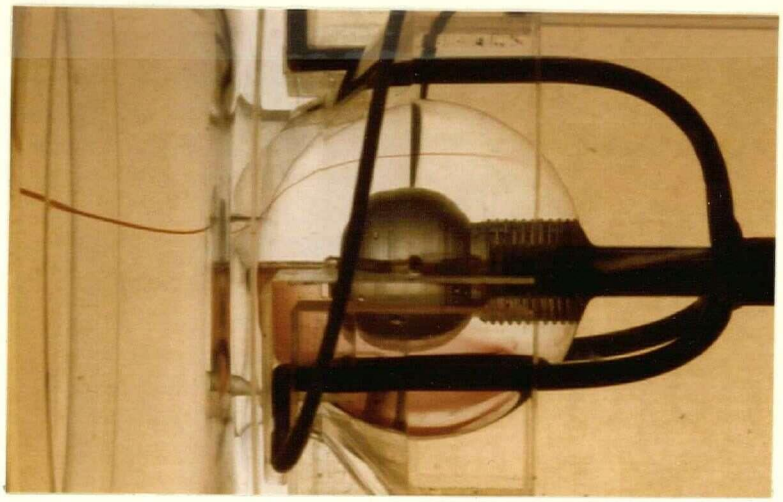

y_b=0.50

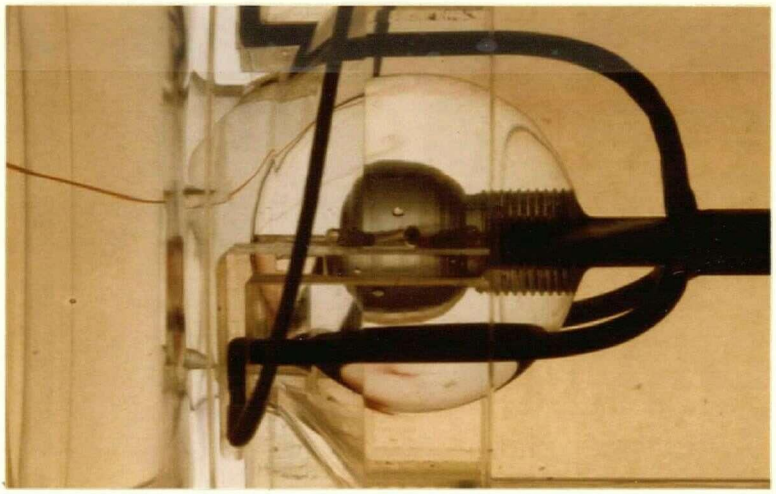

y_b=0.75

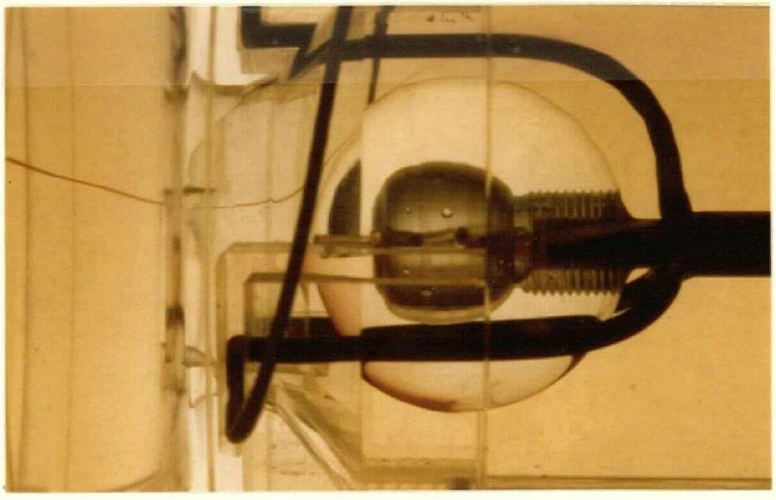

y_b=1.0

Figure 4-27 A flow visualization study showing the effect of valve openings on the flow past a spherical poppet during the closed bypass condition: (c) R_n = 900

drastically thin and eventually break up in the wake. Of particular importance is the location of the separating shear layer and its movement with poppet position. Although it would be somewhat fortuitous to assign numerical values, downstream movement of the separation point with progressive closing of the valve is quite apparent at all the three Reynolds numbers. This is quite significant as now the poppet of the prosthetic device has a periodically oscillating boundary layer with associated wake that also grows periodically. Obviously, this adds to the turbulent character of the wake which appears to be the main cause of concern in successful operation of the device.

4.3.4 Poppet oscillation and Beta number

Having obtained some understanding of the hydrodynamics of the poppet during stationary condition, the next logical step was to explore the effect of pulsation frequency as represented by the Beta number. Using the dimensional analysis of Appendix I and the results of a single sphere described earlier, an experimental program was organized to obtain appreciation of the fluid dynamics of an oscillating poppet. This section presents results on the time history of the static pressure distribution in the Reynolds number range of 300-650. Both the forward and reverse stroke of the poppet are considered with the oscillation frequency

ranging over 6 - 60 cpm (B_n = 19-61). One of the important requirements in this set of experiments was a careful simulation of the displacement-time history of the poppet as observed in a patient with such a prosthetic device (Figure 4-7). The results are complemented by the flow visualization which provides better understanding as to the physical character of the flow.

Figure 4-28 studies dependence of the surface pressure profiles on the Beta number, Reynolds number and valve opening, thus summarizing a rather extensive amount of information in a concise form. At the outset, one reconizes a degree of similarity among all the plots. In general, during the forward stroke, the pressure decreases from the front stagnation value reaching a minimum around 80° followed by a slight increase. It appears that, irrespective of the pulsation frequency, the Reynolds number effect is rather insignificant for larger valve openings ($y_b > 0.20$). This is consistent with the trend observed earlier for the stationary poppet occupying different positions inside the valve (Figure 4-20b). However, for narrow valve settings ($y_b < 0.2$), R_n influence is rather substantial, particularly in the negative pressure region. In general, an increase in R_n leads to a decrease in the wake pressure. Based on the data for stationary poppet inside the valve (Figure 4-24), this again is an expected behavior.

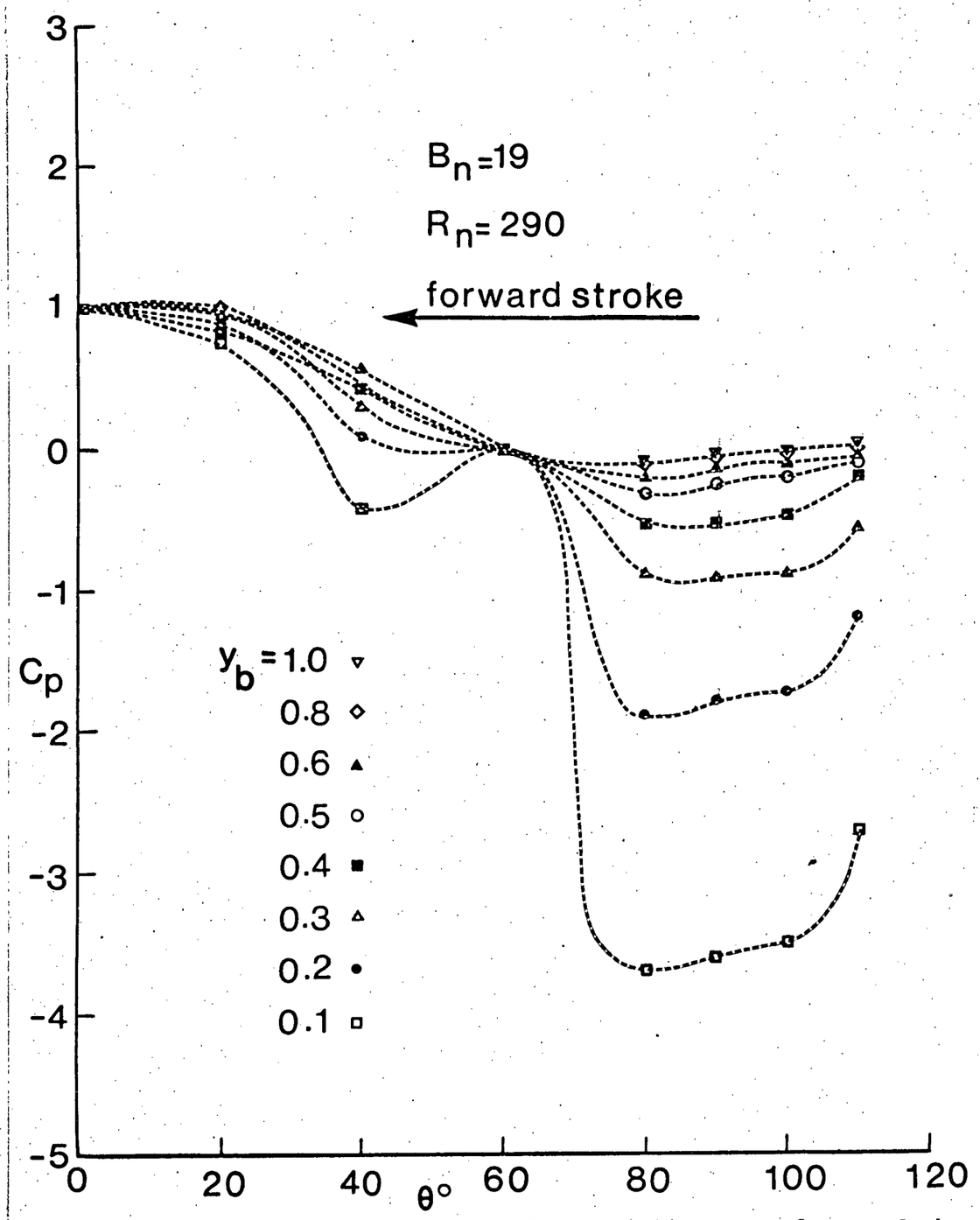

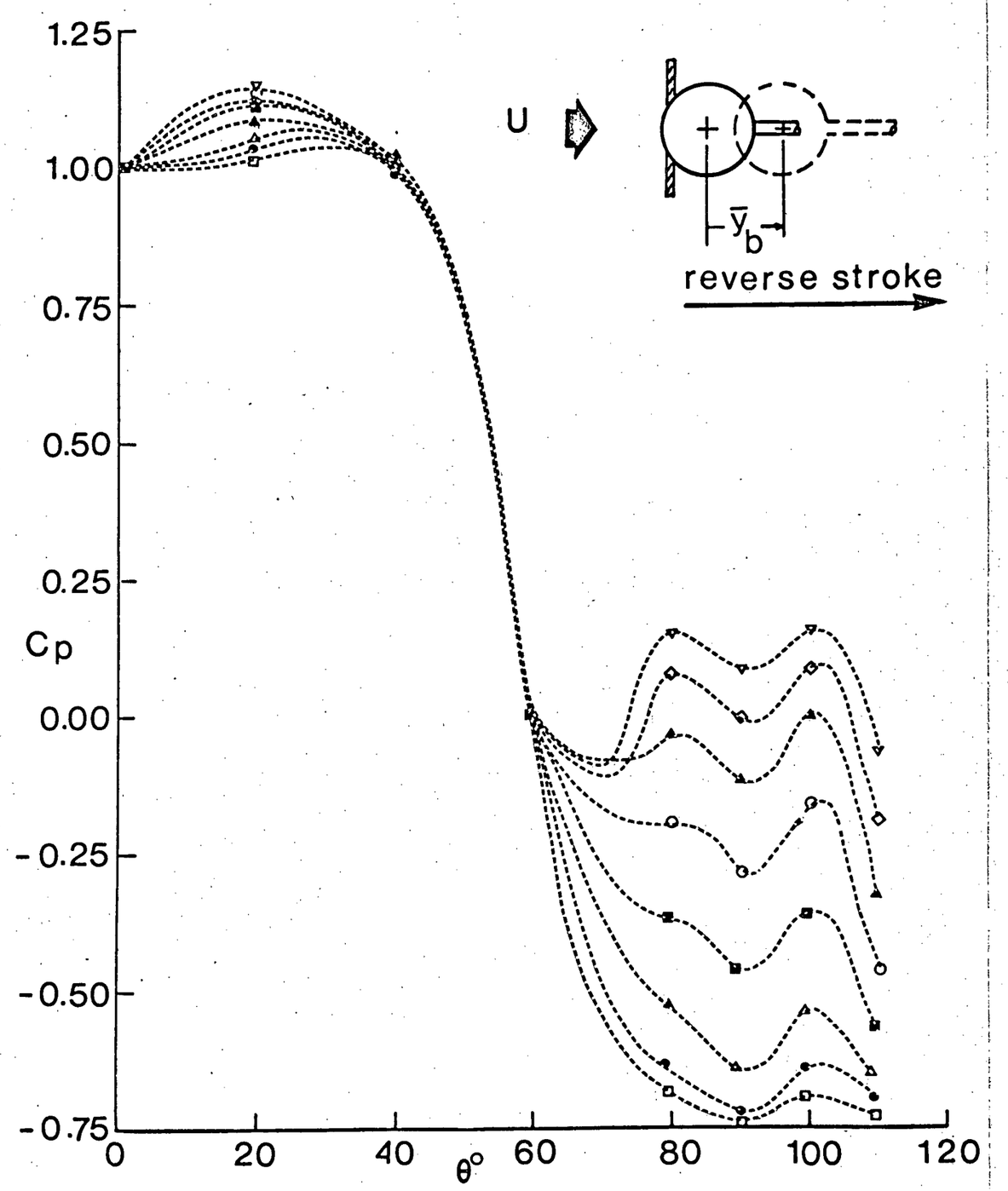

Figure 4-28 Dependence of the surface pressure profiles on the Beta number, Reynolds number, and valve opening: (a) B_n = 19, R_n = 290

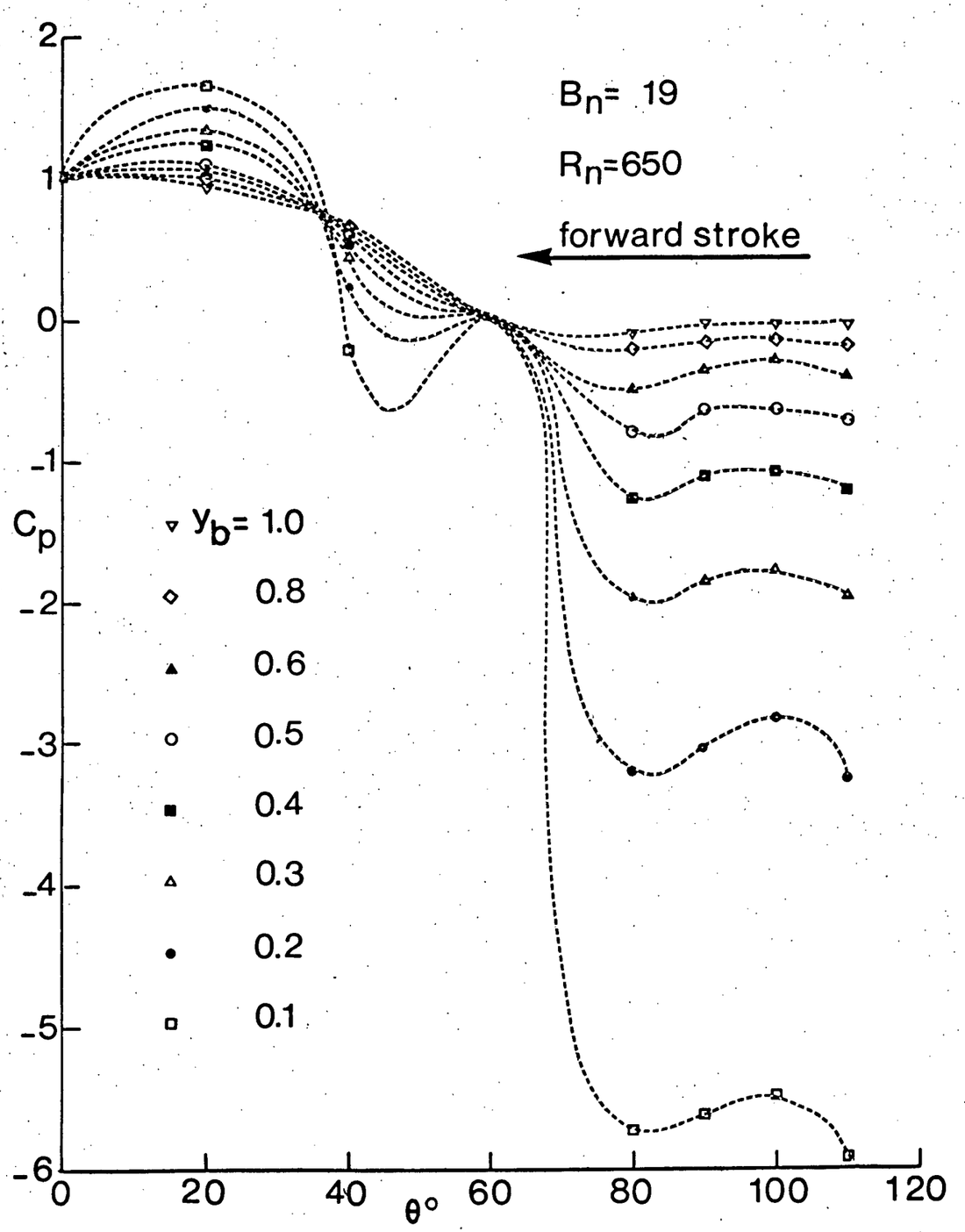

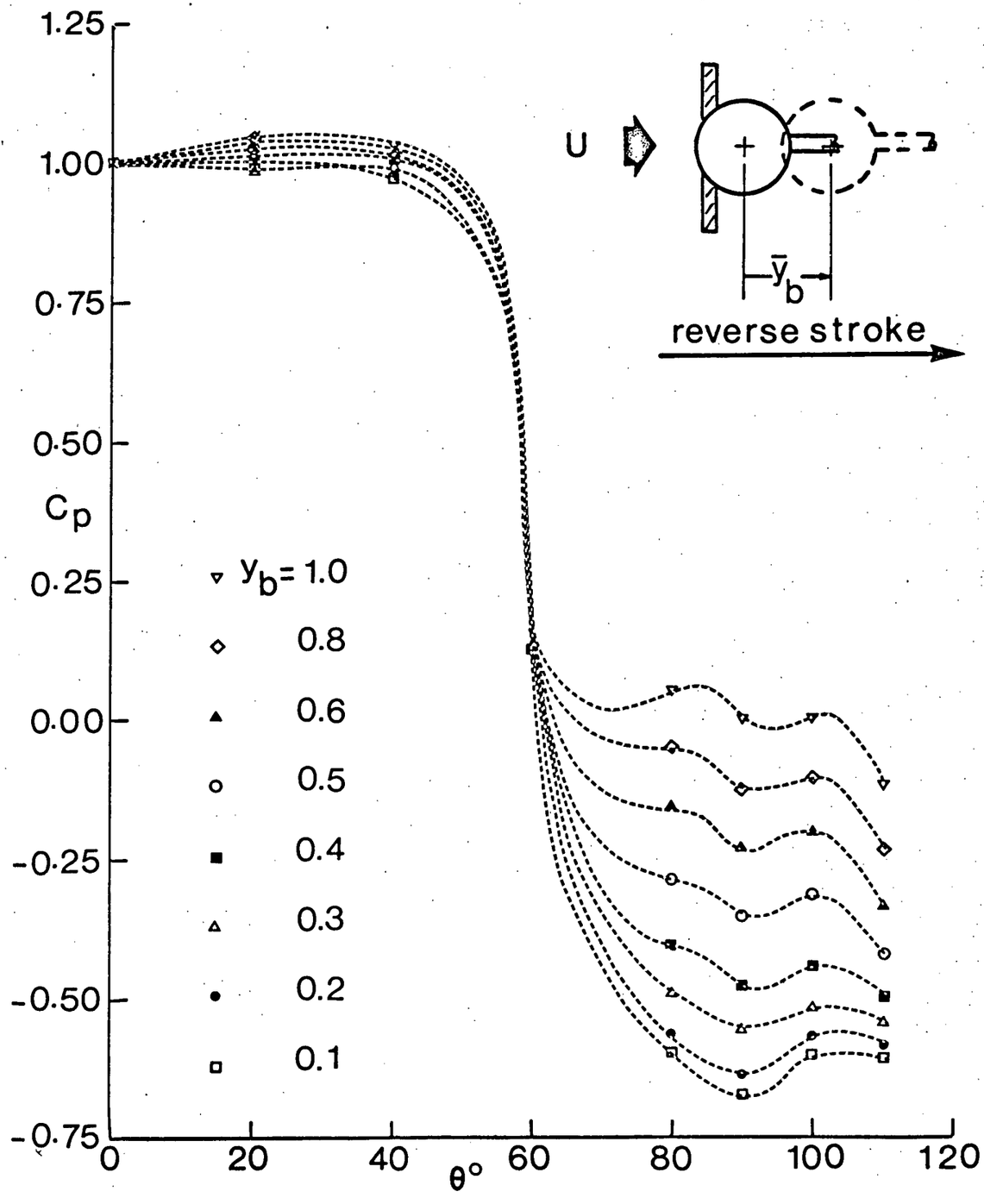

Figure 4-28 Dependence of the surface pressure profiles on the Beta number, Reynolds number, and valve opening: (b) B_n = 19, R_n = 650

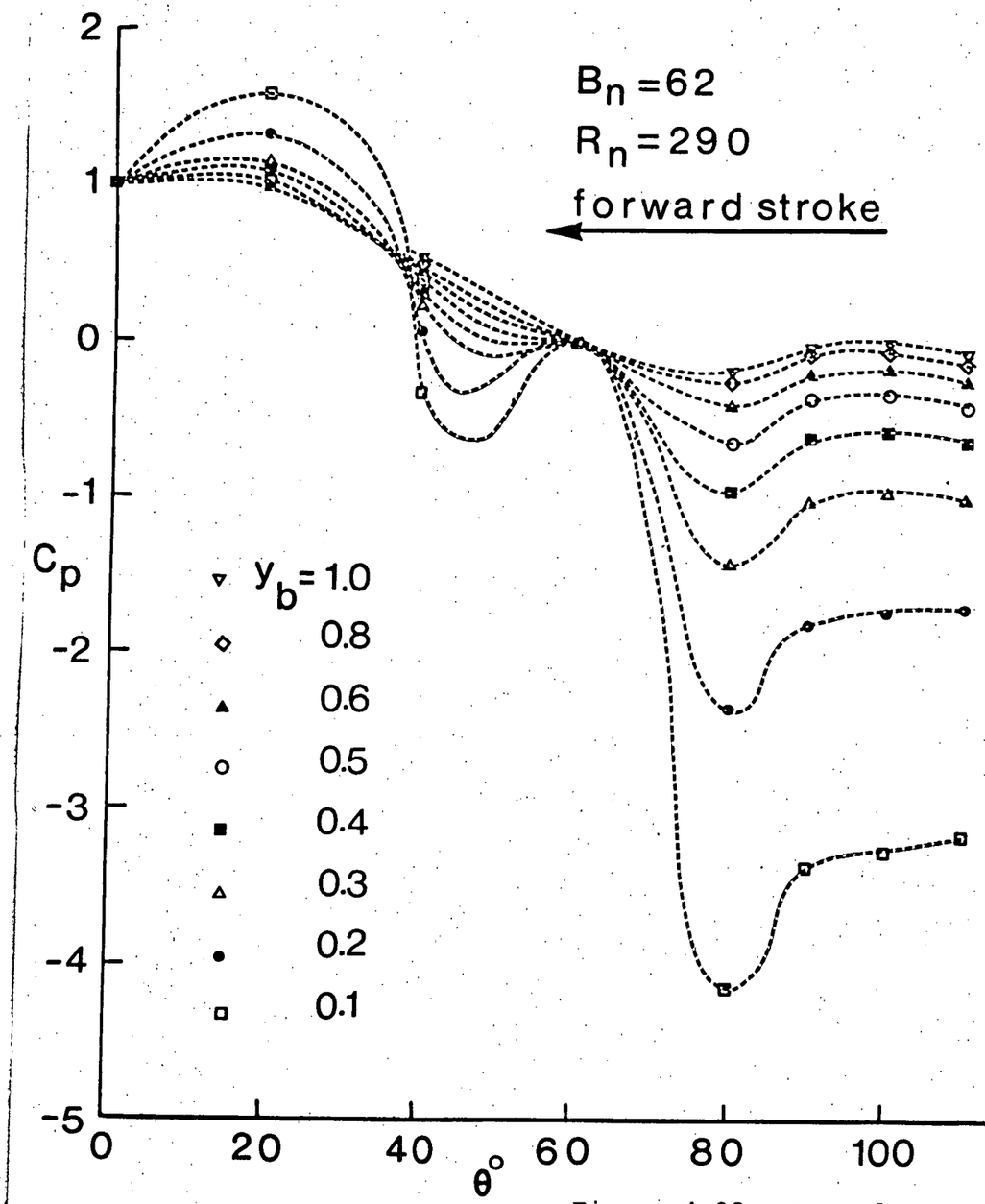

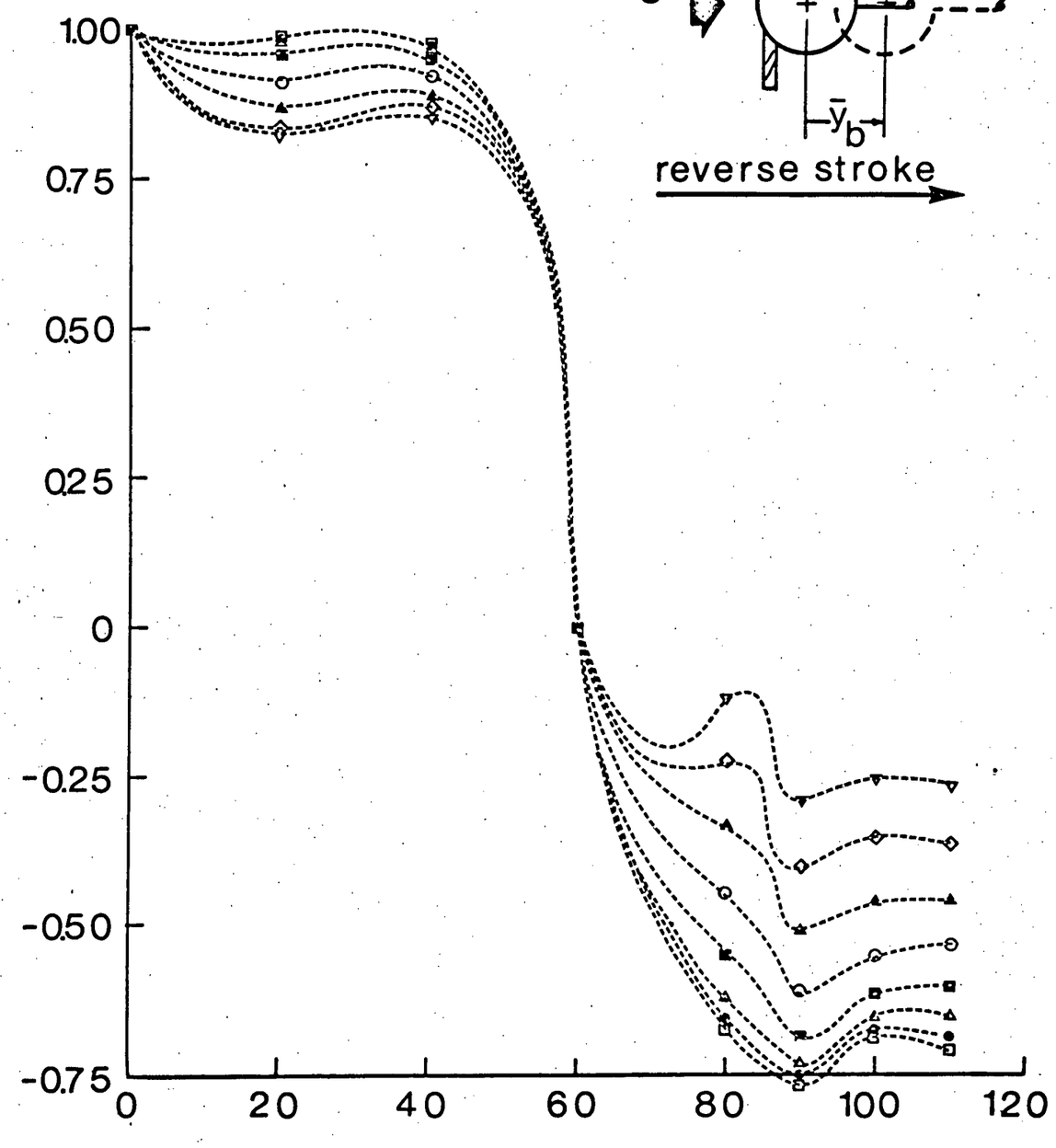

Figure 4-28 Dependence of the surface pressure profiles on the Beta number, Reynolds number, and valve opening: (c) $B_n = 62$, $R_n = 290$

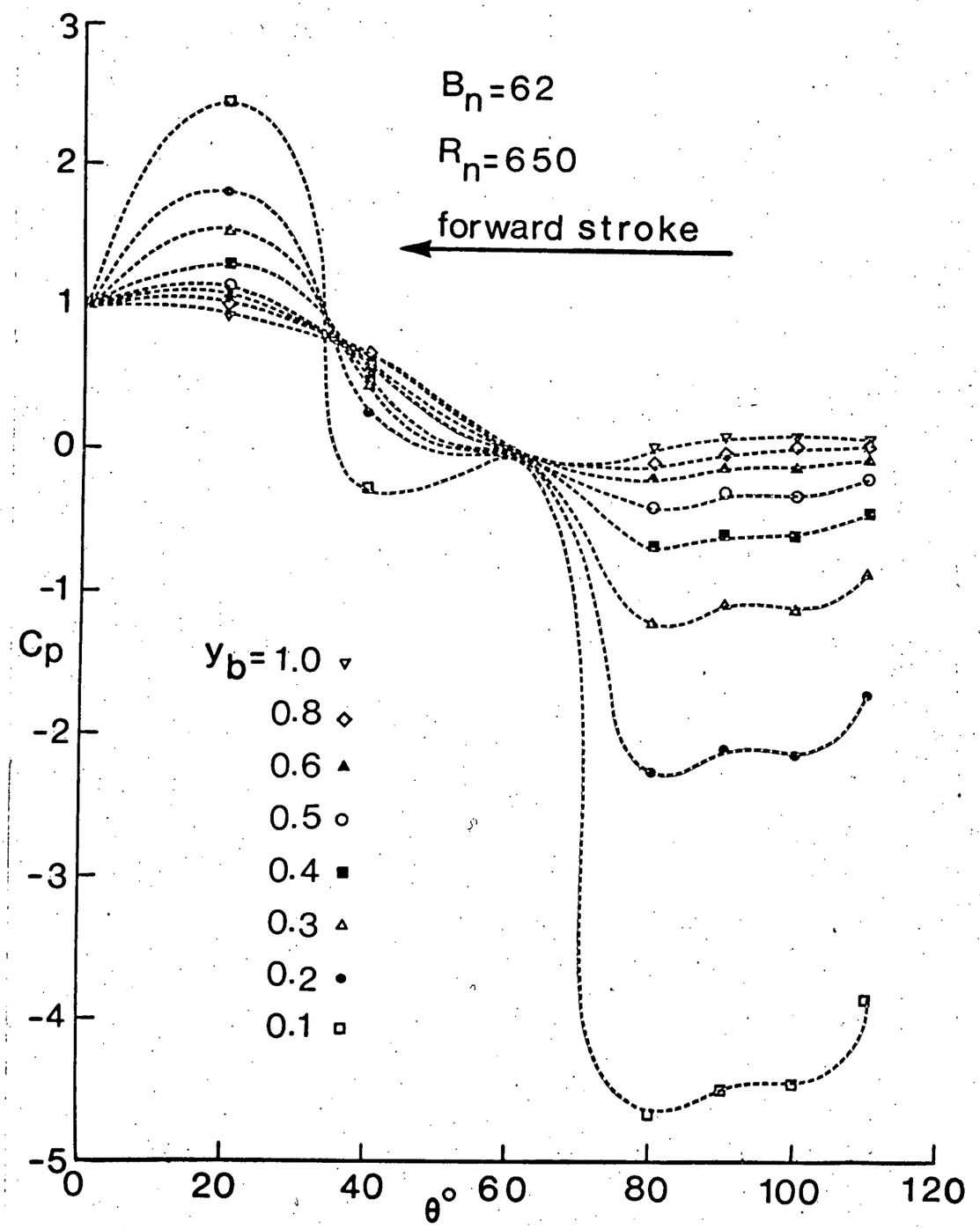

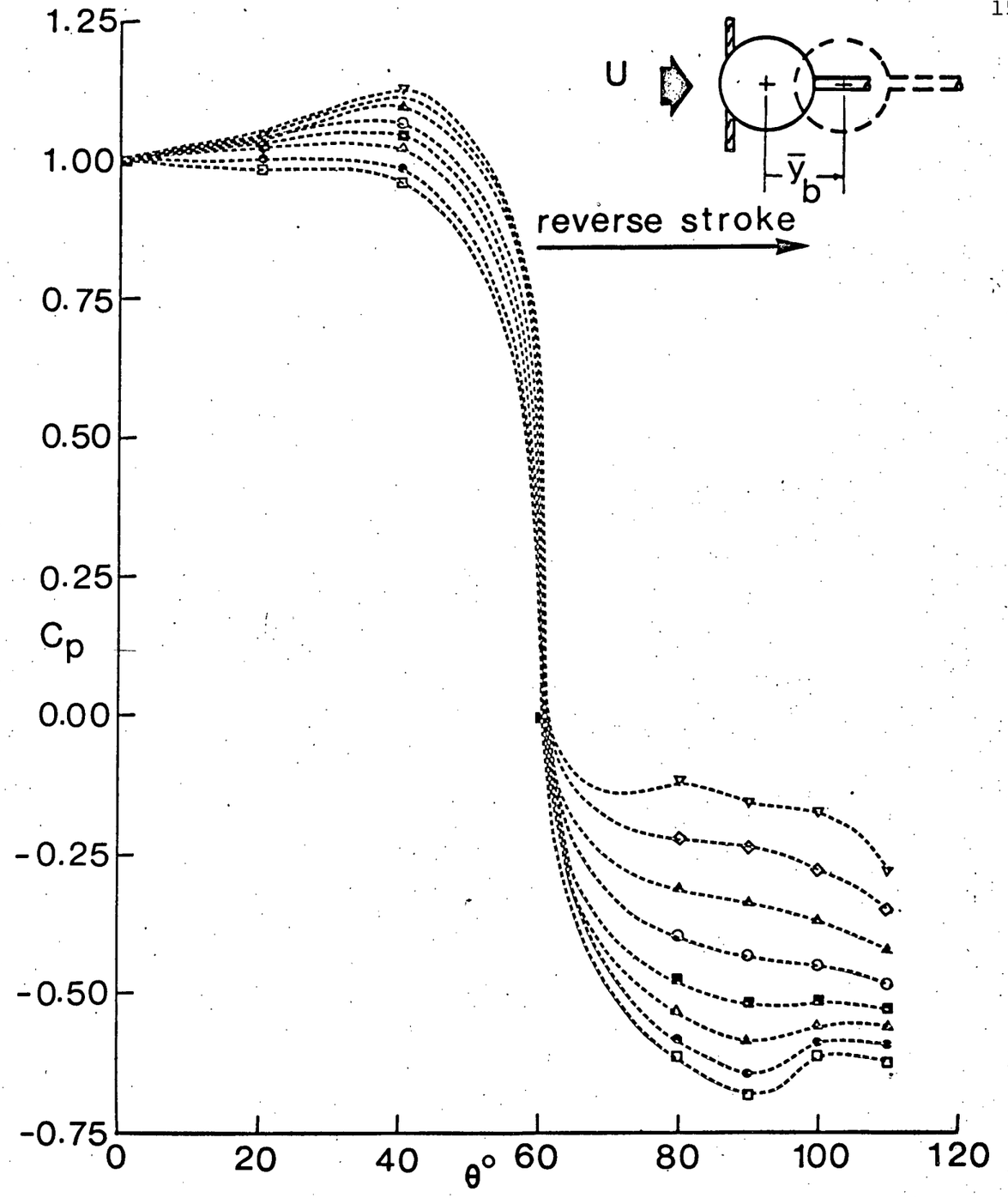

Figure 4-28 Dependence of the surface pressure profiles on the Beta number, Reynolds number, and valve opening: (d) B_n = 62, R_n = 650

Moving to the effect of pulsation frequency on the pressure profile, for a given R_n, it appears to be primarily confined to the negative pressure region and for smaller valve openings ($0 \leq y_b \leq 0.20$). This is better appreciated through Figure 4-29 where pressure variations are plotted as functions of four different values of the Beta number. A degree of similarity with the single pulsating sphere studied earlier (Figure 4-18a) is quite apparent. Of particular interest is the time history of the pressure as a function of the poppet position for a given value of the Reynolds number and Beta number. As the poppet moves closer to the seat, narrowing the valve opening, the back pressure decreases quite sharply. We may recall similar behavior for the stationary poppet (Figure 4-23). However, here due to a relatively higher velocity (poppet velocity plus mean flow velocity during forward stroke) effect of the valve opening on C_p is much greater than that in the stationary case. Note the high negative pressure in the wake region for $y_b < 0.50$. The phenomenon, which is a direct consequence of the main flow being blocked by the poppet, is cyclic and has the same frequency as that of the poppet. The resulting large periodic shear stresses may cause not only distruction and coagulation of the cells leading to clotting as pointed out before,but may also account for rupturing of the suture lines in the implanted prosthetic valve, as occasionally observed.

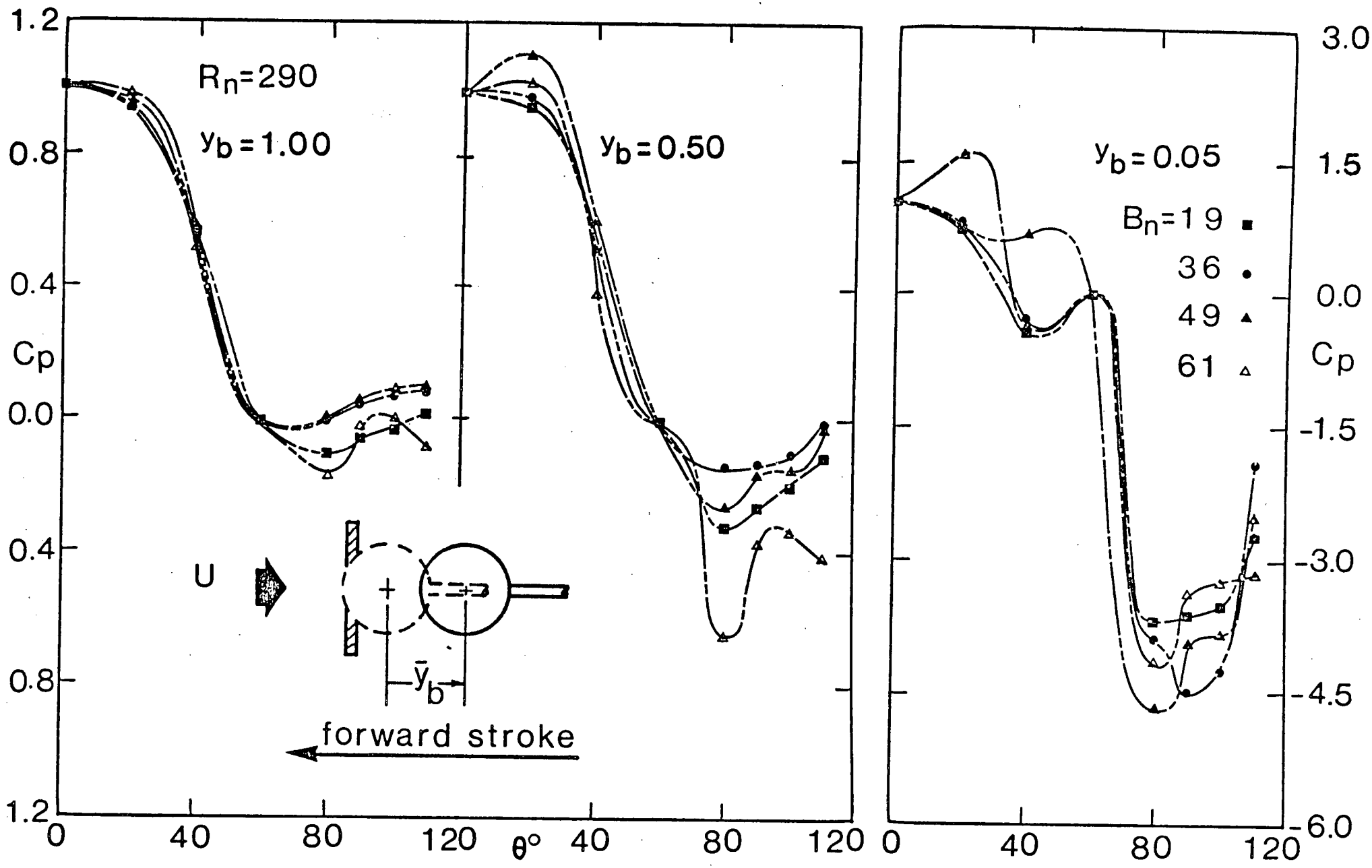

Figure 4-29 Effect of the Beta number on the surface pressure profile for a given R_n: (a) R_n = 290: (i) forward stroke;

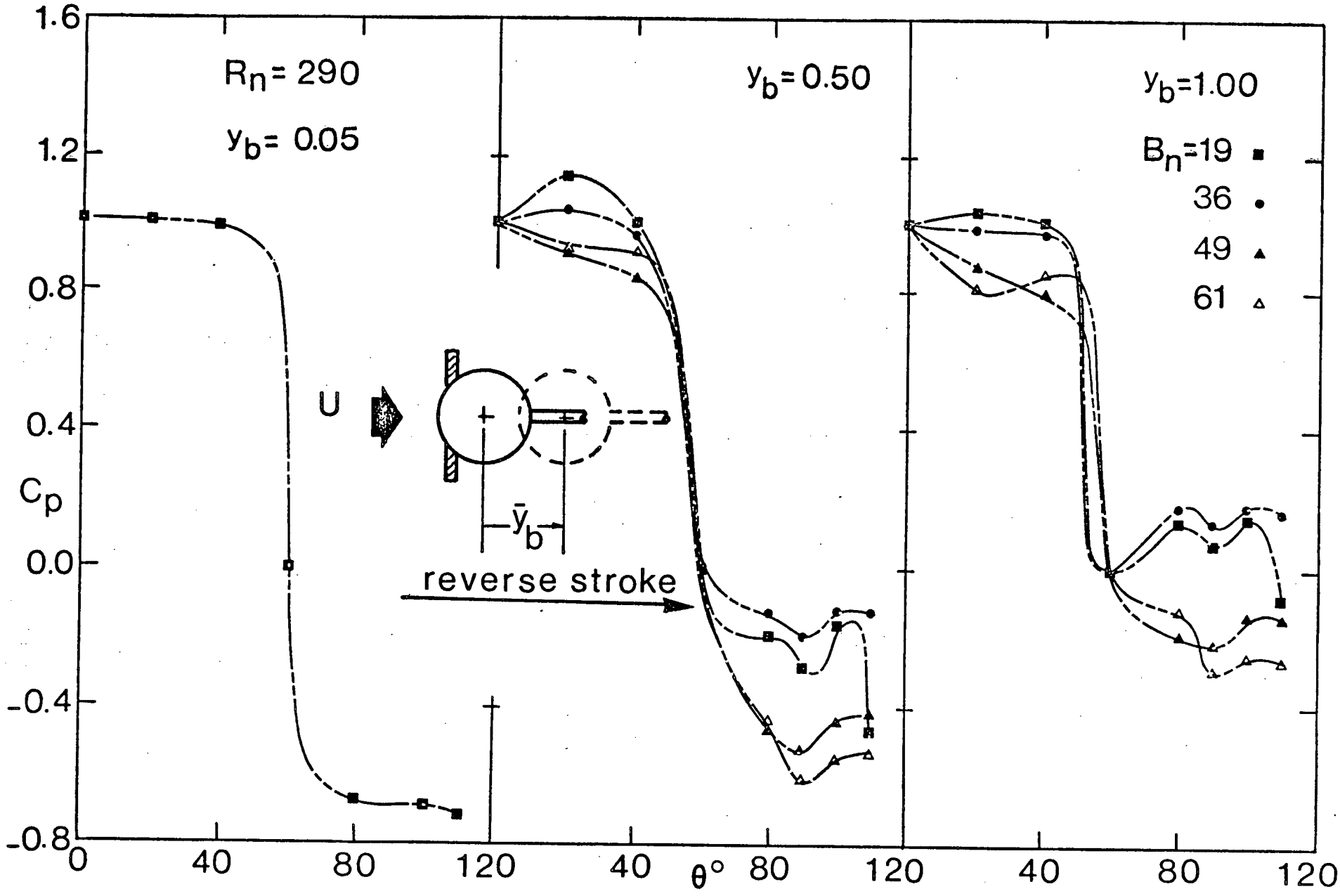

Figure 4-29 Effect of the Beta number on the surface pressure profile for a given R_n: (á) R_n = 290: (ii) reverse stroke

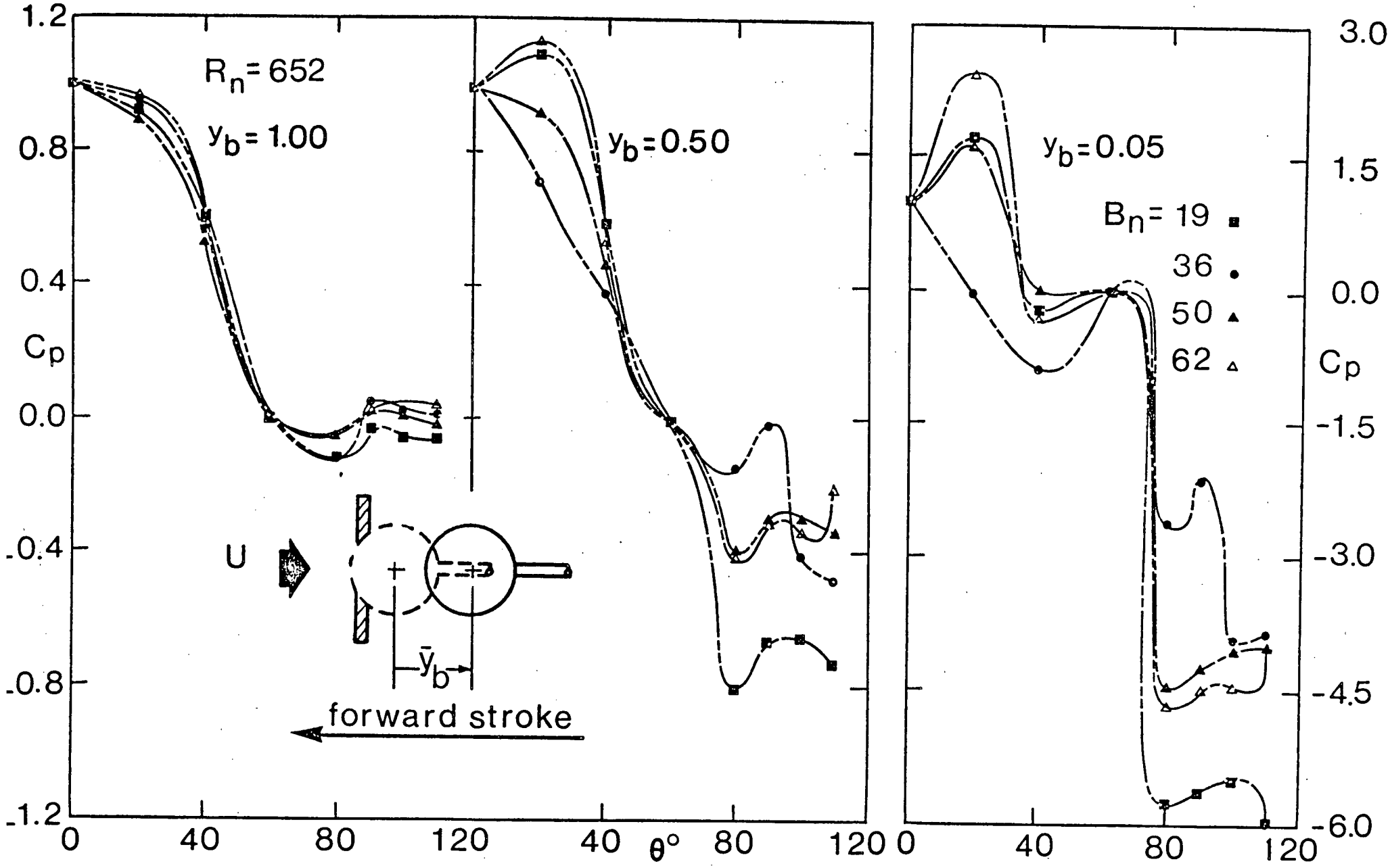

Figure 4-29 Effect of the Beta number on the surface pressure profile for a given R_n: (b) R_n = 652: (i) forward stroke

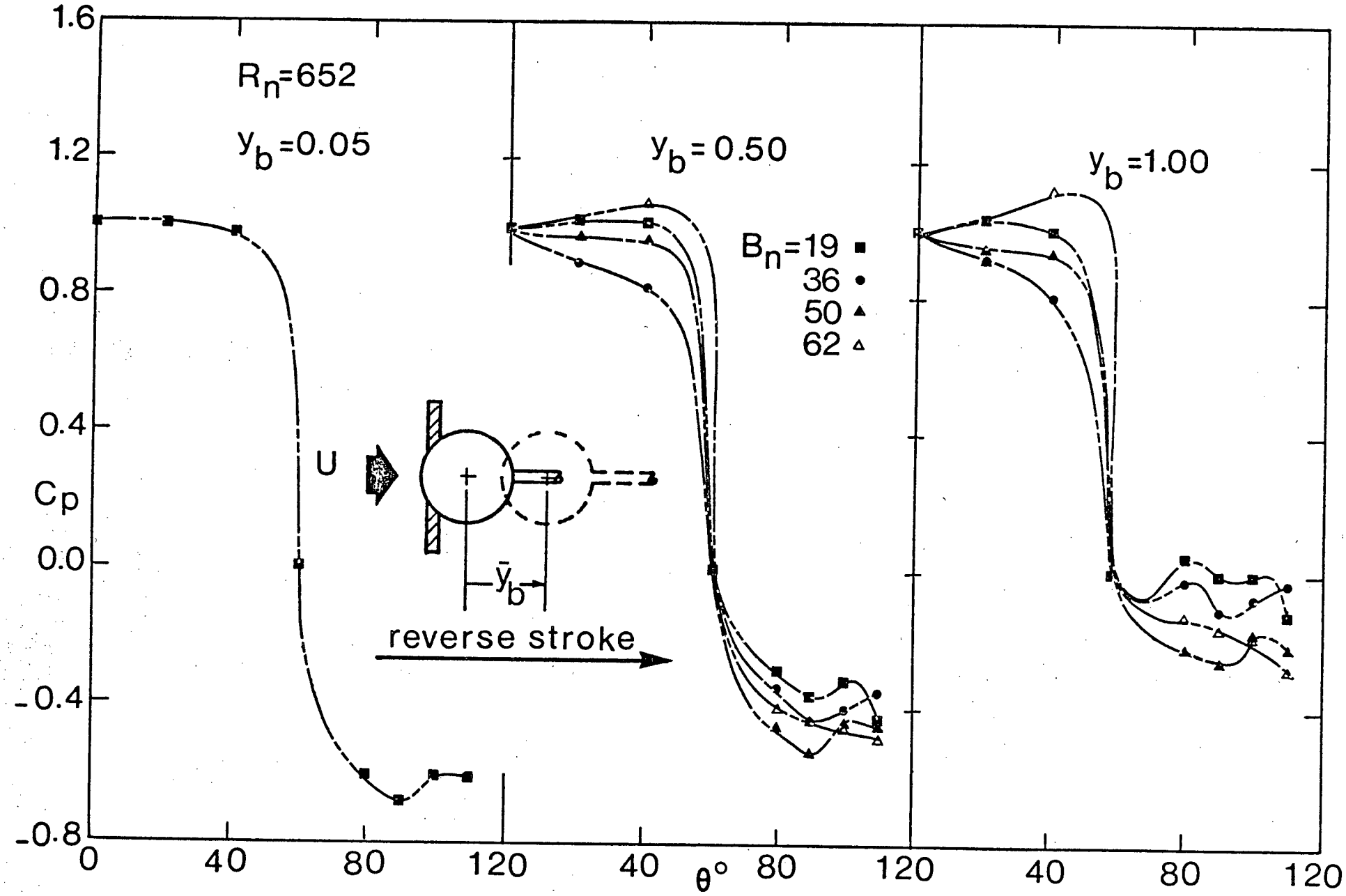

Figure 4-29 Effect of the Beta number on the surface pressure profile for a given R_n: (b) R_n = 652: (ii) reverse stroke

Discussion so far was concerned with the forward portion of the pulsation cycle. Coming to the reverse stroke, it is apparent that the general character of the plots remains essentially the same. However, there are several significant differences. As against the forward case, now the effects of the Reynolds number and Beta number on the pressure profiles are negligible even for small openings. Furthermore, notice the drastic reductions in negative pressures for small openings ($y_b < 0.3$). During the forward cycle this portion of narrow valve openings corresponded to the deceleration while during the reverse stroke the same portion represents an accelerating poppet. This accelerating motion with increase in opening does not result in a stable jet and consequently the lower negative pressures. On the other hand, for larger openings during the reverse stroke pressure coefficients are less positive compared to those for the forward case, thus emphasizing the R_n effect discussed before (i.e. higher Reynolds number in the range $100 \leq R_n \leq 1200$ leads to higher positive pressures but for $1200 < R_n < 5800$ the R_n effects seems to be negligible; Section 4.3.3, Figure 4-26).

No attempt is made here to explain the observed dependence of surface pressures on various systems parameters, as any such effort would be, at best, mere speculation. We are dealing with a highly complex system consisting of intricate geometry and numerous variables. One is thus

forced to be satisfied with the description of the observed behavior and correlate its possible influence in light of the recorded prosthetic valve performance. On the other hand, the results clearly emphasize the usefulness of studies of a single sphere by itself and when occupying various stationary positions in the valve. Although different in details, a general similarity in the plots is quite evident. Hence the discussion given earlier in Sections 4.3.1 - 4.3.3 may have some relevance here.

A flow visualization study helped gain better appreciation of this rather complex character of the fluid dynamics problem. As explained before, the flow pattern was visualized using the dye injection procedure and recorded through a 16 mm high speed photography.

An analysis of the movie clearly showed acceleration and deceleration of flow during the cycle through extension and compression of the dye filaments. Formation of nodal points on the streamlines suggested pressure build-up upstream during the valve closure. The streamlines on the sphere were, in general, inclined to and executed rotational motion about the horizontal axis indicating helical character of the separating vortex ring (Figure 4-30).

By far the most striking contribution of the flow visualization was a vivid confirmation as to the time dependent character of the separation position during the

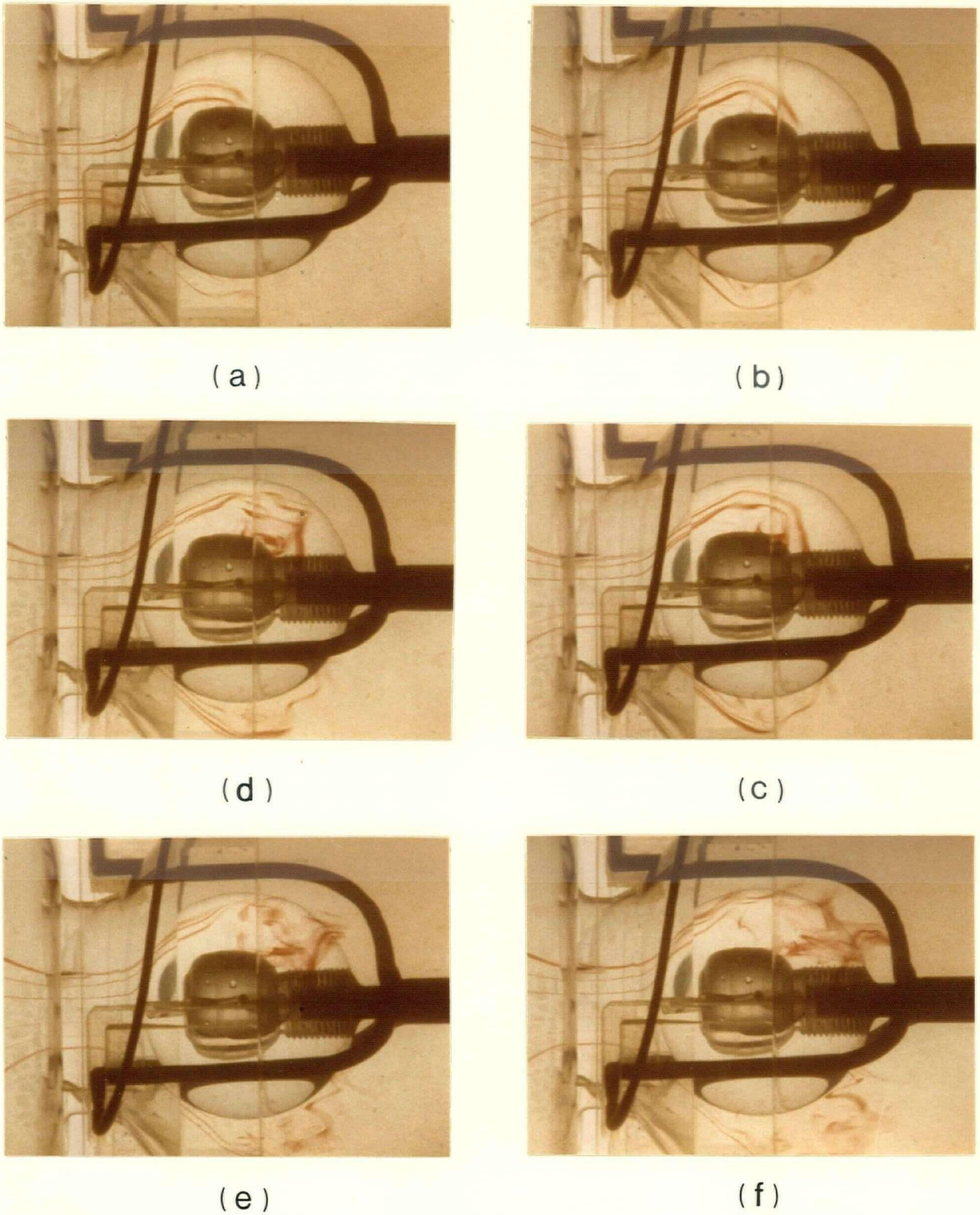

Figure 4-30 Typical photographs illustrating rotational motion of streamlines about the horizontal axis as captured by the 16mm movie

poppet oscillation. Although it would be imprecise to assign numerical values to data obtained through such a crude visualization procedure, the trends were quite distinct. They substantiated general behavior of the separation movement as predicted analytically by Lin[131].

Contraction of the flow past the inlet orifice was evident through the crowding of streamlines. This was followed by jetting of the fluid in the exit bell as indicated by stretching of the dye filament, which finally disintegrated in the turbulent wake (Figure 4-31). Of considerable practical interest was the flow reversal, illustrated by the back flow of the dye filaments during the valve closure, suggesting the possibility of regurgitation. Surprising as it may seem, the movie showed periods of almost stagnant condition in the wake, particularly at a higher pulsation frequency and when the poppet was moving forward to close the valve, which may stimulate deposition of the dissociated blood constituents and thus promote clotting.

4.4 Conclusion

It would be useful to review some of the more significant results of the experimental investigation:

(i) The designed glycerol tunnel performs satisfactorily and produces essentially flat velocity profiles, at least over the central 10 cm. of

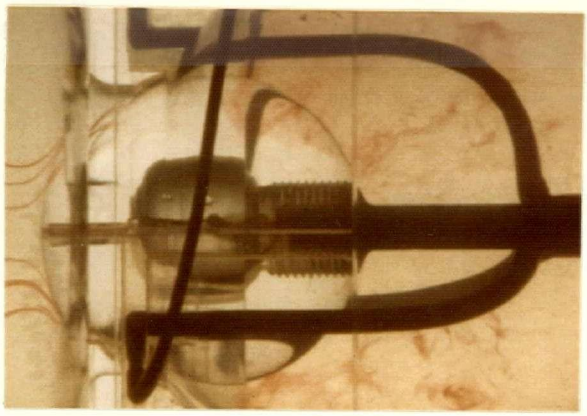

$y_b = 0.05$

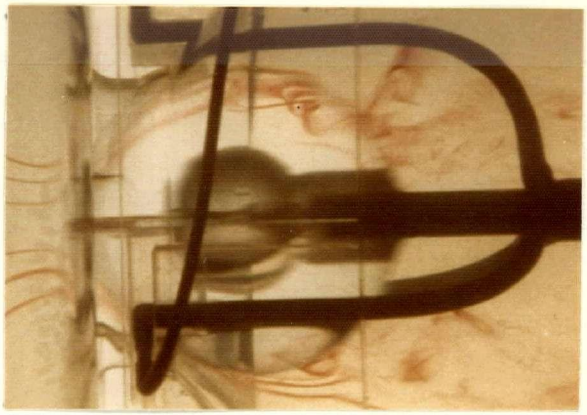

$y_b = 0.20$

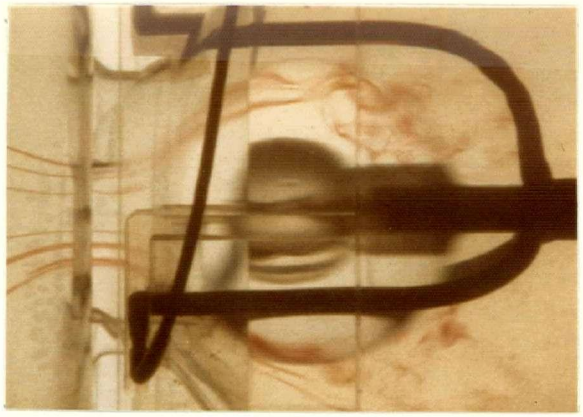

$y_b = 0.50$

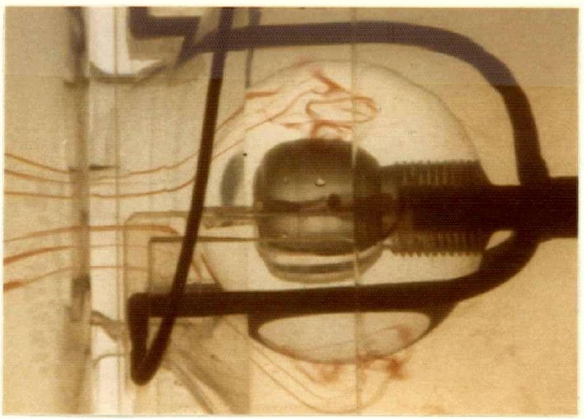

$y_b = 0.90$

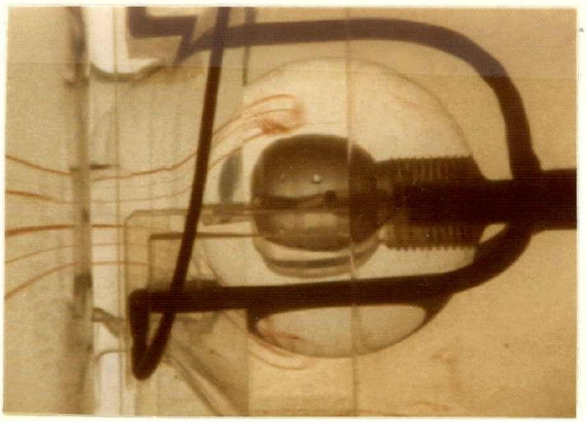

$y_b = 0.95$

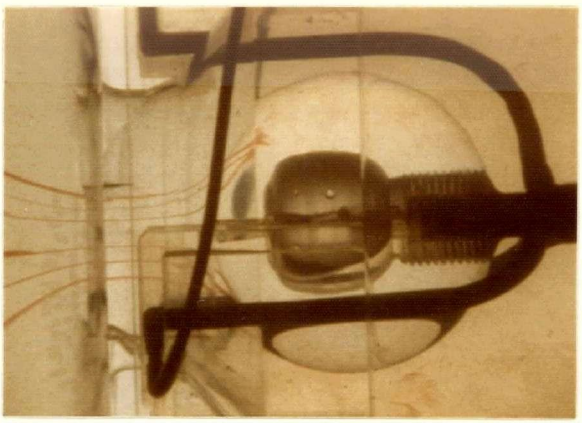

$y_b = 1.0$

Figure 4-31 A flow visualization study illustrating several important characters (time-dependent separation, contraction through the inlet orifice, jeting of fluid in the exit bell, turbulent wake, etc.) of the flow during pulsatile motion of the poppet inside the valve

the tunnel section, which are acceptable for the test program. In general, the uniform portion of the profile decreases with an increase in velocity or distance from the tunnel inlet.

(ii) Introduction of a model in the tunnel test section substantially modifies the velocity profiles. The spherical model, with a small blockage ratio, tends to improve the velocity profile, i.e. it extends the region of nearly uniform flow. On the other hand, the aortic valve model affects the profiles adversely. The valve opening also has direct influence on the velocity profiles and hence on C_p distributions on the surface of the poppet.

(iii) Use of the average velocity in the test section (based on the mean flow rate) as a reference velocity promises to promote repeatability and comparison of data regardless of the test facility used. Furthermore, defining C_p as:

$$C_p = \frac{P_\theta - P_{ref}}{P_0 - P_{ref}}$$

tends to compensate for blockage effects, irregularity of the velocity profiles and possible errors in pressure measurements caused

by electrical drifts of the pressure measuring system. Furthermore, in conjunction with the Reynolds number (based on the suggested average velocity), it promises to assist in duplication and comparison of similar data by other investigators using different test facilities.

(iv) A vertical stem supporting the spherical model has negligible influence on the pressure distribution if the sphere to stem diameter ratio is greater than seven.

(v) For pressure distribution on the surface of a sphere, the Reynolds number effects are primarily confined to the region downstream of the zero pressure point. Locations of the minimum pressure and the separation points tend to shift forward with an increase in R_n. Of particular interest is the sudden rise in the magnitude of the minimum pressure and the average base pressure downstream of it around $R_n = 240 - 475$. As confirmed by the flow visualization, this is associated with the onset of instability of the vortex ring.

(vi) Drag coefficient obtained by integrating pressure agrees rather well with the available experimental and theoretical results and thus tends to substantiate reliability of the pressure data.

(vii) Pressure distribution on the downstream section of a pulsating sphere ($60° \leq \theta \leq 110°$) displays a direct dependence upon the time history of the poppet position. A decrease in y_s causes increase in the minimum and average wake pressures together with a forward movement of the separation point during the forward stroke. However, C_p is essentially independent of the Reynolds number. Effect of the Beta number is confined to local changes in the character of the base pressure plots without substantially affecting their average magnitudes. Although during the reverse stroke the general character of the pressure profiles remains essentially the same, their magnitudes and sensitivity to the position parameters are markedly different.

(viii) As in the case of a single sphere by itself, R_n effects are confined to the wake region for a poppet occupying different positions in the valve (bypass open). The R_n influence, which is more significant for $y_b < 0.20$, is essentially reflected in increase of the wake pressure. On the other hand, valve opening for a given Reynolds number substantially affects the pressure distribution over the entire surface of the poppet. With a progressive reduction in y_b (i.e. valve closing),

the pressure on the frontal section of the sphere increases while that on the downstream section diminishes, leading to a reversal of the flow. A dramatic rise in the negative pressure coefficient at $y_b \leq 0.1$ in the near wake region has far-reaching significance. This would suggest large shearing stresses leading to possible deformation and destruction of the red blood cells. The presence of vorticity distribution and the associated centrifugal field in the wake are the prime suspects promoting dissociation of the blood into its constituents and finally their deposition on the body of the valve.

(ix) In general, pressure distribution on the poppet occupying different positions inside the valve, with bypass closed, exhibits the same trends as those observed during the open bypass case with one significant difference: closing of the bypass tends to increase the pressure on the downstream region of the poppet (i.e. $\theta \gtrsim 60°$). This is attributed to the jet-like flow issuing from the exit bell leading to a higher effective R_n. Of particular importance is the location of the separating shear layer and its movement

with the poppet position. Now the poppet of the prosthetic device has a periodically oscillating boundary layer with associated wake that also grows periodically. Obviously, this adds to the turbulent character of the wake, which appears to be the main cause of concern in successful operation of the device.

(x) For the poppet oscillating inside the valve, irrespective of the pulsation frequency, the Reynolds number effect is rather insignificant for larger valve openings ($y_b > 0.2$). However, for narrow valve settings ($y_b < 0.2$), R_n influence is substantial: an increase in R_n leads to a decrease in the wake pressure. Effect of the pulsation frequency is primarily confined to the negative pressure region at smaller valve openings ($0 \leq y_b \leq 0.20$). On the other hand, influence of the valve opening on C_p is quite striking and much greater than that in the stationary case. High negative pressure in the wake region for $y_b < 0.50$, which is a direct consequence of the main flow being obstructed by the poppet, is cyclic and has the same frequency as that of the poppet. The resulting large periodic shear stresses may cause not only distortion and coagulation of the cells leading

to clotting as pointed out earlier but may also account for rupturing of the suture lines in the implanted prosthetic valve, as occasionally observed.

(xi) Flow visualization proved to be quite useful in providing better appreciation of this rather complex fluid dynamics problem. Formation, symmetric elongation, onset of asymmetry and instability followed by turbulent shedding of the vortex ring were clearly illustrated by the dye injection procedure. Forward movement of the separation point with increasing R_n (single sphere) and its rearward movement with a progressive closure of the valve were also vividly observable. A visual study of the cyclic acceleration and deceleration of the flow, helical character of the separating vortex ring, flow reversal, stagnant condition of fluid in the wake followed by a period of high turbulent motion, etc., not only complemented the test data but also helped understand the phenomenon better.

5. CLOSING COMMENTS

5.1 Concluding Remarks

The primary objectives of the research program have been twofold:

(i) to design, construct, calibrate and instrument a liquid tunnel facility particularly suited for low Reynolds number research in the range $75 \leq R_n \leq 5000$;

(ii) to utilize the facility to study hydrodynamic performance of an artificial aortic ball valve under simulated condition with a hope to gain some insight into the problems encountered in its operation.

One can say with a measure of satisfaction that both the objectives have been realized to an extent. However, I must hasten to add that in a very real sense, the thesis represents only a beginning in exploration of the challenging and equally interesting problem. I have barely touched upon the fringes of an extremely complex problem which only now I am able to understand a little better. Probably the progress of knowledge rests on such modest steps.

The liquid tunnel with controlled variation of the Reynolds number should represent a welcome addition to

the departmental facilities. It would undoubtedly be utilized in further investigation of a variety of aspects associated with this and other bioengineering oriented programs. However, what is more important to recognize is the fact that with its precise temperature control of the working fluid, test section with optically flat glass sides (ideally suited for Schlieren photography and laser doppler anemometry), carefully designed hydraulic and electronic circuitry for pulse duplication, recirculation and filtering loop, etc. the tunnel represents an ideal tool for studying a variety of fundemental problems in fluid mechanics.

The pressure distribution data on the surface of a sphere in the Reynolds number range $74 \leq R_n \leq 5838$ represents a significant contribution in the area of fundamental fluid mechanics. More importantly, the flow visualization of the formation, growth and instability of the vortex ring and its correlation with the accompanying pressure variation provides better appreciation of the physics of the phenomenon, and remain unrecorded so far.

Coming to the hydrodynamics of the prosthetic heart valve proper, the project appears to be the first systematic attempt at establishing fluid dynamic characteristics of the widely used configuration. This is very important as now we have a reference that can be used to evaluate merits of any future inovations in the design of such prosthesis.

In obtaining pressure results over the entire range of variation of nine dimensionless Π numbers during the carefully simulated displacement-time history of the valve lies the strength of the project. It throws some welcome light on several fundamental questions concerning blood clotting and hemolysis. The dramatic rise in the negative pressure for small valve openings suggests large shearing stresses leading to possible deformation and destruction of the red blood cells. The wake vorticity and the associated centrifugal field are probably the two fundamental factors promoting dissociation of the blood and deposition of its constituents on the valve. Periodic character of the phenomenon only accentuates the problem and may also be responsible for ruptured suture lines.

Contribution of the flow visualization in such a study can hardly be overemphasized. A visual study of the cyclic acceleration and deceleration of the flow, helical character of the separating vortex ring, flow reversal, stagnant condition of the fluid in the wake, periods of high turbulent motion, etc. not only complemented the test data but also helped to understand the phenomenon better.

5.2 Recommendation for Future Work

The investigation reported here suggests several topics for future exploration. Much can be learned about the problem through a well-organized experimental program. However, the number of system variables involved are rather enormous hence, any attempts in achieving precise dynamic similarity is likely to demand considerable time and patience. Although ideally one would like to employ a model that reproduces the actual prosthesis in all its details — structural, geometrical and fluid dynamic — practical considerations would require us to establish relative significance of the parameters involved and dictate some judiciously thought out compromises. Only a few of the more significant avenues of future efforts, which are likely to be rewarding, are briefly indicated here.

(i) The obvious logical extension of the present work would be to aim at precise duplication of the:
   (a) flexible character of the surrounding;
   (b) pulsatile character of the flow;
   (c) tappered character of the aorta at the implantation site;
   (d) non-Newtonian character of the flow using, may be, blood compatible synthetic polymers[136].

(ii) Character of the fluid in the near wake region plays an important role in governing the valve

performance. Hence, a study leading to information concerning periodic movement of the separation points, mean and unsteady velocity profiles of the separating shear layers, transition to turbulence, mechanism of the first vortex formation together with generation, dissipation, diffusion and retention of vorticity, etc. would go a long way in providing better appreciation of the process. Of particular interest would be a detailed study of the turbulent character of the flow, both near the poppet surface as well as in the wake. Attention may also be directed towards the measurement of the surface shear stress using flush mounted hot films. These have far reaching implications, as the data would identify regions in the fluid field most responsible for deformation and destruction of the red blood cells.

(iii) Serious efforts should be made to assess blockage effects due to the poppet operating in the confined aorta and under adverse pressure gradient. Such a study as a function of the Reynolds and Beta numbers should provide useful information concerning the wake-body interaction. A preliminary study of this aspect is already in progress.

(iv) With the test facility and instrumentation having been well organized, it would be useful to undertake a study concerning the fluid dynamics of an accelerating sphere with different time-displacement histories. The experiments may be conducted under stationary and streaming conditions of the fluid with the desired pressure gradient. This would help assess validity of the existing theories[126-134] and contribute towards evolution of a better model for an analytical approach to such a complex problem.

(v) A systematic study of the drag force acting on the sphere during opening and closing conditions would be of considerable interest. This would assist in reshaping the exit bell such that the intensity of the impact between the cage and poppet is minimized. Obviously, this would reduce the wear of the components involved.

(vi) One approach that seems promising in improving the valve design would be to study the effectiveness of momentum injection in delaying separation. Several attractive configurations are possible (Figure 5-1). Preliminary tests suggest a reduction in the size of the wake and hence the rate of deposition of the blood constituent on the cage.

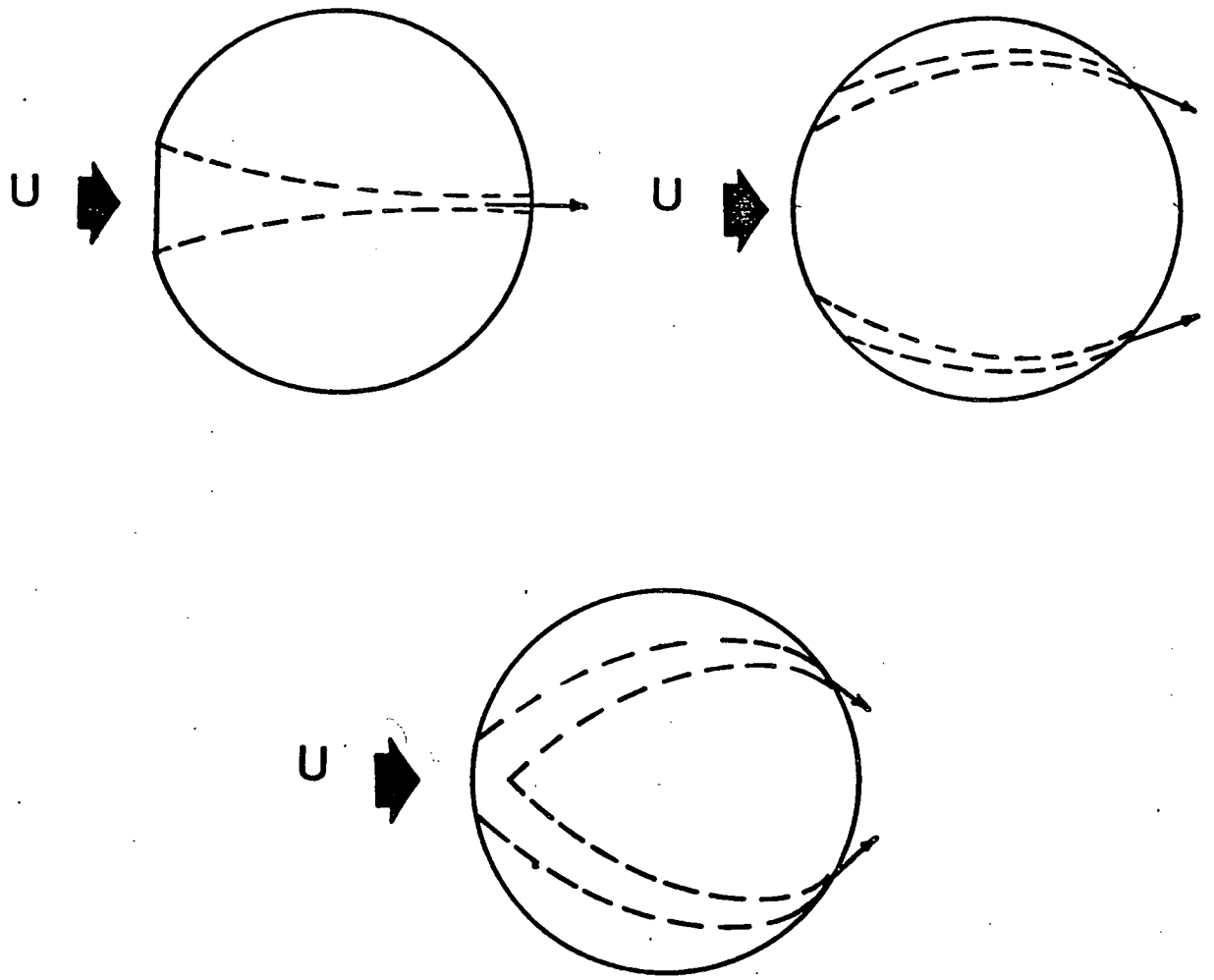

Figure 5-1 A schematic diagram showing several configurations for momentum injection

BIBLIOGRAPHY

1. Smithy, H.G., and Parker, E.F., "Experimental Aortic Valvulotomy," Surgery, Gynacology and Obstetrics, Vol. 84, No. 4A, April 1947, pp. 625-628.

2. Smithy, H.G., Pratt-Thomas, H.R., and Deyerle, H.P., "Aortic Valvulotomy," Surgery, Gynacology and Obstetrics, Vol. 86, No. 5, May 1948, pp. 513-523.

3. Denton, G.R., "Plastic Prosthesis (without moving parts) for the Atrio-Ventricular Valves," Proc. of the Thirty-Sixth Clinical Congress, Surgery Forum, American College of Surgeons, Boston, Massachusetts, October 1950, pp. 239-245.

4. Hufnagel, C.A., Harvey, W.P., Rabil, P.J., and McDermott, T.F., "Surgical Correction of Aortic Insufficiency," Surgery, Vol. 35, No. 5, May 1954, pp. 673-683.

5. Ross, J., Jr., Copper, T., and Brockenbrough, E.C., "Experimental Replacement of the Pulmonic Valve with a Tricuspid Semilunar Prosthesis," J. Thoracic and Cardiovascular Surgery, Vol. 42, No. 3, September 1961, pp. 371-378.

6. Magovern, G.J., Kent, E.M., and Cromie, H.W., "Sutureless Artificial Heart Valves," Circulation, Vol. XXVII, No. 4, April 1963, pp. 784-788.

7. Gott, V.L., Daggett, R.L., Whiffen, J.D., Kopke, D.E., Rowe, G.G., and Young, W.P., "A Hinged-Leaflet Valve for Total Replacement of the Human Aortic Valve," J. Thoracic and Cardiovascular Surgery, Vol. 48, No. 5, November 1964, pp. 713-725.

8. Bahnson, H.T., Spencer, F.C., Busse, E.F.G., and Davis, F.W., "Cusp Replacement and Cornary Artery Perfusion in Open Operation on the Aortic Valve," Ann. of Surgery, Vol. 152, No. 3, September 1960, pp. 494-505.

9. Mohri, H., Hessel, E.A., Nelson, R.J., Anderson, H.N., Dillard, D.H., and Merendino, K.A., "Design and Durability Test of Silastic Trileaflet Aortic Valve Prostheses," J. Thoracic and Cardiovascular Surgery, Vol. 65, No. 4, April 1973, pp. 576-582.

10. Starr, A., Edwards, M.L., McCord, C.W., and Griswold, H.E., "Aortic Replacement Clinical Experience with a Semirigid Ball-Valve Prosthesis," Circulation, Vol. XXVII, No. 4, April 1963, pp. 779-783.

11. Gott, V., Daggett, R.L., Botham, R.J., Koepke, D.E., Zarnstroff, W.C., and Young, W.P., "The Development of a Prosthetic Heart Valve Utilizing a Rigid Housing and Flexible Butterfly-Wing Leaflet," Tran. of the American Society for Artificial Internal Organs, Vol. 8, No. 1, January 1962, pp. 72-78.

12. Björk, V.O., "A New Central-Flow Tilting Disc Valve Prosthesis," J. Thoracic and Cardiovascular Surgery, Vol. 60, No. 3, September 1970, pp. 355-374.

13. Kalke, B.R., Carlson, R.G., and Lillehei, C.W., "Hingeless Double Leaflet Prosthetic Heart Valve for Aortic, Mitral or Tricuspid Positions," Biomedical Sciences Instrumentation, Vol. 4, Plenum Press, New York, 1967, pp. 190-196.

14. Wada, J., Komatsu, S., Ikeda, K., Kitaya, T., Tanuka, N., and Yamud, H., "A New Hingeless Valve," Prosthetic Heart Valves, Editor-in-Chief: L.A. Brewer, Charles C. Thomas-Publisher, Springfield, Ill., 1969, pp. 304-318.

15. Björk, V.O., Cullhead, I., and Lodin, H., "Aortic Valve Prosthesis (Teflon), Two Year Follow-up," J. Thoracic and Cardiovascular Surgery, Vol. 45, No. 5, May 1963, pp. 635-644.

16. Larson, R.E., and Kirklen, J.W., "Early and Late Results of Partial and Total Replacement of the Aortic Valve with Individual Teflon Cusps," J. Thoracic and Cardiovascular Surgery, Vol. 47, No. 6, June 1964, pp. 720-724.

17. Byörk, V.O., "Aortic Valve Replacement," Thorax, Vol. 19, No. 4, July 1964, pp. 369-378.

18. Oliva, P.R., Johnson, M.L., Pomerantz, M., and Levene, A., "Dysfunction of the Beal Mitral Prosthesis and its Detection by Cineflouroscopy and Echocardiography," The American Journal of Cardiology, Vol. 31, March 1973, pp. 393-396.

19. Hendrson, B.J., Mithas, A.S., LeRoux, B.T., and Gotsman, M.S., "Haemolysis Related to Mitral Valve Replacement with the Beall Valve Prosthesis," Thorax, Vol. 28, 1973, pp. 488-491.

20. DuPriest, Jr., R.W., Semler, H.J., Oyama, A.A., and Nohlgren, J.E., "Sudden Death Due to Dislodgement of Disc Occluder of Wada-Cutter Prosthesis," J. Thoracic and Cardiovascular Surgery, Vol. 66, No. 1, July 1973, pp. 93-95.

21. Smith, G.H., and Chandra, K., "Massive Aortic Imcompetence Associated with the Björk-Shiley Prosthesis," Thorax, Vol. 28, No. 5, September 1973, pp. 627-630.

22. Messmer, B.J., Rothlin, M., and Senning, A., "Early Disc Dislodgement: An Unusual Complication after Insertion of a Björk-Shiley Mitral Valve Prosthesis," J. Thoracic and Cardiovascular Surgery, Vol. 65, No. 3, March 1973, pp. 386-390.

23. Morrow, A.G., Clark, W.D., Harrison, D.C., and Braunwald, E., "Prosthetic Replacement of the Mitral Valve: Operative Method and the Results of Preoperative and Postoperative Hemodynamic Assessment," Circulation, (Suppl. 1), Vol. XXIX, No. 4, April 1964, pp. 2-13.

24. Jundson, W.E., Ardiz, J., Starch, T.B.J., and Jennings, R.S., "Postoperative Evaluation of the Prosthetic Replacement of Aortic and Mitral Valves," Circulation, (Suppl. 1), Vol. XXIX, No. 4, April 1964, pp. 14-29.

25. Garamella, J.J., Lynch, M.F., Schmidt, W.R., and Jenson, N.K., "Fatal Clotting of the Starr-Edwards Mitral Ball Valve Nineteen Months Postoperatively," J. Thoracic and Cardiovascular Surgery, Vol. 47, No. 5, May 1964, pp. 673-680.

26. Reed, W.A., and Dunn, M., "Fatal Hemolysis Following Ball Valve Replacement of the Aortic Valve," J. Thoracic and Cardiovascular Surgery, Vol. 48, No. 3, September 1964, pp. 436-442.

27. Lillehei, C.W., Levy, M.J., Lillehei, R.C., Wang, Y., and Bonnabeau, R.C., Jr., "Mitral, Aortic, and Tricuspid Valve Replacement with the Ball Valve," Surgery, Vol. 51, No. 1, January 1965, pp. 184-204.

28. Herr, R., Starr, A., McCord, C.W., and Wood, J.A., "Special Problems Following Valve Replacement: Embolus, Leak, Infection, Red Cell Damage," Ann. Thoracic Surgery, Vol. 1, No. 4, July 1965, pp. 403-415.

29. Cross, S.F., Silver, A.W., et al. "Discussion on the Paper Entitled: Special Problems Following Valve Replacement (Ref. 28)," Ann. Thoracic Surgery, Vol. 1, No. 4, July 1965, pp. 410-415.

30. Gunstensen, J., "Acute Dysfunction of Starr-Edwards Mitral Prostheses," Thorax, Vol. 26, No. 2, March 1971, pp. 163-166.

31. Schottenfeld, M., Wisheart, J.D., Ross, J.K., Lincoln, J.C.R., and Ross, D.N., "Cloth Destruction and Haemolysis with Totally Cloth-Covered Starr-Edwards Prostheses," Thorax, Vol. 26, No. 2, March 1971, pp. 159-162.

32. Joassin, A., and Edwards, J.E., "Late Causes of Death After Mitral Valve Replacement," J. Thoracic and Cardiovascular Surgery, Vol. 65, No. 2, February 1973, pp. 255-263.

33. Najafi, H., and DeWall, R.A., "Fatal Obstruction of the Aortic Root by Starr-Edwards Aortic Ball Valve Prostheses," J. Thoracic Cardiovascular Surgery, Vol. 180, No. 51, February 1966,pp. 180-184.

34. Lillehei, R.C., Dietzman, R.H., and Block, J.H., "Hypotension and Low Output Syndrome Following Cardiopulmonary Bypass," Cardiac Surgery, Appleton-Century Crofts, Division of Meredith Publishing Company, New York, 1967, pp. 437-456.

35. Björk, V.O., Intoni, F., and Meissel, A., "A Mechanical Pulse Duplicator for Testing Prosthetic Mitral and Aortic Valves," Thorax, Vol. 17, No. 3, 1962, pp. 280-283.

36. Starkey, W.L., Sirak, H.D., Collins, J.A., and Hagen, B.T., "The Design and Development of a Cardiac Simulator for the Evaluation of Heart-Valve Prosthesis," J. Thoracic and Cardiovascular Surgery, Vol. 46, No. 2, August 1963, pp. 207-211.

37. Steinmetz, G.P., Jr., May, K.J., Mueller, V., Anderson, H.N., and Merendino, K.A., "An Improved Accelerated Fatigue Machine and Pulse Simulator for Testing and Developing Prosthetic Cardiac Valves," J. Thoracic and Cardiovascular Surgery, Vol. 47, No. 2, February 1964, pp. 186-198.

38. Calvert, G.C., Drabble, J., Serafin, R., and Temple, L.J., "An Aortic Pulse Duplicator of Simple Design," J. Thoracic and Cardiovascular Surgery, Vol. 47, No. 5, May 1964, pp. 633-643.

39. Lighthill, M.J., "Physiological Fluid Dynamics: A Survey," J. Fluid Mechanics, Vol. 52, Pt. 3, April 1972, pp. 475-497.

40. Kuchar, N.R., and S.O. Strach, "Flow in the Entrance Regions of Circular Elastic Tubes," Biomedical Fluid Mechanics Symposium, American Society of Mechanical Engineers, 1966, pp. 45-69.

41. Young, F.D., Cholvin, N.R., "Application of the Concept of Similitude to Pulsatile Blood Flow Studies," Biomedical Fluid Mechanics Symposium, American Society of Mechanical Engineers, 1966, pp. 78-88.

42. Koorjian, S., Keller, D.P., Pierie, W.R., Starr, A., and Herr, R., "Criteria and System for Testing Artificial Heart Valves in Vitro," Prosthetic Heart Valves, Editor-in-Chief: L.A. Brewer III, Charles C. Thomas Publisher, Springfield, Ill., 1969, pp. 92-112.

43. Kinzing, G.E., Kubovick, R.J., and Marmo, J.F., "Pressure Distribution Downstream from a Heart Valve for Steady Flow in a Foam Damped Silastic Tube," J. Biomedical Materials Research, Vol. 2, No. 2, June 1969, pp. 207-212.

44. Pettifor, A.H., and Mockros, L.F., "Hydrodynamic Characteristics of Prosthetic Aortic Valves," The Annals of Thoracic Surgery, Vol. 9, No. 2, February 1970, pp. 122-135.

45. Mueller, T.J., Lloyd, J.R., Lower, J.L., Struble, W.T., and Underwood, F.N., "On the Separated Flow Produced by a Fully Open Disc-Type Prosthetic Heart Valve," Biomechanics Symposium, Properties of Biological Fluids and Solids: Mechanics of Tissues and Organs, American Society of Mechanical Engineers, Vol. 2, June 1973, pp. 97-98.

46. Smith, H.L., Essex, E., and Baldes, E.J., "A Study of the Movements of the Heart Valves and Heart Sounds," Ann. Internal Medicine, Vol. 33, No. 6, December 1950, pp. 1357-1359.

47. Kantrowitz, A., Hurwitz, E.S., and Herskowitz, A., "A Cinematographic Study of the Function of the Mitral Valve in Situ," Surgical Forum Proceedings of the Forum Sessions, Thirty Seventh Clinical Congress of the Americal College of Surgeons, San Francisco, California, Vol. 2, November 1951, pp. 204-206.

48. McMillan, I.K.R., Daley, R., and Matthews, M.B., "The Movement of the Aortic and Pulmonary Valves Studied Postmortem by Colour Cinematography," Brit. Heart J.,Vol. 14, No. 1, 1952, pp. 42-46.

49. McMillan, I.K.R., "Aortic Stenosis: A Postmortem Cinephotographic Study of Valve Action," Brit. Heart Journal, Vol. 17, No. 1, 1955, pp. 56-62.

50. Leyse, R.M., Quinton, E., Blumberg, J.B., Harrison, H.G., May, K.J., Jr., and Merendino, A.K., "A System for the Study of Cardiovascular Flow Patterns," Prosthetic Valves for Cardiac Surgery, Editor-in-Chief: K.A. Meredino, Charles C. Thomas Publisher, Springfield, Ill., 1961, pp. 56-70.

51. Meisner, T.E., and Rushmer, R.F., "Eddy Formation and Turbulence in Flowing Liquids," Circulation Research, Vol. 12, No. 5, May 1963, pp. 455-463.

52. Davila, J.C., "The Development of Artificial Heart Valves," Plastic in Surgical Implants, ASTM Special Technical Publication No. 386, Philadelphia, American Society for Testing Materials, 1964, pp. 1-16.

53. Davila, J.C., Palmer, T.E., Sethi, R.S., DeLaurentis, D.A., Enriquez, F., Rincon, N., and Lautsch, E.V., "The Problem of Thrombosis in Artificial Cardiac Valves," Heart Substitutes: Mechanical and Transplant, Charles C.Thomas Publisher, Springfield, Ill.,1966,pp.25-53.

54. Temple, L.J., Serafin, R., Calvert, N.G., and Drabble, T.M., "Principles of Fluid Mechanics Applied to Some Situations in the Human Circulation and Particularly to the Testing of Valves in a Pulse Duplicator," Thorax, Vol. 19, 1964, pp. 261-267.

55. Wright, J.T.M., and Temple, L.J., "An Improved Method for Determining the Flow Characteristics of Prosthetic Mitral Heart Valves," Thorax, Vol. 26, No. 1, January 1971, pp. 81-88.

56. Davey, T.B., Kaufman, B., and Smeloff, E.A., "Pulsatile Flow Studies of Prosthetic Heart Valves," J. Thoracic and Cardiovascular Surgery, Vol. 51, No. 2, February 1966, pp. 264-267.

57. Smeloff, E.A., Huntley, A.C., Davey, T.B., Kaufman, B., and Gerbode, F., "Comparative Study of Prosthetic Heart Valves," J. Thoracic and Cardiovascular Surgery, Vol. 52, No. 6, December 1966, pp. 841-848.

58. Weiting, D.W., Hall, C.W., Kreisle, L.F., Liotta, D., and DeBakey, M.E., "Design of a System for Analyzing Flow Behavior of Prosthetic Human Heart Valves," Cardiovascular Research Center Bulletin, Vol. 5, No. 2, October-December 1966, pp. 41-57.

59. Wieting, D.W., Hall, C.W., Liotta, D., and DeBakey, M.E., "Dynamic Flow Behavior of Artificial Heart Valves," Prosthetic Heart Valves, Editor-in-Chief: L.A. Brewer III, Charles C. Thomas Publisher, Springfield Ill., 1966, pp. 34-51.

60. Cruz, A.B., Jr., Kaster, R.L., Simmons, R.L., Bruneau, L., and Lillehei, C.W., "Flow Characteristics of the Meniscus Prosthetic Heart Valve," J. Thoracic and Cardiovascular Surgery, Vol. 49, No. 5, May 1965, pp. 813-817.

61. Kalvin, M., Leitz, K.H., and Kolff, W.J., "Comparative Testing of Artificial Heart Valves in a Mock Circulation," Prosthetic Heart Valves, Editor-in-Chief: L.A. Brewer III, Charles C. Thomas Publisher, Springfield, Ill., 1969, pp. 114-136.

62. Kaster, R.L., Mantini, E., Tanaka, S., and Lillehei, C.W., "Analysis of Dynamic Characteristics of Heart Valves in a Pulse Duplication - Analog Computer System," Biomedical Sciences Instrumentation, Vol. 4, May, 1967, pp. 112-118.

63. Kaster, R.L., Bonnabeau, R.C., Jr., Tanka, S., and Lillehei, C.W., "Comparative Analysis of In Vitro Flow Characteristics of Seven Types of Prosthetic Heart Valves," Prosthetic Heart Valves, Editor-in-Chief: L.A. Brewer III, Charles C. Thomas Publisher, Springfield, Ill., 1969, pp. 137-147.

64. Wright, J.T.M., "The Flow Characteristics of Some Commercially Available Prosthetic Mitral Valves," Developments in Biomedical Engineering, Editor: M.M. Black, Butler & Tanner Ltd., Frome and London, 1972, pp. 33-51.

65. Viggers, R.F., Prosthetic Replacement of the Aortic Valve, Charles C. Thomas Publisher, Springfield, Ill., 1972, pp. 64-80.

66. Wieselsberger, C., "Wietere Feststellungen Über die Gesetze des Flüssigkeits-und Luff Widerstandes," Zeitschrift für Physik, Vol. 23, 1922, pp. 219-224.

67. Liebster, H., and Schiller, L., "Vorträge and Diskussionen..Von der 88 Versammluny Deutscher Naturforcher und Arzte in Innsbruck," Annalen der Physik, Vol. 25, No. 24, December 15, 1924, pp. 670-672.

68. Lunnon, R.G., "Fluid Resistance to Moving Spheres," Proceedings of the Royal Society of London, Ser. A., Vol. 118, No. 780, April 2, 1928, pp. 680-694.

69. Schlichting, H. Boundary Layer Theory, Sixth Ed., McGraw-Hill, New York, 1968, Chapter 1, p. 17.

70. Torobin, L.B., and Gauvin, W.H., "Fundamental Aspects of Solids-Gas Flow, Part I: Introductory Concepts and Idealized Sphere Motion in Viscous Regime," The Canadian Journal of Chemical Engineering, Vol. 37, No. 4, August 1959, pp. 129-141; also "Part II: The Sphere Wake in Steady Laminar Fluids," Vol. 37, No. 5, October 1959, pp. 167-176; "Part III: Accelerated Motion of a Particle in a Fluid," Vol. 37, No. 6, December 1959, pp. 224-236; "Part IV: The Effects of Particle Rotation, Roughness and Shape," Vol. 38, No. 5, October 1960, pp. 142-153; "Part V: The Effects of Fluid Turbulence on the Particle Drag Coefficient," Vol. 38, No. 6, December 1960, pp. 189-200.

71. Heinrich, H.G., Niccum, R.J., and Haak, E.L., "The Drag Coefficient of a Sphere Corresponding to a 'One Meter Robin Sphere' Descending from 260,000 ft. Altitude (Reynolds Nos. 789 to 23,448 Mach. Nos. 0.056 to 0.90," Research and Development of Robin Meteorological Rocket Balloon, Vol. II, Contract AF 19(604)-8034 AD480309, Univ. of Minnesota, Minneapolis, Minn., May 1963.

72. Sivier, K.R., "Subsonic Sphere Drag Measurements at Intermediate Reynolds Numbers," Ph.D. thesis, 1967, The Univ. of Michigan, Ann Arbor, Mich.

73. Zarin, N.A., "Measurement of Non-Continuum and Turbulence Effects on Subsonic Sphere Drag," Ph.D. thesis, 1969, The Univ. of Michigan, Ann Arbor, Mich.

74. Ross, F.W., and Willmarth, W.W., "Experimental Results on Sphere and Disk Drag," AIAA Journal, Vol. 9, No. 2, Feb. 1971, pp. 285-291.

75. Bailey, A.B., and Hiatt, J., "Sphere Drag Coefficients for a Broad Range of Mach and Reynolds Numbers," AIAA Journal, Vol. 10, No. 11, November 1972, pp. 1436-1440.

76. Taneda, S., "Experimental Investigation of the Wake Behind a Sphere at Low Reynolds Numbers," Journal of the Physical Society of Japan, Vol. 11, No. 10, October 1956, pp. 1104-1108.

77. Magarvey, R.H., and Bishop, R.L., "Transition Ranges for Three-Dimensional Wakes," Canadian J. Physics, Vol. 39, No. 10, October 1961, pp. 1418-1422.

78. Lee, K., and Barrow, H., "Some Observations on Transport Processes in the Wake of a Sphere in Low Speed Flow," International J. Heat and Mass Transfer, Vol. 8, March 1965, pp. 403-409.

79. Goldburg, A., and Florsheim, B.H., "Transition and Strouhal Number for the Incompressible Wake of Various Bodies," Physics of Fluids, Vol. 9, No. 1, January 1966, pp. 45-50.

80. Calvert, J.R., "Some Experiments on the Flow Past a Sphere," Aeronautical Journal, Vol. 76, No. 4, April 1972, pp. 248-250.

81. Mujumdar, A.S., and Douglas, W.J.M., "Eddy-Shedding from a Sphere in Turbulent Free-Streams," International J. Heat Mass Transfer, Vol. 13, October 1970, pp. 1627-1629.

82. Stokes, G.G., "On the Theories of the Internal Friction of Fluids in Motion, and of Equilibrium and Motion of Elastic Solids," Trans. Camb. Phil. Soc., Vol. 9, Pt. II, 1851, pp. 8-106.

83. Whitehead, A.N., "Second Approximations to Viscous Fluid Motion," Quart. J. Math., Vol. 23, 1889, pp. 143-152.

84. Proudman, I., and Pearson, J.R.A., "Expansion at Small Reynolds Number for the Flow Past a Sphere and Circular Cylinder," J. Fluid Mechanics, Vol. 2, Pt. 3, May 1957, pp. 237-262.

85. Oseen, C.W., "Über Die Stokes'sche Formal und Über eine Verwandte Aufgube in der Hydrodynamik," Ark. for Mat. Astr. O Fysik., Vol. 6, No. 29, September 1910.

86. Goldstein, S., "The Steady Flow of Viscous Fluid Past a Fixed Spherical Obstacle at Small Reynolds Numbers," Proc. Roy. Soc., Series A, Vol. 123, No. 791, March 1929, pp. 225-235.

87. Toniotika, S., and Aoi, T., "The Steady Flow of Viscous Fluid Past A Sphere and Circular Cylinder at Small Reynolds Numbers," Quart. J. Mech. Appl. Math., Vol. 3, Pt. 2 , 1950, pp. 140-161.

88. Pearcey, T., and McHugh, B., "Calculation of Viscous Flow Around Spheres at Low Reynolds Numbers," Philosophical Magazine, Ser. 7, Vol. 46, No. 378, July 1955, pp. 783-794.

89. Kawaguti, M., "An Approximate Solution for Viscous Flow at Low Speeds," Tokyo, Institute of Science and Technology Report, Vol. 2, May-June 1948, pp. 66-71.

90. Kawaguti, M., "Numerical Solution for the Viscous Flow Past a Sphere," Tokyo, Institute of Science and Technology Report, Vol. 4, May-June 1950, pp. 154-158.

91. Fox, L., "A Short Account of Relaxation Methods," Quart. J. Mech. Appl. Math., Vol. 1, 1948, pp. 253-280.

92. Fox, L., and Southwell, R.V., "Relaxation Methods Applied to Engineering Problems," Phil. Trans., Series A, Vol. 239, No. 810, October 1945, pp. 419-460.

93. Allen, D.N. de G., and Dennis, S.C.R., "The Application of Relaxation Methods to the Solution of Differential Equations in Three Dimensions," Quart. J. Mech., Vol. 4, Part 2, 1951, pp. 199-208.

94. Jenson, V.G., "Viscous Flow Round a Sphere at Low Reynolds Numbers (<40)," Proc. Roy. Soc., Series A, Vol. 249, No. 1257, January 1959, pp. 346-366.

95. Hamielec, A.E., Hoffman, T.W., and Ross, L.L., "Numerical Solution of the Navier-Stokes Equation for Flow Past Spheres, Part I - Viscous Flow Around Spheres with and without Radial Mass Efflux," J. of The American Institute of Chemical Engineers, Vol. 13, No. 2, March 1967, pp. 212-219.

96. LeClair, B.P., Hamielec, A.E., and Pruppacher, H.R., "A Numerical Study of the Drag on a Sphere at Low and Intermediate Reynolds Numbers," J. Atmospheric Sciences, Vol. 27, No. 2, March 1970, pp. 308-315.

97. Pruppacher, H.R., LeClair, B.P., and Hamielec, A.E., "Some Relations Between Drag and Flow Pattern of Viscous Flow Past a Sphere and a Cylinder at Low and Intermediate Reynolds Numbers," J. Fluid Mechanics, Vol. 44, Pt. 4, 1970, pp. 781-790.

98. Dennis, S.C.R., and Walker, M.S., "The Steady Motion of a Viscous Fluid Past a Sphere," Aero. Res. Council Report, No. 26105, Aug. 1964.

99. Rimon, Y., and Cheng, S.I., "Numerical Solution of a Uniform Flow over a Sphere at Intermediate Reynolds Numbers," Physics of Fluids, Vol. 12, No. 5, May 1969, pp. 949-959.

100. Dennis, S.C.R., and Walker, J.D.A., "Calculation of the Steady Flow Past a Sphere at Low and Moderate Reynolds Numbers," J. Fluid Mechanics, Vol. 48, Part 4, 1971, pp. 771-789.

101. Van Dyke, M., Perturbation Methods in Fluid Mechanics, Academic Press, New York and London, 1964.

102. Seed, W.A., and Wood, N.B., "Velocity Patterns in Aorta," Cardiovascular Research, Vol. 5, No. 3, July 1971, pp. 319-330.

103. Abdurashitov, S.A., Vershinin, I.M., et al., "Characteristics of Centrifugal Pumps with Water and Viscous Liquids," Russian Engineering J. Vol. 45, No. 1, 1965, pp. 23-26.

104. Hicks, T.G., and Edwards, T.W., Pump Application Engineering, McGraw-Hill Book Company, 1971, pp. 138-140.

105. Rotem, Z., "The Heated Surface Probe for Measuring Shear Stress at the Wall in Laminar Boundary Layers," Canadian J. Chemical Engineering, Vol. 45, June 1967, pp. 175-178.

106. Acrivos, A., and Taylor, T.D., "Heat and Mass Transfer from Single Spheres in Stokes Flow," Physics of Fluids, Vol. 5, No. 4, April 1962, pp. 387-394.

107. Barker, M., "On the Use of Very Small Pitot-Tubes for Measuring Wind Velocity," Proc. Roy. Soc., Series A, Vol. 101, No. 712, August 1922, pp. 435-445.

108. Rasmussen, C.G., "The Air Bubble Problem in Water Flow Hot-Film Anemometry," Disa Information, No. 5, June 1967, pp. 21-26.

109. Morrow, T.G., "Effects of Dirt Accumulation on Hot-Wire and Hot-Film Sensors," Fluid Dynamic Measurements in the Industrial and Medical Environments, Proceeding of the Disa Conference held at the Univer. of Leicester, Vol. 1, April 1972, pp. 122-124.

110. Pinchon, J., "Comparison of Some Methods of Calibrating Hot-Film Probes in Water," Disa Information, No. 10, October 1970, pp. 15-21.

111. Kalashnikov, V.N., and Kudin, A.M., "Calibration of Hot-Film Probes in Water and in Polymer Solutions," Disa Information, No. 14, March 1973, pp. 15-18.

112. Batchelor, G.K., An Introduction to Fluid Dynamics, Cambridge University Press, 1967, pp. 201-204.

113. Batchelor, G.K., and Townsend, A.A., "Decay of Turbulence in the Final Period," Proc. Roy. Soc., Series A, Vol. 194, No. 1039, November 1948, pp. 527-543.

114. Dryden, H.L., and Schubauer, G.B., "The Use of Damping Screens for the Reduction of Wind-Tunnel Turbulence," J. Aeronautical Sciences, Vol. 14, No. 4, April 1947, pp. 221-228.

115. Schubauer, G.B., and Spungenberg, W.G., "Effects of Screens in Wide Angle Diffusers, NACA TN 1610, 1948.

116. Schubauer, G.B., Spangenberg, W.G., and Klebanoff, P.S., "Aerodynamic Characteristics of Damping Screens," NACA TN 2001, 1950.

117. Han, L.S., "Hydrodynamic Entrance Lengths for Incompressible Laminar Flow in Rectangular Ducts," Trans. ASME, Series E, J. Appl. Mechanics, Vol. 27, No. 3, September 1960, pp. 403-409.

118. Lumley, J.L., "Passage of a Turbulent Stream Through Honeycomb of Large Length-to-Diameter Ratio," Trans. ASME, Series D, J. Basic Engineering, Vol. 86, No. 2, June 1964, pp. 218-220.

119. Lumley, J.L., and Mamahon, J.F., "Reducing Water Tunnel Turbulence by Means of a Honeycomb," ASME Fluids Engineering Conference, Chicago, Ill., May 8-11, 1967, Paper No. 67-FE-5.

120. Holmes, D.B., and Vermeulen, J.R., "Velocity Profiles in Ducts with Rectangular Cross Sections," Chemical Engineering Science, Vol. 23, No. 7, August 1968, pp. 717-722.

121. Taback, I., "The Response of Pressure Measuring Systems to Oscillating Pressures," NACA TN 1819, 1949.

122. Iberall, A.S., "Attenuation of Oscillatory Pressure in Instrument Lines," Journal of Research, National Bureau of Standards, Vol. 45, July 1950, pp. 85-108.

123. D'Souza, A.F., and Oldenburger, R., "Dynamic Response of Fluid Lines," Trans. ASME, Series D, Journal of Basic Engineering, Vol. 86, No. 3, September 1964, pp. 589-598.

124. Grove, A.S., Shair, F.H., Petersen, F.E., and Acrivos, A., "An Experimental Investigation of the Steady Separated Flow Past a Circular Cylinder," J. Fluid Mechanics, Vol. 19, Pt. 1, May 1964, pp. 60-80.

125. Acrivos, A., Leal, L.G., Snowden, D.D., and Pan, F., "Further Experiments on Steady Separated Flows Past Bluff Objects," J. Fluid Mechanics, Vol. 34, Pt. 1, 1968, pp. 25-48.

126. Abraham, F.F., "Functional Dependence of Drag Coefficient of a Sphere on Reynolds Number," Physics of Fluids, Vol. 13, No. 8, August 1970, pp. 2194-2195.

127. Stoke, G.G., Mathematical and Physical Papers, Vol. 3, 1851, p. 1.

128. Basset, A.B., A Treatise on Hydrodynamics, Vol. 2, Ch. 21, Deighton, Bell and Co., Cambridge, 1888 (also Dover Publications Inc., New York, 1961).

129. Boussinesq, M.J., "Sur la résistance qu-oppose un liquide indéfini en repos, sans pesanteur, au mouvement varié d'une sphère solide qu'il mouille sur toute sa surface, quand les vitesses restent bien continues et assez faibles pour que leurs carrés et produits soient négligeables," Academic des sciences, Paris Comptes Renaus, Vol. 100, 1885, pp. 935-937.

130. Oseen, C.W., Hydrodynamik, Akademische Verlagsgesellschaft, Leipzig, 1927.

131. Lin, C.C., "Motion in the Boundary Layer with a Rapidly Oscillating External Flow," Proc. 9th Intern. Con. Appl. Mech., Brussels, Vol. 4, 1957, pp. 155-167.

132. Odar, F., and Hamilton, W.S., "Forces on a Sphere Accelerating in a Viscous Fluid," J. Fluid Mechanics, Vol. 18, Pt. 2, February 1964, pp. 302-314.

133. Odar, F., "Verification of the Proposed Equation for Calculation of the Forces on a Sphere Accelerating in a Viscous Fluid," J. Fluid Mechanics, Vol. 25, 1966, pp. 591-592.

134. Odar, F., "Unsteady Motion of a Sphere Along a Circular Path in a Viscous Fluid," Transaction of the ASME, Series E, Journal of Appl. Mech., Vol. 35, No. 4, December 1968, pp. 652-654.

135. Fung, Y.C., Perrone, N., and Anliker, M., Biomechanics: Its Foundations and Objectives, Prentice-Hall Inc., Englewood Cliffs, 1972, pp. 507-523.

136. Bruck, S.D., Blood Compatible Synthetic Polymers, Charles C. Thomas Publisher, Springfield, Ill., 1974.

137. Kline, S.J., Similitude and Approximation Theory, McGraw-Hill, New York, 1965.

138. Buckingham, E., "Model Experiments and the Form of Empirical Equations," Trans. ASME, Vol. 37, No. 1487, June 1915, pp. 263-296.

139. Gimenez, J.L., Winters, W.L., Davila, J.C., Connell, J., and Klein, K.S., "Dynamics of the Starr-Edwards Ball Valve Prosthesis: A Cine-Fluorographic and Ultrasonic Study in Humans," The American Journal of the Medical Sciences, Vol. 250, No. 6, December 1965, pp. 652-657.

140. Dayem, M.K.A., and Raftery, E.B., "Phonocardiogram of the Ball-and-Cage Aortic Valve Prosthesis," British Heart Journal, Vol. 29, No. 3, 1967, pp. 446-452.

141. Winters, W.L., Gimenez, J.L., and Soloff, L.A., "Clinical Application of Ultrasound in the Analysis of Prosthetic Ball Valve Function," The American Journal of Cardiology, Vol. 19, No. 1, January 1967, pp. 97-107.

142. Björk, V.O., Grenvik, A., Hergog, P., and Holmdhahl, M.H., "Aortic Ball Valve Resistance," Thorax, Vol. 21, No. 2, March 1966, pp. 118-120.

143. Benchimol, A., and Matsuo, S., "Ejection Time Before and After Aortic Valve Replacement," The American Journal of Cardiology, Vol. 27, No. 3, March 1971, pp. 244-249.

144. Bristow, J.D., McCord, C.W.D., Starr, A., Ritzmann, L.W., and Griswold, H.E., "Clinical and Hemodynamic Results of Aortic Valvular Replacement with a Ball-Valve Prosthesis, Supplement to Circulation, Vol. 29, No. 4, April 1964, pp. 36-46.

145. Brandfonbrener, M., Landowne, M., and Shock, N.W., "Changes in Cardiac Output with Age," Circulation, Vol. 12, No. 4, October 1955, pp. 557-566.

146. Levine, H.J., Neil, W.A., Wagman, R.J., Krasnow, N., and Gorlin, R., "The Effect of Exercise on Mean Left Ventricular Ejection Rate in Man," Journal of Clinical Investigation, Vol. 41, No. 5, 1962, pp. 1050-1058.

147. Yu, N.P., Pulmonary Blood Volume in Health and Disease, Lea and Febiger Publishers, Philadelphia, 1969, p. 142.

148. Merril, E.W., "Rheology of Blood," Physiological Reviews, Vol. 49, No. 4, October 1969, pp. 863-888.

149. Albritton, E.C., Standard Valves in Blood, W.B. Saunders Company, Philadelphia and London, 1952, p. 5.

150. Van Wazer, J.R., Lyons, J.W., Kim, K.Y., and Colwell, R.E., Viscosity and Flow Measurement, Interscience Publishers, a division of John Wiley and Sons, New York, London, 1963.

151. Charm, S., and Kurland, "Viscometry of Human Blood for Shear Rates of 0-1000,000 Sec.$^{-1}$," Nature, Vol. 206, No. 4984, May 8, 1965, pp. 617-618.

152. Cassen, W., "A Flow Equation for Pigment-Oil Suspensions of the Printing Ink Type," Rheology of Disperse Systems, editor: C.C. Mill, Pergmon Press, 1959, pp. 84-104.

153. Metrill, E.W., Benis, A.M., Gilliland, E.R., Sherwood, T.K., and Salzman, E.W., "Pressure-Flow Relations of Human Blood in Hollow Fibers at Low Flow Rates, J. Applied Physiology, Vol. 20, No. 5, September 1965, pp. 954-967.

154. Dinsdale, A., and Moore, F., Viscosity and its Measurements, Chapman and Hall, London, 1962.

155. Hylen, J.C., Kloster, F.E., Herr, R.H., Hull, P.Q., Ames, A.W., Starr, A., and Griswald, H.E., "Phono-cardiographic Diagnosis of Aortic Ball Valve Variance," Circulation, Vol. 38, No. 1, July 1968, pp. 90-102.

156. Dring, R.P., "A Theoretical and Experimental Investigation of Disturbance Amplification in External Laminar Natural Convection," Ph.D. thesis, Cornell University, June 1968.

157. Ranstadler, P.W., "Stable Operation of Hot-Film Probes in Water," ASME Symposium on Measurement in Unsteady Flow, Editors: R.E. McNair, G.L. Mellor, and R.E. Kronauer, Worchester, Mass., May 1962, pp. 83-84.

158. Richardson, E.V., and McQuivery, R.S., "Measurements of Turbulence in Waters," Journal of the Hydraulic Division, ASCE, Vol. 94, No. 2, March 1968, pp. 411-430.

159. Richardson, E.V., McQuivery, R.S., Sandborn, V.A., and Jog, P.M., "Comparison Between Hot-Film and Hot-Wire Measurements of Turbulence," Proceedings: 10th Midwestern Mechanics Conference, Editors: J.E. Cermak and J.R. Goodman, Colorado State University, Fort Collins, Colorado, August 1967, pp. 1213-1223.

160. Collis, D.C., and Williams, M.J., "Two Dimensional Convection from Heated Wires at Low Reynolds Numbers," J. of Fluid Mechanics, Vol. 6, Pt. 3, October 1959, pp. 357-384.

161. Wood, W.W., "Calculations for Anemometry with Fine Hot Wires," J. Fluid Mechanics, Vol. 32, Pt. 1, 1968, pp. 9-19.

162. Perry, A.E., and Morrison, G.L., "A Study of the Constant-Temperature Hot-Wire Anemometer," J. Fluid Mechanics, Vol. 47, Pt. 3, 1971, pp. 577-599.

163. Moore, F.K., Theory of Laminar Flows, Princeton University Press, Princeton, New Jersey, 1964, p. 127.

164. Rotem, Z., and Claassen, L., "Natural Convection above Unconfined Horizontal Surfaces," J. Fluid Mechanics, Vol. 38, Pt. 1, 1969, pp. 173-192.

165. Sokolowski, M., "Heat Flow in a Wedge with Discontinuous Boundary Conditions," Archiwum Mechaniki Stosowanej, Vol. 4, No. 13, 1961, pp. 433-455.

APPENDIX I

SIMILARITY PARAMETERS

I.1 Preliminary Comments

There are three commonly used procedures for developing similarity criteria for a given problem: evaluation of force ratios, dimensional analysis, and critical study of the governing equations of the system. Each method has its own advantages and limitations, and these have been discussed in detail by Kline[137]. Here the method of dimensional analysis based on the well known Buckingham's Π-theorem[138] is employed to arrive at the dimensionless group of numbers governing the problem. As the procedure is rather routine, only the essential ideas are touched upon.

The usual problem is one of predicting some characteristic function y of a system in terms of a set of independent variables x_i, i.e.

$$y = f(x_1, x_2, \cdots, x_i) \quad . \qquad \ldots . (I\text{-}1)$$

Application of the Π-theorem leads to a new set of variables for the problem.

$$\Pi_1 = f_1(\Pi_2, \Pi_3, \cdots, \Pi_j) \quad \ldots . (I-2)$$

where the value of j is governed by the number of variables and the independent basic dimensions required to describe these variables. The characteristics of Π terms are that they are dimensionless and independent. It follows that if functional relationships for Π_1 are the same for two systems, i.e. the same phenomenon is involved in both the systems, then

$$\Pi_1 = \Pi_{1m} \text{ if } \Pi_2 = \Pi_{2m}, \cdots, \Pi_j = \Pi_{jm} \quad \ldots . (I-3)$$

where the subscript m refers to the model. The scaling relationships for the dependent variable y and the independent variables x_i follow immediately from (I-3). Although this procedure is simple in principle, there are two inherent difficulties:

(i) the validity of the analysis depends on the correct selection of the variables x_i;

(ii) it is not always possible to satisfy the design conditions specified by (I-3), i.e. there exists a possibility of model distortion.

I.2 Similarity Criteria for Artificial Aortic Valves

The dependent variable is considered to be the pressure on the surface of the spherical poppet, P_θ, and the variables that are assumed to influence the pressure are listed in Table 1.

This list, by no means complete, is believed to include more significant parameters likely to affect the pressure. Of course, the velocity distribution upstream and downstream of the valve, flexibility of the surrounding aorta, time history of the poppet acceleration, etc. will have some influence upon the pressure. Unfortunately, it is very difficult to account for them primarily because of the lack of any available measured information about these parameters. The dimensional analysis gives a set of Π numbers as listed in Table 2.

Π_1, Π_2 correspond to the ratio of the ball velocity to the mean flow velocity for opening and closing of the valve, respectively. The importance of these two parameters are well substantiated by post-operative evaluation of prosthetic replacements[139-141]. Π_3 is a measure of the relative time that the valve stays open and closed. The significance of this factor also has been established by published medical reports[142,143]. Π_4 relates the total ejection time and the heart rate, quite critical parameters of the problem, whose importance cannot be overemphasized[142,143].

TABLE I-1

Independent Variables of the Problem

Variable	Symbol	Dimension	Comments
Velocity	U	LT^{-1}	Average based on the cardiac index
Pulsation Frequency	f	T^{-1}	Based on average heart rates of patients with artificial aortic valves
Ball Diameter	D	L	Aortic ball valve diameter, an average based on more commonly used models
Orifice Diameter	d	L	Orifice diameter of the heart valve
Stroke	s	L	Stroke length based on the manufacturer's specification
Valve Opening	$\bar{y}_b$	L	Aortic ball valve opening as measured from the fully closed position
Opening Time	t_0	T	Time of travel from fully closed to fully open positions
Open Time	t_{s0}	T	Time elapsed during which the valve remains fully open
Closing Time	t_c	T	Time of travel from fully open to fully closed position
Closed Time	t_{sc}	T	Elapsed time during which the valve remains fully closed
Density	ρ	FT^2L^{-4}	Assumed constant
Viscosity	μ	FTL^{-2}	Corresponds to blood assumed Newtonian

Π_5, also called Beta number, is an index of inertial effects due to the oscillating flow as compared to the viscous effects. Reynolds number Π_6, of course, must play an important role. The remaining three dimensionless numbers are associated with geometry of the system.

TABLE I-2

A Selection of Dimensionless Numbers for the Problem

$\Pi_1 = (s/t_0)/U = U_0/U$	$\Pi_5 = D(f/\nu)^{1/2} = B_n$
$\Pi_2 = (s/t_c)/U = U_c/U$	$\Pi_6 = UD/\nu = R_n$
$\Pi_3 = t_{so}/t_{sc}$	$\Pi_7 = s/D$
$\Pi_4 = f(t_0+t_c+t_{s0})$	$\Pi_8 = d/D$
	$\Pi_9 = \bar{y}_b/s$

I.3 Range of Values of the Relevant Parameters in the Living System

I.3.1 Average blood velocity in the aortic root based on the cardiac index

Two sets of data on the aortic valve have been reported in the literature, by Bristol et al.[144] and Judson et al.,[24] which lead to somewhat different ranges of variation for this parameter. For comparison, the average blood velocity has been obtained using information from both these sources.

(a) Average velocity based on data by Bristol et al.

Cardiac index = volume flow rate in the aortic passage per unit body surface area

Rest: 2.26-3.39 L/min/M^2

Mean* = 2.756 L/min/M^2

Exercise: 2.85-4.73 L/min/M^2

Mean = 3.717 L/min/M^2

Valve size = 9A - 12A, model 1000, Starr and Edwards

Ball diameter = 0.655 - 0.748 in.

Orifice diameter = 0.610 - 0.685 in.

Mounting diameter = 0.920 - 1.070 in., aortic area (A) = 4.29 - 5.8 cm^2

---

*Mean refers to average based on the number of patients examined.

Blood density (ρ) = 1.055 gr/cc (based on the standard value, see Section I3.3)

U = average blood velocity based on cardiac index

= (body surface area)(cardiac index)/A

Rest: 10.77 - 21.84 cm/sec

Mean = 15.24 cm/sec

Exercise: 13.58 - 30.47 cm/sec

Mean = 22.0 cm/sec

(b) Average velocity based on data by Judson et al.

Cardiac index = volume flow rate in the aortic passage per unit body surface area

Rest: 2.18 - 3.36 L/min/M^2

Mean = 2.967 L/min/M^2

Exercise 2.65 - 7.75 L/min/M^2

Mean = 4.957 L/min/M^2

Valve size = 9A - 13A, model 1000, Starr & Edwards

Ball diameter = 0.6555 - 0.815 in.

Orifice diameter = 0.610 - 0.730 in.

Mounting diameter = 0.920 - 1.160 in., aortic area = 4.29 - 6.8 cm^2

U = average blood velocity based on cardiac index

Rest: 8.86 - 23.71 cm/sec

Mean = 9.33 cm/sec

Exercise: 10.77 - 49.93 cm/sec

Mean = 15.60 cm/sec

I.3.2 Heart rate

Based on extensive tests on numerous healthy adults (without prosthetic valve) conducted by several investigators[145-147], it can be concluded that the normal sinus rhythm ranges over 57 - 111 beats/min. at rest (exercise: 72 - 164 beats/min.) with the mean rhythm of 69 - 85 beats/min. (exercise: 117 beats/min.). On the other hand, for patients with aortic replacements the beat rate has been observed to vary over 56 - 138 (exercise: 90 - 150; Judson et al.[24]), and 62 - 118 (exercise: 82 - 140; Bristol et al.[145]) beats/min. at rest with the mean values of 74 (exercise 114) and 74.3 (exercise 103.5), respectively. In each case, the data represent an average of a large number of samples and hence accounts for observed differences due to age, weight, body surface area, sex and environment.

I.3.3 Properties of blood

Human blood is a suspension of particles in a complex aqueous solution (plasma) of organic and inorganic

substances. In addition, about 7%, by weight, of the blood is macromolecules called proteins. The volume fraction of the particles is of the order of 50%, but the red cells constitute about 97% of the total cell volume in the blood with cell concentration of about 5 million per mm^3. The red cells have a discoid shape of about 8μ maximum diameter but are flexible enough to pass easily through capillaries of about one-half this dimension. In normal blood, the red cells aggregate, face-to-face. Usually these aggregates contain 6 - 10 red cells in a stack, such a primary aggregate being called rouleaux. Secondary aggregation of the rouleaux also occurs. When blood is sheared these secondary aggregates and rouleaux break up, and at sufficiently high shear rates, the cells exist as individuals. However, if the shear rate reduces to about zero, these aggregate structures reform very rapidly.

The other cells (white cell and platelets) are normally not numerous enough to affect the fluid dynamic behavior of blood. Because of this, and as platelets in particular can cause experimental difficulties in viscometer, most blood rheological studies are performed with suspensions which have had most of the white cells and platelets removed. However, it should be pointed out that platelets play an important role in the formation of blood clots and, in this manner may seriously interfere with the flow.

Considering these factors, the rheological properties of blood might be expected to be rather complex.

This is indeed the case, and the complexity becomes apparent when one examines a recent review of the blood rheology literatures by Merril[148]. Although numerous reports have been published on the subject, the results show considerable scatter and may present some difficulty in the selection of appropriate values.

In contrast to the rheological properties, determination of blood density is a relatively simple matter. Its specific gravity has been found[149] to vary over the range 1.052 - 1.061. The reference here is the water at 4°C.

Problems associated with the measurement of blood viscosity are quite challenging. So far, it has not been possible to predict pressure-velocity relationships for blood over a wide range of conditions without employing empirical functions. Consequently, many models have been proposed for blood. Employing these models in conjunction with experimental data obtained with various viscometers, the rheological properties of blood have been compiled.

Almost all researchers have used one or more of the three types of viscometers: (i) the capillary tube type; (ii) the concentric cylinder type; and (iii) the cone and plate configuration. Each of these offers several advantages and limitations. Some of these are related to peculiarities of the instrument while others relate to the characteristics of blood.

(i) Tube viscometers

Here a fluid is allowed to flow from a reservoir down a tube of precisely known dimensions and the volume conveyed in a given time under a given pressure is recorded. For a simple steady laminar flow in the tube, the corresponding shear stress and shear rate at the tube wall are given[150] by

$$\tau_w = \Delta Pr/2L \qquad \ldots .(I-4)$$

$$\gamma_w = \Delta Pr/2\mu L \qquad \ldots .(I-5)$$

where

r = tube radius

L = axial distance

ΔP = pressure difference between two points distance L apart

μ = coefficient of dynamic viscosity.

Equation (I-4) is valid regardless of the nature of the fluid. However, the shear rate variation, Equation (I-5), depends on the velocity distribution which, in turn, is determined by the nature of the fluid.

Recently, Charm and Kurland[151] have shown that blood obeys Cassen's[152] equation at shear rate from 1 to

100,000 $sec.^{-1}$ and that the general expression[153] for blood viscometry is

$$\tau^{1/2} = K\gamma^{1/2} + \sigma^{1/2} \qquad \ldots . (I\text{-}6)$$

or

$$(\Delta Pr/2L)^{1/2} = \mu_c(4\dot{Q}/\pi r^3)^{1/2} + \sigma^{1/2}$$

where

μ_c = Cassen viscosity

σ = yield stress

$\dot{Q}$ = volume flow rate

Thus a plot of $\dot{Q}^{1/2}$ against $(\Delta P/L)^{1/2}$ should be a straight line from whose slope K can be obtained and whose intercept at $\Delta P/L = 0$ gives $\sigma^{1/2}$.

If the tube viscometer is too narrow, however, the recorded viscosity of a heterogeneous suspension such as blood may become dependent upon the diameter of the tube (Fahraeus-Lindqvist effect). Corrections may also be required for flow pattern changes, anomalous pressure gradient at the inlet and outlet of the tube, and meniscus effects.

The tube viscometer has been used extensively for work on blood because it is inexpensive, requires only a small volume of fluid, is easy to use and gives good reproducibility. Moreover, it simulates extra vivum, to a degree, the flow of blood in vivo. Unfortunately, in the

case of a non-Newtonian fluid each viscosity plot covers a wide range of shear rate for which allowance has to be made and, if the tube is narrow, wall effects may influence the results.

(ii) Co-axial cylinder viscometers

The fluid is held in a cylindrical pot containing a concentrically mounted bob. The pot is rotated at a constant velocity and the viscous drag transmitted through the fluid is measured by the angular deflection of the inner cylinder or by the torque required to return it to its original position. This torque is balanced by the moment due to viscous shear so that for a Newtonian fluid

$$\mu = M(r_2^2 - r_1^2)/(4\pi r_1^2 r_2^2 L\omega) \quad \ldots . (I-7)$$

where

M = measured torque

r_1 = radius of inner cylinder

r_2 = radius of outer cylinder

L = height of inner cylinder

ω = angular velocity of outer cylinder.

The viscosity of an unknown fluid can then be found from the torque which it transmits at a predetermined angular velocity.

For non-Newtonian fluids the shearing stress is no longer directly proportional to the rate of shear and thus the measured torque M is not directly proportional to the angular velocity ω. For example, for a plastic fluid or Bingham body[150]

$$\mu = M(r_2^2-r_1^2)/(4\pi r_1^2 r_2^2 L\omega) - (\sigma/\omega)\ln(r_2/r_1) \quad ..(I-8)$$

The co-axial cylinder viscometer has the advantage of shearing a great portion of the fluid at something approaching a constant rate of shear. On the other hand, end effects on the cylinders are sometimes difficult to overcome or allow for, particularly in the case of non-Newtonian fluids. A well designed instrument is expensive, particularly if it is to work on small samples of fluid at low rate of shear (which is often necessary in the case of blood).

(iii) Cone-plate viscometers

The fluid is contained in the space between a cone of very large apex angle and a flat surface normal to its axis. One unit is rotated and the drag transmitted by the fluid is measured on the other. In order that idealized flow exist in the fluid space between the cone and plate, it is necessary that inertial effects be negligible and that α, the angle between the cone and plate, be very small (less

than 4°). Due to the system geometry the perpendicular distance between the cone and the plate increases proportionally with the radius ($z = r \tan \alpha$). Moreover, the linear relative velocity of the cone or the plate is proportional to the radius so that the rate of shear in the fluid is constant throughout.

For the case where the cone rotates at speed ω, the shear rate γ and shear stress τ are given by

$$\gamma = \omega/\alpha \qquad \ldots . \text{(I-9)}$$

$$\tau = 3M/2\pi r^3 . \qquad \ldots . \text{(I-10)}$$

Thus for a Newtonian fluid

$$\mu = 3M\alpha/2\pi r^3\omega \quad . \qquad \ldots . \text{(I-11)}$$

Equations (I-9) and (I-10) are generally used without correction for plotting flow curves of non-Newtonian fluids[154], the viscometer first being calibrated with Newtonian fluids of known viscosity. The apparent viscosity of the unknown non-Newtonian fluid is then found at various rates of shear and the corresponding shear stress obtained from Equation (I-11). The flow curve can then be constructed readily.

The cone-plate viscometer possesses many advantages over the co-axial cylinder instrument and, in addition,

normally requires a smaller sample. However, the distance over which shearing takes place may be so small that the discontinuous nature of fluid such as blood could affect the magnitude of the transmitted stress. The long length and short width of the air fluid interface at the perimeter of the shearing surfaces may also, in certain circumstances, affect stress transmission unless it can be allowed for by the inclusion of a guard ring or other special design features. Furthermore, there is the possibility of circulation developing between the cone and the plate during the shearing of certain non-Newtonian fluids and suspensions, leading to incorrect results.

From the foregoing it is clear that the problems of evaluating rheological properties of normal human blood are overwhelming and in spite of extensive experimental research no precise value can be pinpointed due to the wide scatter in data and the problem of reproducibility. An average value of $\mu = 3.196$ centipoises, usually quoted in hand books[149], thus offers a good compromise.

I.3.4 Physical dimensions of the Starr-Edwards aortic ball valves

Physical dimensions of the human heart and associated appendages vary considerably requiring, preferably, personalized construction of prosthetic replacements. This presents a rather formidable problem of manufacture where

standardization is naturally preferred. For example, Edwards Laboratories has produced at least fifty types of aortic valves accounting for different models and sizes. The range of variation of important parameters and their main values, based on the information supplied by the manufacturer through private communication, are listed below.

Ball diameter = 0.482 - 0.868 in.; mean 0.681 in.

Stroke = 0.232 - 0.405 in.; mean 0.348 in.

Orifice diameter = 0.420 - 0.757 in.; mean 0.594 in.

Mounting diameter = 0.618 - 1.207 in.; mean 0.938 in.

I.3.5 Travel and rest times for the poppet

As seen in Figure 2-13, displacement history of the ball travel includes four important time parameters: opening, opening duration, closing, closing duration. 'Opening time' represents the time taken by a poppet to travel between fully closed to fully open positions (i.e. from the seat to the tip of the cage). This is followed by a dwell period during which the valve remains fully open. It is referred to as 'opening duration'. Now the poppet starts its return journey which ends with full closing of the valve. This represents 'closing time'. The following dwell period before initiation of the new cycle is called 'closing duration'. From physiological consideration a parameter of importance is the 'ejection time' (E_t) indicating duration

over which blood is pumped into aorta. Considering the fact that the flow reverses during the terminal period of the impending closure of the valve, the ejection time is approximately represented by $E_t \simeq t_0 + t_{s0} + t_c$. The recorded information on these parameters is rather sketchy. Among the useful reports are those by Gimenez et al.[139] and Hylene et al.[155] Unfortunately, even the mean values given by them vary significantly as indicated below:

TABLE I-3

Significant Time Parameters for an Aortic Valve Prosthesis

Time Parameters	Gimenez et al.	Hylene et al.
Opening time, t_0	50 m sec.	59 m sec.
Opening duration, t_{s0}	125 m sec.	110 m sec.*
Closing time, t_c	50 m sec.	89 m sec.*
Closing duration, t_{sc}	310 m sec.	419 m sec.
Ejection time, E_t	225 m sec.	258 m sec.

Of interest would be the values of these parameters for patients (with prosthetic valves) with abnormal sinus rhythm. Based on the information obtained at Shaughnessey

*Calculated and/or estimated from the carotid profiles.

Hospital it appears that, although t_0 and t_c remain in the ranges given above, t_{s0} and t_{sc} may show considerable deviation.

I.4 Range of Variation of the Dimensionless Parameters

The wide range of variations of the system parameters would be reflected in the corresponding variation of the dimensionless numbers involved in the dynamic simulation. Obviously with nine Π numbers this presents a rather challenging experimental project. Fortunately, the test program showed some parameters to be more significant than others. The ranges of dimensionless numbers as obtained using the information given in Section I.3 and those used during the actual test are presented in Table I-4.

TABLE I-4

Observed Values of the Dimensionless Numbers and Those Used in Experiments

Dimensionless Number	Observed Range	Experimental Range
$\Pi_1 = (s/t_0)/U = U_0/U$	0.88 - 1.06	1.0 - 2.0
$\Pi_2 = (s/t_c)/U = U_c/U$	0.80 - 1.06	1.0 - 2.0
$\Pi_3 = t_{s0}/t_{sc}$	0.30 - 0.35	0.255 - 0.950
$\Pi_4 = f(t_0+t_c+t_{s0}) = fE_t$	0.298 - 0.460	0.299 - 0.530
$\Pi_5 = D(f/\nu)^{1/2}$	27.68 - 34.36	18.60 - 61.20
$\Pi_6 = UD/\nu$	533 - 1257	290 - 1200
$\Pi_7 = s/D$	0.467 - 0.488	0.02 - 0.500
$\Pi_8 = d/D$	0.871 - 0.872	0.871
$\Pi_9 = \bar{y}_b/s$	0 - 1.0	0 - 1.0

APPENDIX II

A THEORETICAL APPROACH TO EVALUATION OF THE HOT FILM PROBE PERFORMANCE

II.1 Introduction

Hot wire anemometer has been used for many years as a research tool in fluid mechanics. Its small dimensions and time constant have allowed precise measurements of steady and time dependent flow velocities. The successful operation of the system has led to its modification for measurements in liquids, particularly water. Although some reliable results have been obtained using the hot wire anemometer in liquids[136], under controlled conditions, recent investigations would seem to indicate that hot films are better suited for use in liquids[157,158].

A hot film probe essentially consists of a platinum film deposited on a glass substrate in the form of a wedge and coated with a quartz protective layer. Gold leads convey the signal to two concentric silver tubes with insulation in between. The outer tube, normally grounded, provides a heavy metal contact for fastening the sensor to the support (Figure II-1). As compared to hot wires, the film sensors have the following advantages:

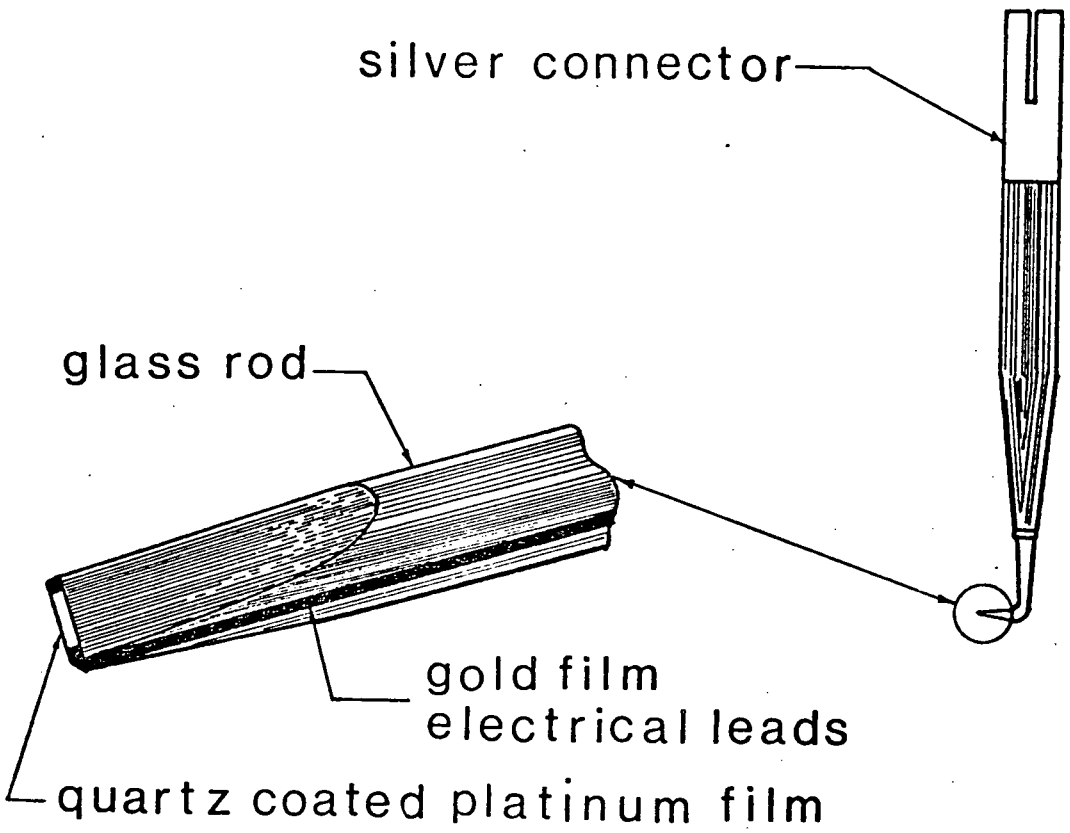

Figure II-1 A schematic drawing of a hot film probe

(i) A hot film probe has better frequency response than a hot wire of the same sensitive area. This is because the sensor is distributed on the surface and hence offers very little thermal inertia as against the circular cross section of the wire.

(ii) In general, film probes exhibit lower heat conduction to the substrate (end losses) for a given power input due to the lower thermal conductivity of the base material. A shorter sensing length can thus be used. On the other hand, size of the silver supports and their proximity to the wire normally results in greater loss due to conduction and free convection.

(iii) Film probes offer more flexibility in the sensor configuration. Wedge, conical, parabolic and flat surface shapes are available.

(iv) Comparatively speaking, probes with heated films are less susceptible to fouling and easier to clean. A thin quartz coating on the surface resists accumulation of foreign matter. Fouling tends to be a direct function of size. On the other hand, hot wire probes oxidize readily, are very fragile and prone to breakage.

Several detailed studies of relative behavior of hot wire and hot film probes and the difficulties encountered in their application in liquid mediums have been reported[158,159] et al. In general, the investigations establish superiority of hot films for liquid application.

II.2 Heat Transfer from a Hot Film Probe

There are several well developed theories reported in literature for evaluating performance of a hot wire anemometer[160,161]. On the other hand, although hot film probes play a rather useful role in the experimental liquid flow studies, no well developed theory systematically accounting for conduction and free convection losses is available, particularly, in the Reynolds number range of 2-350 (based on average flow rate and film width). This is indeed surprising, since the fact that in this range of R_n viscous effects are of the same order as those due to inertia, was first recognized by Barker[107] as early as in 1922. Thus it has been necessary to resort to careful calibration for each shape of the probe. The theory presented here represents a modest step towards minimizing dependence on such tedious experimentation.

The thermal energy loss from a film may be due to forced and free convection, conduction, and radiation of heat to the fluid and to the glass support. At higher

velocities the primary heat loss is by forced convection, the contribution through other sources being negligible, and may be considered as secondary.

The convective heat loss from the film is much greater in liquid than in gas, consequently demanding additional heat flux to keep the film at a constant temperature. Hence, the application of hot film anemometers in liquids is limited to low velocities. However, in this case, only radiation effects tend to be negligible, heat loss by the other modes being significant. Therefore, theoretical analysis of a film probe, particularly in the low velocity range, should account for the losses by both forced and free convection.

From similarity arguments it follows that, for forced convective heat transfer, the Nusselt number is a function of Prandtl and Reynolds numbers only. For heat transfer in a laminar boundary layer and $N_p >> 1$, the function takes the form[105]

$$N_u(x) = C(x) N_p^{1/3} R_n^{1/2} \qquad \ldots . (II\text{-}1)$$

where $x = \chi/b$, dimensionless downstream coordinate along the probe face,

$$C(x) = \{[B(x)]^{1/2}/[9^{1/3}\Gamma(4/3)]\} * \left\{\int_0^x [B(\xi)]^{1/2} d\xi\right\}^{1/3} \qquad \ldots . (II\text{-}2)$$

$$B(x) = \hat{C}[(1+m)/2]^{1/2}\, x^{(3m-1)/2} \quad \ldots\ldots (II-3)$$

$$\hat{C} = f''(0)$$

$$= 0.887 \text{ (based on data by Moore}^{163}\text{)}$$

$$m = \psi/(2-\psi) \quad \ldots\ldots (II-4)$$

$$\psi = \delta/2\Pi, \quad \delta = \text{the wedge angle.} \quad \ldots\ldots (II-5)$$

For the film probe used (DISA type 55A83), $\delta = 80°$. With this, equation (II-1), after integration and simplification, is reduced to

$$N_u(x) = 0.4748\, N_p^{1/3} R_n^{1/2}\, x^{-5/14}$$

the average Nusselt number over the wedge face is obtained as

$$\bar{N}_u = \int_0^1 N_u(x)\,dx$$

$$= 0.7386\, N_p^{1/3}\, R_n^{1/2}$$

$$\therefore\ Q_l = 0.7386(2\ell K_f)(T_w - T_f) N_p^{1/3} R_n^{1/2}. \quad \ldots\ldots (II-6)$$

Heat transfer by natural convection depends on the orientation of the film relative to the gravitational field. For a flat plate inclined to the horizontal (half of the

wedge shaped hot film) the heat loss from the heated surface to the fluid due to convection and conduction, assuming constant wall temperature, may be evaluated by [164]

$$\bar{N}_u = 0.7668(G_r N_p)^{1/5}$$

$$\text{i.e. } Q_2 = 0.7668(2\ell K_f)(T_w - T_f)(G_r N_p)^{1/5} \quad \ldots\ldots (II\text{-}7)$$

providing that $N_p \gg 1$ and the wedge angle obeys the relation

$$\delta = 0 \mid tg^{-1}(G_r N_p x^3)^{-1/5} \mid .$$

Fortunately, both the conditions are satisfied here. Finally, the heat conduction to the quartz support can be estimated from

$$Q_3 = 2C_3 K_g \ell b (T_w - T_f)/b \quad \ldots\ldots (II\text{-}8)$$

where

K_g = thermal conductivity of the quartz support
ℓ = film length
b = film width
T_f = bulk temperature of the fluid
T_w = wall temperature
C_3 = constant of proportionality.

The value of C_3 can be evaluated, approximately, by using a special equation for heat flow in a two dimensional wedge as given by Sokolowski[165] (here $\ell/b = 5$). Taking the average heat flow as $\frac{1}{x}\int_{10^{-7}}^{1} q(x)dx$ to avoid singularity at $x = 0$, the constant C_3 is found to be 0.38.

The total heat flux from the film may now be written as the sum of the contributions represented by Equations (II-6), (II-7) and (II-8). This can then be equated to the power supplied to the film. Thus,

$$R_0 I^2/4.2 = [C_1 \frac{K_f}{K_g} N_p^{1/3} R_n^{1/2} + C_2 \frac{K_f}{K_g} (G_r N_p)^{1/5} + C_3]*$$

$$*2\ell K_g(T_w - T_f) \qquad \ldots .(II-9)$$

$$= C_4\ 2\ K_g(T_w - T_f)$$

where

I = probe current

C_1 = 0.7386

C_2 = 0.7668.

As suggested by the manufacturer, the difference between temperature of the wall and the fluid may be expressed by

$$T_w - T_f = \frac{a}{\lambda}$$

$$= \left(\frac{R_0 - R_c}{R_c}\right) \frac{1}{\lambda} \quad . \qquad \ldots . \text{(II-10)}$$

With this, Equation (II-9) can be rewritten as

$$I^2(a+1)/a = \frac{8.4 K_g \ell C_4}{\lambda R_c} \qquad \ldots . \text{(II-11)}$$

where λ = coefficient of thermal resistivity.

Now the voltage output of a DISA 55A01 constant temperature anemometer is the bridge voltage, which is related to the probe current by

$$I = 1.04\ V/(100.6 + R_c) \quad . \qquad \ldots . \text{(II-12)}$$

Inserting (II-12) in (II-11), the following relation between bridge voltage and flow velocity is obtained:

$$V^2 \hat{C}_3 = \hat{C}_2 + \hat{C}_1 U^{1/2} \qquad \ldots . \text{(II-13)}$$

where

$$\hat{C}_3 = [(a+1)/a\{100.6 + R_c(1+a)\}^2] *$$

$$*1.08\ \lambda\ R_c/8.4\ K_g \ell$$

$$\hat{C}_2 = C_3 + C_2 \frac{K_f}{K_g} (G_r\ N_p)^{1/5}$$

$$\hat{C}_1 = C_1 \frac{K_f}{K_g} N_p^{1/3} (b/\nu)^{1/2} \quad .$$

II.3 Experimental Verification and Discussion

To assess validity of the approach, coefficients $\hat{C}_1$, $\hat{C}_2$, and $\hat{C}_3$ were found experimentally. This was accomplished by calibrating two different probes in a water-glycerol solution, 55% by weight, for two overheat ratios (Figure II-2). Employing the least square fit, the calibration data were fitted into a straight line of the form

$$V^2 = F_1 U^{1/2} + F_2 \quad . \qquad \ldots . (II\text{-}14)$$

Knowing F_1 and F_2, and calculating $\hat{C}_3$ for the probe in question, coefficients $\hat{C}_2$ and $\hat{C}_1$ are determined. Pertinent information for the two hot film probes are listed in Table II-1, while experimental and theoretical values for F_1 and F_2 are compared in Table II-2.

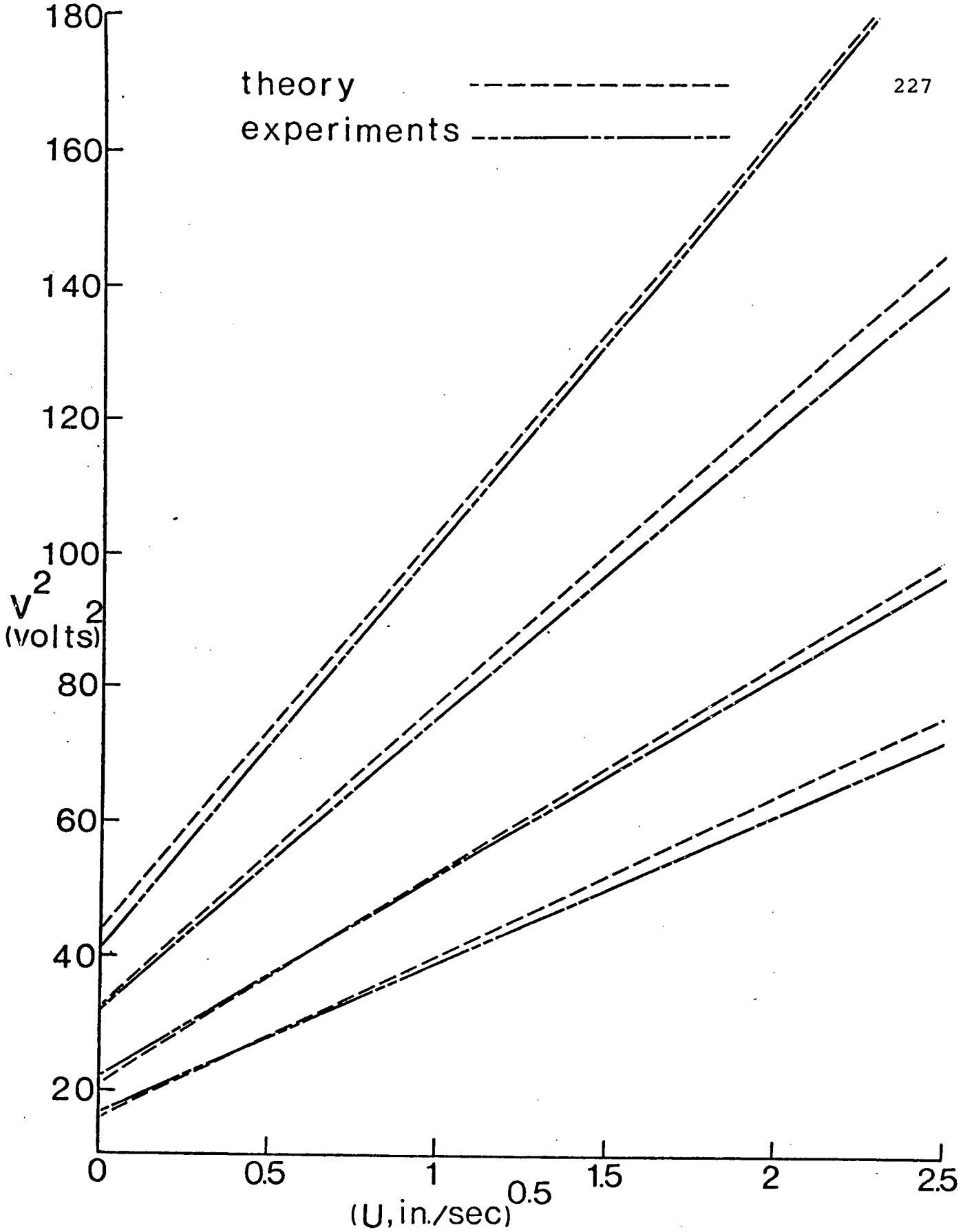

Figure II-2 Theoretical and experimental calibration plots for the hot film probes used

TABLE II-1

Pertinent Data for the Hot Film Probes

	Probe No.	
	1	2
ℓ, film length, cm	0.10	0.10
b, film width, cm	0.02	0.02
λ, temperature coefficient of film resistance, $^\circ C^{-1}$	4.41×10^{-3}	4.4×10^{-3}
K_g, heat conductivity of the glass support, $[(cal/sec.cm^2)/(^\circ C/cm)]$	2.7×10^{-3}	2.7×10^{-3}
R_c, probe cold resistance, Ω	7.8	10.3

TABLE II-2

Heat Transfer Parameters for Hot Film Probes

Probe No.	Overheat Ratio	F_1		% Error F_1	F_2		% Error F_2
		Theory	Experiment		Theory	Experiment	
1	0.051	31.17	29.84	-4.45	21.19	21.79	3.14
	0.103	60.24	61.20	1.26	43.19	40.18	-7.48
2	0.049	23.82	22.06	-7.69	16.09	16.82	+4.36
	0.097	45.50	43.77	-3.43	32.36	31.60	-2.42

Figure II-2 presents theoretical and experimental calibration plots for the hot film probes used. The agreement may be considered quite satisfactory particularly when one realizes the fact that the results depend heavily on the resistivity and conductivity of the glass support, accuracy of the wedge angle, and relation (II-12) governing the amplifier characteristics, etc., which are quoted by the manufacturer (usually as constant values) and can change from probe to probe. Any discrepancy in the slope ($F_1 = \hat{C}_1/\hat{C}_3$) can be minimized by better determination of the probe and fluid physical parameters, specifically b, ℓ, K_f, and λ. The accurate evaluation of these parameters will also improve reliability of the V^2 intercept (i.e. F_2) for the probes. Furthermore, recognizing that F_2 is substantially affected by the value of the constant $\hat{C}_3$, its accuracy will improve with that of $\hat{C}_3$, i.e. by eliminating the assumption of two dimensionality of the wedge and improving upon the power law character of the temperature variation as used in the Sokolowski theory. In any case, even in the absence of any further sophistication, the theory as it stands gives results of sufficient accuracy for practical applications.